Title
Conservation, evolutionary and physiological ecology of plant drought tolerance: from ecotypes to ecosystems

Author
Dias Barros Medeiros, Camila Barros

Publication Date
2021

UNIVERSITY OF CALIFORNIA

Los Angeles

Conservation, evolutionary and physiological ecology of plant drought tolerance: from ecotypes to ecosystems

A dissertation submitted in partial satisfaction of the

requirements for the degree Doctor of Philosophy

in Biology

by

Camila Dias Barros Medeiros

2021

ABSTRACT OF THE DISSERTATION

Conservation, evolutionary and physiological ecology of plant drought tolerance: from ecotypes to ecosystems

by

Camila Dias Barros Medeiros

Doctor of Philosophy in Biology

University of California, Los Angeles, 2021

Professor Lawren Sack, Chair

Due to the projected increases climatic variability, including an increased frequency of extreme climatic events, such and droughts, flooding and fires, the mechanisms that plants use to access, transport and conserve water require critical and quantitative understanding. While there is a growing consensus that traits, such as the leaf osmotic potential at turgor loss point (π_{tlp}), determine plants' abilities to maintain photosynthetic performance and survive droughts, there has been little work to understand their inter-relationships, evolution, and how they scale up to overall plant performance and ecosystem functioning. During my PhD I focused on the integration of leaf and whole-plant traits to explain and predict plant vital rates and vegetation distributions with respect to climate. I showed that the stomatal conductance of *Arabidopsis* ecotypes and its relationship with climate is developmentally determined by the area of epidermal pavement cells and the stomatal initiation rate, and not the stomatal size. I determined that traits of California native oak

species evolve in modules and that traits of Hawaiian native species from contrasting forests varied strongly and influenced species' vital rates, with stronger relationships when stratifying by tree size. I also showed that species' climate distributions across California can be predicted from traits and that traits and trait-trait intercorrelations change along a gradient of aridity in California. Ultimately, this work provided a new synthesis of the variation of trait-climate relationships across scales, opening new avenues for the inclusion of mechanistically informative traits to parameterize process-based models to test the ability to predict growth and mortality rates from trait networks, spatial neighborhoods, local topography, and climate across forests worldwide.

The dissertation of Camila Dias Barros Medeiros is approved.

Priyanga Amarasekare

Thomas Gillespie

Nathan J. B. Kraft

Lawren Sack, Committee Chair

University of California, Los Angeles

2021

To my beloved parents and friends who always believed in me,

even when I didn't.

TABLE OF CONTENTS

LIST OF TABLES

CHAPTER 6

LIST OF SUPPLEMENTARY TABLES

LIST OF FIGURES

LIST OF SUPPLEMENTARY FIGURES

ACKNOWLEDGEMENTS

A PhD is not a journey one can complete alone-- at least I know I wouldn't. This title has been added to my name, but there's a whole village of amazing people who lifted me up and pushed me forward, and without whom I would have never made it here.

First, thank you to Lawren, my mentor and advisor, for teaching me so much. Thank you for welcoming me in your lab when you knew very little about me, for believing in my potential and for pushing me to keep going when I needed the most. You always had my back and your positive energy and encouragement made all the difference in the past six years. Thank you for being so understanding and for helping keep your students safe during the turmoil of the past couple of years. I will be forever thankful for all the opportunities you've given me through science to travel to many beautiful forests and meet amazing collaborators all over the US. I am very fortunate to have been trained by such an incredible scientist and someone I admire so much.

To the Sack lab-- this PhD was a long and winding road, but you've made it so much fun! Leila and Chris, I'm so happy I got to go through everything with you. Our friendship is one of my biggest non-PhD PhD accomplishments! Leila, you are one of the kindest, smartest and funniest people I have ever met. Thank you for always being there for me, for welcoming into your family (thank you Rebecca, Jim, Florence and Biff!) and for the effort you put into keeping our cohort and lab together. Chris, you are the most-coolest and fun person I know! Thank you for always being so patient and supportive, for the partnership always and especially during fieldwork. You taught me to be more patient and optimistic, and you make the hard times lighter to go through! Joseph, thank you for the partnership and friendship! Our field adventures across the US are some of the highlights of my PhD; thank you for letting me get to know you and for staying by my side and growing with me these past few years! Santiago, thank you for the great times

together exploring California and for so many hilarious moments and stories. Christine, thank you for teaching me so much about hydraulics and being a good scientist and person! You are such an inspiration! Megan, thank you for the laughs, emergency coding support and long talks about drag queens! Grace, thank you for all the fun times and deep conversations. You made life in EEB very exciting! Marvin, thank you for all the laughs, cooking conversations and food adventures. Stay amazing! Alec, thank you for your partnership and for partaking in the science gossiping with me on the bus ride home. Marissa, thank you for your friendship, support and wisdom. Jess, my fellow true crime aficionado, thank you for the laughs, hugs and for always being so supportive and caring. To all of my undergraduate students who taught me so much and who helped me collect an absurd amount of data.

To my Kraft lab friends, thank you for all the support and fun times together! Special thanks to Marcel, for everything-- your generosity and patience, for teaching me to code and for indulging in long nerdy plant conversations with me. Gaurav, thank you for sharing your knowledge so selflessly and for always being down for an adventure, be it in nature or Downtown LA! Andy and Jane, thank you for always being so supportive and encouraging.

To my UCLA EEB cohort, Aji, Alayna, Brandon, Bruno, Chris, Clive, Dita, Emily, Gaurav, Hayley, Leila, Marcel, Paige, Rachel, Scott, Shawn, Zack-- thank you for the adventures, goofy moments and for opening your selves up and helping build this community where we feel comfortable to be vulnerable and help each other learn and grow. I will always cherish our evenings at Sepi's, the G&G and the late-night coding sessions in the LS lunch room. I especially want to thank Rachel for living with me all these years. Your confidence, generosity with your community and overall approach to life are inspiring.

Thank you to Tessa Villaseñor, Jocelyn Yamadera, Humberto Barba, Alberto Gonzalez, Joel Latimer and Ora Rutherford-Green for helping me navigate the bureaucracy and practical aspects of being a PhD student. Tessa, thank you for advocating for me and for all the work you do to bring our department together.

To my mentors from CIRTL, Erin O'Leary, Katie Dixie and Rachel Kennison-- thank you for sharing so much with me about teaching and for helping me become a much more confident, purposeful and empathetic teacher.

I am grateful to my many collaborators and to my committee members, Priyanga Amarasekare, Nathan Kraft and Thomas Gillespie for their guidance, encouragement and feedback on my work across the years.

To my LFV mentors and friends, Mauro Guida, Marciel Teixeira, Hiram Falcão, Rebeca Rivas, Karla Figueiredo and Gabriella Frosi-- thank you for introducing me to what is now my career and passion, for your guidance, generosity and friendship. I will always be grateful for the opportunity to learn from and collaborate with you.

To Carol, Gabriela, Larissa and Maíra-- you are my rocks, my sisters, part of my heart. You've been my partners in this academic journey and our adventures (and misadventures!) will always be the best part of college! Carola, thank you for the partnership, drunk late-night conversations and the warm bed and coffee whenever I'm in town. Gabi, thank you for making me laugh, for teaching me the power of generosity and for making me feel so loved. Lari, thank you for the never-ending support and for never letting me give up. Maíra, thank you for showing me a whole new world and for always being there for me!

To Eliziel-- I'm so happy we found each other! Thank you for always being there for me, for being someone I can be 100% myself with. I can't wait to be together again to talk about everything while drinking fancy coffee. You are brilliant and you know it!

Most of all, thank you to my parents, who always encouraged me stay curious and gave me the best education they could. Thank you for teaching me the value of hard work and independence, for giving me space to figure out who I am and what I wanted to do. I wouldn't be who I am today if it wasn't for your hard work, support and love.

Coauthored work: **Chapter 2** is from Medeiros CD, TN Buckley, K Sartori, C Violle, F Vasseur, LR Fletcher and L Sack (*in prep*) Developmental basis for the adaptation of maximum stomatal conductance to climate in *Arabidopsis*. K Sartori, F Vasseur and C Violle planned the experiment and collected samples, LR Fletcher and TN Buckley contributed to analyses and L Sack mentored the project. **Chapter 3** is from Medeiros CD, A Sorfazian, A Mead, V Sork and L Sack (*in prep*) Evolution of trait modules across California native oaks. A Mead contributed to field sampling, A Sorfazian contributed to data collection, V Sork funded nutrient analyses and L Sack mentored the project. **Chapter 4** is from Medeiros CD, C Scoffoni, G John, M Bartlett, F Inman-Narahari, R Ostertag, S Cordell, C Giardina and L Sack (2019) An extensive suite of functional traits distinguishes Hawaiian wet and dry forests and enables prediction of species vital rates. *Functional Ecology* 33:712-34. C Scoffoni, G John, M Bartlett and F Inman-Narahari contributed to data collection, F Inman-Narahari, R Ostertag, S Cordell and C Giardina organized and collected forest census data, L Sack mentored and contributed to all stages of the project. **Chapter 5** is from Medeiros CD, C Henry, S Trueba, I Anghel, SDDL Guerrero, A Pivovaroff, LR Fletcher, GP John, JA Lutz, RM Alonzo and L Sack (*in prep*) The prediction of

species and ecosystem climate distributions on the basis of mechanistic functional traits. RM Alonzo, LR Fletcher, SDDL Guerrero, C Henry and JA Lutz contributed to field sampling, S Trueba, A Pivovaroff and GP John contributed to field sampling and data collection, I Anghel contributed to analyses, L Sack mentored and contributed to all stages of the project. **Chapter 6** is from Medeiros CD, C Henry, S Trueba, SDDL Guerrero, A Pivovaroff, LR Fletcher, GP John, JA Lutz, RM Alonzo and L Sack (*in prep*) Variation in plant trait networks across a gradient of aridity in California. RM Alonzo, LR Fletcher, SDDL Guerrero, C Henry and JA Lutz contributed to field sampling, S Trueba, A Pivovaroff and GP John contributed to field sampling and data collection, L Sack mentored and contributed to all stages of the project.

Funding: This work was generously supported by the Brazilian National Research Council (CNPq) through the Brazilian Science Without Borders Program (grant number: 202813/2014-2), the UCLA EEB Vavra Fellowship and research grants, the La Kretz Center Graduate research grants, the UCNRS Stunt Ranch Reserve research grants, the Ecological Society of America (Forrest Shreve Award), the National Science Foundation grants (grant 1557906 to TN Buckley; grant 2017949 to JA Lutz; grants 1457279, 1951244 and 2017949 to L Sack; grant 1444611 to L Sack and V Sork), the European Research Council (ERC; 'CONSTRAINTS': grant ERC-StG-2014-639706- CONSTRAINTS to C Violle) and the USDA National Institute of Food and Agriculture (Award #2020-67013-30913 and Hatch Project 1016439 to TN Buckley).

VITA

PROFESSIONAL PREPARATION

2012 BA in Biological Sciences (Universidade Federal de Pernambuco- Recife, Brazil)
2015 MS in Plant Science; Emphasis: Ecology (Universidade Federal de Pernambuco- Recife, Brazil)

PUBLICATIONS

Medeiros CD, C Scoffoni, G John, M Bartlett, F Inman-Narahari, R Ostertag, S Cordell, C Giardina, and L Sack. 2019. An extensive suite of functional traits distinguishes Hawaiian wet and dry forests and enables prediction of species vital rates. *Funct Ecol* 33:712-34.

Falcão HM, **CD Medeiros**, JS Almeida-Cortez, and MG Santos (2017) Leaf construction cost is related to water availability in three species of different growth forms in a Brazilian tropical dry forest. *Theor Exp Plant Physiol* 29:95-108.

Medeiros CD, HM Falcão, JS Almeida-Cortez, DYAC Santos, AFM Oliveira, and MG Santos. 2017. Leaf epicuticular wax content changes under different rainfall regimes, and its removal affects the leaf chlorophyll content and gas exchanges of *Aspidosperma pyrifolium* in a seasonally dry tropical forest. *S Afr J Bot* 111: 267–274.

Falcão HM, **CD Medeiros**, BLR Silva, EVSB Sampaio, JS Almeida-Cortez, and MG Santos (2015) Phenotypic plasticity and ecophysiological strategies in a tropical dry forest chronosequence: a study case with *Poincianella pyramidalis*. *For Ecol Manag* 340: 62–69.

Oliveira MT, V Matzek, **CD Medeiros**, R Rivas, HM Falcão, and MG Santos (2014) Stress tolerance and ecophysiological ability of an invader and a native species in a seasonally dry tropical forest. *Plos One* 9(8): e105514.

Oliveira MT, **CD Medeiros**, G Frosi, and MG Santos (2014) Different mechanisms drive the performance of native and invasive woody species in response to leaf phosphorus supply during periods of drought stress and recovery. *Plant Physiol Biochem* 82: 66-75.

Medeiros CD, JRC Ferreira-Neto, MT Oliveira, R Rivas, V Pandolfi, EA Kido, JI Baldani, and MG Santos. 2013. Photosynthesis, antioxidant activities and transcriptional responses in two sugarcane (*Saccharum officinarum* L.) cultivars under salt stress. *Acta Phys Plant* 36: 447-459.

Medeiros CD, MT Oliveira, R Rivas, JI Baldani, EA Kido, and MG Santos (2012) Gas exchange, growth, and antioxidant activity in sugarcane under biological nitrogen fixation. *Photosynthetica* 50: 519-528.

SYNERGISTIC ACTIVITIES

- Conference presentations at the Ecological Society of America (2016-18, 2020-21), the American Geophysical Union (2019-20), UCLA's EEB Department Symposium (2018-20), UCLA's EEB EEP (2017, 19), the Botany Conference (2020) and the Evolution Conference (2021).
- Teaching Assistant Consultant for UCLA's Department of Molecular and Cell Developmental Biology (MCDB) and for the Life Sciences Division (2019-20). Associate at the Center for the Integration of Research, Teaching and Learning (2019-present).

- Guest lecturer of the UCLA EEB Plant Physiology course (2018) and volunteer instructor at the UCLA Annual TA Conference (Active Learning Strategies for Lab Sections Workshop).
- Mentor of 38 undergraduate students, including a UCLA URFP recipient (2016-21).
- Reviewer for *Annals of Botany*, *Conservation Physiology, Ecology Letters*, *Functional Ecology*, *Plant and Soil*, *Plant, Cell and Environment* and *Tree Physiology*.
- Participant in the PHYS-Fest (2016), Likelihood Methods in Ecology (2017) and Applications of Spatial Data: Ecological Niche Modeling Tutorial (NIMBioS; 2018) workshops.
- Member of the Ecological Society of America (2015-present) and the American Geophysical Union (2019-present).

CHAPTER 1

PREMISE OF THE DISSERTATION

Functional traits are morphological, physiological or phenological attributes measurable at the individual level that influence plant growth, reproduction and survival and thereby fitness (Lavorel & Garnier 2002; Violle *et al.* 2007), and thus can be used to predict vital rates (Poorter *et al.* 2008; Adler *et al.* 2014; Uriarte *et al.* 2016), habitat preferences (Shipley *et al.* 2017) and spatial distributions (Stahl *et al.* 2014). For decades, functional traits have been applied by ecologists performing research at large biogeographic scales with an emphasis on easy-to-measure traits that can be determined for entire communities (Grime 1979; Wright *et al.* 2004; Díaz *et al.* 2016; Messier *et al.* 2017). Instead of measuring all aspects of the ecology and physiology, which was presumed to require focusing on small species sets, this approach focuses on small sets of informative parameters in entire communities and ecosystems (Mcgill *et al.* 2006). This trait-based approach presents a clear advantage: the ability to study patterns even across species worldwide (Wright *et al.* 2004; Westoby & Wright 2006; Díaz *et al.* 2016).

However, the functional trait approach has to be applied with caution—traits may not be meaningful alone, since they vary in coordination with other traits (Sack *et al.* 2013; He *et al.* 2020; Sack & Buckley 2020). To truly understand the ecological response and the mechanisms involved, there has been a focus on the selection and quantification of closely coordinated traits thought to most importantly represent function (Cornelissen *et al.* 2003; Westoby & Wright 2006). Oversimplification of the trait-based approach can lead to equivocal conclusions with serious consequences to the development of the field and to the understanding of natural ecosystems, ultimately leading to wrong management of natural landscapes (Lavorel & Garnier 2002; Sack *et*

al. 2013). Indeed, several have argued that more extensive suites of traits would enable stronger predictive and explanatory power (Reich 2014; Paine *et al.* 2015; Greenwood *et al.* 2017; Yang *et al.* 2018), and this argument has conceptual support because mechanistic models of growth and survival are sensitive to a broad set of traits as inputs (Marks & Lechowicz 2006; Sterck *et al.* 2006; Osborne & Sack 2012).

In this context, the inclusion of more physiology-intensive parameters seems be the most promising next step to further the development of trait-based ecology, moving beyond simple and easy-to-measure parameters with little biological relevance to species distribution patterns and closer to a mechanistically oriented functional ecology. Thus, my PhD work focused on integrating trait-based approaches in physiology, evolution and ecology, in particular linking leaf and whole-plant function and vital rates and vegetation distributions to reach an integrative perspective of plant's responses to environmental drivers and create models to explain and predict species ranges. In each successive chapter of my dissertation, I scale up to higher levels of organization and function, from ecotypes to ecosystems. I quantified a comprehensive set of leaf, stem and whole-plant traits and their relationships with climate across: ecotypes of a model species (Chapter 2), different species from the same genus (Chapter 3), species from contrasting forest types (Chapter 4) and different ecosystem types across the California Floristic Province (CAFP; Chapters 5 and 6).

In Chapter 2, I quantify the variation and interrelationships of leaf epidermal traits across *Arabidopsis* ecotypes and partition the developmental drivers of a central trait for the regulation of water use efficiency and photosynthesis, the maximum theoretical stomatal conductance, g_{max}. I show that g_{max} and its relationship with climate is developmentally determined by the area of epidermal pavement cells and the stomatal initiation rate, and not the stomatal size. This finding

has important implications for the advancement of plant breeding for more photosynthetically efficient plants, that can now shift their efforts to genes that regulate epidermal pavement cell size and stomatal initiation. These results also have important implications for models of ecosystem fluxes, since many have been scaling up from stomatal size and density to plant and ecosystem growth rates and NPP (Wang *et al.* 2015).

In Chapter 3, I quantify the variation and interrelationships of functional traits across California Oak species and show that trait evolution driven by adaptation to spatial heterogeneity in climate has resulted in the emergence of semi-independent trait modules relating to structure and function. I also performed an analysis of plant trait networks (PTNs), which creates clusters based on statistical relationships, to identify the contribution of shared evolutionary history to the formation of trait modules (Flores-Moreno *et al.* 2019; Kleyer *et al.* 2019; He *et al.* 2020). I show that traits evolve within clusters, highlighting the emergence of integrated phenotypes that provide drought tolerance and pointing to the necessity of considering the benefits and costs contributed by multiple traits to overall climate adaptation (He *et al.* 2020; Sack & Buckley 2020).

In Chapter 4, I quantify the variation and interrelationships of functional traits across species sampled from a wet montane and a lowland dry forest (MWF and LDF respectively) to test for the presence of functional modules and the relationships between functional traits and relative growth rate (*RGR*) and mortality rate (*m*) while accounting for plant size. I show that traits are overall more variable in the MWF than LDF and are correlated within modules, as we found in Chapter 3. I was also able to predict species' *RGR* and *m* across forests using multiple traits and uncovered stronger relationships when stratifying by tree size. These findings are consistent with a powerful role of broad suites of functional traits in contributing to forest species' distributions, integrated plant design, and vital rates (Marks & Lechowicz 2006; Sterck *et al.* 2006, 2011; Poorter

et al. 2008; Osborne & Sack 2012; Adler *et al.* 2014; Stahl *et al.* 2014; Uriarte *et al.* 2016; He *et al.* 2020).

In Chapter 5, I quantify the variation of functional traits across species sampled from different ecosystems along a gradient of aridity in the California Floristic Province, CAFP, to test the ability of functional traits to predict species' preferred climates. This is important because anticipating and mitigating shifts in the distributions of species and ecosystems under climate change depends on understanding their preferred climate and their vulnerability. In this chapter I show that mechanistic traits enable strong prediction of the mean maximum temperature, rainfall and aridity of the climatic range of diverse plant species and ecosystems, and that species that have less xeromorphic traits are projected to face greater climate aridification. The ability to predict a species' preferred climate from its traits has potential to improve global dynamic vegetation models, and thereby to predict the impact of climate change, and to inform the design and prioritization of conservation efforts to protect the most vulnerable species.

In Chapter 6, I show how the intercorrelations of an extensive suite of functional traits vary across ecosystems along the same gradient of aridity from Chapter 5. Because plant ecological and physiological strategies are the result of multiple interactions among traits, a deeper understanding of how traits are integrated within different axes of function can clarify how they contribute to species' ecological specializations, biogeographic distributions, and tolerance of climate change, building on the evidence I showed in Chapters 3 and 4 (Messier *et al.* 2017; Flores-Moreno *et al.* 2019; Kleyer *et al.* 2019; He *et al.* 2020). I found that functional traits and their pairwise relationships varied strongly across ecosystems, with PTNs becoming more interconnected and more complex from high to low aridity environments, indicating that under more intense

environmental pressure plant communities tend to become more functionally redundant (Cowling *et al.* 1994; Pillar *et al.* 2013; Biggs *et al.* 2020).

The use of extensive suites of functional traits while accounting for species shared evolutionary histories and plant size provided insight into the modular nature of trait function and overall physiological, evolutionary and ecological strategies of different plant species and ecosystems. The PTNs also enabled greater clarity and improved examination of the wider range of key plant traits, reinforcing that traits have limited meaning when alone.

Overall, my thesis work provides a new level of comprehensive trait measurement and analysis within multiple contexts and scales, toward providing a new resolution of the importance of physiological and structural diversity on ecological processes and contributing to state-of-the-art predictive tools to study community assembly and species distributions.

REFERENCES

Adler, P.B., Salguero-Gomez, R., Compagnoni, A., Hsu, J.S., Ray-Mukherjee, J., Mbeau-Ache, C., *et al.* (2014). Functional traits explain variation in plant life history strategies. *Proc Natl Acad Sci USA*, 111, 740–745.

Biggs, C.R., Yeager, L.A., Bolser, D.G., Bonsell, C., Dichiera, A.M., Hou, Z., *et al.* (2020). Does functional redundancy affect ecological stability and resilience? A review and meta-analysis. *Ecosphere*, 11.

Cornelissen, J.H.C., Lavorel, S., Garnier, E., Díaz, S., Buchmann, N., Gurvich, D.E., *et al.* (2003). A handbook of protocols for standardised and easy measurement of plant functional traits worldwide. *Aust J Bot*, 51, 335–380.

Cowling, R.M., Esler, K.J., Midgley, G.F. & Honig, M.A. (1994). Plant functional diversity, species diversity and climate in arid and semi-arid southern Africa. *Journal of Arid Environments*, 27, 141–158.

Díaz, S., Kattge, J., Cornelissen, J.H.C., Wright, I.J., Lavorel, S., Dray, S., *et al.* (2016). The global spectrum of plant form and function. *Nature*, 529, 167–171.

Flores-Moreno, H., Fazayeli, F., Banerjee, A., Datta, A., Kattge, J., Butler, E.E., *et al.* (2019). Robustness of trait connections across environmental gradients and growth forms. *Global Ecol Biogeogr*, 28, 1806–1826.

Greenwood, S., Ruiz-Benito, P., Martínez-Vilalta, J., Lloret, F., Kitzberger, T., Allen, C.D., *et al.* (2017). Tree mortality across biomes is promoted by drought intensity, lower wood density and higher specific leaf area. *Ecol Lett*.

Grime, J.P. (1979). *Plant strategies and vegetation processes*. 1st edn. Wiley, Chichester.

He, N., Li, Y., Liu, C., Xu, L., Li, M., Zhang, J., *et al.* (2020). Plant Trait Networks: Improved Resolution of the Dimensionality of Adaptation. *Trends Ecol Evol*, 35, 908–918.

Kleyer, M., Trinogga, J., Cebrián-Piqueras, M.A., Trenkamp, A., Fløjgaard, C., Ejrnaes, R., *et al.* (2019). Trait correlation network analysis identifies biomass allocation traits and stem specific length as hub traits in herbaceous perennial plants. *J Ecol*, 107, 829–842.

Lavorel, S. & Garnier, E. (2002). Predicting changes in community composition and ecosystem functioning from plant traits: revisiting the Holy Grail. *Funct Ecol*, 16, 545–556.

Marks, C.O. & Lechowicz, M.J. (2006). Alternative designs and the evolution of functional diversity. *Am Nat*, 167, 55–66.

Mcgill, B., Enquist, B., Weiher, E. & Westoby, M. (2006). Rebuilding community ecology from functional traits. *Trends Ecol Evol*, 21, 178–185.

Messier, J., Lechowicz, M.J., McGill, B.J., Violle, C., Enquist, B.J. & Cornelissen, H. (2017). Interspecific integration of trait dimensions at local scales: the plant phenotype as an integrated network. *J Ecol*.

Osborne, C.P. & Sack, L. (2012). Evolution of C $_4$ plants: a new hypothesis for an interaction of CO $_2$ and water relations mediated by plant hydraulics. *Phil Trans R Soc B*, 367, 583–600.

Paine, C.E.T., Amissah, L., Auge, H., Baraloto, C., Baruffol, M., Bourland, N., *et al.* (2015). Globally, functional traits are weak predictors of juvenile tree growth, and we do not know why. *J Ecol*, 103, 978–989.

Pillar, V.D., Blanco, C.C., Müller, S.C., Sosinski, E.E., Joner, F. & Duarte, L.D.S. (2013). Functional redundancy and stability in plant communities. *J Veg Sci*, 24, 963–974.

Poorter, L., Wright, S.J., Paz, H., Ackerly, D.D., Condit, R., Ibarra-Manríquez, G., *et al.* (2008). Are functional traits good predictors of demographic rates? Evidence from five neotropical forests. *Ecology*, 89, 1908–1920.

Reich, P.B. (2014). The world-wide 'fast-slow' plant economics spectrum: a traits manifesto. *J Ecol*, 102, 275–301.

Sack, L. & Buckley, T.N. (2020). Trait multi-functionality in plant stress response. *Integr Comp Biol*, 60, 98–112.

Sack, L., Scoffoni, C., John, G.P., Poorter, H., Mason, C.M., Mendez-Alonzo, R., *et al.* (2013). How do leaf veins influence the worldwide leaf economic spectrum? Review and synthesis. *J Exp Bot*, 64, 4053–4080.

Shipley, B., Belluau, M., Kühn, I., Soudzilovskaia, N.A., Bahn, M., Penuelas, J., *et al.* (2017). Predicting habitat affinities of plant species using commonly measured functional traits. *J Veg Sci*, 28, 1082–1095.

Stahl, U., Reu, B. & Wirth, C. (2014). Predicting species' range limits from functional traits for the tree flora of North America. *Proc Natl Acad Sci USA*, 111, 13739–13744.

Sterck, F., Markesteijn, L., Schieving, F. & Poorter, L. (2011). Functional traits determine trade-offs and niches in a tropical forest community. *Proc Natl Acad Sci USA*, 108, 20627–20632.

Sterck, F.J., Van Gelder, H.A. & Poorter, L. (2006). Mechanical branch constraints contribute to life-history variation across tree species in a Bolivian forest. *J Ecology*, 94, 1192–1200.

Uriarte, M., Lasky, J.R., Boukili, V.K. & Chazdon, R.L. (2016). A trait-mediated, neighbourhood approach to quantify climate impacts on successional dynamics of tropical rainforests. *Funct Ecol*, 30, 157–167.

Violle, C., Navas, M.-L., Vile, D., Kazakou, E., Fortunel, C., Hummel, I., *et al.* (2007). Let the concept of trait be functional! *Oikos*, 116, 882–892.

Wang, R., Yu, G., He, N., Wang, Q., Zhao, N., Xu, Z., *et al.* (2015). Latitudinal variation of leaf stomatal traits from species to community level in forests: linkage with ecosystem productivity. *Sci Rep*.

Westoby, M. & Wright, I.J. (2006). Land-plant ecology on the basis of functional traits. *Trends Ecol Evol*, 21, 261–268.

Wright, I.J., Reich, P.B., Westoby, M., Ackerly, D.D., Baruch, Z., Bongers, F., *et al.* (2004). The worldwide leaf economics spectrum. *Nature*, 428, 821–827.

Yang, J., Cao, M. & Swenson, N.G. (2018). Why functional traits do not predict tree demographic rates. *Trends Ecol Evol*, 33, 326–336.

CHAPTER 2

DEVELOPMENTAL BASIS FOR THE ADAPTATION OF MAXIMUM STOMATAL CONDUCTANCE TO CLIMATE IN *ARABIDOPSIS*

ABSTRACT

Stomata, the micro-pores on leaves, regulate CO_2 uptake and water loss, thus directly influencing plant growth and stress tolerance. The relationships between the stomatal density and size (*d* and *s*, respectively) and epidermal pavement cell size (*e*), and their consequences for the anatomical maximum stomatal conductance, g_{max}, have been widely investigated, with key theory attributing higher g_{max} to a greater density of smaller stomata. However, little is known about how the adaptation of g_{max} to climate depends on its developmental drivers, that is, *e*, *s* and the stomatal initiation rate (*i*). We measured epidermal traits for the abaxial and adaxial surfaces of 152 ecotypes of model species *Arabidopsis thaliana* grown in a greenhouse common garden, quantified how much of the variation in g_{max} was accounted for by the developmental drivers *e*, *i* and *s* and tested their relationships with the native climate of the origin of each ecotype. All epidermal traits varied strongly across ecotypes, and g_{max} was strongly related to mean annual temperature, precipitation and length of the growing season. The g_{max} of *A. thaliana* ecotypes was determined mainly by *e* and *i*, with a minimal role of *s*, and the adaptation of g_{max} to climate was determined by shifts in both *e* and *i* with climate. These results provide new resolution of the underlying developmental basis for g_{max} and its adaptive shifts with climate.

INTRODUCTION

The stomata are pores on the leaf surface involved in the regulation of CO_2 uptake and water loss to the atmosphere (Willmer & Fricker 1995; Wang *et al.* 2015). Stomata first appeared between the late Silurian to early Devonian periods, simultaneously with the cuticle and vascular tissues, when plants transitioned from the aquatic to the terrestrial environment (Willmer & Fricker 1995) and represent the ultimate interface between plants and the atmosphere. Stomatal size and density are key drivers of the theoretical maximum anatomical stomatal conductance, g_{max}, and consequently strongly constrain water uptake and photosynthesis (Buckley 2005; Sack & Buckley 2016), and thus directly influence plant growth and stress tolerance.

The critical importance of stomata, and their ability to open and close to optimize carbon gain relative to water loss, has long inspired plant scientists to investigate how their numbers and dimensions vary across species, ecotypes and ontogenetic stages (Salisbury 1927; Doheny-Adams *et al.* 2012; Dow *et al.* 2014; Wang *et al.* 2015; Dittberner *et al.* 2018). An extensive body of research has focused on the relationship between stomatal area, *s*, and density, *d*, with numerous reports of a negative relationship between *d* and *s* (Franks & Farquhar 2007; Ohsumi *et al.* 2007; Franks *et al.* 2009; Camargo & Marenco 2011; Wang *et al.* 2015; Dittberner *et al.* 2018; Kardiman & Ræbild 2018; Yin *et al.* 2020), which has been considered a trade-off resulting from a spatial constraint in the leaves (Wang *et al.* 2015; Dittberner *et al.* 2018), and to intrinsically determine g_{max}, such that a higher density of smaller stomata is responsible for higher g_{max} (Fig. 2.1a) (Franks *et al.* 2009). However, *d* is itself a function of underlying developmental traits, that is, *s*, and the epidermal pavement cell area, *e*, and the stomatal index, *i* (Salisbury 1927; Sack & Buckley 2016). Thus, g_{max} can be disentangled into its developmental drivers, that is, *e*, *i* and *s* according to explicit mathematical models (Fig. 2.1b) (Sack & Buckley 2016). Yet, the causal roles of *e*, *i* and *s* in

determining d and g_{max} and their adaptation to climate have not been established within and across species.

We measured epidermal traits for the abaxial and adaxial surfaces of 152 ecotypes of *Arabidopsis thaliana* L. Heynh (hereafter "Arabidopsis") grown in a greenhouse common garden. Arabidopsis is an annual herb widely distributed across the Northern hemisphere with populations adapted to contrasting climates ("ecotypes"; Fig. 2.2a), from cold and/or dry to warm and/or wet (Sharbel *et al.* 2000; Hoffmann 2002; Weigel & Mott 2009). More than a thousand ecotypes with known geographic origin have been sequenced to date (Alonso-Blanco *et al.* 2016), making Arabidopsis an ideal system to for ecology and development questions within an evolutionary framework (Sharbel *et al.* 2000; Alonso-Blanco *et al.* 2016), particularly given the phenology and physiology of different ecotypes represent adaptation to drought and cold stresses. Previous studies have shown that across species, adaptation to colder and drier climates may be associated with higher d and g_{max}, for plants that "avoid" drought or cold, through rapid growth in wetter and warmer season and/or warmer times of day, or with lower d and g_{max}, for plants that achieve tolerance through slow growth and reduced resource demand (Carlson *et al.* 2016; Hughes *et al.* 2017). In Arabidopsis ecotypes, many studies have shown that adaptation to cold often involves slower growth and longer times to flowering (Sanda *et al.* 1997; Kazan & Lyons 2016; Exposito-Alonso 2020), and one previous study has shown that d is higher in cold climates (Dittberner *et al.* 2018).

We tested the degree that differences in e, i and s contribute to the variation in d and g_{max} across ecotypes of a single plant species and how g_{max} and its anatomical drivers shift in response to climate. We hypothesized that ecotypes with higher i values would translate into a higher proportion of stomata, leading to higher d and g_{max} (Fig. 2.2f-h), whereas higher e, and to a lesser

extent, higher *s*, would lead to more spaced apart stomata, and thus lower *d* and g_{max} (Fig. 2.2c-e) (Franks & Farquhar 2007). We expected *e* and *i* to be the traits with largest influence on *d* and g_{max} (Appendix Table 2.1 and Fig. 2.1b; (Franks *et al.* 2009; Sack & Buckley 2016)). Further, we expected relationships between *e*, *i* and *s* may arise from development and to constrain g_{max}. We hypothesized a positive relationship between *e* and *s*, based on studies across species that showed that cell sizes are coordinated, potentially due to their associations with genome size (Beaulieu *et al.* 2008); such a relationship would increase the dependence of high and g_{max} on small cell dimensions, that is, *e*, *s* and related measures, including guard cell length and width (CG_l and GC_w) and the inner and outer stomatal pore lengths (SP_{il} and SP_{ol}). We further hypothesized a positive relationship between *e* and *i*, as the differentiation of greater numbers of stomata from meristemoid epidermal cells would be enabled by a greater duration of pavement cell expansion (Nadeau 2002; Bergmann & Sack 2007; Lau & Bergmann 2012). Thus, we (i) quantified the variation and interrelationships of leaf epidermal traits across *Arabidopsis* ecotypes, (ii) partitioned the developmental drivers of g_{max} and (iii) determined the adaptation of g_{max} and its drivers to the native climate of the origin of the ecotypes.

METHODS

Plant material and growing conditions

We grew 152 ecotypes of *Arabidopsis thaliana*, 137 sampled from the 1,001 Genomes Consortium populations (Alonso-Blanco *et al.* 2016) and 15 from the RegMap populations (Horton *et al.* 2012). These ecotypes were selected to represent the extent of the natural distribution of the species (Fig. 2.2a).

Seeds were sown in moist organic compost and stratified in a cold chamber at 4°C for four days. Three seedlings per ecotype were then transferred to individual pots filled with organic compost (Neuhaus N2) and watered twice a week for the duration of the experiment (140 days from sowing to harvest). Pots were randomly distributed across four tables in blocks, with one replicate per ecotype per table. The tables were placed in a greenhouse with a controlled temperature of 18°C during the day and 16°C during the night, and rotated daily to reduce block effects within the greenhouse. A supplemental lighting system was used to maintain a constant 12.5 h day-length.

Trait measurements

For all trait measurements we harvested a fully expanded and light-exposed leaf, or the last developed leaf at the bolting stage of each of three individuals per ecotype. The leaves were fixed in formalin–acetic acid–alcohol solution (FAA) for at least two days and then transferred to a pure glycerol medium for storage. First, the leaf area (*LA*) was measured from images obtained using a flatbed scanner (Pérez-Harguindeguy *et al.* 2013). Epidermal anatomy traits were measured on microscopy images taken of nail varnish impressions of both leaf surfaces (Medeiros *et al.* 2019). To determine leaf-level values for traits, for cell dimensions, we calculated an average value as the arithmetic mean of the abaxial (ABA) and adaxial (ADA) values (traits with subscript "avg"). For leaf-level cell densities and g_{max} we calculated a total trait value as the sum of ABA and ADA values (traits with subscript "total").

From the microscope images of the nail varnish peels we measured stomatal density (*d*; number of stomata per mm^2), stomatal differentiation rate (or index; the number of stomata per numbers of stomata plus epidermal pavement cells, *i*), stomatal area (*s*), guard cell length and

width (GC_l, GC_w), inner and outer stomatal pore length (SP_{il}, SP_{ol}) and epidermal pavement cell area (e) in the abaxial (ABA) and adaxial (ADA) surfaces (Sack *et al.* 2006; Medeiros *et al.* 2019).

The cell dimensions were obtained from four stomatal complexes and three epidermal pavement cells per image. Each image was divided into four quadrants and one stomatal complex per quadrant was measured to reduce selection bias. Due to the large variation in epidermal pavement cell shape and size in Arabidopsis (Pillitteri & Dong 2013), we standardized selection of cells for measurement and averaged measurements of one small subsidiary cell, a typical epidermal pavement cell and a large pavement cell (Boudolf *et al.* 2004; Bergmann & Sack 2007; Pillitteri & Dong 2013). All images were analyzed and traits were measured using the software ImageJ (http://imagej.nih.gov/ij/).

From the anatomical measurements we calculated the maximum theoretical stomatal conductance (g_{max}):

$$g_{\max} = \frac{bmds}{s^{0.5}}, \qquad \text{(Eqn 1)}$$

where b is a biophysical constant given as $b = \frac{D}{v}$, D represents the diffusivity of CO_2 and water in air $m^2\ s^{-1}$ and v is the molar volume of air $m^3\ mol^{-1}$, so $b = 0.00126$; m is a morphological constant based on scaling factors representing the proportionality of stomatal dimensions $m = \frac{\pi c^2}{j^{0.5} 4hj + \pi}$, with c, h, and j treated as constants for the estimation of g_{max} c, h and $j = 0.5$; d is stomatal density, and s is stomatal area (Franks & Farquhar 2007; Franks *et al.* 2009; McElwain *et al.* 2016; Sack & Buckley 2016).

Climate of ecotypes' geographic origins and flowering time

We obtained ecotype coordinates from the 1,001 Genomes Consortium (Alonso-Blanco *et al.* 2016) and RegMap panel (Horton *et al.* 2012) and used R software [version 3.4.4 (R Core Team 2020)] to extract climate variables of the geographic origin of the ecotypes with known coordinates (149 of the 152 ecotypes). From open-access raster layers, we extracted a total of 51 environmental parameters, 34 relating to air temperature and precipitation [WorldClim; (Hijmans *et al.* 2005)], aridity [CGIAR-CSI, NCAR-UCAR; (Zomer *et al.* 2008)] and soil characteristics [ISRIC Soilgrids; (Hengl *et al.* 2017)]. The raster layers with the same resolution were stacked using the *stack* function from the '*raster'* package (Hijmans & van Etten 2012) and the environmental parameters for each geographic coordinate were extracted using the *extract* function from the '*dismo'* package (Hijmans *et al.* 2011). From those variables, we also calculated 17 environmental parameters that describe the length of and climate during the growing season (see Chapter 2 legend in the Data Supplement for complete list of variables). The growing season was determined as the months that have abundant soil moisture (mean precipitation in mm $\geq$ 2 * mean temperature in degrees Celsius) and minimum temperature above 4ºC, since below this temperature water becomes too viscous to pass through membrane (Lasky *et al.* 2012).

We also obtained the flowering time at 10ºC and 16ºC (F_{10} and F_{16}, respectively) for each of the 137 ecotypes included in the 1,001 Genomes Consortium and the present study (Alonso-Blanco *et al.* 2016).

Statistical and comparative analyses

All statistical analyses were performed and plots created using R software [version 4.0.2 (R Core Team 2020)] and packages available from the CRAN platform.

To quantify the trait variation across ecotypes we performed ANOVAs using the *aov* function, with functional traits coded as the dependent variable and ecotype as the independent variable (Sokal & Rohlf 2012; R Core Team 2020). Anatomical traits were log-normally distributed and thus $\log_{10}$-transformed prior to analyses.

To test the relationships among anatomical traits and between traits and the climate of the origin of each ecotype, we used two approaches: one ahistorical and one evolutionary. In the ahistorical approach we used ordinary least squares regression analyses and in the evolutionary approach we performed generalized mixed-effects regression analyses with a Kinship matrix as random effect (Yu *et al.* 2006). We chose this framework because it is more powerful in reducing types I and II errors in datasets with complex familial relationships and population structure of relatedness than other frameworks, such as phylogenetic generalized least-squares analyses (Yu *et al.* 2006). Analyses were performed for untransformed and $\log_{10}$-transformed data, to test for either approximately linear or non-linear (i.e., approximate power-law) relationships respectively. Variables that included both negative and positive numbers were incremented by a constant equal to the lowest ecotype mean +1 before log-transformation, such that 1 was the lowest value for that variable.

To determine the contribution of leaf anatomical parameters e, i and s to g_{max} we conducted a causal partitioning analysis, in which we partitioned differences in g_{max} among ecotypes into contributions from the underlying variables using the partitioning approach of (Buckley & Diaz-Espejo 2015). In this approach, a finite difference δy in some function f of N underlying variables x_j (j=1 to N) between two states, an initial or "reference state" ($y_r = f(x_{1r}, x_{2r}, ...)$) and a final or "comparison" state ($y_c = f(x_{1c}, x_{2c}, ...)$), is partitioned into contributions from changes in each variable, by numerically integrating the partial derivative of f with respect to the variable in

question ($\partial f/\partial x_j$) over an imaginary path between the two states, with each variable assumed to change linearly between its values in each state. Thus, the % contribution of variable x_k ($C[x_k]$) to the difference in y ($\delta y = y_c - y_r$) between the two states is given by

$$C(x_k) = 100 \cdot \frac{\int_r^c \frac{\partial f}{\partial x_k} dx_k}{\sum_{j=1}^{N} \int_r^c \frac{\partial f}{\partial x_j} dx_j} = 100 \cdot \frac{\int_r^c \frac{\partial f}{\partial x_k} dx_k}{y_c - y_r}. \qquad \text{(Eqn 2)}$$

Each contribution is expressed relative to the sum of all contributions, so the contributions add up to 100%. We used this method to partition: (i) abaxial g_{max} into contributions from abaxial values of *e*, *i*, and *s*, (ii) adaxial g_{max} into contributions from adaxial values of *e*, *i* and *s*, (iii) total g_{max} into contributions from abaxial and adaxial g_{max}, and (iv) total g_{max} into contributions from both abaxial and adaxial values of *e*, *i* and *s*. In each case, we repeated these calculations for every possible pairwise comparison between ecotypes (for 152 ecotypes, this gives 152!/[150!×2!] = 152×151/2 = 11,476 pairwise comparisons), with values for the two ecotypes in each pair representing the reference and comparison states respectively, and each numerical integration using 1,000 steps. We then calculated the median contributions (values of *C*) for each variable over the 11,476 comparisons.

RESULTS

Variation in leaf anatomical traits across ecotypes

We found strong variation in all leaf anatomical traits across ecotypes from contrasting native climates, with similar values in the abaxial and adaxial surfaces (ANOVAs; $p<0.001$; Table S2.1 and Fig. 2.2a). The leaf area (*LA*) was the most variable trait with a 10-fold variation across

ecotypes, followed by the maximum anatomical stomatal conductance ($g_{max\ total}$), average epidermal cell area (e_{avg}), stomatal density (d_{total}), stomatal index (i_{avg}) and stomatal area (s_{avg}), which varied two- to four-fold across ecotypes (Fig. 2.2b-g). Guard cell and stomatal pore dimensions, $GC_{l\ avg}$, $GC_{w\ avg}$, $SP_{il\ avg}$ and $SP_{ol\ avg}$ varied from 1.6 to 1.9-fold (Table S2.1).

Coordination of leaf anatomical traits

We found strong coordination among leaf anatomical traits and high similarity between results obtained from ahistorical and evolutionary analyses (Tables S2.2 and S2.3); we present in the text evolutionary analyses based on linear mixed effects regression with a Kinship matrix as a random effect, hereafter, "kin", and ahistorical analyses based on ordinary least squares regression, hereafter, "ols",only when the evolutionary relationships were not significant; both analyses are presented in the figures and supplements (Table S2.2 and Fig. 2.3).

Arabidopsis ecotypes with larger leaves had larger epidermal cells and smaller stomata on both leaf surfaces and, consequently, had lower d and g_{max} in both leaf surfaces ($|r_{kin}|$ ranging from 0.24 to 0.36; $p<0.05$; Table S2.3). Ecotypes with large LA also had a negative relationship with the t_{ADA} (r_{kin} = -0.23; $p<0.05$; Table S2.3).

For the abaxial surface i_{ABA} was the trait most strongly and positively correlated with both d_{ABA} and $g_{max\ ABA}$ (r_{kin} = 0.56 and 0.55, respectively; $p<0.01$; Table S2.3 and Fig. 2.3b, e), followed closely by e_{ABA}, which was negatively correlated with both d_{ABA} and $g_{max\ ABA}$ (r_{kin} = -0.49 and -0.47, respectively; $p<0.001$; Table S2.3 and Fig. 2.3a, d). As hypothesized, e_{ABA} and i_{ABA} were also positively correlated (r_{kin} = 0.40; $p<0.001$; Table S2.3 and Fig. 2.3g). Notably, s_{ABA} was only weakly negatively correlated with d_{ABA} (r_{ols} = -0.23; $p<0.01$; Table S2.2 and Fig. 2.3f) and not correlated with e_{ABA}, i_{ABA} and $g_{max\ ABA}$ (Fig. 2.3c, h-i). For the adaxial surface i_{ADA} was also the

trait most strongly and positively correlated with both d_{ADA} and $g_{max\ ADA}$ (r_{kin} = 0.74 and 0.73, respectively; p<0.01; Table S2.3 and Fig. S2.2), followed by e_{ADA}, which was negatively correlated with both d_{ADA} and $g_{max\ ADA}$ (r_{kin} = -0.43 and -0.42, respectively; p<0.001; Table S2.3 and Fig. S2.2). s_{ADA} was positively correlated with $g_{max\ ADA}$ (r_{kin} = 0.22; p<0.05; Table S2.3 and Fig. S2.2). e_{ADA} and i_{ADA} were positively correlated and both were independent from s (r_{kin} = 0.23; p<0.001; Table S2.3 and Fig. S2.2).

We also tested the relationships between guard cell dimensions and stomatal pore length with g_{max} and its anatomical drivers (Table S2.3). $SP_{il\ ABA}$, $SP_{ol\ ABA}$, $GC_{l\ ABA}$ and $GC_{w\ ABA}$ were positively correlated with s_{ABA} (r_{kin} ranging from 0.30 to 0.80; p<0.05). $SP_{il\ ABA}$ was negatively correlated with d_{ABA} and i_{ABA} (r_{kin} = -0.20 and -0.23, respectively; p<0.05), $SP_{ol\ ABA}$ was negatively correlated with d_{ABA} (r_{kin} = -0.24; p<0.05), $GC_{l\ ABA}$ was negatively correlated with d_{ABA} (r_{kin} = -0.28; p<0.001) and positively correlated with e_{ABA} (r_{kin} = 0.19; p<0.05) and $GC_{w\ ABA}$ was positively correlated with $g_{max\ ABA}$ (r_{kin} = 0.21; p<0.05) (Table S2.3). For the adaxial surface, $SP_{il\ ADA}$, $SP_{ol\ ADA}$, $GC_{l\ ADA}$ and $GC_{w\ ADA}$ were positively correlated with s_{ADA} (r_{kin} ranging from 0.32 to 0.76; p<0.05). $SP_{il\ ADA}$ was negatively correlated with d_{ADA}, i_{ADA} and $g_{max\ ADA}$ (r_{kin} ranging from -0.20 and -0.23; p<0.05), $SP_{ol\ ADA}$ was negatively correlated with d_{ADA} (r_{kin} = -0.22; p<0.05), $GC_{l\ ABA}$ was negatively correlated with d_{ADA} (r_{kin} = -0.26; p<0.01) and positively correlated with e_{ADA} (r_{kin} = 0.18; p<0.05) and $GC_{w\ ADA}$ was positively correlated with $g_{max\ ADA}$ (r_{kin} = 0.26; p<0.05) (Table S2.3).

Relationship of epidermal traits and climate

We found strong coordination of leaf anatomical traits with the native climate of ecotype origins. The $g_{max\ total}$ and d_{total} were correlated with 32 and 29 of the 53 climate variables included in our

study, respectively; overall, $g_{max\ total}$ and d_{total} were negatively correlated with mean annual temperature, precipitation of the growing season and soil water variables, and positively correlated with the flowering times and Spring and Winter drought frequencies (Table S2.3). Among the hypothesized anatomical drivers of $g_{max\ total}$, e_{avg} and i_{avg} were correlated with 20 each and s_{avg} with three of the climate variables included in our study (Table S2.3).

In Figure 4 we summarize the overall patterns of trait-climate relationships across Arabidopsis ecotypes. g_{max} and i were negatively correlated with the mean annual temperature (*MAT*) and the precipitation of the growing season (ppt_{GS}) and positively correlated with the flowering time at 16ºC (FT_{16}) ($|r_{kin}|$ ranged from 0.19 to 0.72; $p<0.05$; Table S2.3 and Fig. 2.4a-c, g-i). i was positively correlated with *MAT* and ppt_{GS} and negatively correlated with FT_{16} ($|r_{kin}|$ ranged from 0.22 to 0.3; $p<0.01$; Table S2.3 and Fig. 2.4d-f). s was not correlated with direct temperature or precipitation variables (Table S2.3 and Fig. 2.4j-l). It was, however, weakly negatively correlated with the seasonality and annual range of temperature and positively correlated with the soil water capacity ($|r_{kin}|$ ranged from 0.17 to 0.18; $p<0.05$; Table S2.3).

We also found relationships between *LA* and climate. *LA* was negatively correlated with the *FT*s, soil water content and the Spring drought frequency and positively correlated with temperature variables, elevation and soil's depth and pH ($|r_{kin}|$ ranged from 0.22 to 0.3; $p<0.01$; Table S2.3).

The drivers of maximum stomatal conductance

Causal partitioning analysis found that differences in g_{max} among ecotypes were driven almost entirely by differences in e and i, and minimally by differences in s (Fig. 2.5). For leaf total g_{max}, the strongest contributors were i_{ADA} and i_{ABA} (median contributions of 36.4% and 26.8%,

respectively), followed by e_{ABA} and e_{ADA} (20.4% and 16.2%, respectively). The median contributions of s_{ADA} and s_{ABA} were 1.8% and -0.9%, respectively. (n.b.: [i] a negative contribution indicates that the underlying variable in question [abaxial stomatal size in this case] usually changed in the direction opposite to the dependent variable [g_{max}]; and [ii] although the contributions calculated for a comparison between two given ecotypes always sum to 100%, the median values of those contributions across all such comparisons may not sum exactly to 100%). For $g_{max\ ABA}$ considered in isolation, e_{ABA} and i_{ABA} contributed approximately equally (51.6% and 50.3%, respectively), and s_{ABA} negligibly (0.1%) (Fig. S2.3); $g_{max\ ADA}$ considered in isolation, i_{ADA} was more than twice as important (64.5%) as e_{ADA} (30.7%), and again s_{ADA} contributed little (3.7%). Finally, differences in $g_{max\ total}$ were driven roughly equally by differences in abaxial and adaxial g_{max} (45.1% and 55.2%, respectively) (Fig. S2.3).

DISCUSSION

Across Arabidopsis ecotypes, g_{max} was determined mainly by *e* and *i*, with a much smaller effect of *s* (Fig. 2.5). The anatomical determination of *d* and g_{max} by *e* and *i* suggests that these traits would be loci for selection, and potential targets for improved crops. By contrast, stomatal size was not a key driver of *d* or g_{max}, indicating that theory that g_{max} is strongly influenced by stomatal packing and the *s* vs. *d* trade-off—which was weak in this study—does not apply across Arabidopsis ecotypes.

The coordination between anatomical drivers of g_{max} with climate across Arabidopsis ecotypes would provide adaptation to cold and drought through a drought-avoidance strategy, *e.g.*, the positive relationship between *e* and *i* and negative relationships between g_{max} and the mean annual temperature and the precipitation and length of the growing season (Table S2.3 and Fig.

2.4) (Xu & Zhou 2008; Basu *et al.* 2016). The variation in leaf anatomical traits across ecotypes was consistent with the wide range of climates this species is found in and was larger for traits expected to be under intense selective pressure, such as g_{max} (Table S2.1 and Fig. 2.2b-j) (Hoffmann 2002; Raven 2002). Traits with the lowest variation were also the less adaptive across ecotypes, such as *s* and guard cell dimensions (Figs. 2.2b-j and 2.4j-l). Indeed, *s* was independent from both *e* and *i*, and from the main climatic drivers of g_{max} (Figs. 2.3 and 2.4).

To our knowledge, this is the first study to show quantitatively that the maximum anatomical stomatal conductance and its relationship with climate, is developmentally determined by the area of epidermal pavement cells and the stomatal initiation rate, and not the stomatal size. This finding has important implications for the advancement of plant breeding for more photosynthetically efficient plants, that can now shift their efforts to genes that regulate epidermal pavement cell size and stomatal initiation. These results also have important implications for models of ecosystem fluxes, since many have been scaling up from stomatal size and density to plant and ecosystem growth rates and NPP (Wang *et al.* 2015).

ACKNOWLEDGEMENTS

We thank Jessica Smith, Timothy Chu, Hanna Lee, Jeffrey Lee, Nicole Lum, Jenny Park, Sophie Sha and Savannah Tan for assistance with imaging and measurements. This work was funded by National Science Foundation Grants 1457279, 1951244, 1557906 and 2017949, and by the USDA National Institute of Food and Agriculture (Award #2020-67013-30913 and Hatch Project 1016439). CM was supported by the Brazilian National Research Council (CNPq) through the Brazilian Science Without Borders Program (grant number: 202813/2014-2).

FIGURE CAPTIONS

Figure 2.1. Anatomical variables contributing to the maximum theoretical anatomical stomatal conductance, $g_{max,}$ and the stomatal density, *d*. (a) Summarizes the classic understanding that g_{max} is determined by *d* and *s* (Franks *et al.* 2009). In (b) we updated the causal model of anatomical determinants of g_{max} (Sack & Buckley 2016). Increasing *e* leads to more spaced out stomata, and thus lower g_{max} and *d*. Higher *i* values translate into higher proportion of stomata, which leads to higher g_{max} and *d*. Increasing *s* is typically associated with low *d*, since all else being equal, larger cells would result in lower density. Consequently, larger *s* is also associated with lower g_{max} (more detailed rationale available in Appendix Table 2.1). (c-k) Panels showing the variation in epidermal morphology of ecotypes with increasing values of (c-e) epidermal pavement cell area, *e*, (f-h) stomatal differentiation rate, *i*, and (i-k) stomatal area, *s*.

Figure 2.2. (a) Map showing the geographic origin of the 149 ecotypes of *Arabidopsis thaliana* included in this study that have geolocated origins. Symbol colors represent a gradient from low (light gray) to high (dark red) mean annual temperature, *MAT*. (b-g) Plots showing the variation in cell morphology of leaves of 152 ecotypes. (b) Epidermal pavement cell area, e_{avg}; (c) stomatal differentiation rate, i_{avg}; (d) stomatal area, s_{avg}; (e) maximum theoretical anatomical stomatal conductance, $g_{max\ total}$, (f) stomatal density, d_{total}, and (g) leaf area, *LA* (Table S2.1). (b-d) show the average of adaxial and abaxial values for cell dimensions and (e-f) show the total values, calculated as the sum of adaxial and abaxial values.

Figure 2.3. Relationships between easy-to-measure anatomical traits (epidermal pavement cell area, e_{ABA}; stomatal differentiation rate, i_{ABA}, and stomatal area, s_{ABA}) measured on the abaxial

surface of 152 ecotypes of *Arabidopsis thaliana* grown under greenhouse conditions with the maximum theoretical anatomical stomatal conductance, $g_{max\ ABA}$ (a-c), and with stomatal density, d_{ABA} (d-f). Panels (g-i) show the relationships among anatomical traits. Symbol colors represent a gradient from low (light gray) to high (dark red) mean annual temperature, *MAT*, of ecotype origins. *$p < 0.05$; **$p < 0.01$; ***$p < 0.01$. Solid and dashed lines represent the ahistorical and historical correlations (ordinary least squares and linear mixed-effects models using a kinship matrix as random effect, respectively; Tables S2.2 and S2.3).

Figure 2.4. Relationships between anatomical traits measured from leaves of 152 ecotypes of *Arabidopsis thaliana* grown under greenhouse conditions with the climate of their origin. Symbol colors represent a gradient from low (light gray) to high (dark red) mean annual temperature, *MAT*, of ecotype origins. The first column shows the relationships with the mean annual temperature, *MAT*; the second with the precipitation of the growing season, ppt_{GS}, and the third with an important life-history trait, the flowering time at 16ºC, FT_{16}. Relationships with (a-c) the maximum theoretical anatomical stomatal conductance, $g_{max\ total}$, (d-f) epidermal pavement cell area, e_{avg}, (g-i) stomatal index, i_{avg}, and (j-l) stomatal area, s_{avg}. *$p < 0.05$; **$p < 0.01$; ***$p < 0.01$. Solid and dashed lines represent the ahistorical and historical correlations (ordinary least squares and linear mixed effects models using a kinship matrix as random effect, respectively; Tables S2.2 and S2.3).

Figure 2.5. Median contributions (%) of differences in anatomical variables (*e*: epidermal cell size; *s*: stomatal size; *i*: stomatal index) to differences in anatomical leaf g_{max} between ecotypes of *Arabidopsis thaliana* grown under greenhouse conditions with the climate of their origin. Medians were calculated over all possible pairwise comparisons between ecotypes (n = 11,476

comparisons). The small negative contribution of abaxial stomatal size indicates that, when two ecotypes were compared, the ecotype with larger g_{max} tended to have smaller stomata (albeit only very slightly so); thus, although smaller stomata should decrease g_{max} for a given value of stomatal index, in practice that effect tended to be greatly outweighed by differences in stomatal index.

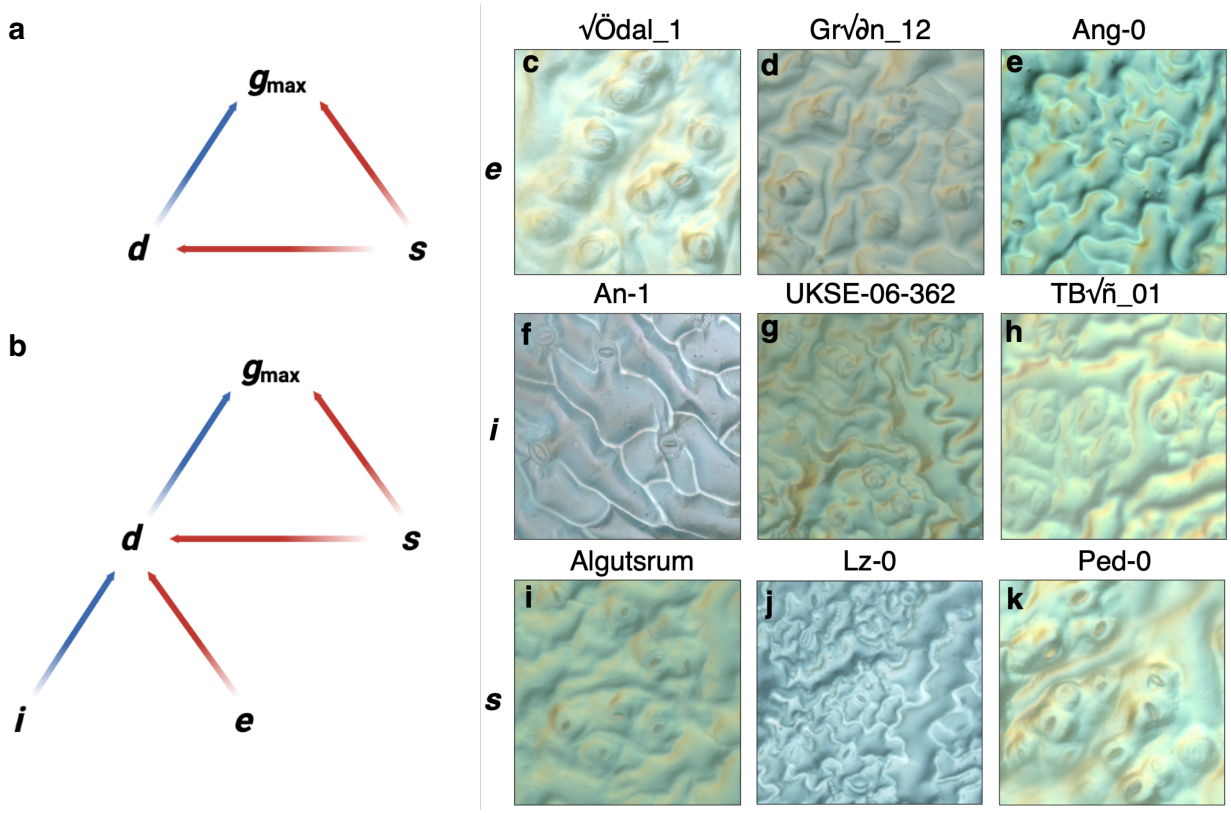
a
gmax
d
s
b
gmax
d
s
i
e
√Ödal_1
Gr√∂n_12
Ang-0
e
c
d
e
An-1
UKSE-06-362
TB√ñ_01
i
f
g
h
Algutsrum
Lz-0
Ped-0
s
i
j
k

Figure 2.1

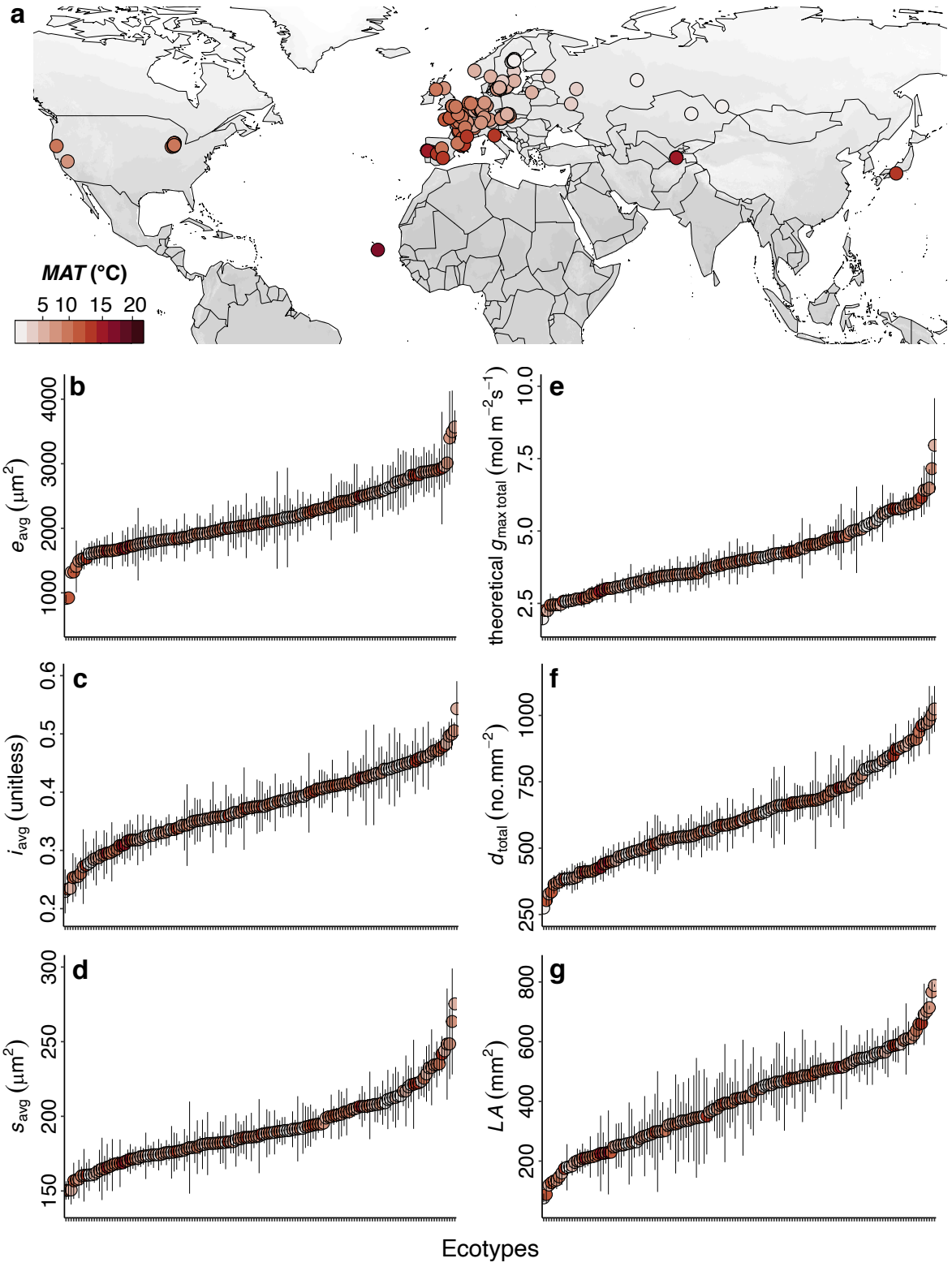
a
MAT (°C)
5 10 15 20
b
e_{avg} (μm^2)
1000 2000 3000 4000
c
i_{avg} (unitless)
0.2 0.3 0.4 0.5 0.6
d
s_{avg} (μm^2)
150 200 250 300
e
theoretical $g_{max\ total}$ (mol $m^{-2}s^{-1}$)
2.5 5.0 7.5 10.0
f
d_{total} (no.mm^{-2})
250 500 750 1000
g
LA (mm^2)
200 400 600 800
Ecotypes

Figure 2.2

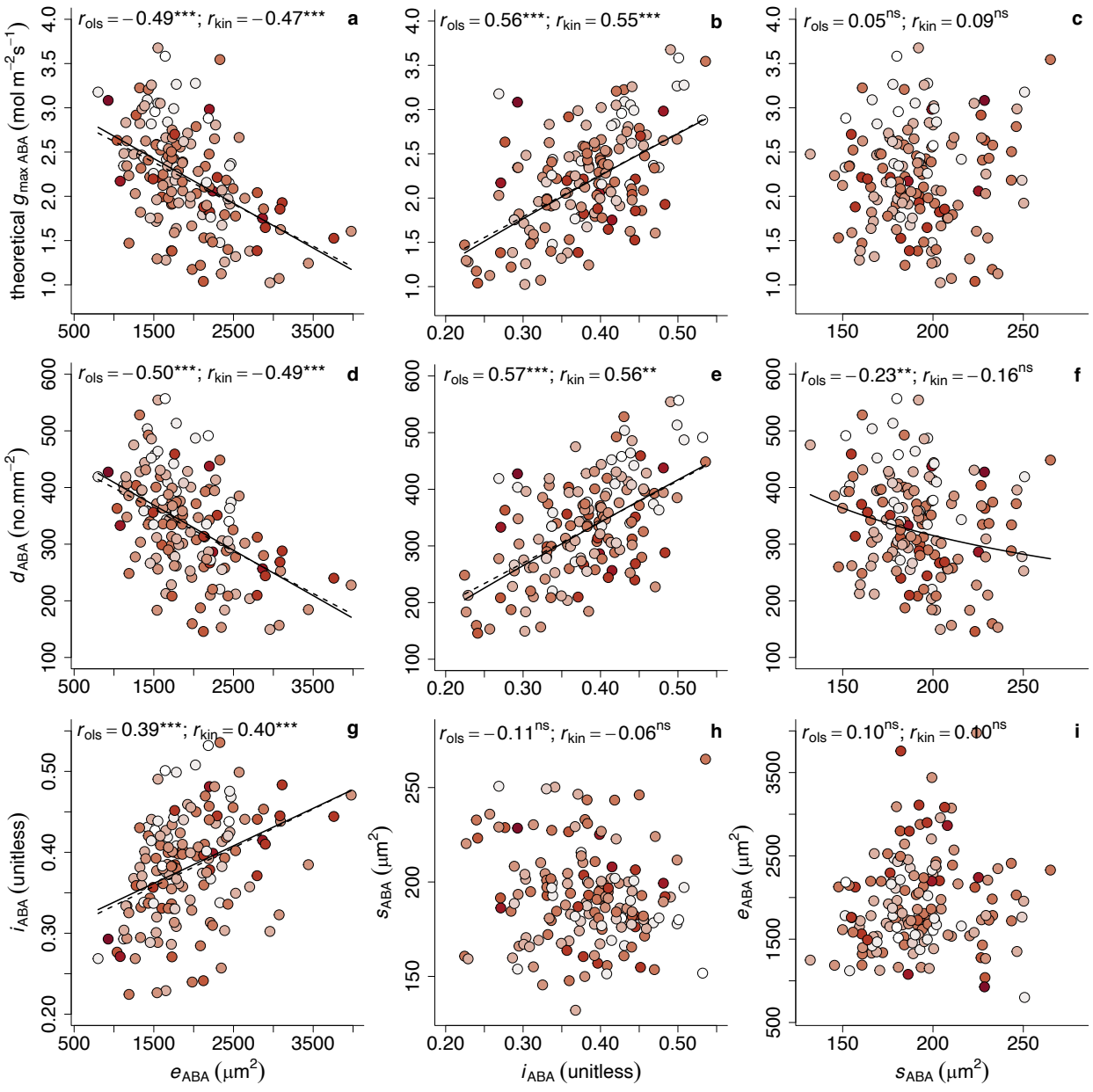
a
$r_{ols} = -0.49^{***}$; $r_{kin} = -0.47^{***}$
theoretical $g_{max\ ABA}$ (mol m^{-2}s^{-1})
b
$r_{ols} = 0.56^{***}$; $r_{kin} = 0.55^{***}$
c
$r_{ols} = 0.05^{ns}$; $r_{kin} = 0.09^{ns}$
d
$r_{ols} = -0.50^{***}$; $r_{kin} = -0.49^{***}$
d_{ABA} (no.mm^{-2})
e
$r_{ols} = 0.57^{***}$; $r_{kin} = 0.56^{**}$
f
$r_{ols} = -0.23^{**}$; $r_{kin} = -0.16^{ns}$
g
$r_{ols} = 0.39^{***}$; $r_{kin} = 0.40^{***}$
i_{ABA} (unitless)
e_{ABA} (μm^2)
h
$r_{ols} = -0.11^{ns}$; $r_{kin} = -0.06^{ns}$
s_{ABA} (μm^2)
i_{ABA} (unitless)
i
$r_{ols} = 0.10^{ns}$; $r_{kin} = 0.10^{ns}$
e_{ABA} (μm^2)
s_{ABA} (μm^2)

Figure 2.3

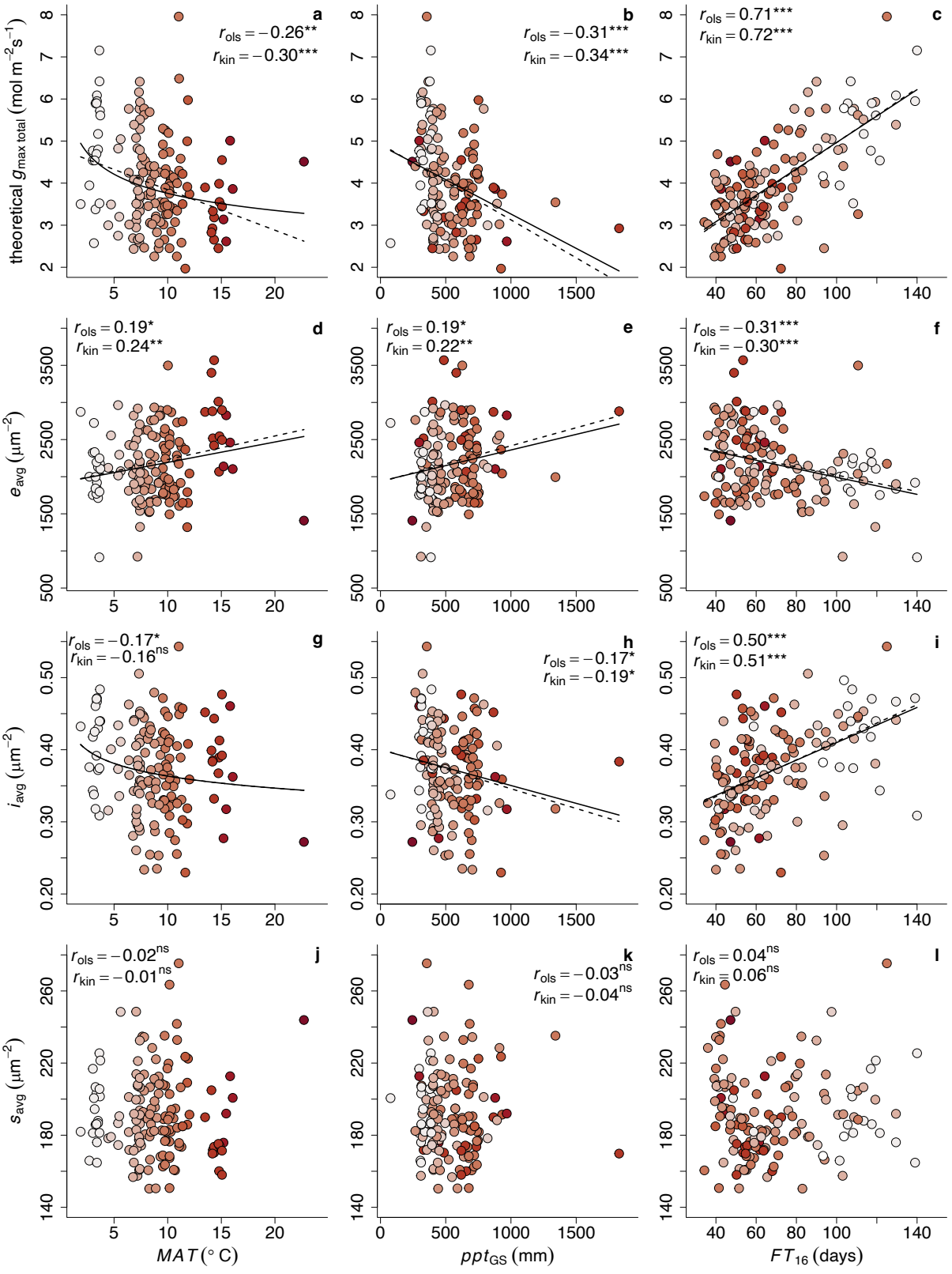
a
b
c
d
e
f
g
h
i
j
k
l
$r_{ols} = -0.26^{**}$
$r_{kin} = -0.30^{***}$
$r_{ols} = -0.31^{***}$
$r_{kin} = -0.34^{***}$
$r_{ols} = 0.71^{***}$
$r_{kin} = 0.72^{***}$
$r_{ols} = 0.19^{*}$
$r_{kin} = 0.24^{**}$
$r_{ols} = 0.19^{*}$
$r_{kin} = 0.22^{**}$
$r_{ols} = -0.31^{***}$
$r_{kin} = -0.30^{***}$
$r_{ols} = -0.17^{*}$
$r_{kin} = -0.16^{ns}$
$r_{ols} = -0.17^{*}$
$r_{kin} = -0.19^{*}$
$r_{ols} = 0.50^{***}$
$r_{kin} = 0.51^{***}$
$r_{ols} = -0.02^{ns}$
$r_{kin} = -0.01^{ns}$
$r_{ols} = -0.03^{ns}$
$r_{kin} = -0.04^{ns}$
$r_{ols} = 0.04^{ns}$
$r_{kin} = 0.06^{ns}$
theoretical $g_{max\ total}$ (mol m^{-2}s^{-1})
e_{avg} (µm^{-2})
i_{avg} (µm^{-2})
s_{avg} (µm^{-2})
MAT (° C)
ppt_{GS} (mm)
FT_{16} (days)

Figure 2.4

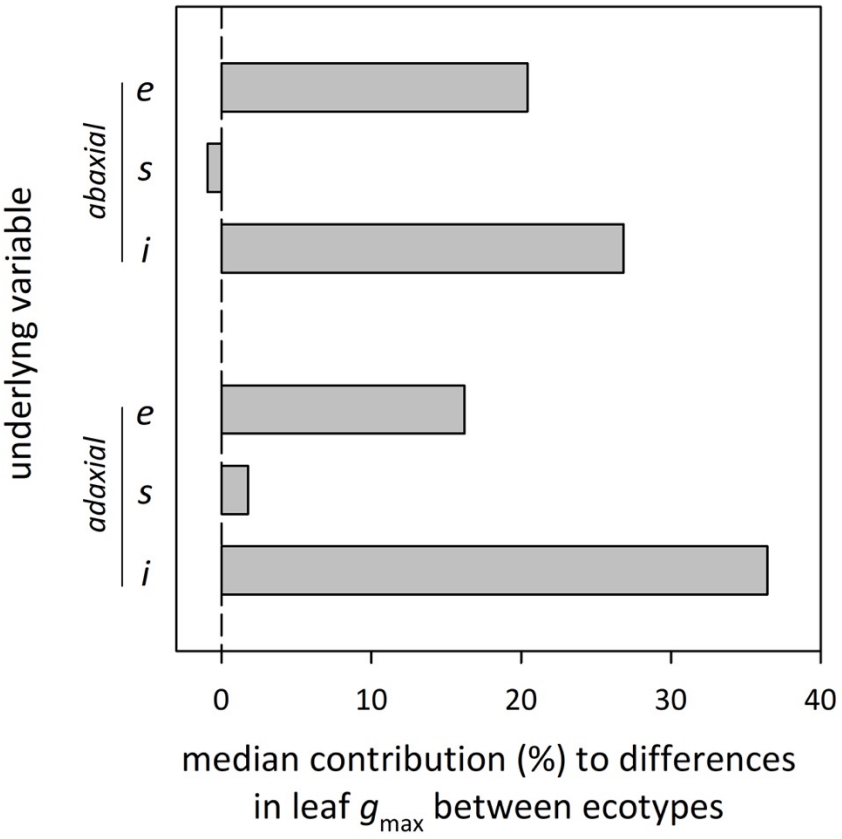
underlyng variable
abaxial
e
s
i
adaxial
e
s
i
0
10
20
30
40
median contribution (%) to differences
in leaf g_{max} between ecotypes

Figure 2.5

Appendix Table 2.1. Expectation and rationale for each trait-trait or trait-climate relationship and whether the expectation was supported by our data. We report the range of correlation coefficients of relationships between traits measured on the abaxial and the adaxial surfaces and their average. The *p*-values shown below were estimated using linear mixed-effects models with a kinship matrix as random effect.

Trait-trait or trait-climate pair	**Expectation and rationale**	**Supported?**
***d* vs. g_{max}**	+. More stomata per area would lead to larger pore area which can reduce the resistance to CO_2 flux and enable greater CO_2 assimilation.	Yes. *r* ranged from 0.96 to 0.98; $p<0.001$.
d* vs. *e	-. Large epidermal pavement cells would cause the stomata to become more spaced apart, thus reducing the stomatal density.	Yes. *r* ranged from -0.43 to -0.49; $p<0.001$.
d* vs. *i	+. High *i* reflects a large frequency of stomata per total epidermal cell number, so stomatal density should be positively correlated with stomatal initiation rate.	Yes. *r* ranged from 0.56 to 0.74; $p<0.001$.
d* vs. *s	-. For a given leaf size, we expect to find a trade-off between stomatal density and size due to a spatial constraint; however, due to the small area occupied by stomata on a typical leaf, we expect this relationship to be weak.	No.
g_{max} vs. *e*	-. For a given leaf size, you would expect a trade-off between the maximum theoretical anatomical stomatal conductance and the epidermal pavement cell size. Due to a spatial constraint, when *e* is large there will be less space available to be occupied by stomata, so the pore area would be smaller, increasing the resistance to CO_2 and lowering the overall g_{max}.	Yes. *r* ranged from = -0.42 to -0.47; $p<0.001$.
g_{max} vs. *i*	+. High *i* reflects a large frequency of stomata per total epidermal cell number, which leads to a larger pore area, reduced resistance to CO_2 flux and greater CO_2 assimilation.	Yes. *r* ranged from 0.55 to 0.73; $p<0.001$
g_{max} vs. *s*	-. Smaller stomata free up more epidermal space for other cell types and functions	No. We found a positive relationship between g_{max} and *s* in the abaxial surface. $r = 0.22$; $p<0.05$.
e* vs. *i	-. For a given number of epidermal cells, we expect large epidermal pavement cells to result in more spaced apart stomata, so *i* would be inversely correlated with *e*. +. Given the independence of *e* and *i*, plants can achieve high *i* despite of having large *e* if the number of epidermal cells is lower.	We found a positive relationship with *r* ranging from 0.22 to 0.40; $p<0.05$.
i* vs. *s	-. When stomatal size is larger there will be less space to be occupied by more stomata, so the stomatal differentiation rate should be inversely correlated with *s*.	No.
s* vs. *e	+. Stomatal size typically scales with epidermal pavement cell size.	Yes. *r* ranged from 0.19 to 0.43; $p<0.05$.

$g_{max\ total}$ vs. *MAT* (mean annual temperature)	+. High g_{max} would enable more efficient cooling of the leaves in grown in warm temperatures. -. Ecotypes adapted to grow fast during a short growth season, i.e., adapted to cold and/or dry climates, would maintain higher g_{max} during the growth period.	We found support for a negative relationship between g_{max} and the *MAT*. r = -0.32; p<0.01.
$g_{max\ total}$ vs. ppt_{GS} (precipitation of the growing season)	+. High water availability would allow plants to maintain their stomata open for longer periods. -. Ecotypes adapted to grow fast during a short growth season, i.e., adapted to cold and/or dry climates, would maintain higher g_{max} during the growth period.	We found support for a negative relationship between g_{max} and the ppt_{GS}. r = -0.34; p<0.001.
$g_{max\ total}$ vs. L_{GS} (length of growing season)	+. Longer potential growing seasons reflect environments with high water availability, which would allow plants to maintain their stomata open for longer periods. -. Ecotypes adapted to grow fast during a short growth season, i.e., adapted to cold and/or dry climates, would maintain higher g_{max} during the growth period (drought-avoiding).	We found support for a negative relationship between g_{max} and L_{GS}. r = -0.34; p<0.001.

SUPPLEMENTARY MATERIALS

Supplementary data captions (see attached Excel Workbook)

Table S2.1. Differences in traits among 152 ecotypes of *Arabidopsis thaliana* as indicated in one-way analyses of variance. Eight of the 11 groups were created based on geographic origin, one group gathers relict ecotypes, one group with the admixed ecotypes and one with ecotypes not included in the 1,001 Genomes Project dataset. Red highlighted cells indicate variables differing significantly across ecotypes ($p \leq 0.05$).

Table S2.2. Associations of traits and environmental variables representing the climate of the origin for 131 ecotypes of *Arabidopsis thaliana* using linear mixed models with ecotypes relatedness included as a random effect (through a kinship matrix; Yu *et al*. 2006). Red highlighted cells indicate significant relationships ($p \leq 0.05$).

Table S2.3. Associations of traits and environmental variables representing the climate of the origin for 131 ecotypes of *Arabidopsis thaliana* using linear mixed models with ecotypes relatedness included as a random effect (through a kinship matrix; Yu *et al*. 2006). Red highlighted cells indicate significant relationships ($p \leq 0.05$).

Supplementary figure captions

Figure S2.1. Relationship between the total maximum theoretical anatomical stomatal conductance, $g_{max\ total}$, with stomatal density, d. Symbol colors represent a gradient from low (light gray) to high (dark red) mean annual temperature, *MAT*, of ecotype origins. ***$p < 0.001$. Solid and dashed lines represent the ahistorical and historical correlations (ordinary least squares and linear mixed effects models using a kinship matrix as random effect, respectively).

Figure S2.2. Relationships between easy-to-measure anatomical traits (epidermal pavement cell area, e_{ADA}; stomatal differentiation rate, i_{ADA}, and stomatal area, s_{ADA}) measured on the adaxial surface of 152 ecotypes of *Arabidopsis thaliana* grown under greenhouse conditions with the maximum theoretical anatomical stomatal conductance, $g_{max\ ADA}$ (a-c), and with stomatal density, d_{ADA} (d-f). Panels (g-i) show the relationships among anatomical traits. Symbol colors represent a gradient from low (light gray) to high (dark red) mean annual temperature, *MAT*, of ecotype origins. *$p < 0.05$; **$p < 0.01$; ***$p < 0.01$. Solid and dashed lines represent the ahistorical and historical correlations (ordinary least squares and linear mixed-effects models using a kinship matrix as random effect, respectively).

Figure S2.3. Median contributions (%) of (a) differences in anatomical variables (*e*: epidermal cell size; *s*: stomatal size; *i*: stomatal index) to differences in single-surface anatomical g_{max} for abaxial (red) and adaxial (blue) surfaces; and (b) differences in abaxial and adaxial anatomical g_{max} to differences in whole-leaf anatomical g_{max}, between ecotypes of *Arabidopsis thaliana* grown under greenhouse conditions with the climate of their origin. Medians were calculated over all possible pairwise comparisons between ecotypes (n = 11,476 comparisons).

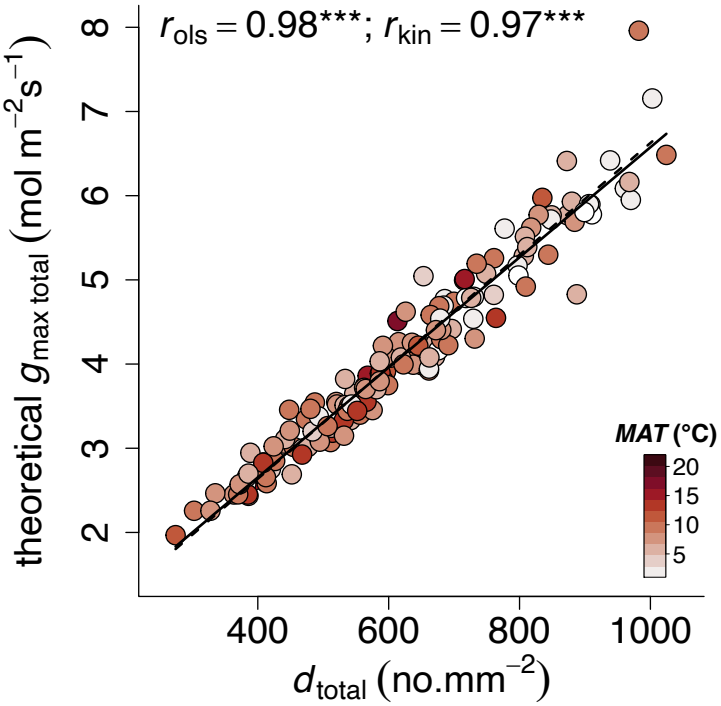
$r_{ols} = 0.98^{***}$; $r_{kin} = 0.97^{***}$
theoretical $g_{max\ total}$ (mol $m^{-2}s^{-1}$)
2
3
4
5
6
7
8
400
600
800
1000
d_{total} (no.mm^{-2})
MAT (°C)
20
15
10
5

Figure S2.1

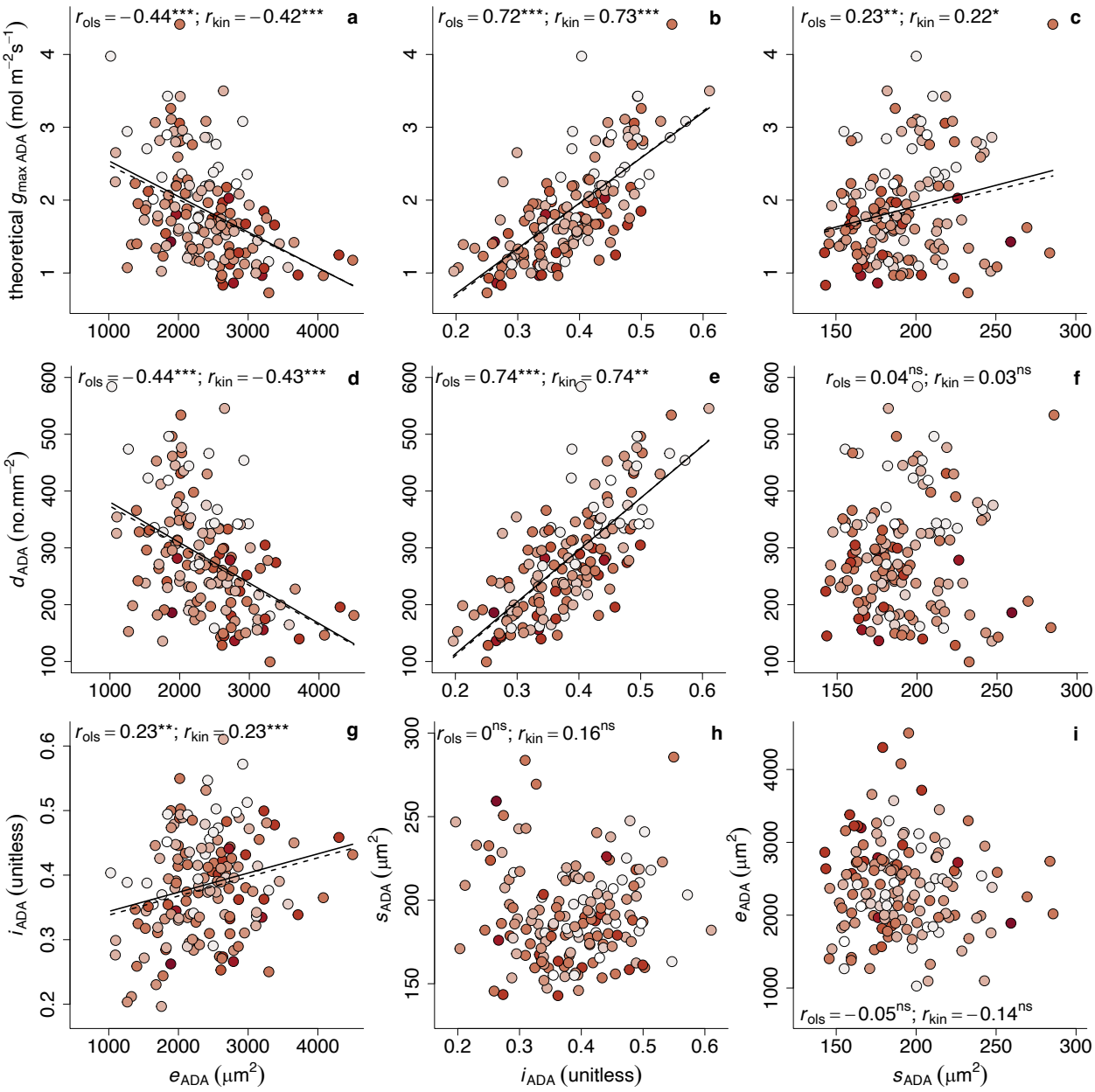
a
b
c
d
e
f
g
h
i
theoretical $g_{max\ ADA}$ (mol m^{-2}s^{-1})
d_{ADA} (no.mm^{-2})
i_{ADA} (unitless)
e_{ADA} (µm^2)
s_{ADA} (µm^2)
$r_{ols} = -0.44^{***}$; $r_{kin} = -0.42^{***}$
$r_{ols} = 0.72^{***}$; $r_{kin} = 0.73^{***}$
$r_{ols} = 0.23^{**}$; $r_{kin} = 0.22^{*}$
$r_{ols} = -0.44^{***}$; $r_{kin} = -0.43^{***}$
$r_{ols} = 0.74^{***}$; $r_{kin} = 0.74^{**}$
$r_{ols} = 0.04^{ns}$; $r_{kin} = 0.03^{ns}$
$r_{ols} = 0.23^{**}$; $r_{kin} = 0.23^{***}$
$r_{ols} = 0^{ns}$; $r_{kin} = 0.16^{ns}$
$r_{ols} = -0.05^{ns}$; $r_{kin} = -0.14^{ns}$

Figure S2.2

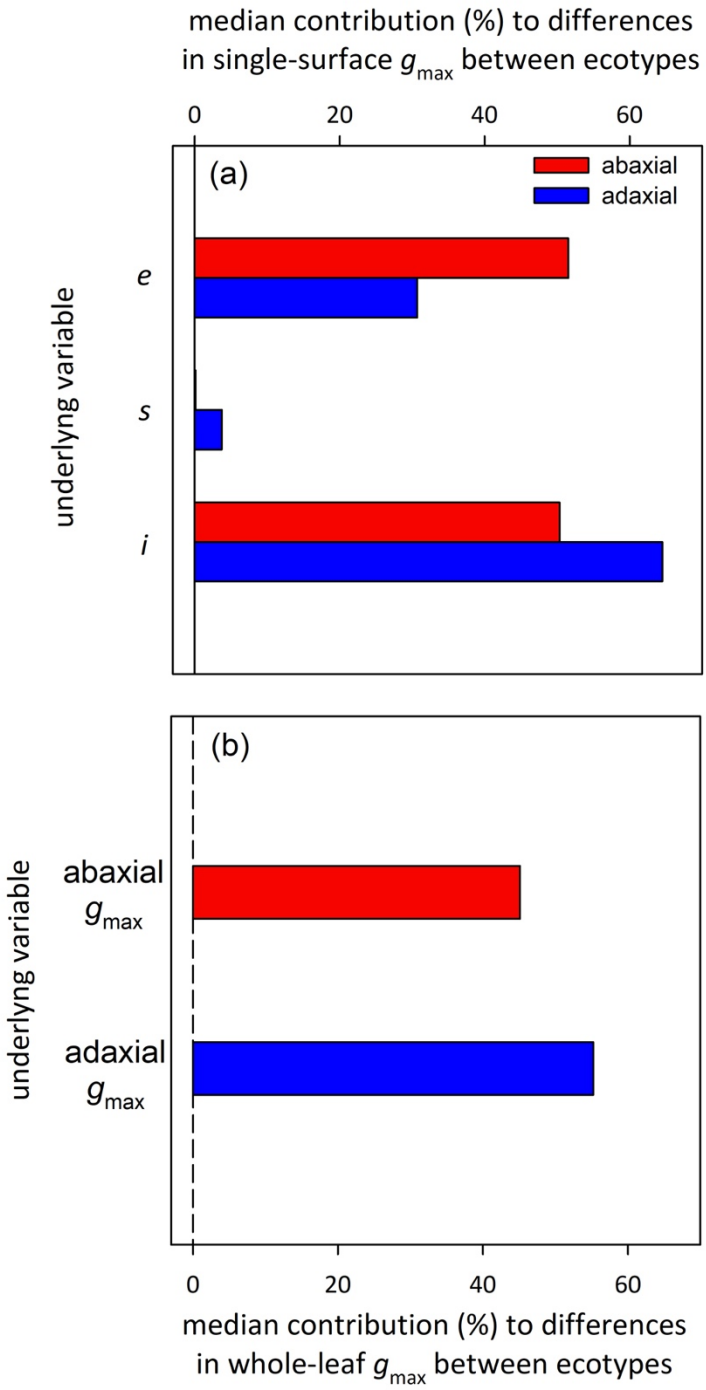
median contribution (%) to differences
in single-surface g_{max} between ecotypes
0
20
40
60
(a)
abaxial
adaxial
underlyng variable
e
s
i
(b)
underlyng variable
abaxial
g_{max}
adaxial
g_{max}
0
20
40
60
median contribution (%) to differences
in whole-leaf g_{max} between ecotypes

Figure S2.3

REFERENCES

Alonso-Blanco, C., Andrade, J., Becker, C., Bemm, F., Bergelson, J., Borgwardt, K.M., *et al.* (2016). 1,135 Genomes reveal the global pattern of polymorphism in *Arabidopsis thaliana*. *Cell*, 166, 481–491.

Basu, S., Ramegowda, V., Kumar, A. & Pereira, A. (2016). Plant adaptation to drought stress. *F1000Res*, 5, 1554.

Beaulieu, J.M., Leitch, I.J., Patel, S., Pendharkar, A. & Knight, C.A. (2008). Genome size is a strong predictor of cell size and stomatal density in angiosperms. *New Phytol*, 179, 975–986.

Bergmann, D.C. & Sack, F.D. (2007). Stomatal development. *Annu Rev Plant Biol*, 58, 163–181.

Boudolf, V., Barrôco, R., Engler, J. de A., Verkest, A., Beeckman, T., Naudts, M., *et al.* (2004). B1-Type Cyclin-Dependent Kinases Are Essential for the Formation of Stomatal Complexes in *Arabidopsis thaliana*. *Plant Cell*, 16, 945–955.

Buckley, T.N. (2005). The control of stomata by water balance. *New Phytol*, 168, 275–292.

Buckley, T.N. & Diaz-Espejo, A. (2015). Partitioning changes in photosynthetic rate into contributions from different variables: Partitioning changes in photosynthesis. *Plant Cell Environ*, 38, 1200–1211.

Camargo, M.A.B. & Marenco, R.A. (2011). Density, size and distribution of stomata in 35 rainforest tree species in Central Amazonia. *Acta Amaz.*, 41, 205–212.

Carlson, J.E., Adams, C.A. & Holsinger, K.E. (2016). Intraspecific variation in stomatal traits, leaf traits and physiology reflects adaptation along aridity gradients in a South African shrub. *Ann Bot*, 117, 195–207.

Dittberner, H., Korte, A., Mettler-Altmann, T., Weber, A.P.M., Monroe, G. & de Meaux, J. (2018). Natural variation in stomata size contributes to the local adaptation of water-use efficiency in *Arabidopsis thaliana*. *Mol Ecol*, 27, 4052–4065.

Doheny-Adams, T., Hunt, L., Franks, P.J., Beerling, D.J. & Gray, J.E. (2012). Genetic manipulation of stomatal density influences stomatal size, plant growth and tolerance to restricted water supply across a growth carbon dioxide gradient. *Phil Trans R Soc B*, 367, 547–555.

Dow, G.J., Bergmann, D.C. & Berry, J.A. (2014). An integrated model of stomatal development and leaf physiology. *New Phytol*, 201, 1218–1226.

Exposito-Alonso, M. (2020). Seasonal timing adaptation across the geographic range of *Arabidopsis thaliana*. *Proc Natl Acad Sci USA*, 117, 9665–9667.

Franks, P.J., Drake, P.L. & Beerling, D.J. (2009). Plasticity in maximum stomatal conductance constrained by negative correlation between stomatal size and density: an analysis using Eucalyptus globulus. *Plant Cell Environ*.

Franks, P.J. & Farquhar, G.D. (2007). The Mechanical Diversity of Stomata and Its Significance in Gas-Exchange Control. *Plant Physiol*, 143, 78–87.

Hengl, T., Mendes de Jesus, J., Heuvelink, G.B.M., Ruiperez Gonzalez, M., Kilibarda, M., Blagotić, A., *et al.* (2017). SoilGrids250m: Global gridded soil information based on machine learning. *PLoS ONE*, 12, e0169748.

Hijmans, R.J., Cameron, S.E., Parra, J.L., Jones, P.G. & Jarvis, A. (2005). Very high resolution interpolated climate surfaces for global land areas. *Int J Climatol*, 25, 1965–1978.

Hijmans, R.J. & van Etten, J. (2012). *raster: Geographic analysis and modeling with raster data*. R.

Hijmans, R.J., Phillips, S., Leathwick, J. & Elith, J. (2011). *Package 'dismo'*. R.

Hoffmann, M.H. (2002). Biogeography of *Arabidopsis thaliana* (L.) Heynh. (Brassicaceae). *J Biogeography*, 29, 125–134.

Horton, M.W., Hancock, A.M., Huang, Y.S., Toomajian, C., Atwell, S., Auton, A., *et al.* (2012). Genome-wide patterns of genetic variation in worldwide Arabidopsis thaliana accessions from the RegMap panel. *Nat Genet*, 44, 212–216.

Hughes, J., Hepworth, C., Dutton, C., Dunn, J.A., Hunt, L., Stephens, J., *et al.* (2017). Reducing stomatal density in barley improves drought tolerance without impacting on yield. *Plant Physiol*, 174, 776–787.

Kardiman, R. & Ræbild, A. (2018). Relationship between stomatal density, size and speed of opening in Sumatran rainforest species. *Tree Physiol*, 38, 696–705.

Kazan, K. & Lyons, R. (2016). The link between flowering time and stress tolerance. *J Exp Bot*, 67, 47–60.

Lasky, J.R., Des Marais, D.L., McKAY, J.K., Richards, J.H., Juenger, T.E. & Keitt, T.H. (2012). Characterizing genomic variation of *Arabidopsis thaliana*: the roles of geography and climate. *Mol Ecol*, 21, 5512–5529.

Lau, O.S. & Bergmann, D.C. (2012). Stomatal development: a plant's perspective on cell polarity, cell fate transitions and intercellular communication. *Development*, 139, 3683–3692.

McElwain, J.C., Yiotis, C. & Lawson, T. (2016). Using modern plant trait relationships between observed and theoretical maximum stomatal conductance and vein density to examine patterns of plant macroevolution. *New Phytol*.

Medeiros, C.D., Scoffoni, C., John, G.P., Bartlett, M.K., Inman-Narahari, F., Ostertag, R., *et al.* (2019). An extensive suite of functional traits distinguishes Hawaiian wet and dry forests and enables prediction of species vital rates. *Funct Ecol*, 33, 712–734.

Nadeau, J.A. (2002). Control of stomatal distribution on the Arabidopsis leaf surface. *Science*, 296, 1697–1700.

Ohsumi, A., Kanemura, T., Homma, K., Horie, T. & Shiraiwa, T. (2007). Genotypic variation of stomatal conductance in relation to stomatal density and length in rice (*Oryza sativa* L.). *Plant Prod Sci*, 10, 322–328.

Pérez-Harguindeguy, N., Díaz, S., Garnier, E., Lavorel, S., Poorter, H., Jaureguiberry, P., *et al.* (2013). New handbook for standardised measurement of plant functional traits worldwide. *Aust J Bot*, 61.

Pillitteri, L.J. & Dong, J. (2013). Stomatal development in Arabidopsis. *The Arabidopsis Book*, 26.

R Core Team. (2020). *R: a language and environment for statistical computing*. R Foundation for Statistical Computing.

Raven, J.A. (2002). Selection pressures on stomatal evolution. *New Phytol*, 153, 371–386.

Sack, L. & Buckley, T.N. (2016). The developmental basis of stomatal density and flux. *Plant Physiol*.

Sack, L., Melcher, P.J., Liu, W.H., Middleton, E. & Pardee, T. (2006). How strong is intracanopy leaf plasticity in temperate deciduous trees? *J Bot*.

Salisbury, E.J. (1927). On the causes and ecological significance of stomatal frequency, with special reference to the woodland flora. *Phil Trans R Soc B*, 216, 1–65.

Sanda, S., John, M. & Amasino, R. (1997). Analysis of flowering time in ecotypes of *Arabidopsis thaliana*. *J Hered*, 88, 69–72.

Sharbel, T., Haubold, B. & Mitchell-Olds, T. (2000). Genetic isolation by distance in *Arabidopsis thaliana*: biogeography and postglacial colonization of Europe. *Mol Ecol*, 9, 2109–2118.

Sokal, R.R. & Rohlf, F.J. (2012). Biometry: the principles and practice of statistics in biological research.

Wang, R., Yu, G., He, N., Wang, Q., Zhao, N., Xu, Z., *et al.* (2015). Latitudinal variation of leaf stomatal traits from species to community level in forests: linkage with ecosystem productivity. *Sci Rep*.

Weigel, D. & Mott, R. (2009). The 1001 genomes project for *Arabidopsis thaliana*. *Genome Biol*, 10, 107.

Willmer, C. & Fricker, M. (1995). *Stomata*. Topics in plant functional biology: 2. 2nd edn. Springer.

Xu, Z. & Zhou, G. (2008). Responses of leaf stomatal density to water status and its relationship with photosynthesis in a grass. *J Exp Bot*, 59, 3317–3325.

Yin, Q., Tian, T., Kou, M., Liu, P., Wang, L., Hao, Z., *et al.* (2020). The relationships between photosynthesis and stomatal traits on the Loess Plateau. *Glob Ecol Conserv*, 23, e01146.

Yu, J., Pressoir, G., Briggs, W.H., Vroh Bi, I., Yamasaki, M., Doebley, J.F., *et al.* (2006). A unified mixed-model method for association mapping that accounts for multiple levels of relatedness. *Nat Genet*, 38, 203–208.

Zomer, R.J., Trabucco, A., Bossio, D.A. & Verchot, L.V. (2008). Climate change mitigation: A spatial analysis of global land suitability for clean development mechanism afforestation and reforestation. *Agric Ecosyst Environ*, 126, 67–80.

CHAPTER 3

EVOLUTION OF TRAIT MODULES ACROSS CALIFORNIA NATIVE OAKS

ABSTRACT

Plants species may adapt to the environment through the optimization of phenotype, which involves multiple functional traits. Previous theory has held that suites of traits often evolve together to enable optimization according to given environments, or along environmental gradients, but contrary views of trait variation have emerged, with some considering that most key plant traits would shift together as a single module (economics spectrum) reflecting fast versus slow growth, and others hypothesizing the evolution of semi-independent structure-function modules. Our main goals were to: (1) test hypotheses for trait co-evolution within and across structure-function modules defined based on ecophysiological theory (plant size, leaf size, flux-related, economics, ecological stoichiometry and drought response modules), (2) identify the contribution of shared evolutionary history on the formation of trait modules within plant trait networks (PTNs), (3) identify the key "hub traits" within the trait networks, that show disproportionate connectivity among the traits, and (4) test the correlated evolution of traits and structure-function modules with species' climatic aridity. Thus, for common garden-grown adult trees of 15 species from three sections of the genus *Quercus* in California (*Lobatae*, *Protobalanus* and *Quercus*), we measured 90 functional traits, including plant and leaf size-related traits, drought tolerance, resource economics, and nutrient stoichiometry and tested their associations and with the climatic aridity of species native ranges of distribution. Traits varied strongly among and within California oak species, and showed significantly more correlations within than among theoretically expected structure-function modules. Indicator traits of several modules (the leaf size, ecological

stoichiometry and drought-tolerance modules) were positively correlated with climatic aridity of species' native distributions, and others were independent (plant size, flux-related and economics modules). Including evolutionary history strongly influenced the analysis of trait network architecture. Network analysis indicated multiple traits showed disproportionate connectivity, including photosynthetic traits and the leaf turgor loss point. The evolution of traits within modules highlights the complexity of the integrated phenotypes, and that several semi-distinct trait suites adapt to climatic aridity, and overall points to the necessity of considering the benefits and costs contributed by multiple traits to overall climate adaptation.

INTRODUCTION

Plant species may adapt to the environment through the optimization of their functional traits (He *et al.* 2020), defined as characteristics of a plant that influence plant growth, reproduction and survival and thereby fitness (Lavorel & Garnier 2002; Violle *et al.* 2007; Medeiros *et al.* 2019). Functional traits are often used in frameworks distinguishing species' ecological strategies and are often inter-related due to co-optimization or trade-offs, which may provide advantages in given environments and result in the emergence of putative structure-function trait clusters or modules (Maire *et al.* 2013; Medeiros *et al.* 2019). Many attempts have been made to summarize the complexity of trait-trait relationships and the resulting functional strategies into a few dimensions (or axes). For example, Grime's Competitive-Stress tolerator-Ruderal Triangle, categorized plants based on the combination of levels of disturbance and stress of the environment they occupy (Grime 1979). Yet, such simple frameworks have since been criticized due to the fact that plants can occupy more diverse environments and can show more diverse trait combinations than such simple schemes describe (Grubb 1985).

More recently, Westoby proposed a model that would be more general than Grime's and would explain species strategies in response to the environment using three dimensions of plant function: specific leaf area, *SLA*, maximum canopy height, H_{max}, and seed mass, *SM* (Leaf-Height-Seed strategy; (Westoby 1998)). Later work on leaf traits found that traits related to rapid growth tended to be positively correlated across species, and negatively with traits related to leaf longevity (Reich 2014). These correlations also hold across globally diverse plant species, and have been described as the worldwide 'Leaf Economics Spectrum', LES (Wright *et al.* 2004), which integrates six key traits related to leaf economics: leaf mass per area (*LMA*), photosynthetic assimilation rates (A_{mass}), leaf nitrogen (*N*), phosphorus (*P*), dark respiration (R_{mass}) and leaf

lifespan (*LL*). The LES, despite being one the most successful and widely discussed frameworks of trait-based ecology, also has been criticized for its attempt to summarize plant ecophysiological "strategies" without accounting for water-related traits or plant organs other than the leaves (Reich 2014). Other models have been proposed since, as complementary, such as the wood and root economics spectra (WES and RES, respectively; (Chave *et al.* 2009; Roumet *et al.* 2016)) and the designation of independent trait spectra related to carbon and water fluxes versus drought tolerance (Sack *et al.* 2003; Hao *et al.* 2010; Li *et al.* 2017). Further, the LES has been expanded in a proposed "global spectrum of form and function" (Díaz *et al.* 2016), which included stem density with the LES traits. Some have also proposed links between functional dimensions, such plant size and flux (Olson *et al.* 2018) and drought tolerance and economics (Oliveira *et al.* 2021), while others argue that all traits are part of a single fast *vs*. slow dimension (Grime 2006). All such proposals for generalized schemes based on correlated traits are challenged by the multifunctionality of traits (i.e., traits that may be optimized to multiple environmental factors) and their contributions to multiple functions (i.e., different combinations of traits may result in the same overall functional strategy) (Marks & Lechowicz 2006; Sack & Buckley 2020).

Recent work has shown that plant trait networks (PTNs) offer a higher resolution of the patterns of traits correlations (Messier *et al.* 2017; Flores-Moreno *et al.* 2019; Kleyer *et al.* 2019; He *et al.* 2020). PTNs enable a comprehensive visualization of the associations among traits and the architecture of PTNs can indicate the overall ecophysiological strategies of different individual plants, species or communities. Notably, while species trait-trait relationships are moderated by species-relatedness or associated with convergent adaptation across a phylogeny (Edwards 2006; Schmerler *et al.* 2012; Fletcher *et al.* 2018; Ramírez-Valiente *et al.* 2020), previous PTN analyses have heretofore not included phylogenetic information that would enable evolutionary insight.

To identify the architecture of trait correlations and the emergence of modules we focus on the genus *Quercus*, which is highly diverse and widespread worldwide, and has very well studied phylogenies for a non-model organism (Cavender-Bares *et al.* 2015; Sork *et al.* 2016; Hipp *et al.* 2018, 2020). Studies within plant genera growing under controlled conditions would make the ideal system to test hypotheses about the evolution of plant traits in clusters (Cavender-Bares *et al.* 2020; Ramírez-Valiente *et al.* 2020). Oak species can be found across the entire CAFP, but some species have more restricted ranges of occupation than others, which allowed us to investigate how trait-trait coordination and trait-climate relationships shaped their current distribution (Ortego *et al.* 2015; Sork *et al.* 2016; Hipp *et al.* 2018) (Fig. S3.1).

Our overarching hypothesis is that trait evolution driven by adaptation to spatial heterogeneity in climate has resulted in the emergence of semi-independent trait modules relating to structure and function, such that traits will be coordinated disproportionately within relative to among modules. Based on the literature describing trait coordination, we assessed evidence in support of six proposed trait modules. Specifically, we explored traits related to plant size, leaf size, water and carbon fluxes, resource economics, nutrient stoichiometry and drought tolerance (Table S1). We measured 90 structural, hydraulic, compositional traits and compiled another 8 traits from the literature for 15 species of California native oaks grown in a common garden (Fig. 1) to test the existence of the aforementioned structure-function modules, their interrelationships and evolution. We also performed an independent analysis of plant trait networks (PTNs), which creates clusters based on statistical relationships, to identify the contribution of shared evolutionary history to the formation of trait modules.

METHODS

Study species and sampling

For this study we sampled 15 of the 21 species of California native oaks, including three representatives from each of the three *Quercus* sections found in North America, *Quercus*, *Lobatae* and *Protobalanus* (Hipp *et al.* 2018) (Fig. 3.1a). All sampled individuals were grown in a common garden at the California Botanic Garden in Claremont, California (34.110738, −117.713913; 507 mm precipitation per year; WorldClim (Hijmans *et al.* 2005); Fig. 3.1a). The common garden approach is ideal to test questions related to trait evolution across species, as it ensures that the observed differences are due to heritable interspecies variation and minimizes confounding environmental variables that may have elicited phenotypically plastic trait variation if plants were sampled in the field (Cordell *et al.* 1998; Dunbar-Co *et al.* 2009; Givnish & Montgomery 2014; Mason & Donovan 2015; Fletcher *et al.* 2018; Cavender-Bares *et al.* 2020). The species varied in growth form (shrubs and trees), leaf habit (evergreen and deciduous), and climate of their native ranges of distribution (Appendix Table 3.1 and Fig. S3.1).

We sampled three to six individuals per species, given availability in the common garden. For each individual, we recorded approximate plant height and used pole pruners to collect the most exposed mature branch grown in the current year, with no signs of damage and herbivory. Branches were carried to the lab in dark plastic bags with moist paper and rehydrated overnight under plastic before harvesting stem sections and fully expanded leaves and stems for all subsequent analyses. We measured traits from three leaves from each of three to six individuals per species, unless noted otherwise in the sections below.

Epidermal morphology and leaf venation traits

We measured epidermal and venation traits on one leaf from each of three to six individuals per species. Epidermal measurements were obtained from microscopy images taken from nail varnish impressions of both leaf surfaces. From microscope images of the nail varnish peels we measured stomatal density (*SD*), stomatal differentiation rate (or index; the number of stomata per numbers of stomata plus epidermal pavement cells, *SI*), stomatal area (*S*), guard cell length and width (GC_l, GC_w), inner and outer stomatal pore length (SP_{il}, SP_{ol}), epidermal pavement cell area (*E*) and trichome density (*TD*). The total number of cells per leaf (N_{cells}) was calculated as the sum of stomata and epidermal pavement cells per leaf. From cell measurements we calculated the maximum theoretical stomatal conductance (G_{max}) (Franks & Farquhar 2007; Sack & Buckley 2016).

For the venation traits, fixed leaves were cleared, stained and scanned for major vein lengths per area (VLA_{major}) and diameter (VD_{major}) and the top, middle and bottom of each leaf were imaged under light microscope for measurements of minor and free ending vein lengths per area (VLA_{minor} and *FEV*s) and diameter (VD_{minor}) (Scoffoni *et al.* 2011). From those measurements, we calculated the major, minor and total leaf vein volume (VV_{major}, VV_{minor} and VV_{total}) as: $\pi \times \left({}^{VD}/_{2}\right)^2 \times VLA$ (Sack *et al.* 2012). All images were analyzed and anatomical traits were measured using the software ImageJ (http://imagej.nih.gov/ij/).

Leaf economics and structure

Leaf saturated mass was measured using an analytical balance (0.01 mg; XS205; Mettler-Toledo, OH, USA) and leaf thickness (*LT*) using digital calipers (0.01 mm; Fowler, Chicago, IL, USA). The leaf area (*LA*) and perimeter (*LP*) were measured using a flatbed scanner and analyzed using

the software ImageJ (http://imagej.nih.gov/ij/). From these measurements we calculated descriptors of leaf shape, including the ratio between *LP* and *LA* (*LP*:*LA*), which quantifies the relative amount of leaf edge, and LP^2 and *LA* (LP^2:*LA*), which removes the geometric dependence on leaf size. After scanning, leaves were oven-dried at 70º for 72 h and their dry mass and area were measured again. Leaf mass per area (*LMA*) was calculated as lamina dry mass divided by saturated area; leaf density (*LD*) as *LMA* divided by *LT*; saturated water content (*SWC*) as (saturated mass minus dry mass) divided by dry mass; water mass per area (*WMA*) as the (saturated mass minus dry mass) divided by saturated area; leaf dry matter content (*LDMC*) as dry mass divided by saturated mass; percentage loss in area after drying (PLA_{dry}) as the percent decline in area from saturated to dry leaves, and percentage loss in thickness after drying ($PLTH_{dry}$) as the percent decline in thickness from saturated to dry leaves (Witkowski & Lamont 1991; Ogburn & Edwards 2012; Pérez-Harguindeguy *et al.* 2013). The petiole area (*PA*) was calculated as the area of a cylinder using the petiole length and diameter; the petiole to leaf area ratio (*PA*:*LA*) was calculated as the petiole area divided by the leaf area.

Wood economics and structure

We measured wood density (*WD*) from one 5 cm-branch segment of each of the studied individuals after bark removal by water-displacement; branch segments were immersed in water and the mass of the displaced water was recorded. Branch segments were then oven-dried at 70º for 120 h and their dry mass was measured. *WD* was calculated as the segment dry mass divided by the mass of displaced water (Pérez-Harguindeguy *et al.* 2013).

Leaf composition

The concentrations of four macronutrients (potassium, calcium, phosphorus and magnesium) and 12 micronutrients (iron, boron, manganese, sodium, zinc, copper, molybdenum, cobalt, aluminum, arsenic, cadmium, rubidium and strontium) were determined from ground oven-dried leaves using high throughput elemental profiling (ionomics; (Salt *et al.* 2008)) by the USDA-ARS/Danforth Center Ionomics facility at the Donald Danforth Plant Science Center. Elemental carbon and nitrogen concentrations and their isotope ratios ($\delta^{13}C$ and $\delta^{15}N$) were measured by the University of California, Berkeley, Center for Stable Isotope Biogeochemistry, by continuous flow dual isotope analysis using a CHNOS Elemental Analyzer interfaced to an IsoPrime100 mass spectrometer (Fry *et al.* 1996; Pérez-Harguindeguy *et al.* 2013). The concentrations of nutrients were converted from mass basis into area-basis by multiplying by *LMA*. The carbon isotope discrimination ($\Delta^{13}C$; in parts per thousand, ‰) was calculated following (Farquhar & Richards 1984). The chlorophyll concentration per area (Chl_{area}) was measured using a SPAD meter ((Monje & Bugbee 1992); SPAD-502, Konica Minolta, Japan), and the chlorophyll concentration per mass was determined by dividing by *LMA* (Chl_{mass}).

Hydraulics traits

Turgor loss point (π_{tlp}) was measured for two leaves per studied individual. We used a vapor-pressure osmometer (Vapro 5520, Wescor, US) to obtain the osmotic concentration of the leaves and used calibration equations to estimate π_{tlp} (Bartlett *et al.* 2012).

The leaf and stem water potentials at point of air entry in the xylem (Pe_{leaf} and Pe_{stem}), water potentials at 50% loss of hydraulic conductivity ($P50_{leaf}$ and $P50_{stem}$), minimum water potential at midday (ψ_{midday}) and maximum xylem vessel length (V_l) were measured by (Skelton

et al. 2018) using the optical method (Brodribb *et al.* 2016) in three branches from at least six individuals of seven of the 15 species included in this study grown in the Pepperwood Preserve in Sonoma County, located on the west coast of California (Skelton *et al.* 2018).

Estimated photosynthetic traits

We estimated maximum rate of carboxylation per mass ($Vc_{max\ mass}$) and electron transport rate ($J_{max\ mass}$) from leaf N and P concentrations per mass (Domingues *et al.* 2010). The ratio between intercellular CO_2 concentration (C_i) and ambient CO_2 concentration (C_a) was estimated from $\Delta^{13}C$ (Farquhar *et al.* 1982; Franks *et al.* 2014). Estimates of leaf lifetime integrated CO_2 assimilation rate (A_{mass}) and stomatal conductance to CO_2 (G_{cleaf}) were derived from $Vc_{max\ mass}$, $J_{max\ mass}$ and isotope composition data using the Farquhar, von Caemmerer and Berry model (Franks *et al.* 2009). To convert $Vc_{max\ mass}$, $J_{max\ mass}$, and A_{mass} to area-basis, we multiplied the trait values by *LMA*. We also calculated the ratio between G_{cleaf} and G_{max}, an index of the degree that stomata are open on average relative to their anatomical maximum aperture (McElwain *et al.* 2016), and the ratio between G_{max} and N_{area}, which is negatively related to water retention for a given investment in photosynthetic machinery (Wright *et al.* 2001).

Plant size

Species maximum height (H_{max}) and seed dry mass values (*SM*) were compiled from the Ecological Flora of California database (https://ucjeps.berkeley.edu/efc/). When not available, the H_{max} was recorded as the maximum value reported on the Jepson eFlora website (https://ucjeps.berkeley.edu/eflora/).

Environmental variables for species' native ranges

We obtained species occurrence data from the Global Biodiversity Information Facility (GBIF; references available in Table S3.2) and we used R software (version 3.4.4 (R Core Team 2020)) to extract and calculate the mean, range and standard deviation of environmental variables of known occurrences across the range of distribution of each species. Occurrence records were downloaded using the '*rgbif*' package (Chamberlain *et al.* 2019) and filtered to keep herbarium records only and remove incomplete (latitude or longitude missing) and duplicated records, non-natural occurrences (e.g., records from botanical gardens, planted urban trees) and to limit the temporal range to 1950-current (Riordan *et al.* 2015; Chamberlain *et al.* 2019). We calculated species climatic envelope using species occurrence points and not maps of distribution ranges because we were interested in the relationship between species' traits and climate, and since occurrence maps are based on ecological niche models (Harrison 1997; Peterson 1999) that are partially calculated from environmental variables, they could potentially introduce circularity into our analyses (Šímová *et al.* 2018).

From open-access raster layers, we extracted a total of 30 environmental parameters relating to air temperature (WorldClim, CRU; (Hijmans *et al.* 2005)), precipitation (WorldClim; (Hijmans *et al.* 2005)), aridity (CGIAR-CSI, NCAR-UCAR; (Zomer *et al.* 2008)) and soil characteristics (ISRIC Soilgrids; (Hengl *et al.* 2017); see Table S3 for detailed description, download links and references for each variable). The raster layers with the same resolution were stacked using the *stack* function from the '*raster'* package (Hijmans & van Etten 2012) and the environmental parameters for each occurrence record were extracted using the *extract* function from the '*dismo'* package (Hijmans *et al.* 2011).

Quantifying the relative connectivity of traits within and across structure-function clusters

The 90 measured traits were organized into eight measurement type categories: epidermal morphology, leaf venation, leaf economics and structure, wood economics and structure, leaf composition, hydraulics, estimated photosynthesis and plant size (Table S3.1). Traits were then assigned to six structure-function clusters, which were defined based on expectations for trait correlation with an "indicator trait", according to theory and empirical evidence in the previous literature considering diverse species (Table S3.1). Thus, traits expected to be related to taller stature were included in the "plant size cluster" (with indicator trait H_{max}); traits expected to be related to leaf size were included in the "leaf size cluster" (with indicator trait *LA*); traits expected to be related to fluxes of carbon and water per leaf area were included in the "flux-related cluster" (with indicator trait G_{max}); traits expected to be related to plant growth rates and tissue longevity were included in the "economics cluster" (with indicator trait *LMA*) and, if traits were also expected to be related to mass-based leaf nutrient concentrations they were included in the "ecological stoichiometry cluster" (with indicator trait N_{mass}); traits expected to be related to drought tolerance (with indicator trait π_{tlp}) were included in the "drought tolerance cluster" (see Table S3.1 for the rationales for assigning each trait into structure-function clusters). Note that given traits were assigned to one or more structure-function clusters, assuming multiple functions and involvement in different physiological processes (Sack & Buckley 2020).

For each *a priori* hypothesized structure-function cluster we quantified the "within-cluster trait connectivity" as the proportion of trait-trait correlations relative to the total number of possible correlations within the cluster, and the "across-cluster trait connectivity" as the number of correlations among traits classified into different structure-function clusters relative to the number of possible trait-trait correlations among clusters (Table S3.8- S3.9).

Plant trait network analysis

To build the plant trait networks (PTNs), functional traits were considered as nodes and trait correlations were considered as edges. First, we built trait-trait correlation matrices from species mean values using ahistorical (ordinary least squares regression, OLS) and historical (phylogenetic generalized least squares, PGLS) relationships. The strength of the trait-trait relationships was described using correlation coefficients (r). To consider trait relationships as edges in the network, we set significance thresholds of $p < 0.05$. The matrices were then converted into adjacency matrices $A = [a_{i,j}]$, where we assigned 1 to relationships that were above the significance threshold and 0 to those below the threshold ($a_{i,j} \in [0,1]$). These networks were visualized and all network parameters were calculated using functions available in the '*igraph'* package (version 1.2.6) in the R Software (R Core Team 2020).

We calculated five parameters to describe the overall topology of the PTNs, three that quantify the "tightness" of the PTN, the edge density (*ed*), the diameter (*d*) and the average path length (*al*); and two parameters to quantify the "complexity" of the PTN, the average clustering coefficient (*ac*) and the modularity (*q*) (He *et al.* 2020). The *ed* is the proportion of connections out of all possible connections, *al* is the network-averaged shortest distance between traits, *d* is the maximum distance between traits in the network; *ac* is the network-averaged clustering coefficient of all traits and *q* is the difference between the within-module connections and a null model where connections among traits are randomly distributed. Higher values of *ed* reflect more interdependence of traits within the network while higher values of *al* and *d* reflect networks that have traits that are more independent of each other. Higher values of *ac* reflect higher division of network into subcomponents and higher *q* values reflect higher tendency of the network to form modules (He *et al.* 2020).

We also calculated parameters to describe the importance of traits within PTNs, two that quantify the "connectedness" of each trait, the degree (*k*) and closeness (*c*); and two that quantify the "centrality" of each trait, the betweenness (*b*), and the clustering coefficient (*cc*). For each trait, *k* is defined as the number of connections for a given trait, *c* represents how far other traits are from the focal trait; *b* is a measure of the number of shortest paths between traits that connect with the focal trait and *cc* is the proportion of connections between a focal trait and its neighboring traits out of all possible connections. Traits with the highest *k* were considered "hub traits" and traits with highest *b* were considered "mediator traits" (He *et al.* 2020).

Statistical and comparative analyses

All statistical analyses were performed and plots created using R software (version 4.0.2 (R Core Team 2020)) and packages available from the CRAN platform. We performed nested ANOVAs to test for differences in functional traits among sections using the *aov* function, with functional traits coded as the dependent variable, section as the independent variable and species nested within section (Sokal & Rohlf 2012; R Core Team 2020). To test for differences in functional traits among species we performed one-way ANOVAs, with functional traits coded as the dependent variable and species as the independent variable (Sokal & Rohlf 2012; R Core Team 2020). Most trait and climate variables were log-nomally distributed and were $\log_{10}$-transformed prior to analyses. Variables that included both negative and positive numbers were incremented by a constant equal to the lowest species mean +1 before log-transformation, such that 1 was the lowest value for that variable (see Tables S3.4-5 for detailed description).

To summarize the variation in functional traits of the oak species, we performed a principal component analyses (PCAs) on species means of the six indicator traits of the structure-function

clusters, H_{max}, *LA*, G_{max}, *LMA*, N_{mass} and π_{tlp}, using the *prcomp* function in the '*stats*' package (R Core Team 2020). All variables were log-scaled prior to analyses. We extracted the species scores (scaled to range from -1 to 1) of PC axes 1 and 2, and used them to summarize trait main axes of variation in subsequent analyses.

To test trait-trait and trait-environment relationships across species, we performed regressions using an ahistorical and an evolutionary approach. In the ahistorical approach we used ordinary least squares regression analyses (OLS) using the *lm* function from the '*stats'* package and in the evolutionary approach we used phylogenetic generalized least-squares analyses (PGLS (Felsenstein 1985; Freckleton *et al.* 2002; Harmon 2019)) using the *pgls* function from the '*caper*' package (Orme *et al.* 2018) with lambda (λ) optimized using maximum likelihood. Pairwise branch distances were calculated for each species pair based on an ultrametric tree modified from the oak phylogeny of (Hipp *et al.* 2020). Analyses were performed in untransformed and log-transformed data, to test for either approximately linear or non-linear (i.e., approximate power-law) relationships, respectively. Here we focus on the results from the evolutionary analyses (hereafter "r_{phy}") and present the ahistorical results (hereafter, "r_{ols}") in the figures and supplemental files (Table S3.6 and Fig. 3.2).

To compare the proportion of correlations uncovered within and across the hypothesized structure-function trait clusters out of all possible correlations we performed proportion tests using the *prop.test* function from the '*stats'* package.

RESULTS

Variation in traits within and across species

Traits varied strongly among and within California oak species. On average across the measured traits, 13% of the total variation was accounted for by section, 44% by species-differences within section, and 43% by individuals within species (nested ANOVAs; Table S3.4). We found that 56 of the 90 traits with individual-level measurements differed significantly across species, including the indicator traits of four of the six structure-function clusters, G_{max} (flux-related cluster), *LMA* (resource economics cluster), N_{mass} (nutrient stoichiometry cluster) and π_{tlp} (drought tolerance cluster) (one-way ANOVAs; Table S3.5 and Fig. S3.2).

Trait-trait coordination among and within structure-function clusters

Overall, traits were more connected within than across the *a priori* defined structure-function clusters. We tested if traits were more correlated within than across the six *a priori* hypothesized structure-function clusters by comparing the proportion of correlations within and across clusters out of all possible correlations, with values closer to one reflecting higher "connectivity" (Tables S3.1, S3.8- S3.9). With the ahistorical approach, we found a connectivity of 0.23 within and 0.18 across structure-function clusters (p <0.001; Table S3.8) and with the evolutionary approach, we found a connectivity of 0.29 within and 0.23 across clusters (p <0.001; Table S3.9). The plant and leaf size clusters were the most intercorrelated, while the flux-related and drought response clusters were the least intercorrelated in both ahistorical and evolutionary analyses (Tables S3.8- S3.9). Traits in the plant size cluster were also the most correlated with traits in other structure-function clusters, while traits in the economics cluster were the least correlated (Tables S3.8- S3.9).

We also plotted the relationships between the indicator traits (i.e., traits we hypothesized would be the most strongly correlated with the structure-function cluster and thus, have the highest number of connections with other traits) and the other traits belonging to the same structure-function cluster (Fig. 3.2). In the plant size cluster, we found that taller oak species have larger leaves and petioles, faster photosynthetic rates and less dense wood, so larger petiole area, *PA*, leaf area, *LA*, CO_2 assimilation rate, A_{mass}, maximum carboxylation and electron rates per mass, $Vc_{max\ mass}$ and $J_{max\ mass}$, and lower wood density, *WD* ($|r_{phy}|$ ranged from 0.58 to 0.84; $p < 0.05$; Table S3.7 and Fig. 2a). In the leaf size cluster, oak species with larger leaves were taller, had larger *PA*, higher major vein diameter, VD_{major} and lower major vein lengths per area, VLA_{major}, and leaf mass per area, *LMA* ($|r_{phy}|$ ranged from 0.75 to 0.93; $p < 0.05$; Table S3.7 and Fig. 3.2b). In the flux-related cluster we found that species with higher maximum stomatal conductance, G_{max}, have higher stomatal density, *SD*, stomatal index, *SI*, guard cell width, GC_w, petiole to leaf area ratio, *PA*:*LA*, and nitrogen concentration per area, N_{area} ($|r_{phy}|$ ranged from 0.54 to 0.95; $p < 0.05$; Table S3.7 and Fig. 3.2c). In the economics cluster, species with high *LMA* had thicker, denser leaves with higher photosynthetic rates and nutrient concentrations per area; they also had lower chlorophyll, photosynthetic rates and nutrients per mass ($|r_{phy}|$ ranged from 0.55 to 1; $p < 0.05$; Table S3.7 and Fig. 3.2d). In the ecological stoichiometry cluster, species with high N_{mass} had higher leaf concentrations of K, Cu, P, Rb, and lower concentrations of B, Na, and C per mass; they also had a higher nitrogen 15 isotope composition, $\delta^{15}N$, and lower C to N ratio, *C*:*N* ($|r_{phy}|$ ranged from 0.62 to 0.99; $p < 0.05$; Table S3.7 and Fig. 3.2e). In the drought response cluster, oak species with higher (less negative) turgor loss point, π_{tlp}, had larger and less lobed leaves (low *LP*:*LA* and LP^2:*LA*) with higher VD_{major}, photosynthetic rates and saturated water content, *SWC*,

and lower saturated water mass per area, *SWMA*, *LMA*, *WD* and minor vein diameter, VD_{minor} ($|r_{phy}|$ ranged from 0.55 to 0.86; $p < 0.05$; Table S3.7 and Fig. 3.2f).

Trait-environment coordination

A principal component analysis of indicator traits from each of the six structure-function clusters for all species identified two dominant axes of variation (Traits-PCA); Traits-PC1 and Traits-PC2 explained 59.6% and 20.3% of variation, respectively (Table S3.3 and Fig. 3.3a). Traits-PC1 represented a gradient from low to high tolerance to drought, with higher scores corresponding to higher *LMA*, more negative π_{tlp} and smaller *LA*, H_{max}, and N_{mass}. Traits-PC2 represented a gradient from low to high G_{max} (Table S3.3 and Fig. 3.3a).

High climatic aridity, i.e., low values of aridity index, *AI*, and high potential evapotranspiration (*PET*), was positively correlated with Traits-PC1 (r_{phy} = 0.54 and 0.61, respectively; $p < 0.05$; Table S3.7 and Fig. 3.3b-c). Traits-PC1 was also negatively correlated with soil depth (r_{phy} = -0.58; $p < 0.05$; Table S3.7). Despite varying largely in climatic aridity of their native ranges, three of the four deciduous species, *Q. kelloggii*, *Q. garryana* and *Q. lobata*, had very similarly low values of Traits-PC1, which reflect their large *LA*, H_{max} and π_{tlp} (Fig. 3.3). Traits-PC2 was not correlated with *AI* nor *PET*, but it was positively correlated with the annual temperature range and negatively correlated with the minimum temperature and soil pH ($|r_{phy}|$ ranging from 0.52 to 0.56; $p < 0.05$; Table S3.7). Indicator traits alone were also correlated with *AI* and *PET* (Tables S3.6- S3.7). *AI* was positively correlated with *LA* and N_{mass} (r_{phy} = 0.57 and 0.61, respectively; $p < 0.05$; Table S3.7) and *PET* was negatively correlated with *LA* and π_{tlp} (r_{phy} = -0.71 and -0.62, respectively; $p < 0.01$; Table S3.7).

Plant trait network architecture and complexity: ahistorical vs. evolutionary networks

The ahistorical and evolutionary networks had similar overall tightness (i.e., dependence of one trait on another); the diameter, *d*, of the two networks was the same, but the evolutionary network had a higher edge density, *ed*, while the ahistorical had a higher average path length, *al* (Table 3.1 and Fig. 3.4). The evolutionary network was overall more complex than the ahistorical; it had a higher clustering coefficient (*ac*; PTN is divided into more subcomponents) and lower modularity (*q*; higher clustering into modules) than the ahistorical PTN (Table 3.1 and Fig. 3.4). The ahistorical network grouped the traits into 44 modules, with 39 composed of one trait, and the evolutionary network grouped traits into 40 modules, 36 of them composed of a single trait (Table S3.10 and Fig. 3.4).

In the ahistorical PTN, the algorithm grouped the traits into five main modules (Fig. 3.4a). The first module included traits related to gas exchange and photosynthetic efficiency: *SD*, *SI*, G_{max} and G_{max}:N_{area} (orange; Fig. 3.4a). The second group consisted of traits that describe stomatal size (*S*, GC_l, SP_{il}, SP_{ol}) and the volume of major veins (pink; Fig. 3.4a). The third and largest group combined traits related to leaf and wood economics, leaf composition and drought tolerance responses, such as *LA*, *LMA*, *WD*, π_{tlp} and VLA_{major} and the area and mass-basis concentrations of leaf nutrients (green; Fig. 3.4a). The fourth group included the GC_W, Al_{mass}, Fe_{mass}, Zn_{mass}, Co_{mass} and Co_{area} (yellow; Fig. 3.4a). The fifth module consisted of VLA_{minor}, Ca_{mass} and Sr_{mass} (blue; Fig. 3.4a).

The evolutionary PTN grouped the traits into four main clusters (Fig. 3.4b). The first, second and third clusters of the evolutionary PTN consisted of virtually the same traits as the ahistorical network (orange, pink and green modules; Table S3.10 and Fig. 3.4b). The fourth and last module, however, consisted of traits related to water use and photosynthetic efficiency, $\Delta^{13}C$,

C_i:C_a and K_{area} (purple; Fig. 3.4b). We also plotted the evolutionary PTN coloring the nodes according to the structure-function cluster we hypothesized them to belong to (Table S3.1 and Fig. S3.3) instead of the clusters formed by the clustering algorithm (Fig. 3.4b). We observed a high similarity between the economics structure-function cluster and the green cluster of the PTN and between the drought response structure-function cluster and the combination of the pink, purple and orange clusters of the PTN (Figs. 3.4b and S3.3).

Trait connectedness: "hub" and "mediator" traits

Hub and mediator traits differed between the ahistorical and evolutionary approaches. In the ahistorical network, the top five hub traits were the chlorophyll concentration per mass, Chl_{mass}, boron concentration per area, B_{area}, carbon concentration per area, C_{area}, carbon to nitrogen ratio, *C*:*N*, and N_{mass} (Table S3.10 and Fig. 3.5a) and the top five mediator traits were the zinc concentration per area, Zn_{area}, sodium concentration per mass, Na_{mass}, the ratio of G_{max}:N_{area}, Chl_{mass} and H_{max} (Table S3.10 and Fig. 3.5b). In the evolutionary network, the top five hub traits were the Chl_{mass}, A_{mass}, *LMA*, B_{area} and *C*:*N* (Table S3.10 and Fig. 3.5c) and the top five mediator traits were H_{max}, *PA*:*LA*, π_{tlp}, aluminum concentration per area, Al_{area}, and the diameter of major veins (Table S3.10 and Fig. 3.5d).

The PTN mostly supported our selection of indicator traits for each structure-function cluster and helped uncover additional potential indicator traits (Table S3.10 and Fig. S3.4). In the plant size cluster, the indicator trait H_{max} was the trait with highest betweeness and A_{mass} was the trait with largest *k* (Fig. S3.4a). In the leaf size cluster, the indicator trait *LA* had the second largest *k* and fourth largest *b*, with *LMA* and H_{max} also being very connected traits (Fig. S3.4b). In the flux-releted cluster, the indicator trait G_{max} had low *k* and *b*; the most interconnected traits in the

flux-related cluster were photosynthesis variables, such A_{mass} and $Vc_{max\ mass}$ and H_{max} (Fig. S3.4c). The *LMA* had the third highest *k* and seventh largest *b* of the economics cluster; other traits were also very connected, such as Chl_{mass} and A_{mass}(Fig. S3.4d). N_{mass} had the second largest *k* of the ecological stoichiometry cluster, but had a low *b*; *C*:*N* and Zn_{mass} were also important traits in the cluster (Fig. S3.4e). In the drought tolerance cluster, traits related to photosynthesis, such as A_{mass} and $Vc_{max\ mass}$ had the largest *k*, and the indicator trait π_{tlp} had the second largest *b*, after H_{max} (Fig. S3.4f).

DISCUSSION

Variation in traits within and across species

We found strong intra- and interspecific variation in traits of California native oak species, which is not surprising, given their high degree of phenotypic variation, convergent evolution and hybridization (Tucker 1974; Sork *et al.* 2016). A high intraspecific variation could be advantageous for species growing under resource-limitation, since a larger range of possible trait values would allow plants to go through plastic trait changes in response to shifts in the environment, potentially leading to higher resilience (Jung *et al.* 2014; Anderegg 2015; González de Andrés *et al.* 2021).

It is also interesting to note that the variation explained by inter and intraspecific differences was not consistent across traits. Traits such as leaf nutrient concentrations had greatest intraspecific variation, which might explained due to differential resource allocation and differences in the soil morphology and composition in different microenvironments across the common garden (Opedal *et al.* 2015). For the large majority of traits, species differences explained most of the variation in traits while the differences across sections explained the least amount of

variation (around 13%). This lack of cohesiveness among species belonging to the same section indicates that species relatedness is not the main determining factor of functional strategies across this set of California native oaks (Tucker 1974).

Trait-trait coordination among and within structure-function clusters

Our results supported the hypothesis that traits would be more inter-correlated with traits that are involved in the same physiological processes, thus evolving as structure-function clusters. We showed that, with the exception of the flux-related cluster, traits involved in similar functional responses are more coordinated and relatively independent of other clusters (Table S3.8- S3.9). This low cohesiveness of the flux-related cluster could be explained by their multifunctionality. Indeed, most of the traits included in the flux-related cluster were hypothesized to be involved in four of the six structure-function clusters (Sack & Buckley 2020). We also found that the inclusion of shared evolutionary histories in our analyses resulted in higher trait-trait coordination, both within and across structure-function modules. This indicates that despite not being an important driver of overall function, species' relatedness can have an important role in determining certain traits, such as stomatal density, guard cell width, G_{max} and trichome density (Table S3.4).

Trait modules evolved with climate

Our results suggest strong adaptation of drought tolerance across the California native *Quercus* species, involving repeated convergent adaptation of key traits. The relationships we uncovered between the structure-function clusters, through their indicator traits, and climatic aridity of their native ranges supported our initial hypotheses (Table S3.1 and Fig. 3.3). Species that reach a smaller height at maturity, possess smaller leaves and lower cencentration of nitrogen in the leaves,

coupled with larger *LMA* and a more negative π_{tlp} are currently distributed in drier climates, where the *AI* is lower and the *PET* is higher (Fig. 3.3), consistent with traits related to high sclerophylly and tolerance to drought (Alonso-Forn *et al.* 2020).

There was a clear decoupling between the traits of three of the four deciduous species (*Q. kelloggii*, *Q. garryana* and *Q. lobata*) included in this study from the climatic aridity of their native ranges (Table S3.3 and Fig 3.3). These species had a variation of approximately 2 fold in their native *AI* and *PET*, but their Traits-PC1 was very similar; in other words, they have large H_{max}, *LA* and N_{mass} coupled with less negative π_{tlp} and low *LMA*. This combination of traits is typically found in drought sensitive species or species growing in resource abundant environments, which is not the case for these three species (Sork *et al.* 2016). However, since they only keep their leaves physiologically active for a few months a year, they compensate by doing most of their growth in a short growth season (which is also the rainy season), supporting a drought avoidance strategy for this subset of species (Sancho-Knapik *et al.* 2021).

Evolution of traits in modules

The PTN approach helped clarify the correlative structure of traits and allowed us to identify trait clusters according to their statistical relationships. Including species shared evolutionary history strongly influenced the architecture of the PTN; the evolutionary network was overall more complex than the ahistorical, with higher *ac* and lower *q*, which reflect a network with more subcomponents or clusters consisting of less traits (Table 3.1; (He *et al.* 2020)). Additionally, the clusters identified with this approach somewhat supported the structure-function clusters we hypothesized *a priori*, especially the economics and the drought response clusters. The differences between the structure-function clusters we hypothesized and the clusters identified by the

algorithm do not necessarily mean there was no statistical support for the other four other clusters; it just highlights the strong coordination of traits and the importance of this global view of plant function. Because of the multifunctionality of traits, some trait-trait relationships will vary depending of the circumstances of the study, so we would also expect to uncover different architectures in PTNs created from contrasting species adapted to different environments. This is ultimately why PTNs are so promising in ecophysiological studies: they help resolve relationships among multiple traits at the same time and visualize how traits might indirectly influence traits related to different functions (Messier *et al.* 2017; Flores-Moreno *et al.* 2019; Kleyer *et al.* 2019; He *et al.* 2020).

The PTN approach also allowed us to identify traits with special importance as hubs and mediators, including photosynthetic traits, such as A_{mass} and $Vc_{max\ mass}$, leaf composition traits, such as *LMA* and *C*:*N*, and π_{tlp} and H_{max} (Figs. 3.5 and S3.4). This does not mean that less connected traits are necessarily less important; these traits might be fundamental to a different dimension of plant function and thus more "mechanistically isolated" from other trait clusters.

Applications and limitations of this study

The evolution of traits within clusters highlights the emergence of integrated phenotypes that provide drought tolerance, and points to the necessity of considering the benefits and costs contributed by multiple traits to overall climate adaptation. The PTN are a very promising approach to visualize multiple traits at the same time, providing us with a more integrative perpective of how the plant phenotype responds to changing environments, while also helping us get closer to the identification of the key traits and/or structure-function clusters.

ACKNOWLEDGEMENTS

We acknowledge the indigenous peoples that stewarded the land studied in this project in previous millenia, including the Kizh, Tongva, Chumash and Micqanaqa'n peoples. We thank Aleena Sorfazian, Alayna Mead and Victoria Sork for collaboration and Alec Baird, Marvin Browne, Nathan Kraft, Yao Li, Marissa Ochoa, Santiago Trueba and Joseph Zailaa for help with sampling, trait measurements and comments on early versions of the manuscript and the Rancho Santa Ana Botanical Garden for giving permission to sample from their living collection. This work was funded by the UCLA EEB Vavra Research Grant awarded to CM. CM was supported by the Brazilian National Research Council (CNPq) through the Brazilian Science Without Borders Program (grant number: 202813/2014-2).

Table 1. Network-level parameters that quantify network tightness (edge density, *ed*, diameter, *d*, and average path length, *al*) and complexity (average clustering coefficient, *ac*, and the modularity, *q*) using ahistorical correlations and evolutionary correlations.

Network property	Parameter	Significance of higher value	Ahistorical	Evolutionary
Tightness	Edge density, *ed*	Traits are less independent	0.197	0.248
	Average path length, *al*	Traits are more independent	2.230	2.022
	Diameter, *d*	Traits are more independent	5	5
Complexity	Average clustering coefficient, *ac*	Network divided into more subcomponents	0.607	0.634
	Modularity, *q*	Higher clustering of traits into modules	0.146	0.117

FIGURE CAPTIONS

Figure 3.1. (a) Map showing the centroid of the range of distribution of the 15 California native oak species sampled in this study with terrain colored according to the aridity index. The star represents the sampling location, Rancho Santa Ana Botanical Garden. (b) Phylogenetic tree of the California native oaks species included in this study (adapted from (Hipp *et al.* 2020)). Colors represent section within the genus *Quercus*: *Lobatae* (red), *Protobalanus* (yellow) and *Quercus* (blue).

Figure 3.2. Relationships between indicator traits (*x*-axes) and traits hypothesized to belong to each structure-function cluster (*y*-axes). Traits that affect plant stature are included in the "plant size cluster"; traits that affect the leaf size are included in the "leaf size cluster"; traits that affect hydraulic conductivity were included in the "flux-related cluster"; traits that affect leaf lifespan were included in the "economics cluster" and, if they are also related to elemental composition they were included in "ecological stoichiometry cluster"; traits that affect species responses to drought (i.e., re related to climatic aridity) were included in the "drought response cluster". Since traits can have multiple functions, they might reflect more than one cluster. Relationships between (a) plant size cluster and the maximum plant height, H_{max}, (b) the leaf size cluster and the leaf area, *LA*; (c) the flux-related cluster and the theoretical maximum stomatal conductance, G_{max}; (d) the economics cluster and the leaf mass per area, *LMA*; (e) the ecological stoichiometry cluster and the nitrogen concentration per leaf mass, N_{mass}; (f) the drought response cluster and the water potential at turgor loss, π_{tlp}. The symbol outline color represents the hypothesized relationship (Table S3.1) and the symbol filling represents the relationship uncovered by our analyses (phylogenetic generalized least squares, PGLS; $p < 0.05$; Table S3.7). Blue and red symbols

represent traits that are, respectively, positively and negatively related to the indicator trait of a given cluster. Gray represents traits with multiple published hypotheses for their relationships with the indicator trait (Table S3.1).

Figure 3.3. Variation in traits and native climate across 15 oak species grown in a common garden. Principal component analysis (PCA; Table S3.3) on (a) indicator traits of each of the six structure-function clusters, maximum plant height, H_{max}, leaf area, *LA*, anatomical maximum stomatal conductance, G_{max}, leaf mass per area, *LMA*, foliar nitrogen concentration per mass, N_{mass}, and turgor loss point, π_{tlp} (multiplied by "-1" prior to PCA). Relationships between the first axis of the traits PCA with (b) the aridity index, *AI,* and (c) the potential evapotranspiration, *PET*. Larger *AI* represents more humid climate, so we present the reversed the *x*-axis to highlight that *PET* and *AI* increase with climatic aridity. Colors represent section within the genus *Quercus*: *Lobatae* (red), *Protobalanus* (yellow) and *Quercus* (blue); symbols represent leaf habit, evergreen (circles) and deciduous (squares). Solid lines describe the fit of the evolutionary analyses (PGLS; Table S3.7) and dashed lines describe the fit of the ahistorical analyses (ordinary least squares regression, OLS; Table S3.6). *$p < 0.05$.

Figure 3.4. Networks of the 90 functional traits measured in 15 species of California native oaks grown in a common garden. Both networks were built from a matrix of trait-trait correlations, with (a) showing the resulting ahistorical network (ordinary least squares regression, OLS; Table S3.6) and (b) showing the evolutionary network (phylogenetic generalized least squares, PGLS; Table S3.7). Correlations were considered significant when $p < 0.05$. Nodes with the same colors were

grouped into the same modules by the clustering algorithm and nodes colored in gray were placed in modules where they were the single component (Table S3.10).

Figure 3.5. Trait-level network parameters describing trait connectivity and centrality in the ahistorical (top row) and evolutionary networks (bottom row). Panels (a) and (c) show the degree of connectedness, *k*, and panels (b) and (d) show the betweeness, *b*. Traits with high values of *k* were considered "hub traits" and traits with high values of *b* were considered "mediator traits". Bars with the same colors were grouped into the same modules by the clustering algorithm (as in Fig. 4) and bars colored in gray were placed in modules where they were the single component. Indicator traits are highlighted in bold and with an asterisk. Here we show the 20 traits with largest *k* and *b* values; see Table S3.10 for complete list.

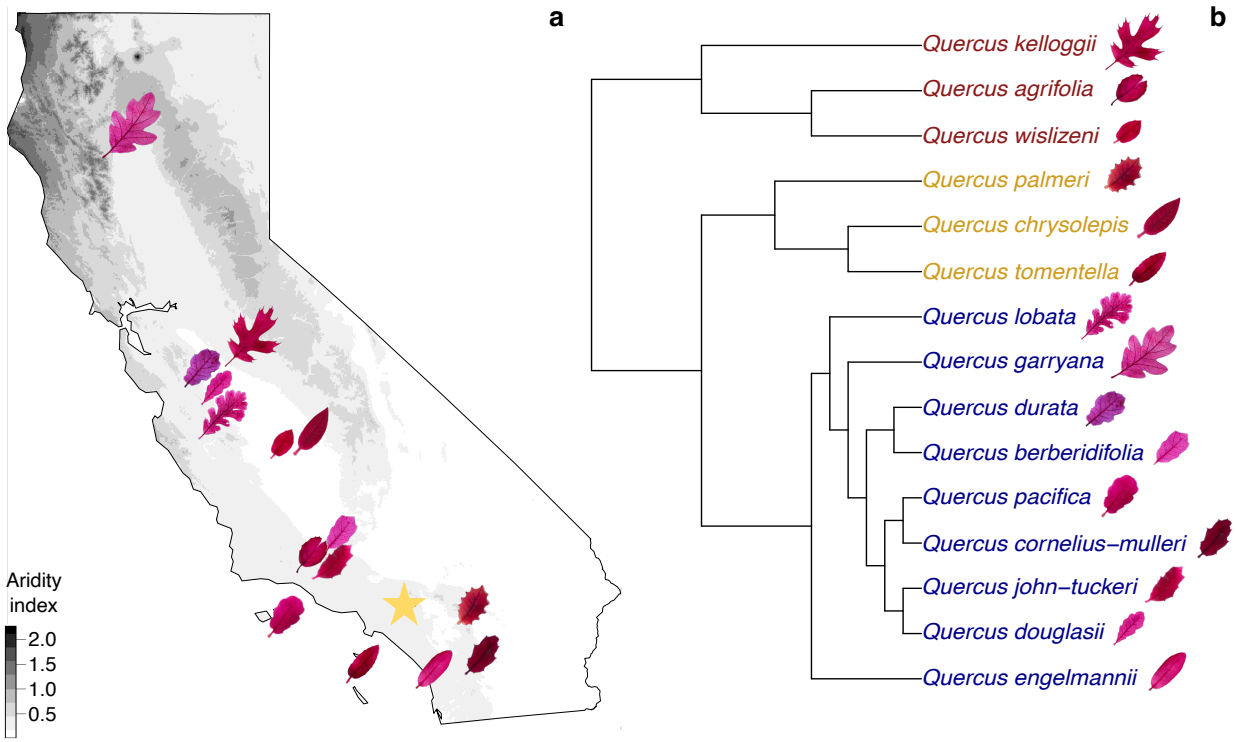
a
b
Aridity index
2.0
1.5
1.0
0.5
Quercus kelloggii
Quercus agrifolia
Quercus wislizeni
Quercus palmeri
Quercus chrysolepis
Quercus tomentella
Quercus lobata
Quercus garryana
Quercus durata
Quercus berberidifolia
Quercus pacifica
Quercus cornelius–mulleri
Quercus john–tuckeri
Quercus douglasii
Quercus engelmannii

Figure 3.1

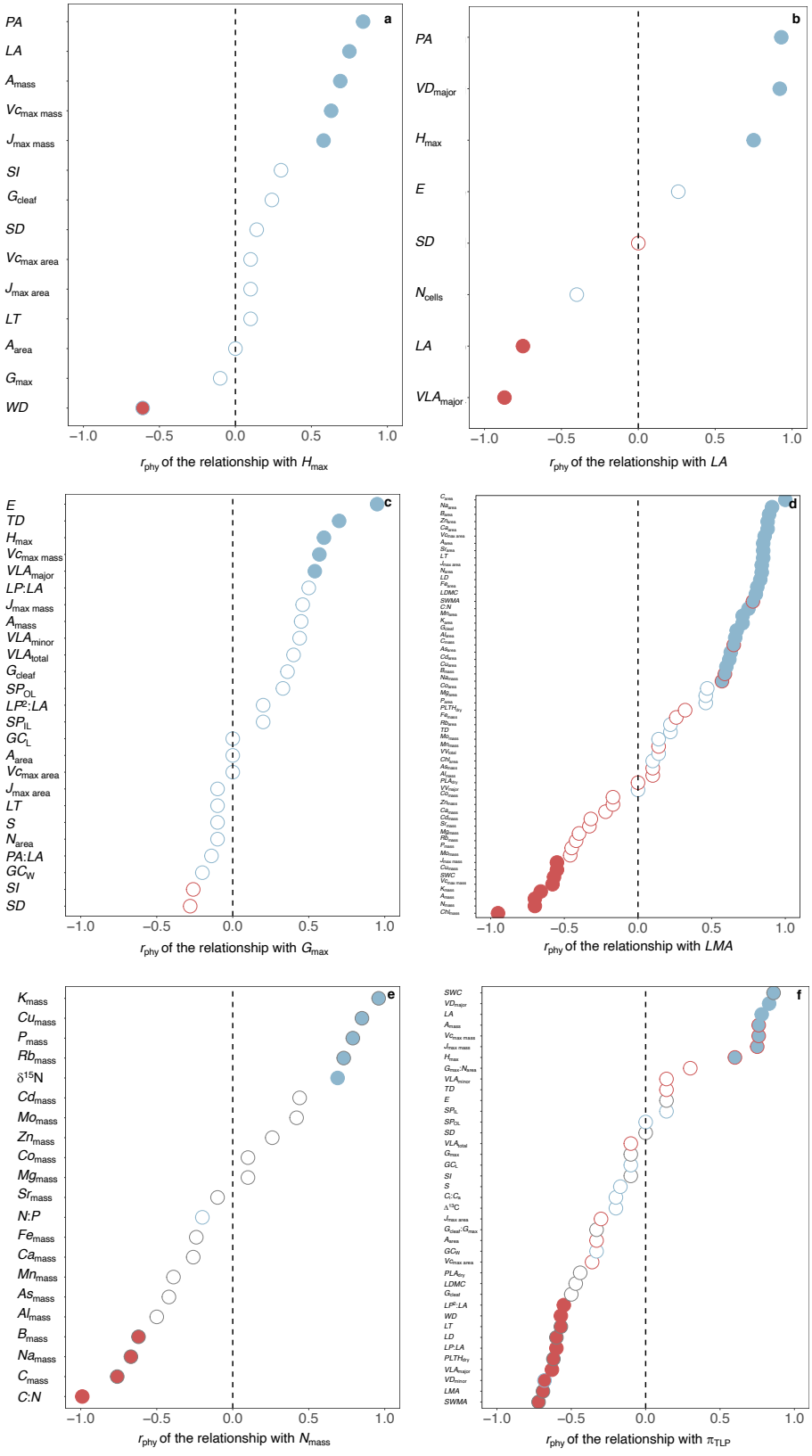
a
PA
LA
Amass
Vcmax mass
Jmax mass
SI
Gcleaf
SD
Vcmax area
Jmax area
LT
Aarea
Gmax
WD
−1.0
−0.5
0.0
0.5
1.0
rphy of the relationship with Hmax
b
PA
VDmajor
Hmax
E
SD
Ncells
LA
VLAmajor
rphy of the relationship with LA
c
E
TD
Hmax
Vcmax mass
VLAmajor
LP:LA
Jmax mass
Amass
VLAminor
VLAtotal
Gcleaf
SPOL
LP2:LA
SPIL
GCL
Aarea
Vcmax area
Jmax area
LT
S
Narea
PA:LA
GCW
SI
SD
rphy of the relationship with Gmax
d
rphy of the relationship with LMA
e
Kmass
Cumass
Pmass
Rbmass
δ15N
Cdmass
Momass
Znmass
Comass
Mgmass
Srmass
N:P
Femass
Camass
Mnmass
Asmass
Almass
Bmass
Namass
Cmass
C:N
rphy of the relationship with Nmass
f
SWC
VDmajor
LA
Amass
Vcmax mass
Jmax mass
Hmax
Gmax:Nmass
VLAminor
TD
E
SPIL
SPOL
SD
VLAtotal
Gmax
GCL
SI
S
C:CL
Δ13C
Jmax area
Gcleaf:Gmax
Aarea
GCW
Vcmax area
PLAdry
LDMC
Gcleaf
LP2:LA
WD
LT
LD
LP:LA
PLTHdry
VLAmajor
VDminor
LMA
SWMA
rphy of the relationship with πTLP

Figure 3.2

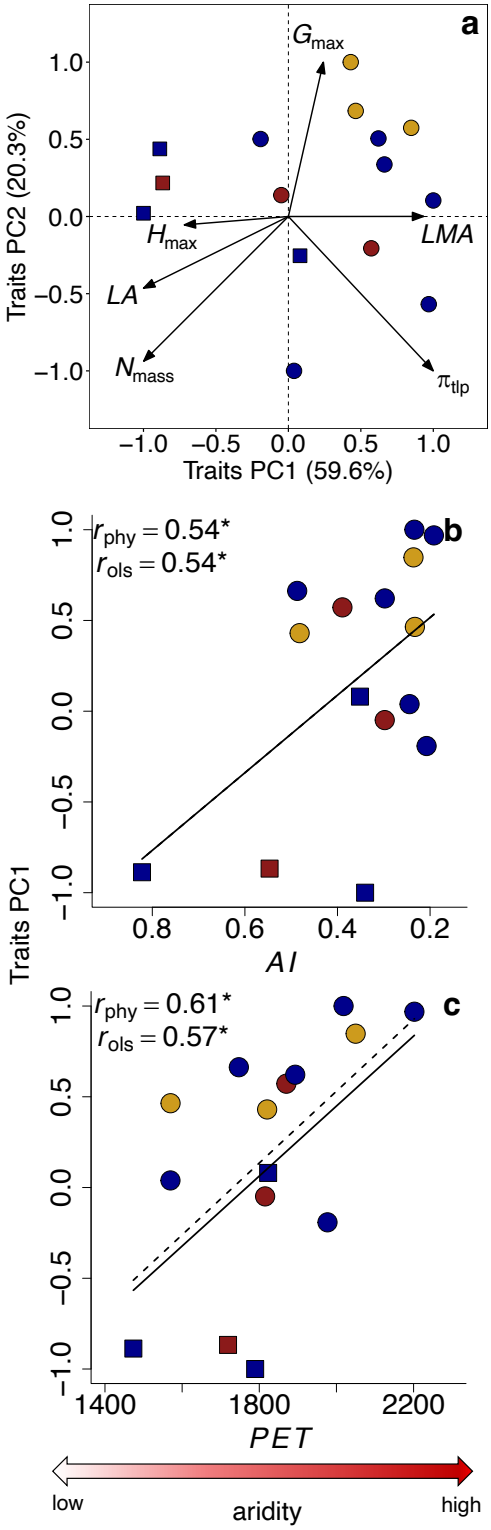
a
G_{max}
H_{max}
LMA
LA
N_{mass}
π_{tlp}
Traits PC2 (20.3%)
Traits PC1 (59.6%)
b
$r_{phy} = 0.54^*$
$r_{ols} = 0.54^*$
Traits PC1
AI
c
$r_{phy} = 0.61^*$
$r_{ols} = 0.57^*$
PET
low
aridity
high

Figure 3.3

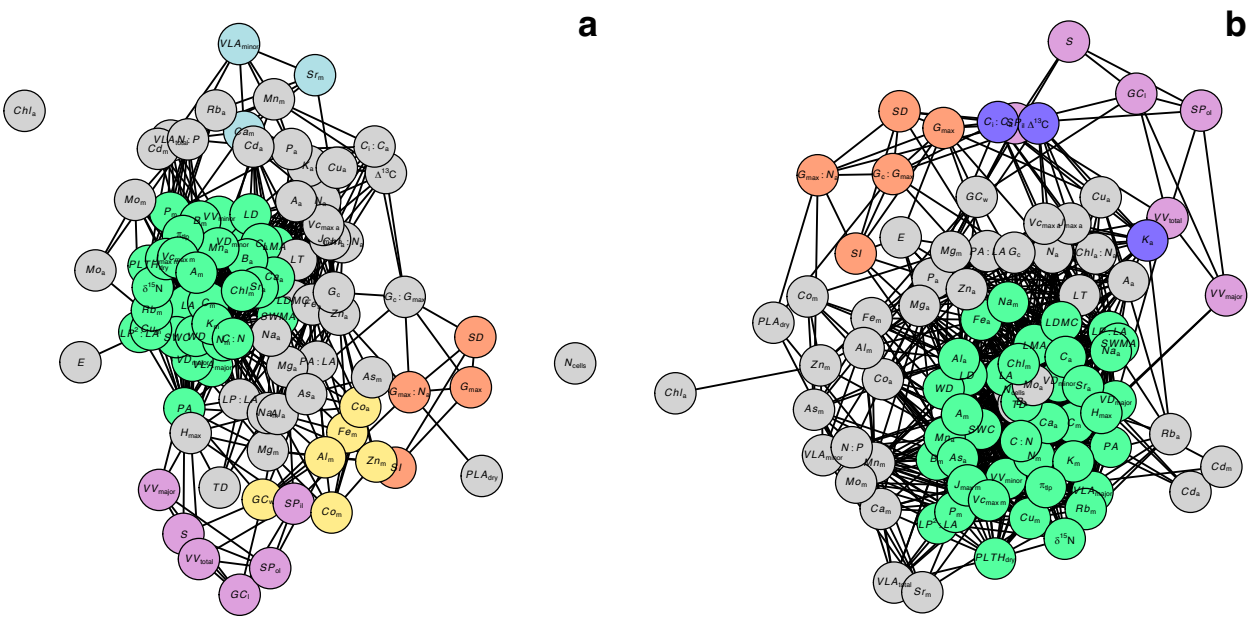

Figure 3.4

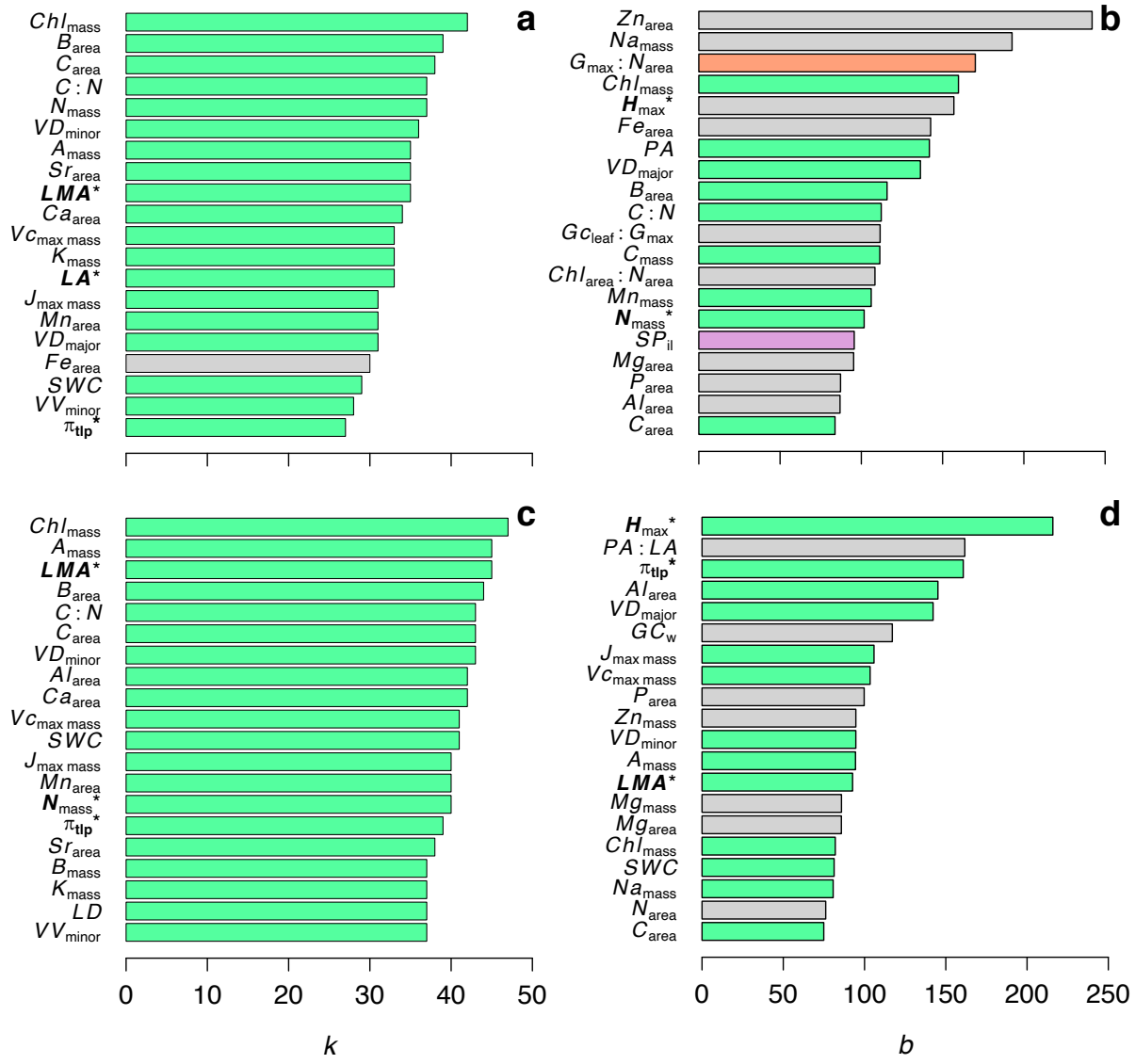
a
Chl_{mass}
B_{area}
C_{area}
$C:N$
N_{mass}
VD_{minor}
A_{mass}
Sr_{area}
$\boldsymbol{LMA}^{*}$
Ca_{area}
$Vc_{max\ mass}$
K_{mass}
$\boldsymbol{LA}^{*}$
$J_{max\ mass}$
Mn_{area}
VD_{major}
Fe_{area}
SWC
VV_{minor}
$\pi_{\boldsymbol{tlp}}^{*}$
b
Zn_{area}
Na_{mass}
$G_{max}:N_{area}$
Chl_{mass}
$\boldsymbol{H}_{max}^{*}$
Fe_{area}
PA
VD_{major}
B_{area}
$C:N$
$Gc_{leaf}:G_{max}$
C_{mass}
$Chl_{area}:N_{area}$
Mn_{mass}
$\boldsymbol{N}_{mass}^{*}$
SP_{il}
Mg_{area}
P_{area}
Al_{area}
C_{area}
c
Chl_{mass}
A_{mass}
$\boldsymbol{LMA}^{*}$
B_{area}
$C:N$
C_{area}
VD_{minor}
Al_{area}
Ca_{area}
$Vc_{max\ mass}$
SWC
$J_{max\ mass}$
Mn_{area}
$\boldsymbol{N}_{mass}^{*}$
$\pi_{\boldsymbol{tlp}}^{*}$
Sr_{area}
B_{mass}
K_{mass}
LD
VV_{minor}
0
10
20
30
40
50
k
d
$\boldsymbol{H}_{max}^{*}$
$PA:LA$
$\pi_{\boldsymbol{tlp}}^{*}$
Al_{area}
VD_{major}
GC_{w}
$J_{max\ mass}$
$Vc_{max\ mass}$
P_{area}
Zn_{mass}
VD_{minor}
A_{mass}
$\boldsymbol{LMA}^{*}$
Mg_{mass}
Mg_{area}
Chl_{mass}
SWC
Na_{mass}
N_{area}
C_{area}
0
50
100
150
200
250
b

Figure 3.5

Appendix Table 3.1. List of the 15 California native *Quercus* species grown in a common garden and included in this study. For each species we provide Latin and common names, section within the genus, growth form, leaf habit (evergreen, E, or deciduous, D), and the mean aridity index (*AI*) and potential evapotranspiration (*PET*) of their natural range of distribution.

Species name	**Code**	**Common name**	**Section**	**Growth form**	**Leaf habit**	***AI***	***PET*** **(mm.year^{-1})**
Quercus agrifolia	QAGR	Coast Live oak	*Lobatae*	Tree	E	0.30	1815
Quercus kelloggii	QKEL	Black oak	*Lobatae*	Tree	D	0.55	1719
Quercus wislizeni	QWIS	Interior live oak	*Lobatae*	Tree	E	0.39	1870
Quercus chrysolepis	QCHR	Canyon Live oak	*Protobalanus*	Tree	E	0.48	1820
Quercus palmeri	QPAL	Palmer oak	*Protobalanus*	Shrub	E	0.24	2050
Quercus tomentella	QTOM	Island oak	*Protobalanus*	Tree	E	0.23	1570
Quercus berberidifolia	QBER	Coastal Shrub oak	*Quercus*	Shrub	E	0.30	1893
Quercus cornelius-mulleri	QCOR	Muller oak	*Quercus*	Shrub	E	0.19	2202
Quercus douglasii	QDOU	Blue oak	*Quercus*	Tree	D	0.35	1823
Quercus durata	QDUR	Leather oak	*Quercus*	Shrub	E	0.49	1747
Quercus engelmannii	QENG	Engelman oak	*Quercus*	Tree	E	0.21	1977
Quercus garryana	QGAR	Oregon oak	*Quercus*	Tree	D	0.82	1474
Quercus john-tuckeri	QJOH	Tucker oak	*Quercus*	Tree	E	0.23	2018
Quercus lobata	QLOB	Valley oak	*Quercus*	Tree	D	0.34	1789
Quercus pacifica	QPAC	Island scrub oak	*Quercus*	Shrub	E	0.24	1570

SUPPLEMENTARY MATERIALS

Supplementary data captions (see attached Excel Workbook)

Table S3.1. List of the 98 traits and three environmental variables quantified for 15 species of California native oaks grown in a common garden. The traits relate to eight measurement categories: epidermal morphology, leaf venation, leaf economics and structure, wood economics and structure, leaf composition, hydraulics, estimated photosynthesis and plant size. For the traits, we provide symbols, units and the functional dimensions each trait reflects, i.e. the "structure-function clusters". Traits that affect plant stature are included in the "plant size cluster"; traits that affect the leaf size are included in the "leaf size cluster"; traits that affect hydraulic conductivity were included in the "flux-related cluster"; traits that affect leaf lifespan were included in the "economics cluster" and, if they are also related to elemental composition they were included in "ecological stoichiometry cluster"; traits that affect species responses to drought (i.e., are related to climatic aridity) were included in the "drought response cluster". Blue and red filled cells represent traits that are, respectively, positively and negatively related to a given cluster. Since traits can have multiple functions, they might reflect more than one cluster.

Table S3.2. List of environmental variables including abbreviations, units, source database, metadata (raster layer title, timeframe of the dataset, the subset of the original dataset that was used to calculate species climate envelope, and the download date), and links to access datasets and references.

Table S3.3. Principal Components Analysis (PCA) axes scores, trait contribution, trait correlational values and importance of components for 15 species of oaks (genus *Quercus*) grown in a common garden and eight traits that reflect different axes of plant-structure variation.

Table S3.4. Differences in functional traits among 15 species of California native oaks belonging to three sections, as indicated in nested analyses of variance, with species nested within section. Traits deviating from assumptions of normality or homoscedasticity were log-transformed prior to the analysis (see legend below). Highlighted cells indicate variables differing significantly across sections or species ($p \leq 0.05$).

Table S3.5. Differences in functional traits among 15 species of California native oaks, as indicated in one-way analyses of variance. Traits deviating from assumptions of normality or homoscedasticity were log-transformed prior to the analysis (see legend below). Highlighted cells indicate variables differing significantly across species ($p \leq 0.05$).

Table S3.6. Associations of traits and environmental variables using ordinary least squares (OLS) regression tests across 15 California native oak species. Highlighted cells indicate significant relationships ($p \leq 0.05$).

Table S3.7. Associations of traits and environmental variables using phylogenetic generalized least squares (PGLS) tests across 15 California native oak species. Highlighted cells indicate significant relationships ($p \leq 0.05$).

Table S3.8. Proportion of correlations uncovered within and across the hypothesized structure-function trait clusters out of all possible correlations using the ahistorical correlations.

Table S3.9. Proportion of correlations uncovered within and across the hypothesized structure-function trait clusters out of all possible correlations using evolutionary correlations.

Table S3.10. Trait-level plant network parameters.

Supplementary figure captions

Figure S3.1. Maps showing the occurrences records of *Quercus* species used to estimate the mean climate of the native range of distribution of the 15 California native oak species sampled in this study. Inset we provide a picture of a typical leaf of one individual per species. Colors represent section within the genus *Quercus*: *Lobatae* (red), *Protobalanus* (yellow) and *Quercus* (blue). Symbols represent leaf habit, evergreen (circles) and deciduous (squares).

Figure S3.2. Within and across species variation in the indicator trait of each structure-function cluster (one-way ANOVAs; Table S3.5). Panel (a) shows the mean height of sampled individuals, *H*, (b) the leaf area, *LA*, (c) the theoretical maximum stomatal conductance, G_{max}, (d) the leaf mass per area, *LMA*, (e) the nitrogen concentration per leaf mass, N_{mass}, and (f) the water potential at turgor loss, π_{tlp}. Colors represent section within the genus *Quercus*: *Lobatae* (red), *Protobalanus* (yellow) and *Quercus* (blue). Symbols represent leaf habit, evergreen (circles) and deciduous (squares).

Figure S3.3. Networks showing the coordination of 90 functional traits measured in 15 species of California native oaks grown in a common garden. Networks were built from a matrix of trait-trait phylogenetic correlations (phylogenetic generalized least squares, PGLS; Table S3.7) and correlations were considered significant when $p < 0.05$. Colored nodes were hypothesized *a priori* to belong to each of the six structure-function clusters; the indicator traits of each cluster are highlighted in darker colors (Table S3.1).

Figure S3.4. Degree of connectedness, *k*, and betweeness, *b*, of the traits hypothesized *a priori* to to belong to each structure-function cluster. The indicator traits of each cluster are highlighted in darker colors (Table S3.1).

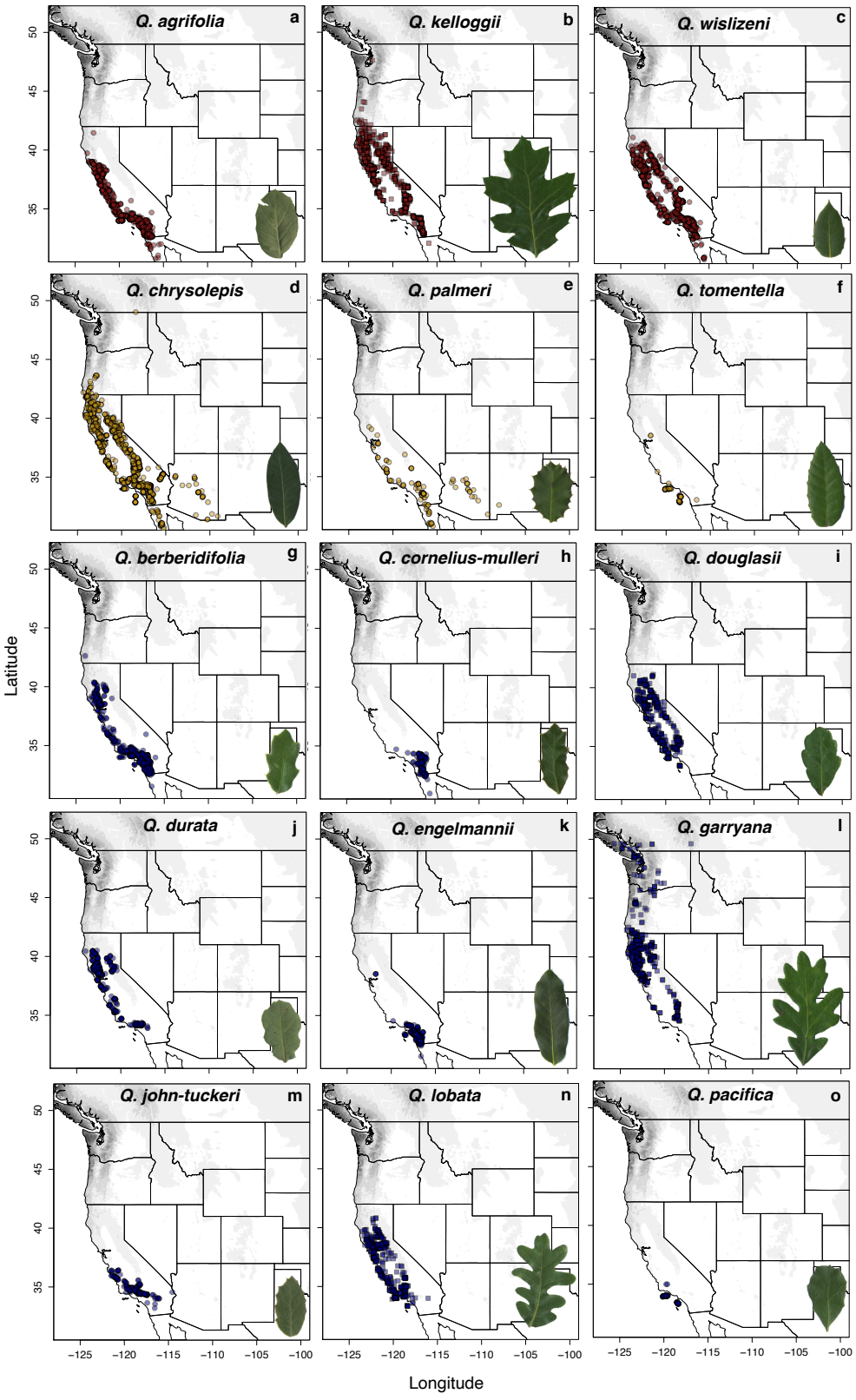
Q. agrifolia
a
Q. kelloggii
b
Q. wislizeni
c
Q. chrysolepis
d
Q. palmeri
e
Q. tomentella
f
Q. berberidifolia
g
Q. cornelius-mulleri
h
Q. douglasii
i
Q. durata
j
Q. engelmannii
k
Q. garryana
l
Q. john-tuckeri
m
Q. lobata
n
Q. pacifica
o
Latitude
Longitude
50
45
40
35
−125
−120
−115
−110
−105
−100

Figure S3.1

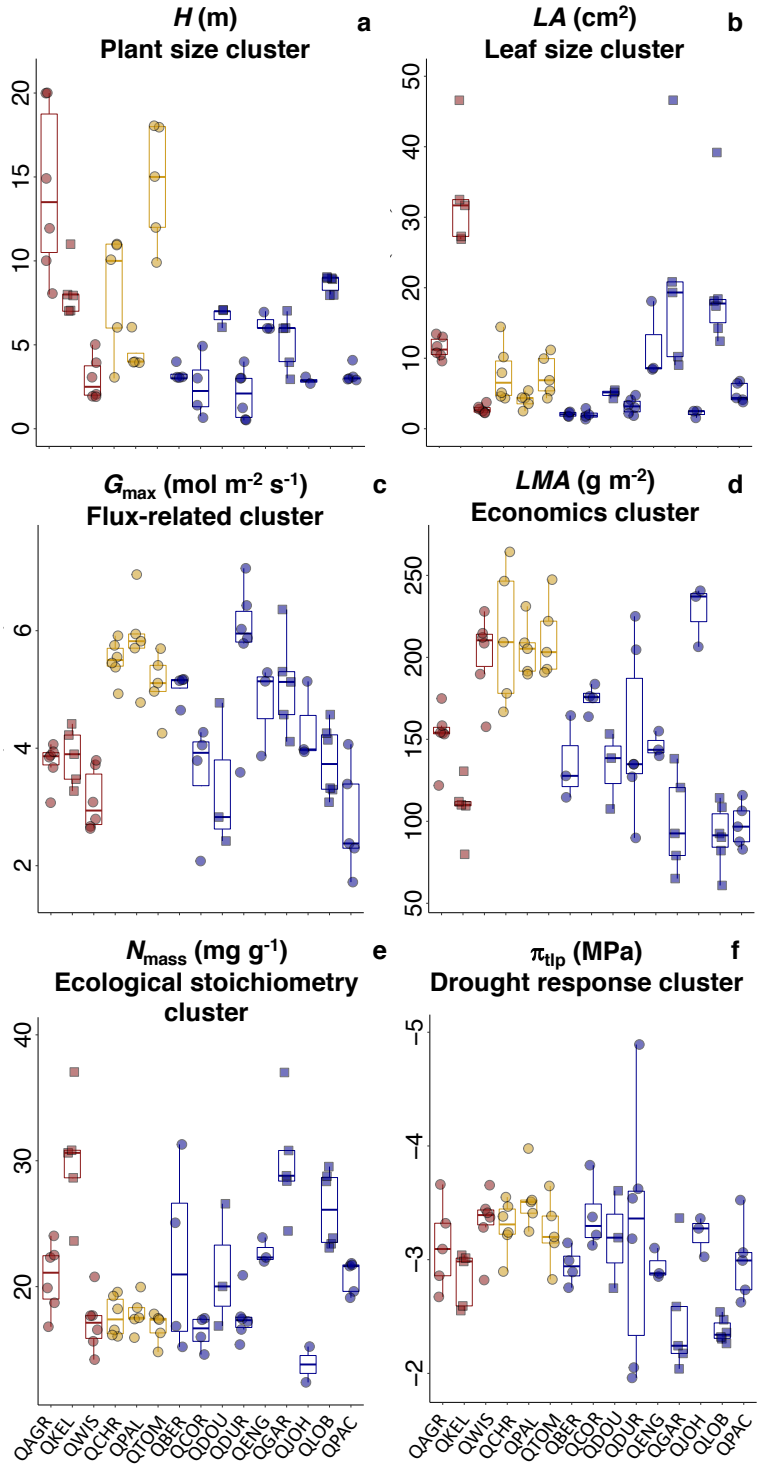
H (m)
Plant size cluster
a
LA (cm²)
Leaf size cluster
b
Gmax (mol m-2 s-1)
Flux-related cluster
c
LMA (g m-2)
Economics cluster
d
Nmass (mg g-1)
Ecological stoichiometry cluster
e
πtlp (MPa)
Drought response cluster
f
QAGR
QKEL
QWIS
QCHR
QPAL
QTOM
QBER
QCOR
QDOU
QDUR
QENG
QGAR
QJOH
QLOB
QPAC

Figure S3.2

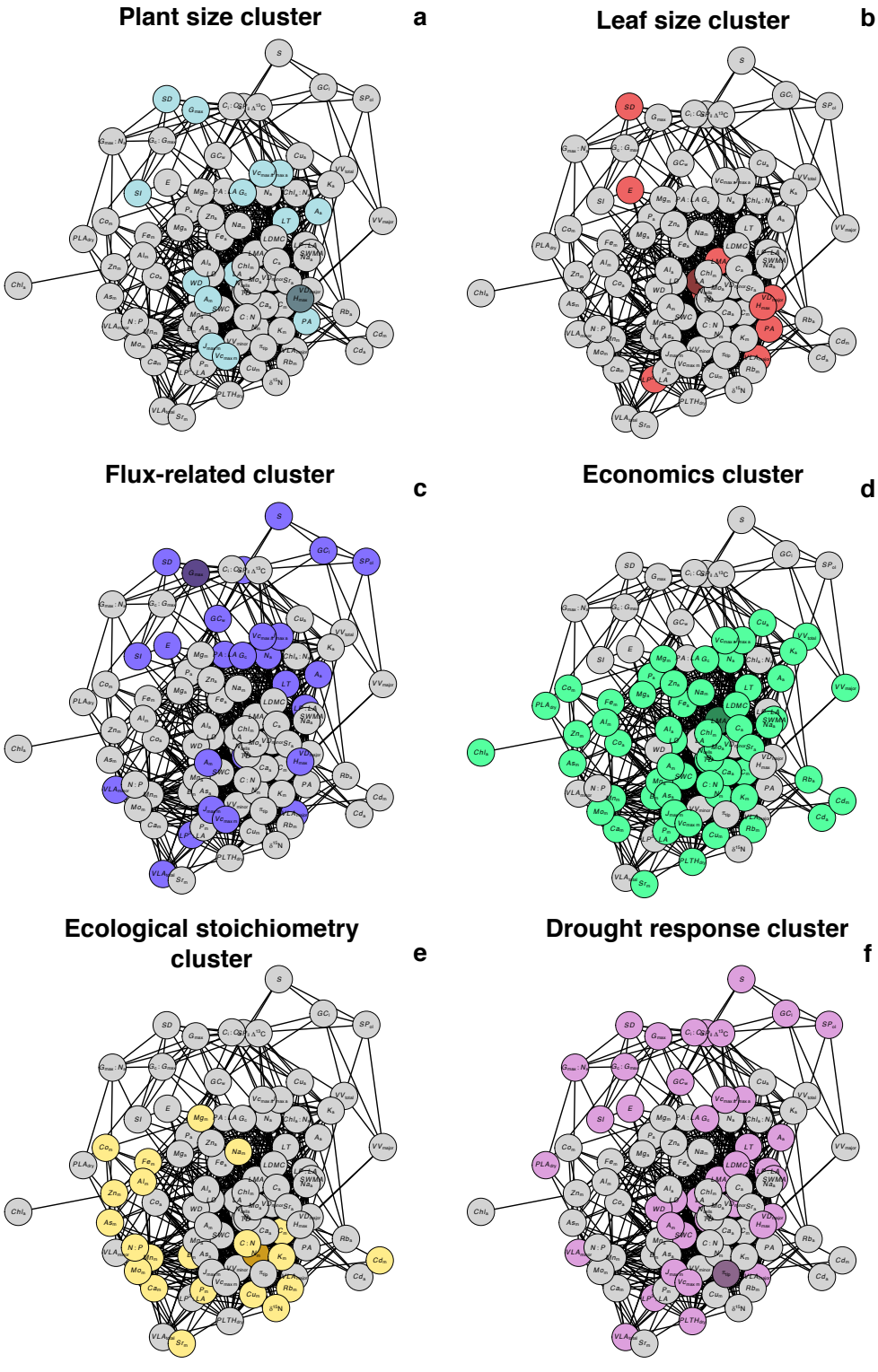
Plant size cluster
a
Leaf size cluster
b
Flux-related cluster
c
Economics cluster
d
Ecological stoichiometry cluster
e
Drought response cluster
f

Figure S3.3

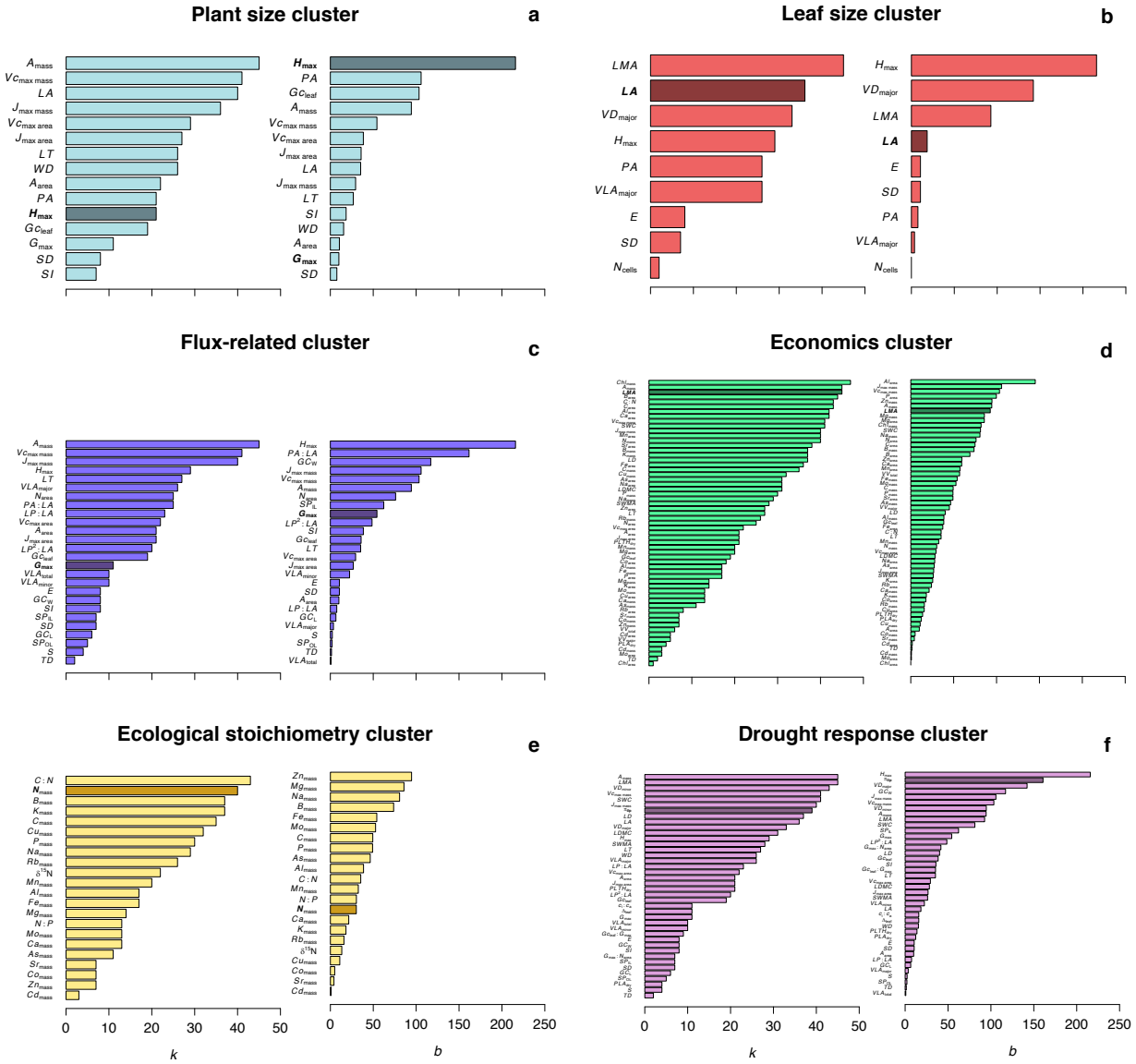
Plant size cluster
a
Leaf size cluster
b
Flux-related cluster
c
Economics cluster
d
Ecological stoichiometry cluster
e
Drought response cluster
f
k
b
k
b

Figure S3.4

REFERENCES

Alonso-Forn, D., Sancho-Knapik, D., Ferrio, J.P., Peguero-Pina, J.J., Bueno, A., Onoda, Y., *et al.* (2020). Revisiting the functional basis of sclerophylly within the leaf economics spectrum of oaks: Different roads to Rome. *Curr Forestry Rep*, 6, 260–281.

Anderegg, W.R.L. (2015). Spatial and temporal variation in plant hydraulic traits and their relevance for climate change impacts on vegetation. *New Phytol*, 205, 1008–1014.

Bartlett, M.K., Scoffoni, C., Ardy, R., Zhang, Y., Sun, S., Cao, K., *et al.* (2012). Rapid determination of comparative drought tolerance traits: using an osmometer to predict turgor loss point. *Methods Ecol Evol*, 3, 880–888.

Brodribb, T.J., Skelton, R.P., McAdam, S.A.M., Bienaimé, D., Lucani, C.J. & Marmottant, P. (2016). Visual quantification of embolism reveals leaf vulnerability to hydraulic failure. *New Phytol*, 209, 1403–1409.

Cavender-Bares, J., G. Fontes, C. & Pinto-Ledezma, J. (2020). Open questions in understanding the adaptive significance of plant functional trait variation within a single lineage. *New Phytol*, 227, 659–663.

Cavender-Bares, J., González-Rodríguez, A., Eaton, D.A.R., Hipp, A.A.L., Beulke, A. & Manos, P.S. (2015). Phylogeny and biogeography of the American live oaks (*Quercus* subsection *Virentes*): a genomic and population genetics approach. *Mol Ecol*, 24, 3668–3687.

Chamberlain, S., Ram, K., Mcglinn, D. & Barve, V. (2019). *rgbif: A programmatic interface to the Web Service methods provided by the Global Biodiversity Information Facility*.

Chave, J., Coomes, D., Jansen, S., Lewis, S.L., Swenson, N.G. & Zanne, A.E. (2009). Towards a worldwide wood economics spectrum. *Ecol Lett*, 12, 351–366.

Cordell, S., Goldstein, G., Mueller-Dombois, D., Webb, D. & Vitousek, P.M. (1998). Physiological and morphological variation in *Metrosideros polymorpha*, a dominant Hawaiian tree species, along an altitudinal gradient: the role of phenotypic plasticity. *Oecologia*, 113, 188–196.

Díaz, S., Kattge, J., Cornelissen, J.H.C., Wright, I.J., Lavorel, S., Dray, S., *et al.* (2016). The global spectrum of plant form and function. *Nature*, 529, 167–171.

Domingues, T.F., Meir, P., Feldpausch, T.R., Saiz, G., Veenendaal, E.M., Schrodt, F., *et al.* (2010). Co-limitation of photosynthetic capacity by nitrogen and phosphorus in West Africa woodlands. *Plant Cell Environ*.

Dunbar-Co, S., Sporck, M.J. & Sack, L. (2009). Leaf trait diversification and design in seven rare taxa of the Hawaiian *Plantago* radiation. *Int J Plant Sci*, 170, 61–75.

Edwards, E.J. (2006). Correlated evolution of stem and leaf hydraulic traits in *Pereskia* (Cactaceae). *New Phytol*, 172, 479–789.

Farquhar, G., O'Leary, M. & Berry, J. (1982). On the Relationship Between Carbon Isotope Discrimination and the Intercellular Carbon Dioxide Concentration in Leaves. *Functional Plant Biol.*, 9, 121.

Farquhar, G.D. & Richards, R.A. (1984). Isotopic composition of plant carbon correlates with water-use efficiency of Wheat genotypes. *Aust J Plant Physiol*, 11, 539–552.

Felsenstein, J. (1985). Phylogenies and the comparative method. *Am Nat*, 125, 1–15.

Fletcher, L.R., Cui, H., Callahan, H., Scoffoni, C., John, G.P., Bartlett, M.K., *et al.* (2018). Evolution of leaf structure and drought tolerance in species of Californian *Ceanothus*. *Am J Bot*, 105, 1672–1687.

Flores-Moreno, H., Fazayeli, F., Banerjee, A., Datta, A., Kattge, J., Butler, E.E., *et al.* (2019). Robustness of trait connections across environmental gradients and growth forms. *Global Ecol Biogeogr*, 28, 1806–1826.

Franks, P.J., Drake, P.L. & Beerling, D.J. (2009). Plasticity in maximum stomatal conductance constrained by negative correlation between stomatal size and density: an analysis using *Eucalyptus globulus*. *Plant Cell Environ*.

Franks, P.J. & Farquhar, G.D. (2007). The mechanical diversity of stomata and its significance in gas-exchange control. *Plant Physiol*, 143, 78–87.

Franks, P.J., Royer, D.L., Beerling, D.J., Van de Water, P.K., Cantrill, D.J., Barbour, M.M., *et al.* (2014). New constraints on atmospheric CO2concentration for the Phanerozoic. *Geophys Res Lett*.

Freckleton, R.P., Harvey, P.H. & Pagel, M. (2002). Phylogenetic analysis and comparative data: a test and review of evidence. *Am Nat*, 160, 712–726.

Fry, B., Ganitt, R., Tholke, K., Neill, C., Michener, R.H., Mersch, F.J., *et al.* (1996). Cryoflow: Cryofocusing Nanomole Amounts of CO2, N2, and SO2 from an Elemental Analyzer for Stable Isotopic Analysis. *Rapid communications in mass spectrometry*.

Givnish, T.J. & Montgomery, R.A. (2014). Common-garden studies on adaptive radiation of photosynthetic physiology among Hawaiian lobeliads. *Proc R Soc B*, 281, 20132944.

González de Andrés, E., Rosas, T., Camarero, J.J. & Martínez-Vilalta, J. (2021). The intraspecific variation of functional traits modulates drought resilience of European beech and pubescent oak. *J Ecol*, 1365-2745.13743.

Grime, J.P. (1979). *Plant strategies and vegetation processes*. 1st edn. Wiley, Chichester.

Grime, J.P. (2006). *Plant strategies, vegetation processes, and ecosystem properties*. 2nd edn. Chichester.

Grubb, P.J. (1985). Plant populations and vegetation in relation to habitat, disturbance and competition: problems of generalization. In: *The population structure of vegetation. Handbook of Vegetation Science.* Springer, Dordrecht.

Hao, G.-Y., Sack, L., Wang, A.-Y., Cao, K.-F. & Goldstein, G. (2010). Differentiation of leaf water flux and drought tolerance traits in hemiepiphytic and non-hemiepiphytic Ficus tree species: Leaf hydraulics and drought tolerance. *Funct Ecol*, 24, 731–740.

Harmon, L.J. (2019). *Phylogenetic comparative methods*.

Harrison, S. (1997). How natural habitat patchiness affects the distribution of diversity in Californian serpentine chaparral. *Ecology*, 78, 1898–1906.

He, N., Li, Y., Liu, C., Xu, L., Li, M., Zhang, J., *et al.* (2020). Plant Trait Networks: Improved Resolution of the Dimensionality of Adaptation. *Trends Ecol Evol*, 35, 908–918.

Hengl, T., Mendes de Jesus, J., Heuvelink, G.B.M., Ruiperez Gonzalez, M., Kilibarda, M., Blagotić, A., *et al.* (2017). SoilGrids250m: Global gridded soil information based on machine learning. *PLoS ONE*, 12, e0169748.

Hijmans, R.J., Cameron, S.E., Parra, J.L., Jones, P.G. & Jarvis, A. (2005). Very high resolution interpolated climate surfaces for global land areas. *Int J Climatol*, 25, 1965–1978.

Hijmans, R.J. & van Etten, J. (2012). *raster: Geographic analysis and modeling with raster data*. R. .

Hijmans, R.J., Phillips, S., Leathwick, J. & Elith, J. (2011). *Package 'dismo'*. R. .

Hipp, A.L., Manos, P.S., González-Rodríguez, A., Hahn, M., Kaproth, M., McVay, J.D., *et al.* (2018). Sympatric parallel diversification of major oak clades in the Americas and the origins of Mexican species diversity. *New Phytol*, 217, 439–452.

Hipp, A.L., Manos, P.S., Hahn, M., Avishai, M., Bodénès, C., Cavender-Bares, J., *et al.* (2020). Genomic landscape of the global oak phylogeny. *New Phytol*, 226, 1198–1212.

Jung, V., Albert, C.H., Violle, C., Kunstler, G., Loucougaray, G. & Spiegelberger, T. (2014). Intraspecific trait variability mediates the response of subalpine grassland communities to extreme drought events. *J Ecol*, 102, 45–53.

Kleyer, M., Trinogga, J., Cebrián-Piqueras, M.A., Trenkamp, A., Fløjgaard, C., Ejrnaes, R., *et al.* (2019). Trait correlation network analysis identifies biomass allocation traits and stem specific length as hub traits in herbaceous perennial plants. *J Ecol*, 107, 829–842.

Lavorel, S. & Garnier, E. (2002). Predicting changes in community composition and ecosystem functioning from plant traits: revisiting the Holy Grail. *Funct Ecol*, 16, 545–556.

Li, H., Liu, B., McCormack, M.L., Ma, Z. & Guo, D. (2017). Diverse belowground resource strategies underlie plant species coexistence and spatial distribution in three grasslands along a precipitation gradient. *New Phytol*, 216, 1140–1150.

Maire, V., Gross, N., Hill, D., Martin, R., Wirth, C., Wright, I.J., *et al.* (2013). Disentangling Coordination among Functional Traits Using an Individual-Centred Model: Impact on Plant Performance at Intra- and Inter-Specific Levels. *PLoS ONE*, 8, e77372.

Marks, C.O. & Lechowicz, M.J. (2006). Alternative designs and the evolution of functional diversity. *Am Nat*, 167, 55–66.

Mason, C.M. & Donovan, L.A. (2015). Evolution of the leaf economics spectrum in herbs: Evidence from environmental divergences in leaf physiology across *Helianthus* (Asteraceae). *Evolution*, 69, 2705–2720.

McElwain, J.C., Yiotis, C. & Lawson, T. (2016). Using modern plant trait relationships between observed and theoretical maximum stomatal conductance and vein density to examine patterns of plant macroevolution. *New Phytol*.

Medeiros, C.D., Scoffoni, C., John, G.P., Bartlett, M.K., Inman-Narahari, F., Ostertag, R., *et al.* (2019). An extensive suite of functional traits distinguishes Hawaiian wet and dry forests and enables prediction of species vital rates. *Funct Ecol*, 33, 712–734.

Messier, J., Lechowicz, M.J., McGill, B.J., Violle, C., Enquist, B.J. & Cornelissen, H. (2017). Interspecific integration of trait dimensions at local scales: the plant phenotype as an integrated network. *J Ecol*.

Monje, O.A. & Bugbee, B. (1992). Inherent Limitations of Nondestructive Chlorophyll Meters: A Comparison of Two Types of Meters. *HortScience*.

Ogburn, R.M. & Edwards, E.J. (2012). Quantifying succulence: a rapid, physiologically meaningful metric of plant water storage. *Plant Cell Environ*.

Oliveira, R.S., Eller, C.B., Barros, F. de V., Hirota, M., Brum, M. & Bittencourt, P. (2021). Linking plant hydraulics and the fast–slow continuum to understand resilience to drought in tropical ecosystems. *New Phytol*, 230, 904–923.

Olson, M.E., Soriano, D., Rosell, J.A., Anfodillo, T., Donoghue, M.J., Edwards, E.J., *et al.* (2018). Plant height and hydraulic vulnerability to drought and cold. *Proc Natl Acad Sci USA*, 115, 7551–7556.

Opedal, Ø.H., Armbruster, W.S. & Graae, B.J. (2015). Linking small-scale topography with microclimate, plant species diversity and intra-specific trait variation in an alpine landscape. *Plant Ecol Divers*, 8, 305–315.

Orme, D., Freckleton, R., Thomas, G., Petzoldt, T., Fritz, S., Isaac, N., *et al.* (2018). *caper: comparative analyses of phylogenetics and evolution in R*.

Ortego, J., Noguerales, V., Gugger, P.F. & Sork, V.L. (2015). Evolutionary and demographic history of the Californian scrub white oak species complex: an integrative approach. *Mol Ecol*, 24, 6188–6208.

Pérez-Harguindeguy, N., Díaz, S., Garnier, E., Lavorel, S., Poorter, H., Jaureguiberry, P., *et al.* (2013). New handbook for standardised measurement of plant functional traits worldwide. *Aust J Bot*, 61.

Peterson, A.T. (1999). Conservatism of ecological niches in evolutionary time. *Science*, 285, 1265–1267.

R Core Team. (2020). *R: a language and environment for statistical computing*. R Foundation for Statistical Computing.

Ramírez-Valiente, J.A., López, R., Hipp, A.L. & Aranda, I. (2020). Correlated evolution of morphology, gas exchange, growth rates and hydraulics as a response to precipitation and temperature regimes in oaks (*Quercus*). *New Phytol*, 227, 794–809.

Reich, P.B. (2014). The world-wide 'fast-slow' plant economics spectrum: a traits manifesto. *J Ecol*, 102, 275–301.

Riordan, E.C., Gillespie, T.W., Pitcher, L., Pincetl, S.S., Jenerette, G.D. & Pataki, D.E. (2015). Threats of future climate change and land use to vulnerable tree species native to Southern California. *Envir Conserv*, 42, 127–138.

Roumet, C., Birouste, M., Picon-Cochard, C., Ghestem, M., Osman, N., Vrignon-Brenas, S., *et al.* (2016). Root structure–function relationships in 74 species: evidence of a root economics spectrum related to carbon economy. *New Phytol*, 210, 815–826.

Sack, L. & Buckley, T.N. (2016). The developmental basis of stomatal density and flux. *Plant Physiol*.

Sack, L. & Buckley, T.N. (2020). Trait multi-functionality in plant stress response. *Integr Comp Biol*, 60, 98–112.

Sack, L., Cowan, P.D., Jaikumar, N. & Holbrook, N.M. (2003). The 'hydrology' of leaves: co-ordination of structure and function in temperate woody species. *Plant, Cell & Environment*.

Sack, L., Scoffoni, C., McKown, A.D., Frole, K., Rawls, M., Havran, J.C., *et al.* (2012). Developmentally based scaling of leaf venation architecture explains global ecological patterns. *Nat Commun*, 3, 837.

Salt, D.E., Baxter, I. & Lahner, B. (2008). Ionomics and the study of the plant ionome. *Annu Rev Plant Biol*, 59, 709–733.

Sancho-Knapik, D., Escudero, A., Mediavilla, S., Scoffoni, C., Zailaa, J., Cavender-Bares, J., *et al.* (2021). Deciduous and evergreen oaks show contrasting adaptive responses in leaf mass per area across environments. *New Phytol*, 230, 521–534.

Schmerler, S.B., Clement, W.L., Beaulieu, J.M., Chatelet, D.S., Sack, L., Donoghue, M.J., *et al.* (2012). Evolution of leaf form correlates with tropical–temperate transitions in *Viburnum* (Adoxaceae). *Proc R Soc B*, 279, 3905–3913.

Scoffoni, C., Rawls, M., McKown, A., Cochard, H. & Sack, L. (2011). Decline of leaf hydraulic conductance with dehydration: Relationship to leaf size and venation architecture. *Plant Physiol*.

Šímová, I., Violle, C., Svenning, J.-C., Kattge, J., Engemann, K., Sandel, B., *et al.* (2018). Spatial patterns and climate relationships of major plant traits in the New World differ between woody and herbaceous species. *J Biogeogr*, 45, 895–916.

Skelton, R.P., Dawson, T.E., Thompson, S.E., Shen, Y., Weitz, A.P. & Ackerly, D. (2018). Low vulnerability to xylem embolism in leaves and stems of north american oaks. *Plant Physiol*, 177, 1066–1077.

Sokal, R.R. & Rohlf, F.J. (2012). Biometry: the principles and practice of statistics in biological research.

Sork, V.L., Riordan, E., Gugger, P.F., Fitz-Gibbon, S., Wei, X. & Ortego, J. (2016). Phylogeny and introgression of California scrub white oaks (*Quercus* section *Quercus*). *Int Oaks*, 27, 61–74.

Tucker, J.M. (1974). Patterns of parallel evolution of leaf form in new world oaks. *TAXON*, 23, 129–154.

Violle, C., Navas, M.-L., Vile, D., Kazakou, E., Fortunel, C., Hummel, I., *et al.* (2007). Let the concept of trait be functional! *Oikos*, 116, 882–892.

Westoby, M. (1998). A leaf-height-seed (LHS) plant ecology strategy scheme. *Plant Soil*, 199, 213–227.

Witkowski, E.T.F. & Lamont, B.B. (1991). Leaf specific mass confounds leaf density and thickness. *Oecologia*.

Wright, I.J., Reich, P.B. & Westoby, M. (2001). Strategy shifts in leaf physiology, structure and nutrient content between species of high- and low-rainfall and high- and low-nutrient habitats. *Funct Ecol*, 15, 423–434.

Wright, I.J., Reich, P.B., Westoby, M., Ackerly, D.D., Baruch, Z., Bongers, F., *et al.* (2004). The worldwide leaf economics spectrum. *Nature*, 428, 821–827.

Zomer, R.J., Trabucco, A., Bossio, D.A. & Verchot, L.V. (2008). Climate change mitigation: A spatial analysis of global land suitability for clean development mechanism afforestation and reforestation. *Agric Ecosyst Environ*, 126, 67–80.

CHAPTER 4

AN EXTENSIVE SUITE OF FUNCTIONAL TRAITS DISTINGUISHES HAWAIIAN WET AND DRY FORESTS AND ENABLES PREDICTION OF SPECIES VITAL RATES

ABSTRACT

The application of functional traits to predict and explain plant species' distributions and vital rates has been a major direction in functional ecology for decades, yet numerous physiological traits have not yet been incorporated into the approach. Using commonly measured traits such as leaf mass per area (*LMA*) and wood density (*WD*), and additional traits related to water transport, gas exchange and resource economics, including leaf vein, stomatal, and wilting traits, we tested hypotheses for Hawaiian wet montane and lowland dry forests (MWF and LDF respectively): (1) forests would differ in a wide range of traits as expected from contrasting adaptation; (2) trait values would be more convergent among dry than wet forest species due to the stronger environmental filtering; (3) traits would be inter-correlated within "modules" supporting given functions; (4) relative growth rate (*RGR*) and mortality rate (*m*) would correlate with a number of specific traits, with (5) stronger relationships when stratifying by tree size, and (6) *RGR* and *m* can be strongly explained from trait-based models. The MWF species' traits were associated with adaptation to high soil moisture and nutrient supply and greater shade tolerance whereas the LDF species' traits were associated with drought tolerance. Thus, on average, MWF species achieved higher maximum heights than LDF species and had leaves with larger epidermal cells, higher maximum stomatal conductance and CO_2 assimilation rate, lower vein lengths per area, higher saturated water content and greater shrinkage when dry, lower dry matter content, higher

phosphorus concentration, lower nitrogen to phosphorus ratio, high chlorophyll to nitrogen ratio, high carbon isotope discrimination, high stomatal conductance to nitrogen ratio, less negative turgor loss point, and lower *WD*. Functional traits were more variable in the MWF than LDF, were correlated within modules, and predicted species' *RGR* and *m* across forests, with stronger relationships when stratifying by tree size. Models based on multiple traits predicted vital rates across forests (R^2 = 0.70-0.72; $P < 0.01$). Our findings are consistent with a powerful role of broad suites of functional traits in contributing to forest species' distributions, integrated plant design, and vital rates.

INTRODUCTION

Functional traits influence plant growth, reproduction and survival and thereby fitness (Lavorel & Garnier 2002; Violle *et al.* 2007), and thus can be used to predict vital rates (Poorter *et al.* 2008; Adler *et al.* 2014; Uriarte *et al.* 2016), habitat preferences (Shipley *et al.* 2017) and spatial distributions (Stahl *et al.* 2014). For decades, most studies have focused on relatively few commonly measured functional traits, with some justification given that overall trait variation can be simplified statistically into a few fundamental dimensions (Díaz *et al.* 2016; Messier *et al.* 2017). However, several have argued that more extensive suites of traits would enable strong predictive and explanatory power (Reich 2014; Paine *et al.* 2015; Greenwood *et al.* 2017; Yang *et al.* 2018), and this argument has conceptual support because mechanistic models of growth and survival are sensitive to a broad set of traits as inputs (Marks & Lechowicz 2006; Sterck *et al.* 2006; Osborne & Sack 2012). The traits measured in this study include well-studied functional traits within the leaf and wood "economics spectra" (LES and WES, respectively), that describe trade-offs in plant carbon balance with given traits contributing to either fast growth and resource turnover, or slow growth and longer tissue lifespans and stress tolerance (Wright *et al.* 2004; Chave *et al.* 2009). In addition, we included a wider set of traits recognized to have proximal physiological influence on water transport, gas exchange and resource economics. The aim of this study was to assess six key hypotheses derived from first principles in trait physiology and ecology (Table 4.1), utilizing 45 traits expected to show contrasting adaptation across forests, and/or to influence relative growth rate (RGR_{dbh} and RGR_{biom}) and mortality (m) (Table 4.2). We pursued this aim while recognizing that many more traits than those we included play important roles, and that species differ in the traits with most important influence on vital rates.

First, we tested the ability of an extensive suite of traits to resolve variation between Hawaiian wet and dry forest species given their contrasting adaptation. We assessed traits which, based on the previous literature, would have specific mechanistic influences on resource acquisition, growth and stress tolerance (Table 4.2, with detailed reasoning in Appendix Table 4.1). In particular, we expected that relative to the dry forest, the wet forest species would have shifted their traits values in the direction beneficial to their adaptation to greater availability of water and soil nutrients. Such trait shifts would include greater mean and maximum plant height (Koch *et al.* 2004; King *et al.* 2006); lower wood density (*WD*; (Hacke *et al.* 2001; Chave *et al.* 2009; Gleason *et al.* 2016)) and seed mass (Gross 1984; Khurana & Singh 2004); higher overall rates of photosynthesis, and rates of electron transport and carboxylation (all per unit leaf area and/or dry mass), and higher values for the ratio of internal to ambient CO_2 (c_i:c_a), related to higher values of carbon isotope discrimination (Δ_{leaf}; (Farquhar *et al.* 1989; Donovan & Ehleringer 1994; Franks *et al.* 2009; Wang *et al.* 2017)); larger and denser stomata and higher stomatal conductance (Hetherington & Woodward 2003; Franks & Farquhar 2007; Beaulieu *et al.* 2008; Franks *et al.* 2009; Wang *et al.* 2015; Sack & Buckley 2016); higher densities of leaf major and minor veins and free ending veins (Sack & Frole 2006; Brodribb *et al.* 2007; Sack & Scoffoni 2013; Iida *et al.* 2016; Scoffoni *et al.* 2016); thinner and larger leaves of higher saturated water content and lower dry mass density, lower water mass and dry mass per area and lower dry matter content with lesser shrinkage in area under dehydration (Evans 1973; Niinemets 2001; Vendramini *et al.* 2002; Wright *et al.* 2004; Westoby & Wright 2006; Bartlett *et al.* 2012b; Ogburn & Edwards 2012; Sack & Scoffoni 2013; Scoffoni *et al.* 2014; Díaz *et al.* 2016); high foliar concentrations of nitrogen (N), phosphorus (P), and chlorophyll, and lower concentration of carbon (Lambers & Poorter 2004; Wright *et al.* 2004; Chaturvedi *et al.* 2011); lower *N*:*P* (Elser *et al.* 2000); and greater stomatal

opening relative to maximum aperture, and relative to N (Wright *et al.* 2001; Franks *et al.* 2009). Given that species of the wet forest are adapted to lower understorey irradiance also led to the expectation of lower rates of photosynthesis and greater Δ_{leaf} (Farquhar *et al.* 1989; Donovan & Ehleringer 1994; Franks *et al.* 2009; Evans 2013), larger leaf area (Niinemets 2001; Chaturvedi *et al.* 2011), lower *LMA* (Walters & Reich 1999; Sack *et al.* 2003b), lower N and P and higher C and chlorophyll concentration (*Chl*; Givnish 1988; (Niinemets 2001; Lusk & Warton 2007; Poorter 2009; Chaturvedi *et al.* 2011); higher *Chl* to N ratio (Givnish 1987); and lower stomatal and vein densities (Givnish 1987; Sack *et al.* 2012; Sack & Scoffoni 2013). The literature also supports contrasting hypotheses in which dry forest species gain drought tolerance by achieving higher photosynthetic activity when water is available, linked with smaller and more numerous stomata and epidermal cells (Maximov 1931; Grubb 1998; Scoffoni *et al.* 2011; Wang *et al.* 2017), higher vein densities (Sack & Scoffoni 2013), and high N and P per mass (Wright *et al.* 2001). We also expected the dry forest species to have more negative turgor loss point (Bartlett *et al.* 2012b), thick and small leaves (Sack *et al.* 2012; Wright *et al.* 2017) and high *WD* (Hacke *et al.* 2001; Chave *et al.* 2009; Gleason *et al.* 2016), and traits associated with high water use efficiency, reflected in as low c_i:c_a and carbon isotope discrimination (Farquhar *et al.* 1989; Donovan & Ehleringer 1994).

Second, we tested the hypothesis that on average, species of the dry forest would have narrower ranges in trait values than the wet forest (Nathan *et al.* 2016). Two main processes of community assembly affect functional diversity at local scale: environmental (or habitat) filtering and biotic interactions (Chesson 2000; Cornwell *et al.* 2006; Asefa *et al.* 2017). In low-resource habitats, environmental filtering is expected to more strongly constrain trait diversity, as would the reduction of biotic interactions which would promote greater niche overlap (Weiher & Keddy 1995; Lebrija-Trejos *et al.* 2010; Nathan *et al.* 2016).

Third, we tested the hypothesis that traits would be inter-correlated in "modules" due to their contributions to given functions (Sack *et al.* 2003a; Li *et al.* 2015a) or "strategies" (Westoby *et al.* 2002). Modules are defined as clusters of traits that show co-variation among themselves, due to-selection, but are relatively independent of other clusters (Wagner & Altenberg 1996; Armbruster *et al.* 2014). Such co-selection has been a main explanation for why plant phenotypes are organized into dimensions (or axes), such as the leaf and wood economic spectra (Wright *et al.* 2004; Chave *et al.* 2009). Several of the newly added traits are expected to be mechanistically related to traits from the LES and WES and are therefore grouped within the same trait modules (Table 4.2).

Fourth, we hypothesized that across species *RGR* and *m* would be positively correlated due to life history trade-offs, and parallel associations with given traits (Kitajima 1994; Russo *et al.* 2010; Wright *et al.* 2010; Philipson *et al.* 2014; Visser *et al.* 2016). Thus, we hypothesized that *RGR* and *m* would relate positively to photosynthetic rate (Donovan & Ehleringer 1994; Franks *et al.* 2009); leaf area (Iida *et al.* 2016), N and P concentrations (Osone *et al.* 2008; Iida *et al.* 2016); the sizes and numbers of stomata (Hetherington & Woodward 2003; Wang *et al.* 2015); maximum stomatal conductance and vein densities (Hetherington & Woodward 2003; Iida *et al.* 2016), and negatively to *LMA* (Osone, Ishida & Tateno 2008; Wright *et al.* 2010; Iida *et al.* 2016); leaf thickness, density and dry matter content (Niinemets 2001; Iida *et al.* 2016); *N*:*P* (Elser *et al.* 2000); and *WD* (Wright *et al.* 2010; Philipson *et al.* 2014; Visser *et al.* 2016). We also tested whether trait relationships with vital rates differed between forests (Kobe & Coates 1997; Lusk & Warton 2007).

Fifth, we expected to uncover more relationships of traits with vital rates when accounting for tree size (Iida *et al.* 2014, 2016; Prado-Junior *et al.* 2016).

Finally, based on the expectations of strong trait-vital rate associations, we hypothesized that *RGR* and *m* can be predicted based on trait-based models.

Our study focused on Hawaiian forests with low species diversity located across highly contrasting environments (Table 4.3) (Price & Clague 2002; Ostertag *et al.* 2014). By testing our framework of hypotheses, we more generally addressed the question of whether considering an extensive suite of mechanistic traits has value for trait-based ecological theory and applications.

METHODS

(For additional details for each methods section, see correspondingly-named section in the supplementary methods, Appendix 4.1)

Study sites

The study was based in forest dynamics plots (FDPs) on Hawai‘i Island within montane wet forest (MWF) and within lowland dry forest (LDF), part of the Hawai‘i Permanent Plot Network established in 2008-9 (HIPPNET; Fig. 4.1; Supplementary Methods; (Ostertag *et al.* 2014)). The MWF and LDF plots contrast strongly in climate and soil composition: the substrate in the MWF is formed from weathered volcanic material, and is old, deep, and moderately well-drained, while LDF has younger, shallow, and highly organic substrate (websoilsurvey.nrcs.usda.gov). The forests also have distinct species, with only *Metrosideros polymorpha* common to both, being the canopy co-dominant in the MWF and limited to a few individuals in the LDF.

Both FDPs were established using the standard methodology of the Center for Tropical Forest Science global FDP network (Condit 1998). From 2008 to 2009, all live, native woody plants ≥1 cm diameter at breast height (DBH, at 130 cm), were tagged and mapped relative to 5 m × 5 m grids installed throughout the plots and measured for DBH (Ostertag *et al.* 2014).

Some of our study questions were addressed by comparing these single forests that were selected to be highly representative of their forest type, an approach previously used in many ecophysiological comparisons of forests (e.g., (Baltzer *et al.* 2008; Markesteijn *et al.* 2010; Blackman *et al.* 2012; Zhu *et al.* 2013; Falcão *et al.* 2015)). Notably, statistical differences between forests are not necessarily generalizable, but enable refined hypotheses for testing in future studies of replicate forests of each type. However, when predicting species' vital rates from traits, statistical significance is expected to reflect a higher generality, as each species represents a replicate data point (Sokal & Rohlf 2012).

Measurement of relative growth rate, mortality

A total of 21,805 individual trees of 29 species from both forest plots were measured for DBH in the first census, 2008, and the 18,745 of those trees that were alive were remeasured in the second census in 2013. From individual plant DBH in both censuses, we used the function '*AGB.tree*' available in the '*CFTS R Package*' (ctfs.si.edu/Public/CTFSRPackage/) to calculate above ground biomass using allometric equations specific for "wet" and "dry" forests that use DBH and wood density as species-specific inputs following (Chave *et al.* 2005). We then calculated relative growth rates in DBH and above-ground biomass (RGR_{dbh} and RGR_{biom}, respectively) as $\frac{\ln(x_{t1})-\ln(x_{t0})}{\Delta t}$, where x is DBH or above-ground biomass and Δt is the time between measurements (in years). RGR_{dbh} is the most commonly used in the literature, but RGR_{biom} is arguably most relevant for relating mechanistically to traits on one hand, and to forest scale processes on the other (Gil-Pelegrín *et al.* 2017). Annual mortality rate (m) was calculated for each of the same 29 species using survival data from both censuses as $m = \left[1 - \left(\frac{N_1}{N_0}\right)^{\frac{1}{\Delta t}}\right] \times 100$, where N_1 is the number of

live individuals at census 2, N_0 is the number of live individuals at census 1, and Δt is the time between measurements (in years; (Sheil *et al.* 1995)). Due to the potential for demographic stochasticity in small populations to affect vital rate estimates, species with <15 individuals were excluded from analyses of *RGR* and *m* (Fiske *et al.* 2008); for RGR_{dbh} the mean coefficient of variation was fivefold higher for species with $n > 15$ than those with $n < 15$ individuals (80% and 16% respectively).

Seed mass and maximum height

Species' mean height (*H*) was calculated across all individuals in the plot, estimated from allometries (Ostertag *et al.* 2014), and maximum height (H_{max}) was calculated as the 95th percentile height of each species. Seed dry mass values were compiled from seed banks across Hawai'i (L. Sack & A. Yoshinaga, unpublished data).

Sampling for leaf and wood trait measurements

We sampled all native woody species from both forest dynamics plots, i.e., 20 species in the MWF and 15 species in the LDF (Table 4.3; Ostertag *et al.* 2014). Data were collected for five randomly selected individuals per species, given availability in the plot, but stomatal and venation traits were measured for only three randomly selected individuals; for this study, those three individuals per species were used for all trait analyses. For each individual, we used pole pruners to collect the most exposed mature branch grown in the current year, with no signs of damage and herbivory. Branches were carried to the lab in plastic with moist paper and rehydrated overnight under plastic before harvesting stem sections and fully expanded leaves and stems for all subsequent analyses. For compound-leafed species (Table 4.3), leaflets were used; for *Acacia koa*, phyllodes were used.

Leaf stomatal and venation traits

We measured stomatal and venation traits on one leaf from each of three individuals per species. Stomatal measurements were obtained from microscopy images taken from nail varnish impressions of both leaf surfaces. We measured stomatal density (*d*) and stomatal index (i.e., differentiation rate, the number of stomata per numbers of stomata plus epidermal pavement cells, *i*), stomatal pore length (SP_L), guard cell length and width (GC_L, GC_W), stomatal area (*s*), and epidermal pavement cell area (*e*) (Sack *et al.* 2006), and calculated the maximum theoretical stomatal conductance (g_{max}; (Franks & Farquhar 2007; Sack & Buckley 2016)).

For the venation traits, fixed leaves were cleared, stained and scanned for major vein density (VLA_{major}) and the top, middle and bottom of each leaf were imaged under light microscope for measurements of minor and free ending vein densities (VLA_{minor} and *FEV*) (Scoffoni *et al.* 2011). *Euphorbia multiformis* var. *microphylla* (EUPMUL; Table 4.3), the single C_4 species in the study (Yang *et al.* 2016), was removed from analyses of across-species correlations of vein traits with vital rates; C_4 species are known to differ from C_3 species in the relationship of photosynthetic rate to vein density, and thus would be expected to differ in their relationships of vital rates to vein traits (Ogle 2003).

Leaf and wood economics and structure, and leaf composition

Leaf structure and composition traits were measured in three leaves per studied individual. Leaf saturated mass was measured using an analytical balance (0.01 mg; XS205; Mettler-Toledo, OH, USA) and leaf thickness (*LT*) using digital calipers (0.01 mm; Fowler, Chicago, IL, USA). The leaf area (*LA*) was measured using a flatbed scanner and analyzed using the software ImageJ (http://imagej.nih.gov/ij/). After scanning, leaves were oven-dried at 70º for 72 h and their dry

mass and area were measured again. Leaf mass per area (*LMA*) was calculated as lamina dry mass divided by saturated area; leaf density (*LD*) as *LMA* divided by *LT*; saturated water content (*SWC*) as (saturated mass minus dry mass) divided by dry mass; water mass per area (*WMA*) as the (saturated mass minus dry mass) divided by saturated area; leaf dry matter content (*LDMC*) as dry mass divided by saturated mass; and percentage loss in area after drying (PLA_{dry}) as the percent decline in area from saturated to dry leaves (Witkowski & Lamont 1991; Ogburn & Edwards 2012; Pérez-Harguindeguy *et al.* 2013).

We measured wood density (*WD*) from one 5 cm-branch segment of each of the studied individuals after bark removal by water-displacement (Pérez-Harguindeguy *et al.* 2013).

The concentration of leaf nitrogen, phosphorus, carbon per mass (N_{mass}, P_{mass} and C_{mass}), and carbon isotope ratio ($\delta^{13}C$) were determined using oven-dried leaves of three individuals per species by the University of Hawaii at Hilo Analytical Laboratory facility (Fry *et al.* 1996; Pérez-Harguindeguy *et al.* 2013). N_{mass} and P_{mass} were converted into N_{area} and P_{area} by multiplying by *LMA*. The carbon isotope discrimination (Δ_{leaf}; in parts per thousand, ‰) was calculated following (Farquhar & Richards 1984). The chlorophyll concentration per area (*Chl*) was measured using a SPAD meter ((Monje & Bugbee 1992); SPAD-502, Konica Minolta, Japan), and the chlorophyll concentration per mass was determined by dividing by *LMA*.

Turgor loss point (π_{tlp}) was measured in three leaves per studied individual. We used a vapor-pressure osmometer (Vapro 5520, Wescor, US) to obtain the osmotic concentration (π_o) of the leaves and used calibration equations to estimate π_{tlp} (Bartlett *et al.* 2012a).

Estimating photosynthetic traits

We estimated maximum rate of carboxylation per mass ($Vcmax_{mass}$) and electron transport rate ($Jmax_{mass}$) from leaf N and P concentrations per mass (Domingues *et al.* 2010). The ratio between intercellular CO_2 concentration (c_i) and ambient CO_2 concentration (c_a) was estimated from Δ_{leaf} (Farquhar *et al.* 1982; Franks *et al.* 2014). Estimates of leaf lifetime integrated CO_2 assimilation rate ($\bar{A}_{mass}$) and stomatal conductance to CO_2 ($\bar{g}_{cleaf}$) were derived from $Vcmax_{mass}$, $Jmax_{mass}$ and isotope composition data using the Farquhar, von Caemmerer and Berry model (Franks *et al.* 2009). To convert $Vcmax_{mass}$, $Jmax_{mass}$, and $\bar{A}_{mass}$ to area-basis, we multiplied the trait values by *LMA*. We also calculated the ratio between $\bar{g}_{cleaf}$ and g_{max}, an index of the degree that stomata are open on average relative to their anatomical maximum aperture (McElwain *et al.* 2016), and the ratio between g_{max} and N_{area}, which is negatively related to water retention for a given investment in photosynthetic machinery (Wright *et al.* 2001).

Statistical analyses

Differences in traits between MWF and LDF species were determined using nested ANOVAs with species nested within forest type, followed by a Tukey test at 5% probability when differences were detected (Sokal & Rohlf 2012). Differences between forests in traits established as species means (*RGR*s, *m*, *H*, H_{max} and *SM*) were tested using *t*-tests. Traits that did not fulfill the normality and homocedasticity assumptions were log-transformed prior to analyses. To test whether trait variation differed between forests, we (a) performed *F*-tests to compare the variances in each trait (Minitab Release 17; State College, Pennsylvania, USA) and (b) calculated the coefficient of variation (CV; %) for each trait in each forest as $CV_{forest} = {}^{\sigma_{forest}}/_{\bar{x}_{forest}} \times 100$ and applied a paired *t*-test across all traits.

Functional traits were grouped into six "modules" according to their contributions to given functions or "strategies": the "stomatal morphology" module included traits such as *d* and *s*; the "leaf venation" module included traits such as VLA_{minor} and *FEV*s; the "leaf and wood economics and structure" module included traits such as *LMA* and *WD*; the "leaf composition" module included leaf nutrient concentrations and $|\pi_{tlp}|$; the "estimated photosynthesis" module included traits such as $\bar{A}_{mass}$ and Vc_{max}; and the "plant size" module included traits such as H_{max} and *SM* (Table 4.2).

To investigate trait-trait and trait-vital rate relationships within and across modules we calculated Pearson's correlations for untransformed and log-transformed data, to test for either approximately linear or non-linear (i.e., approximate power-law) relationships respectively, and the higher correlation value is reported in the text. These analyses were applied to all species from both forests (Table S4.4; described in the main text) and to species of each forest separately (Tables S4.5-S4.6).

We focus on frequentist statistical approaches, following the bulk of previous studies on trait-vital rate relationships. However, in the case of analyzing size-dependent changes in the relationships between vital rates (RGR_{dbh} and *m*) and functional traits, we utilized a hierarchical Bayesian approach following (Iida *et al.* 2014), the most sophisticated previous approach for resolving such an influence. Detailed description of parameters, priors and MCMC settings are provided in the Appendix (supplementary methods, Appendix 4.1), and model code is available on GitHub (https://github.com/camilamedeiros/Medeiros_et_al_2018).

RGR_{dbh} for each individual *i*th tree of species *j* ($RGR\text{dbh}_{ij}$), was modeled as a linear function of the natural logarithm of the initial diameter, $DBH1_{ij}$, based on two parameters estimated for

species *j* (α_{kj}; k=1, 2) and given the input of the initial stem diameter ($DBH1_i$), the final stem diameter ($DBH2_i$) and the census interval of the *i*th tree (Δt_i).

$$RGR\mathrm{dbh}_{ij} = \alpha_{1j} + \alpha_{2j} \times \ln(DBH1_i) \quad \text{(Eq1)}$$

$$\ln(DBH2_i) = \ln(DBH1_i) + RGR\mathrm{dbh}_{ij} \times \Delta t_i \quad \text{(Eq2)}$$

To estimate *m* for each individual *i*th tree belonging to species *j* (m_{ij}), we first calculated the probability of survival of the *i*th individual tree (p_i) from observations of whether the tree survived the census period (S_i = 1) or not (S_i = 0). We assumed that S_i followed a Bernoulli distribution of the probability of survival (p_i).

$$S_i \sim Bernoulli(p_i) \quad \text{(Eq3)}$$

The p_i of the *i*th tree was calculated from the per capita annual mortality rate, m_{ij}, adjusted to the census interval (Δt_i). which was a function of three species-specific parameters β_{kj} (k = 1, 2, 3).

$$p_i = \exp(-m_{ij} \times \Delta t_i) \quad \text{(Eq4)}$$

$$\ln(m_{ij}) = \beta_{1j} + \beta_{2j} \times \ln(DBH1_i) + \beta_{3j} \times DBH1_i \quad \text{(Eq5)}$$

Posteriors were estimated via Markov Chain Monte Carlo implemented in JAGS (Just Another Gibbs Sampler; (Plummer 2007)) from R, using the package '*R2Jags'*. These analyses were carried out including all species from both forests.

To analyze trait-demographic rate relationships for given plant size classes, we first calculated RGR_{dbh} and *m* using equations 1 and 5, respectively, by using the posterior distribution of species-specific parameters α_1 and α_2 for RGR_{dbh} (Table S4.7) and β_{1j}, β_{2j} and β_{3j} for *m* (Table S4.7) and substituting the *DBH*1 term for a reference diameter at 1-cm DBH classes (Iida *et al.* 2014). When the DBH of a size class exceeded a given species' actual maximum DBH (calculated as the 95th percentile of the species' individuals in the plots), that species was dropped from the

analysis in larger size classes. We then calculated the Kendall correlation coefficient (τ) between the RGR_{dbh} and m (calculated for each species in each 1-cm *DBH* class) and species' mean values for functional traits. We decided to use Kendall correlation following (Iida *et al.* 2014) because of the typical non-normality of the size-class stratified vital rates (Prado-Junior *et al.* 2016). The maximum DBH class included in our analysis was 10 cm because analysis of correlations lost power with lower species numbers available to test at larger plant sizes ($n < 9$). To reduce the rate of false positive discoveries, the correlations were considered significant only when 99% of the probability distribution (used as credible interval) of τ did not include zero, rather than 95% as in previous studies (Iida *et al.* 2014).

Finally, to test the ability of traits to predict plant RGR_{dbh}, RGR_{biom} and m, we built multiple regression models that included as independent variables functional traits and a term for forest membership (site; coded as 0 for MWF species and 1 for LDF species). We selected 7 traits to include in the models, based on consideration of the 26 traits hypothesized *a priori* to mechanistically influence RGR_{dbh}, RGR_{biom} and m. To avoid collinearity, we did not choose traits that were partially redundant, i.e., correlated, calculated in part from the same measurements, and involved within similar physiological processes and within the same trait category; e.g., we considered *LMA* and not leaf thickness, given that *LMA* equals leaf thickness × density; Table 4.2). We selected the trait most strongly correlated with vital rates from each trait module in Table 4.2, except for the "Leaf and wood economics and structure" module, from which we selected one leaf- and one wood-related trait.

To compare model performance, we included only species that had complete observations for all traits (final sample size = 16 species; Table S4.8). To select the trait-based models that best predicted RGR_{dbh}, RGR_{biom} and m, we used forward, backward and bidirectional procedures of

variable selection and compared models using Akaike Criterion (AIC) and Bayesian Information Criterion (BIC) using the '*stepAIC*' function in the '*MASS*' package (Table S4.9) and calculated the AIC corrected for small sample sizes (AICc) (Hurvich & Tsai 1989; Hastie & Pregibon 1992; Venables & Ripley 2002). To find the percentage contribution of each variable to the prediction of RGR_{dbh}, RGR_{biom} and m, we performed a Hierarchical Partitioning Analysis using the '*hier.part'* package (Chevan & Sutherland 1991).

All statistical analyses and plots were performed using R software (R Core Team 2018) and packages available from the CRAN platform.

RESULTS

Variation in vital rates and functional traits between forests types

On average, m was 39% higher in species from LDF than in species from MWF. Although several MWF species had higher growth rates than those of LDF, species means for RGR_{dbh} and RGR_{biom} were statistically similar in the MWF and LDF (Fig. 4.2).

Traits varied strongly between and within forests. On average across the measured traits, 16% of the total variation was accounted for by forest type, 73% by species-differences within forests, and 11% by individuals within species (nested ANOVAs; Table S4.1). The MWF showed stronger trait variation than the LDF; the variance was higher in the MWF for 20 traits, in the LDF for 6 traits and not different between forests on the remaining 19 traits (F-tests; Table S4.3), and on average across all traits, the coefficient of variation (CV) was 13.5 ± 0.8% in the MWF and 10.1 ± 0.6% in the LDF (paired t-test; $P < 0.001$).

Species from MWF and LDF differed in 24 of the 45 functional traits (53%) used to test hypotheses (Table 4.2, S4.1-S4.2; Fig. 4.2). MWF species had higher values on average for

stomatal index (i) and area (s) and dimensions of guard cells (GC_L, GC_W and SP_L) and epidermal pavement cells (e), and MWF species had on average a 70% higher g_{max} (Fig. 4.2; Table 4.2-S4.1). Additionally, SWC and PLA_{dry} were 47-49% higher in the MWF than in the LDF species, and $\bar{A}_{mass}$, $\bar{g}_{cleaf}$ and c_i:c_a ratio were 28-33% higher for the MWF than the LDF (Fig. 4.2; Table 4.2-S4.1). The MWF species had 49 and 17% higher values than LDF respectively for P_{mass} and g_{max}:N_{area} species, and 82% higher H_{max} (Table 4.2-S4.1-S4.2; Fig. 4.2).

Conversely, species from the LDF had higher values on average for VLA_{major}, VLA_{minor}, VLA_{total}, and $FEVs$ 46-70% than the MWF, and $LDMC$, WD and $N:P$ 22-42% higher (Fig. 4.2; Table 4.2-S1). The LDF species also had a π_{tlp} more negative by 0.6 MPa on average, and 25% lower Δ_{leaf} than MWF species (Fig. 4.2; Table 4.2-S4.1).

Associations among vital rates

Across forests, the two measures of relative growth rates (RGR_{dbh} and RGR_{biom}) were strongly intercorrelated (r = 0.97; P < 0.001), and both were correlated with m (r = 0.55 and 0.57, respectively; P < 0.05; Fig. 4.3A-B). Within the LDF but not the MWF, m was positively correlated with RGR_{dbh} and RGR_{biom} (r = 0.76 and 0.93, respectively; P < 0.05; Tables S4.5-S4.6).

When using the Bayesian approach to account for plant sizes, we found positive correlations between m and both RGR_{dbh} and RGR_{biom} in all size classes ($\tau > 0$; Fig. 4.3C-D).

Trait-trait coordination

Traits were highly inter-correlated within functional modules (i.e., stomatal morphology traits, venation traits, leaf and wood economics and structure traits, and compositional traits) when considering species from both forests together, and in the MWF and LDF separately (Appendix 4.2. Supplementary results, "*Trait-trait coordination*"; Tables S4.4, S4.5 and S4.6).

Trait relationships with plant vital rates

Overall, eight traits were correlated with RGR_{dbh} and/or RGR_{biom} and seven were correlated with m (Table S4.4). Of the 26 traits hypothesized to correlate with vital rates, three traits were correlated with RGR_{dbh}, seven with RGR_{biom}, and two with m across all 35 species (Table S4.4). Thus, RGR_{dbh} and RGR_{biom} were positively correlated with d, i and g_{max} (r ranged from 0.57-0.64; $P < 0.05$; Table S4.4 and S4.8; Fig. 4.4A-B), RGR_{biom} was negatively correlated with LMA and VLA_{minor} (r = -0.5 and -0.56, respectively; $P < 0.05$; Table S4.5 and S4.9; Fig. 4.4D-E) and positively correlated with P_{mass} and $\bar{A}_{mass}$ (r = 0.48 and 0.51, respectively; $P < 0.05$; Table S4.4 and S4.8; Fig. 4.4C,F), and m was positively correlated with both N_{mass} and $\bar{A}_{mass}$ (r = 0.5 and 0.61, respectively; $P < 0.05$; Table S4.8; Fig. 4.4G-H).

Given that species' RGRs did not differ between forests, trait-RGR correlations within forests were tested but not explored (Tables 4.2, S4.2, S4.5 and S4.6). However, the forests differed in m, and in its trait correlations. In the MWF, m was positively correlated with LMA, LD, N_{area}, P_{area}, and P_{mass}, and with photosynthetic traits on both mass and area-basis, $Jmax_{area}$, $Jmax_{mass}$, $Vcmax_{area}$, $Vcmax_{mass}$, $\bar{A}_{area}$, $\bar{A}_{mass}$, and $\bar{g}_{cleaf}$ (r ranged from 0.72 and 0.89; $P < 0.05$; Table S4.5). In the LDF, m was negatively correlated with LA, LMA, LT, $Jmax_{area}$, $Vcmax_{area}$, $\bar{A}_{area}$ and $\bar{g}_{cleaf}$ (r ranged from -0.76 and -0.91; $P < 0.05$; Table S4.6). Notably, the direction of the correlation across species between m and LMA differed between forests, resulting in positive relationships between m and area-based photosynthetic traits in the MWF and negative relationships in the LDF (Fig 4.5A-B). Further, m was positively correlated with P_{mass} in the MWF (r = 0.89; $P < 0.01$; Table S4.5; Fig. 4.5C), and negatively correlated with LA in the LDF (r = -0.76; $P < 0.05$; Table S4.6; Fig. 4.5D).

Functional traits and size-dependent plant relative growth and mortality rates

Many more trait correlations with relative growth rate were resolved when accounting for tree size using the Bayesian approach. Whereas three traits were correlated with RGR_{dbh} without accounting for size class, when using the Bayesian approach to account for plant sizes, 18 traits were correlated with RGR_{dbh} within at least one size class. Within given size classes RGR_{dbh} was positively correlated with *d*, *i*, g_{max}, *LDMC, LD,* C_{mass}, c_i:c_a, $\bar{g}_{cleaf}$, g_{max}:N_{area} (Fig. 4.6A), H_{mean}, and H_{max}, and negatively correlated with *e*, *SWC*, *WMA*, *LA*, PLA_{dry}, $\bar{g}_{cleaf}$:g_{max} and *SM* ($\tau > 0$).

When accounting for plant size, we found correlations of *m* with 18 traits. In all size classes, *m* was positively correlated with N_{mass}, $Jmax_{mass}$, $Vcmax_{mass}$ and $\bar{A}_{mass}$ ($\tau > 0$), and negatively correlated with *LT* ($\tau < 0$). Within given size classes *m* was positively correlated with *d* (Fig. 4.6C), VLA_{major}, N_{area}, P_{mass} (Fig. 4.6D), *N:P*, and $\bar{g}_{cleaf}$, and negatively correlated with *s*, $GC_{L,}$ $GC_{W,}$ *WMA*, C_{mass}, Chl_{area}:N_{area}, and g_{max}:N_{area} ($\tau > 0$).

Notably, the finding of a greater number of significant relationships between traits and vital rates when stratifying by tree size was not based on the (appropriate) use of different correlation methods selected according to the distribution of the data, i.e., the Pearson *r* for the analyses of trait-vital rate correlations when averaging across all individuals for each species, and the Kendall tau when testing these correlations while stratifying by plant size (see Methods). To test this, we also determined the trait-vital rate correlations using Kendall tau when averaging across all individuals for each species, and as for the Pearson test, seven traits were correlated with RGR_{dbh} and/or RGR_{biom} and seven were correlated with *m*. Thus, the finding that more trait-vital rate relationships are significant when stratifying by plant size is robust to the use of different correlation tests.

Predicting RGR_{dbh}, RGR_{biom} and m from functional traits

To predict RGR_{dbh}, RGR_{biom} and m, we built multiple regression models that included the seven nonredundant traits most strongly correlated with vital rates among the 26 hypothesized *a priori* to influence vital rates (d, VLA_{minor}, LMA, WD, N_{mass}, P_{mass} and $\bar{A}_{mass}$) and a term for forest membership (site; coded as 0 for MWF species and 1 for LDF species). The variable selection procedures (Table S4.9) indicated that d, VLA_{minor}, P_{mass} and $\bar{A}_{mass}$ were the best predictors for RGR_{dbh} (adjusted $R^2 = 0.72$; $P < 0.001$; Table 4.4, Fig. 4.7A); d, VLA_{minor}, LMA and P_{mass} for RGR_{biom} (adjusted $R^2 = 0.70$; $P < 0.01$; Table 4.3, Fig. 4.7B); and VLA_{minor}, LMA, P_{mass}, $\bar{A}_{mass}$ and *site* for m (adjusted $R^2 = 0.71$; $P < 0.001$; Table 4.4, Fig. 4.7C).

DISCUSSION

Trait variation between Hawaiian wet and dry forests

We found strong novel trait variation between Hawaiian wet and dry forests, demonstrating that these forests are highly distinct not only in climate and species composition, but also in diversity across an extensive set of traits. While previous studies have shown that wet and dry forests differ in functional traits (Santiago *et al.* 2004; Wright *et al.* 2004; Markesteijn *et al.* 2010; Brenes-Arguedas *et al.* 2013; Fine *et al.* 2015), by including a far wider range of traits related to resource acquisitiveness and stress tolerance, our analyses highlight their power in multiple comparative and predictive applications of trait-based ecology.

The trait differences between forests aligned with their variation in vital rates. While the species of the two forests did not differ on average in *RGR*, the MWF species showed lower mortality rates than the LDF species, consistent with previous work showing higher mortality in drier forests elsewhere (Suarez & Kitzberger 2010; Gaviria *et al.* 2017). The lower mortality of

the MWF species is consistent with the greater supply of water and soil nutrients, related to greater accumulated weathering, organic material formation, N-fixation, and nutrient retention capacity, and its richer microbial community. The positive relationship of *RGRs* and *m* across all species was consistent with that found across species in temperate (Seiwa 2007; Iida *et al.* 2014) and tropical forests (Kitajima 1994; Wright *et al.* 2010; Philipson *et al.* 2014). Our finding of greater trait variation within the wet forest than the dry forest supports the expectations from first principles that the low resource availability in the dry forest would act as a strong environmental filter resulting in functional convergence, and/or promote greater niche overlap among species in the dry forest via fewer potential biotic interactions (Weiher & Keddy 1995; Lebrija-Trejos *et al.* 2010; Kraft *et al.* 2014; Nathan *et al.* 2016).

The greater soil resources in the MWF led to the expectation that species would possess traits associated with photosynthetic productivity and rapid growth. Consistent with this expectation, MWF species had higher values on average for *i* and *s*, dimensions of guard cells (GC_L, GC_W and SP_L) and *e*, g_{max}, *SWC,* PLA_{dry}, P_{mass}, Chl_{area}:N_{area}, $\bar{A}_{mass}$, $\bar{g}_{cleaf}$, c_i:c_a, g_{max}:N_{area}, Δ_{leaf} and H_{max} and lower values for *LDMC, WD*, and *N:P*. By contrast, the higher temperature and lower rainfall of the LDF led to the expectation that species would possess drought tolerance traits. Indeed, LDF species had higher vein densities, $|\pi_{tlp}|$, *WD*, and *LDMC* and lower values for PLA_{dry}, stomatal dimensions, *SWC* and c_i:c_a ratio and $\bar{A}_{mass}$. Finally, the greater understorey shade of the MWF led to expectations of shade adaptation, confirmed for the lower values for vein densities and *LDMC* (Farquhar *et al.* 1989; Stratton *et al.* 2000; Niinemets 2001; Wright *et al.* 2004; Baltzer *et al.* 2008; Chave *et al.* 2009; Li *et al.* 2015a). Beyond these average differences among forests, trait values were consistent with known life history differences among species within and across forests. For example, *Acacia koa*, the fastest growing species overall, had notably high values for

stomatal dimensions and index, and estimated rates of electron transport and gas exchange; drought tolerant *Osteomeles anthyllidifolia*, had high $|\pi_{tlp}|$ and *WD* and low c_i:c_a ratio and $\bar{A}_{mass}$; and shade tolerant *Hedyotis hillebrandii* had high values for stomatal dimensions and *LA*, and low vein densities and *WD*.

Trait correlations across species of wet and dry forests

Our work supported the hypothesis that traits would be inter-correlated, within modules corresponding to a given organ or function (Sack *et al.* 2003a; Li *et al.* 2015a). These trait associations can indicate allometric relationships that arise developmentally, as are found among stomatal traits, vein densities and leaf size (Brodribb *et al.* 2010; Sack *et al.* 2012). Other trait-trait relationships within modules would arise from co-selection for optimal function, e.g., traits related to maximum gas exchange and *RGR* (Scoffoni *et al.* 2016), such as high g_{max} and P_{mass}; drought tolerance (Bartlett *et al.* 2016), such as high $|\pi_{tlp}|$ and $\bar{A}_{mass}$; or shade tolerance (Givnish *et al.* 2005), such as high *LA* and low *WD*.

The numerous trait correlations across species results in a reduced trait "dimensionality", by which most trait variation may be captured by few axes (Díaz *et al.* 2016). However, that finding does not in fact imply that traits are functionally redundant, as correlated traits can contribute semi-distinctly to function and their consideration as separate parameters improves predictive and mechanistic modeling (Sterck *et al.* 2011; John *et al.* 2017). For example, while *LMA* is correlated with other traits that share structural or compositional bases (Finegan *et al.* 2015; John *et al.* 2017) such as *LDMC* or *WMA*, photosynthetic rates and nutrient concentrations, these traits can play non-redundant roles in determining functions such as shade and drought tolerance and in influencing *RGR* and *m* (Tables S4.4-S4.6 and S4.10 for *RGR* traits).

Trait associations with relative growth rates and mortality rates

Several novel trait correlations were found with mean *RGR*s and *m* across species that were expected from theory and that have potential for generality, including the relationships of RGR_{dbh}, RGR_{biom} and/or *m* to $\bar{A}_{mass}$, and *d*, and several relationships were confirmed, such as with H_{max}, *LMA* and *WD*, that were reported in previous studies of temperate (Iida *et al.* 2016) and/or tropical forests (Wright *et al.* 2010; Hérault *et al.* 2011; Finegan *et al.* 2015; Liu *et al.* 2016). The contrasting correlations of traits with *m* between the MWF and LDF, such as *LMA* and $\bar{A}_{area}$ (Fig. 4.6A-B), and the correlations of traits with *m* in one but not the other forest, such as for *LA* and P_{mass} (Fig. 4.6C-D), highlight the context-dependence of trait-vital rate relationships. In the MWF, a high *LMA* was associated with higher *m*, as expected given ist representing the more shade-tolerant species in the understory, which tend to have higher mortality (Kobe & Coates 1997; Lusk & Warton 2007). Conversely, in the LDF, high *LMA* was related to lower *m*, as expected given its representing greater drought tolerance via a lower surface area: volume ratio, and/or a greater mechanical protection contributing to longer leaf lifespan and reduced respiration costs (Westoby *et al.* 2002; Wright *et al.* 2004; Falcão *et al.* 2015).

Hawaiian forests also showed contrasting relationships of certain traits to vital rates than previously reported. For example, vein density contributes mechanistically to greater hydraulic conductance, photosynthetic productivity and *RGR* across diverse species, all else being equal (Sack & Frole 2006; Sack & Scoffoni 2013; Li *et al.* 2015a; Iida *et al.* 2016; Scoffoni *et al.* 2016; Brodribb *et al.* 2017). However, *RGR* was negatively related to vein density across the species of both forests. This negative correlation may reflect the covariation of vein density with other traits negatively related to *RGR*, including traits not considered, such as root traits, and/or it may arise from the high values for LDF species, which is consistent to their adaptation to higher potential

growth in the more limited periods when water is available, though this growth is not achieved integrated over time (Sack & Scoffoni 2013)).

Our study also confirmed the hypothesis that stratifying by plant size improved the frequency of correlations of vital rates with given traits. Stratifying by size has previously been shown to improve resolution of correlations of *RGR* and *m* with traits such as vein densities, *LA*, *LMA*, *SWC*, *LT*, N_{mass} and P_{mass}, *WD* and H_{max} (Iida *et al.* 2014, 2016; Prado-Junior *et al.* 2016), and our study expanded this finding to a wider range of traits. Stratifying by size reduces the confounding influence of ontogenetic shifts in vital rates on cross-species comparisons (Hérault *et al.* 2011). Notably, while we examined trait correlations with *RGR* and *m* for plants of given sizes, as in previous studies conducting this analysis, our trait values were only for the sampled trees of typical mature size. Future studies may further improve resolution of correlations by also considering ontogenetic variation in trait values.

Trait-based predictions of vital rates

Our study showed the value of a broad suite of functional traits for predicting vital rates. Models based on 7 selected traits could explain more than 70% of the variation in RGR_{dbh}, RGR_{biom} and *m* (Table 4.4-S4.9, Fig. 4.7). The most parsimonious models for all three vital rates retained minor vein density and P per mass, and two of them included stomatal density, time integrated CO_2 assimilation rate and *LMA*. These findings highlight the potential of an approach based on an extensive suite of functional traits and the continued need to refine our mechanistic understanding of how suites of traits drive processes at the scale of individuals and whole forests.

Conclusions and limitations of the study

We conclude that the use of an extensive suite of functional traits contributes power to (1) discover and resolve variation across species of forests, as expected from their contrasting adaptation, (2) compare functional convergence across ecosystems, (3) highlight novel trait-trait and (4) trait-vital rate associations, and (5) the mediating role of plant size in these associations, and (6) to predict *RGR* and *m* across species. Recent studies have applied trait data to mechanistic process models to predict forest vital rates, niche differentiation and productivity (Marks & Lechowicz 2006; Sterck *et al.* 2011; Fyllas *et al.* 2014). We propose that including an extensive suite of traits in such models will be a powerful avenue for future research on the functional ecology of contrasting communities, including vital rates and ultimately their responses to climate change and shifts in species' distributions. An important avenue for future research is to consider the incorporation extended traits into estimating and testing species' habitat preferences within and across forests, extending from recent work showing substantial power even based on few traits, such as leaf size, wood density, *LMA*, and seed size (Shipley *et al.* 2017).

We note that some of our study questions were carried out by comparing single forests of each type, and our findings suggest that the approach has value for further testing replicate forests of each type. Additionally, models are needed of the specific processes involved in vital rates, in which traits can be included along with climate, to resolve how specific trait variation scales up to influencing *RGR* and *m*. Our approach focused on the correlations of single traits and suites of traits with *RGR* and *m*, a central approach in trait-based ecology. However, given that upper level processes such as growth or species niche preferences depend on multiple traits, correlations may not reflect causal mechanisms, due to patterns of covariation with other traits (John *et al.* 2017; Shipley *et al.* 2017). Further, while our models predicting vital rates included site as a factor, that

approach does not fully incorporate trait-climate interactions, suggesting the value of mechanistic trait-based models that include climatic factors.

Including an extensive suite of functional traits can sharpen our characterization of species adaptation to their ecosystem and climatic preferences as well as predicting vital rates. Including traits in mechanistic process models for growth and species' distributions will increase predictive power further. Such prediction is increasingly critical for species conservation, especially in ecosystems like Hawaiian forests, which are threatened in the face of development and ongoing climate change (Fortini *et al.* 2013) . Future work should also consider intraspecific variation in the wider set of traits, and its role in shaping species distributions within and between forests, as well as trait determination of microsite differences among species (Inman-Narahari *et al.* 2014). Given the power to predict vital rates, this work can enable scaling up from the traits of component species to ecosystem and eventually global vegetation processes, highlighting the enormous promise of increasing mechanistic information—from measurements, to analyses, to models—for clarifying and predicting processes in species and community ecology.

ACKNOWLEDGMENTS

Permits were obtained for work in the HETF through the Institute of Pacific Islands Forestry and the Hawai‘i Division of Forestry and Wildlife. Department of Land and Natural Resources. This work was supported by the National Science Foundation, the Brazilian National Research Council (CNPq) and Brazilian Science Without Borders Program (grant number: 202813/2014-2). We thank Adam Sibley, Brittney Chau, Nisha Choothakan, Tiffany Dang, Chirag Govardhan, Jonnby Laguardia, Jeffrey Lee, Tram Nguyen, Sara Rashidi, Erin Solis and Dustin Wong for lab and field assistance and Nathan Kraft and Marcel Vaz for discussion.

Table 4.1. Framework of hypotheses derived from first principles of trait-based physiology and ecology to test the application of an extensive suite of traits to resolve variation among forests and to enable prediction of vital rates across species.

Hypothesis	Explanation based on first principles	References	Test	Support?
1. Wet and dry forest species would differ in numerous traits as expected from contrasting adaptation	Adaptation to contrasting climate and soil would lead to variation among species in numerous functional traits important in plant performance	(Schimper 1898; Marks & Lechowicz 2006; Fine *et al.* 2015; Levine *et al.* 2017)	Nested ANOVAs for individual-level traits and *t*-tests for species-level traits	Yes
2. Trait values would be more convergent among dry than wet forest species due to the selective pressure imposed by low resource availability	Environmental filtering is expected to reduce functional diversity by constraining the range of possible trait states across habitats.	(Cornwell *et al.* 2006; Mayfield *et al.* 2009; Lebrija-Trejos *et al.* 2010; Kraft *et al.* 2014; Nathan *et al.* 2016; Asefa *et al.* 2017)	*t*-test on the coefficient of variation in traits from MWF and LDF; F-tests on the variance of each trait between MWF and LDF	Yes
3. Traits would be inter-correlated within functional "modules"	Selection on multiple traits across environments would lead to trait-trait correlations within organs and functional modules due to common developmental pathway or function or benefit in given environments	(Sack *et al.* 2003a; Givnish *et al.* 2005; Poorter *et al.* 2014; Li *et al.* 2015b)	Pearson's correlations between traits within functional "modules"	Yes
4. *RGR* and *m* would correlate with specific traits	Given traits contribute mechanistically directly to *RGR*s and *m* in given habitats	(Kitajima 1994; Grime 2006; Marks & Lechowicz 2006; Wright *et al.* 2010; Sack *et al.* 2013)	Pearson's correlations between specific traits and vital rates	Yes
5. *RGR* and *m* would correlate with traits more frequently when stratifying by tree size	Ontogenetic- and size-related trends in traits and vital rates mean that trait-vital rate correlations would be reduced given comparison of species mean values when species vary in size distributions; stratifying by size should therefore strengthen trait-vital rate relationships	(Iida *et al.* 2014; Prado-Junior *et al.* 2016)	Bayesian model to estimate vital rates in given sizes followed by Kendall's correlations between traits and vital rates at each size	Yes
6. *RGR* and *m* can be predicted based on trait-based models.	Given relationships of vital rates with given traits, combinations of traits should be strongly predictive	(Poorter *et al.* 2008; Uriarte *et al.* 2016; Thomas & Vesk 2017)	Linear regression	Yes

Table 4.2. Study traits relating to stomatal morphology, leaf venation, leaf and wood economics and structure, leaf composition, and estimated photosynthesis and plant size, and the vital rates measured for species from a montane wet forest (W) and a lowland dry forest (D) in Hawai‘i. For the traits, we provide symbols; units; hypotheses for given traits differences between forests and results from statistical tests; and hypotheses for correlations with vital rates (relative growth rate and mortality) and results from Pearson's correlation tests (when one result is presented this represents species from both forests together, and when two results are presented these represent species in the wet and dry forests separately); and references supporting the hypotheses. ns indicates no significant difference at $P < 0.05$. "W" represents the expectation that, all else being equal, given the specific hypothesis, the wet forest would have a higher trait value than the dry forest on average; "D" that the dry forest would have the higher trait value on average; and "either" denotes the existence of multiple published hypotheses whereby either MWF or LDF could be expected to have the higher trait value (Table S4.1). Positive signs (+) indicate the expectation or finding of a positive correlation with relative growth rate and mortality rate; negative signs (-) indicate the opposite. For detailed reasoning behind each hypothesis and references see Supplemental Table S4.1. *$P < 0.05$; **$P < 0.01$; ***$P < 0.001$.

Trait/ Vital rate	**Symbol**	**Unit**	***Hypotheses* W or D higher?**	**W or D higher?**	***Hypotheses* trait-vital rate correlation**	**Direction of trait-vital rate correlation**	**Source**
Stomatal morphology							
Stomatal density	d	stomata μm^{-2}	either	ns	+	+**	1-5
Stomatal differentiation rate (or index)	i	stomata $cell^{-1}$	either	W*	+	+**	2-6
Stomatal area	s	μm^2	W	W*	+	ns	1; 5; 7
Guard cell length	GC_L	µm	W	W*			"
Guard cell width	GC_W	µm	W	W**			"
Pore length	SP_L	µm	W	W*			"
Epidermal cell area	e	μm^2	W	W*			8
Maximum stomatal conductance	g_{max}	mmol m^{-2} s^{-1}	either	W*	+	+*	2-5; 9-10

Leaf venation							
Major vein density	VLA_{major}	mm^{-1}	either	D***	+	ns	2-4, 11-15
Minor vein density	VLA_{minor}	mm^{-1}	either	D***	+	ns ns	"
Total vein density	VLA_{total}	mm^{-1}	either	D***	+	ns	"
Free ending vein density	FEV	mm^{-2}	either	D**			"
Leaf and wood economics and structure							
Leaf area	*LA*	cm^2	W	ns	+	W ns; D -*	16-18
Leaf mass per area	*LMA*	$g\ m^{-2}$	either	ns	-	W +*; D -*	12;18-23
Leaf thickness	*LT*	mm	either	ns	-	-*	"
Leaf density	*LD*	$g\ cm^{-3}$	either	ns	-	W +*; D -*	"
Leaf dry matter content	*LDMC*	$g\ g^{-1}$	D	D*	-	ns	18; 24
Saturated water content	*SWC*	$g\ g^{-1}$	either	W**			25-27
Water mass per area	*WMA*	$g\ m^{-2}$	D	ns			"
Percentage loss area (dry)	PLA_{dry}	%	W	W**			28-29
Wood density	*WD*	$g\ cm^{-3}$	either	D***	-	ns	5; 30-32
Leaf composition							
Nitrogen concentration per leaf area	N_{area}	$g\ m^{-2}$	either	ns	+	W +*; D -*	2-5; 20
Nitrogen concentration per leaf mass	N_{mass}	$mg\ g^{-1}$	either	ns	+	+*	"
Phosphorus concentration per leaf area	P_{area}	$g\ m^{-2}$	either	ns	+	W +*; D -*	"
Phosphorus concentration per leaf mass	P_{mass}	$mg\ g^{-1}$	either	W**	+	+*	"
Chlorophyll concentration	Chl_{area}	SPAD	either	ns			2-4; 33
Chlorophyll per mass	Chl_{mass}	SPAD $g^{-1}\ m^2$	either	ns			"
Carbon concentration per leaf mass	C_{mass}	$mg\ g^{-1}$	W	ns			34-35
Nitrogen/ phosphorus ratio	*N*:*P*	-	either	D**	-	ns	35
Chlorophyll/ nitrogen per area ratio	Chl_{area}:N_{area}	SPAD $g^{-1}\ m^2$	W	ns			5
Carbon isotope discrimination	Δ_{leaf}	‰	W	W***			36-37
|Turgor loss point|	$\|\pi_{tlp}\|$	MPa	D	D***			28
Estimated photosynthesis							

Electron transport rate per area	$Jmax_{area}$	µmol m^{-2} s^{-1}	either	ns	+	W +*; D -*	2-4; 36-38
Electron transport rate per mass	$Jmax_{mass}$	nmol g^{-1} s^{-1}	either	ns	+	+*	"
Maximum rate of carboxylation per area	$Vcmax_{area}$	µmol m^{-2} s^{-1}	either	ns	+	W +*; D -*	"
Maximum rate of carboxylation per mass	$Vcmax_{mass}$	nmol g^{-1} s^{-1}	either	ns	+	+*	"
Ratio between intercellular and ambient CO_2 concentrations	c_i:c_a	-	either	W***	+	ns	36-38
Time integrated leaf CO_2 assimilation rate per area	$\bar{A}_{area}$	µmol m^{-2} s^{-1}	either	ns	+	W +*; D -*	9
Time integrated leaf CO_2 assimilation rate per mass	$\bar{A}_{mass}$	nmol g^{-1} s^{-1}	either	W***	+	+*	"
Time integrated stomatal conductance	$\bar{g}_{cleaf}$	mmol m^{-2} s^{-1}	either	W**	+	W +*; D -*	"
Time integrated/ maximum stomatal conductance ratio	$\bar{g}_{cleaf}$: g_{max}	-	either	ns			2-4; 9
Maximum stomatal conductance/ nitrogen per area ratio	g_{max}:N_{area}	mmol g^{-1} s^{-1}	W	W**			40
Plant size							
Mean height	H	m	W	ns			46-47
Maximum height	H_{max}	m	W	W*			"
Seed mass	SM	mg	D	ns			48-49
Vital rates							
Relative growth rate (diameter increment)	RGR_{dbh}	cm cm^{-1} $year^{-1}$	either	ns			5; 20; 41
Relative growth rate (biomass increment)	RGR_{biom}	Kg Kg^{-1} $year^{-1}$	either	ns			"
Mortality rate	m	% $year^{-1}$	either	D**			42-45

References: 1. Hetherington & Woodward (2003); 2. Maximov (1931); 3. Grubb (1998); 4. Scoffoni *et al.* (2011); 5. Givnish (1988); 6. Sack & Buckley (2016); 7. Franks & Farquhar (2007); 8. Beaulieu *et al.* (2008); 9. Franks & Beerling (2009); 10. Wang *et al.* (2015); 11. Sack & Frole (2006); 12. Brodribb et al. (2007); 13. Sack & Scoffoni (2013); 14. Iida *et al.* (2016); 15. Scoffoni *et al.* (2016); 16. Sack *et al.* (2012); 17. Wright *et al.* (2017); 18. Niinemets (2001); 19. Evans (1973); 20. Wright *et al.* (2004); 21. Westoby & Wright (2006); 22. Lusk & Warton (2007); 23. Poorter et al. (2009); 24. Diaz *et al.* (2016); 25. Vendramini *et al.* (2002); 26. Sack *et al.* (2005); 27. Ogburn *et al.* (2012); 28. Bartlett *et al.* (2012); 29. Scoffoni *et al.* (2014); 30. Hacke *et al.* (2001); 31.Chave *et al.* (2009); 32. Gleason *et al.* (2016); 33. Chatuverdi *et al.* (2011); 34. Lambers & Poorter (2004); 35. Elser *et al.* (2000); 36. Farquhar *et al.* (1989); 37. Donovan & Ehleringer (1994); 38. Evans (2013); 39. Wang *et al.* (2017); 40. Wright et al. (2001); 41. Gibert, A. *et al.* (2016); 42. Wright *et al.* (2010); 43. McDowell *et al.* (2008); 44. McDowell *et al.* (2018); 45. Kobe & Coates (1997); 46. Koch *et al.* (2004); 47. King *et al.* (2006); 48. Gross (1984); 49. Khurana & Singh (2004).

Table 4.3. List of all species from the montane wet forest (MWF) and lowland dry forest (LDF) sites in Hawai‘i with family, species code, growth form, leaf habit (evergreen, E; or deciduous, D) and type (simple, S; compound, C; or phyllode, P) and forest stratum. Nomenclature follows (Wagner *et al.* 1999).

Species	Family	Code	Growth Form	Leaf habit and type	Forest stratum
Montane Wet Forest (MWF)					
Acacia koa A. Gray	Fabaceae	ACAKOA	Tree	E, P	Canopy
Broussaisia arguta Gaud.	Hydrangeaceae	BROARG	Shrub	E, S	Understorey
Cheirodendron trigynum (Gaud.) A. Heller	Araliaceae	CHETRI	Tree	E, C	Canopy
Cibotium chamissoi Kaulf.	Cibotiaceae	CIBCHA	Tree fern	E, C	Understorey
Cibotium glaucum (Sm.) Hook. & Arn.	Cibotiaceae	CIBGLA	Tree fern	E, C	Understorey
Cibotium menziesii Hook.	Cibotiaceae	CIBMEN	Tree fern	E, C	Understorey
Clermontia parviflora Gaud. ex A. Gray	Campanulaceae	CLEPAR	Shrub	E, C	Understorey
Coprosma rhynchocarpa A. Gray	Rubiaceae	COPRHY	Tree	E, S	Sub-canopy
Hedyotis hillebrandii (Fosb.) W.L. Wagner & D.R. Herbst	Rubiaceae	HEDHIL	Shrub/Small tree	E, S	Understorey
Ilex anomala Hook. & Arn.	Aquifoliaceae	ILEANO	Tree	E, S	Sub-canopy
Leptecophylla tameiameiae (Cham. & Schltdl.) C.M. Weiller	Epacridaceae	LEPTAM	Shrub	E, S	Understorey
Melicope clusiifolia (A. Gray) T.G. Hartley & B.C. Stone	Rutaceae	MELCLU	Shrub/Small tree	E, S	Understorey
Metrosideros polymorpha Gaud.	Myrtaceae	METPOL_W	Shrub/Tall tree	E, S	Canopy
Myrsine lessertiana A. DC	Myrsinaceae	MYRLES	Tree	E, S	Sub-canopy
Myrsine sandwicensis A. DC	Myrsinaceae	MYRSAN	Shrub/Small tree	E, S	Understorey
Perrottetia sandwicensis A. Gray	Celastraceae	PERSAN	Shrub/Small tree	E, S	Understorey
Pipturus albidus (Hook. & Arn.) A. Gray	Urticaceae	PIPALB	Shrub	E, S	Understorey
Psychotria hawaiiensis (A. Gray) Fosberg	Rubiaceae	PSYHAW	Tree	E, S	Sub-canopy
Trematolobelia grandifolia (Rock) O. Deg.	Campanulaceae	TREGRA	Shrub	E, S	Understorey
Vaccinium calycinum Sm.	Ericaceae	VACCAL	Shrub	E, S	Understorey
Lowland Dry Forest (LDF)					
Euphorbia multiformis Gaud. ex Hook. & Arn.	Euphorbiaceae	EUPMUL	Shrub	D, S	Understorey
Diospyros sandwicensis (A. DC) Fosberg	Ebenaceae	DIOSAN	Tree	E, S	Canopy
Dodonaea viscosa Jacq.	Sapindaceae	DODVIS	Shrub	E, S	Understorey
Erythrina sandwicensis O. Deg.	Fabaceae	ERYSAN	Tree	D, C	Canopy

Metrosideros polymorpha Gaud.	Myrtaceae	METPOL_D	Shrub/Tall tree	E, S	Canopy
Myoporum sandwicense A. Gray	Scrophulariaceae	MYOSAN	Shrub/Small tree	D, S	Understorey
Osteomeles anthyllidifolia (Sm.) Lindl.	Rosaceae	OSTANT	Shrub	E, C	Understorey
Pittosporum terminalioides Planch. ex A.G	Pittosporaceae	PITTER	Tree	E, S	Understorey
Pleomele hawaiiensis O. Deg. & I. Deg.	Asparagaceae	PLEHAW	Tree	E, S	Sub-canopy
Psydrax odorata (G. Forst.) A.C. Sm. & S.P. Darwin	Rubiaceae	PSYODO	Shrub/Small tree	E, S	Understorey
Santalum paniculatum Hook. & Arn.	Santalaceae	SANPAN	Shrub/Tree	E, S	Canopy
Senna gaudichaudii (Hook. & Arn.) H. Irwin & Barneby	Fabaceae	SENGAU	Shrub	D, C	Understorey
Sophora chrysophylla (Salisb.) Seem.	Fabaceae	SOPCHR	Shrub/Tree	D, C	Canopy
Sida fallax Walp.	Malvaceae	SIDFAL	Shrub	E, S	Understorey
Wikstroemia sandwicensis Meisn.	Thymelaeaceae	WIKSAN	Shrub/Tree	E, S	Understorey

Table 4.4. Models selected by maximum likelihood to estimate relative growth rate in terms of diameter at breast height (A, RGR_{dbh}) or above ground biomass (B, RGR_{biom}) or mortality rate (C, m). Independent variables included in the tested models included were those of each module (Table S4.7) that were most correlated with each dependent variable. We present the Pearson's correlation coefficients on untransformed and log transformed data for the predicted variable and the independent variable, the multiple regression coefficient estimates and percent contribution of each trait to model fit. Full models and detailed model selection procedures using AICcs are presented in Table S4.8.

Model	Pearson's correlation coefficient	Multiple regression analyses coefficient estimate	Hierarchical partition analyses (%)
A) $\boldsymbol{RGR_{dbh} \sim d + VLA_{minor} + P_{mass} + \bar{A}_{mass}}$			
intercept	-	2.09e^{-02}*	-
d	0.67**, 0.43	7.76e^{-05}***	53.2
VLA_{minor}	-0.44, -0.49	-3.32e^{-03}*	27.6
P_{mass}	0.39, 0.25	-2.43e^{-02}*	10.9
$\bar{A}_{mass}$	0.36, 0.28	2.51e^{-04}	8.32
Adjusted multiple R^2	-	**0.72*** **	-
B) $\boldsymbol{RGR_{biom} \sim d + VLA_{minor} + LMA + P_{mass}}$			
intercept	-	6.58e^{-02}*	-
d	0.65**, 0.4	2.01e^{-04}***	51.9
VLA_{minor}	-0.50, -0.56*	-4.78e^{-03}*	20.0
LMA	-0.35, -0.48	-2.32 e^{-04}	13.7
P_{mass}	0.39, 0.25	-2.30e^{-02}	14.4
Adjusted multiple R^2	-	**0.70****	-
C) $\boldsymbol{m \sim VLA_{minor} + LMA + P_{mass} + \bar{A}_{mass} + site}$			
intercept	-	-2.59	-
$\bar{A}_{mass}$	0.49, 0.73**	0.18**	39.1
$site$	-	6.65**	31.2
LMA	-0.35, -0.38	-0.03	15.9
P_{mass}	0.16,0.42	-3.39	7.73
VLA_{minor}	-0.13, -0.17	-0.60	6.09
Adjusted multiple R^2	-	**0.70****	-

*$P < 0.05$; **$P < 0.01$; ***$P < 0.001$

FIGURE CAPTIONS

Figure 4.1. Contour map of the Pālamanui (LDF) and Laupāhoehoe (MWF) 4-ha plots on Hawai‘i Island.

Figure 4.2. Radar graph illustrating percent difference in trait means between MWF and LDF species. The LDF species means were fixed arbitrarily as the 100% reference values (the dark red dotted line) and the black line indicates the percent difference between MWF species and LDF species. Traits are arranged according to putative traits modules previously defined (Table 4.1). Bold and *, $P < 0.05$.

Figure 4.3. Relationships between relative growth rate (*RGR*) and mortality rate (*m*) across species of Hawaiian wet and dry forest. The top panels show the relationships across species mean values for *m* and (A) relative growth rate in terms of diameter at breast height, RGR_{dbh} (B) and relative growth rate in terms of above-ground biomass, RGR_{biom}. The bottom panels show that the correlation of mortality with *RGR* is robust across size modules by plotting the Kendall correlation coefficient (τ) between *m* and (C) RGR_{dbh} and (D) RGR_{biom} against plant size class, with the gray line showing the number of species in each 1-cm diameter class (lower in larger size classes). *$P < 0.05$, **$P < 0.01$, ***$P < 0.001$. Top row: black symbols, Montane Wet Forest (MWF) species; gray symbols, Lowland Dry Forest (LDF). $RGR_{dbh} = 0.01 + 0.001 * m$; $RGR_{biom} = 0.03 * m^{0.35}$. Bottom row: filled and open symbols represent significant correlations. We use Pearson correlation coefficient in plots A and B because the species means for *m,* RGR_{dbh} and RGR_{biom} calculated across all individuals were normally distributed or became so after log-transformation, whereas we used Kendall's correlation coefficient in plots C and D because after stratifying by plant size,

m remained non-normally distributed even after transformation. Notably, the RGR-m relationships can be discerned with either coefficient; when calculating Kendall's coefficient for panels A and B, Kendall's τ was 0.32 (P = 0.07) and 0.35 (P = 0.048) respectively; for panels C and D, correlations were considered significant when the 99% credible interval of τ did not include zero.

Figure 4.4. Trait-vital rate relationships across Hawaiian wet and dry forest species, including relationships between relative growth rate in terms of diameter at breast height (RGR_{dbh}) and (A) stomatal density and (B) maximum stomatal conductance; between relative growth rate in terms of above-ground biomass (RGR_{biom}) and (C) time integrated CO_2 assimilation rate per mass, (D) leaf mass per area, (E) minor vein density, and (E) phosphorus per mass; and between mortality rate (m) and (G) time integrated CO_2 assimilation rate per leaf dry mass, (H) nitrogen per leaf dry mass. Black symbols, Montane Wet Forest (MWF) species; gray symbols, Lowland Dry Forest (LDF). $RGR_{dbh} = 3.02e^{-03} + 5.51e^{-05} * d$; $RGR_{dbh} = 0.01 + 0.004 * g_{max}$; $RGR_{biom} = 10e^{-03} * \bar{A}_{mass}^{1.35}$; $RGR_{biom} = 2.53 * LMA^{-0.858}$; $RGR_{biom} = 0.17 * VLA_{minor}^{-0.87}$; $RGR_{biom} = 0.041 * P_{mass}^{0.97}$; $m = 8e^{-05} * \bar{A}_{mass}^{2.40}$; $m = 0.04 * N_{mass}^{1.67}$. $*P < 0.05$, $**P < 0.01$, $***P < 0.001$.

Figure 4.5. Contrasting relationships between mortality rate and functional traits across forests, including (A) leaf mass per area, (B) time integrated CO_2 assimilation rate per leaf area, (C) phosphorus concentration per leaf mass and (D) individual leaf area. Black symbols and curve, Montane Wet Forest (MWF) species; gray symbols and curve, Lowland Dry Forest (LDF). In (E), the black line and r represent the fit and Pearson's regression coefficient including only wet forest species and the gray line are for LDF species only. $m_{MWF} = 5e^{-04} * LMA^{1.89}$ and $m_{LDF} = 4e^{8} * LMA^{-}$

$^{3.74}$; m_{MWF} = -0.72 + 0.44 * $\bar{A}_{area}$ and m_{LDF} = 764699 * $\bar{A}_{area}^{-5.43}$; m = 1.73 * $P_{mass}^{2.38}$; m = 74.53 * $LA^{-1.46}$. *P < 0.05, **P < 0.01, ***P < 0.001.

Figure 4.6. Estimating the influence of plant on the correlation of relative growth rate and mortality with given functional traits. Each panel shows the plot of the size-dependent Kendall correlation coefficient (τ) between: (A) relative growth rate and maximum stomatal conductance and nitrogen per area ratio, g_{max}:N_{area}; (B) relative growth rate and maximum height, H_{max}; (C) mortality rate and stomatal density, d; and (D) mortality rate and phosphorus concentration, P_{mass}. Open symbols represent non-significant results (the 99% credible interval of τ included zero) and filled symbols significant correlations (the 99% credible interval of τ did not include zero). The gray line shows the number of species in each 1-cm diameter class.

Figure 4.7. Relationship between observed growth rate in terms of diameter at breast height (RGR_{dbh}), above-ground biomass (RGR_{biom}) and mortality rate (m) and the values predicted from models using the plant traits most correlated with each dependent variable: (A) RGR_{dbh} = 2.09e^{-02} + (7.76e^{-05} * d) – (3.32e^{-03} * VLA_{minor}) – (2.43e^{-02} * P_{mass}) + (2.51e^{-04} * $\bar{A}_{mass}$); (B) RGR_{biom} = 6.58 e^{-02} + (2.01e^{-04} * d) – (4.78e^{-03} * VLA_{minor}) – (2.32e^{-04} * LMA) – (2.3e^{-02} * P_{mass}); (C) m = -2.59 - (0.60 * VLA_{minor}) – (0.03 * LMA) – (3.39 * P_{mass}) + (0.18 * $\bar{A}_{mass}$) + (6.64 * $site$). The dashed line represents the 1:1 relationship. *P < 0.05, **P < 0.01, ***P < 0.001.

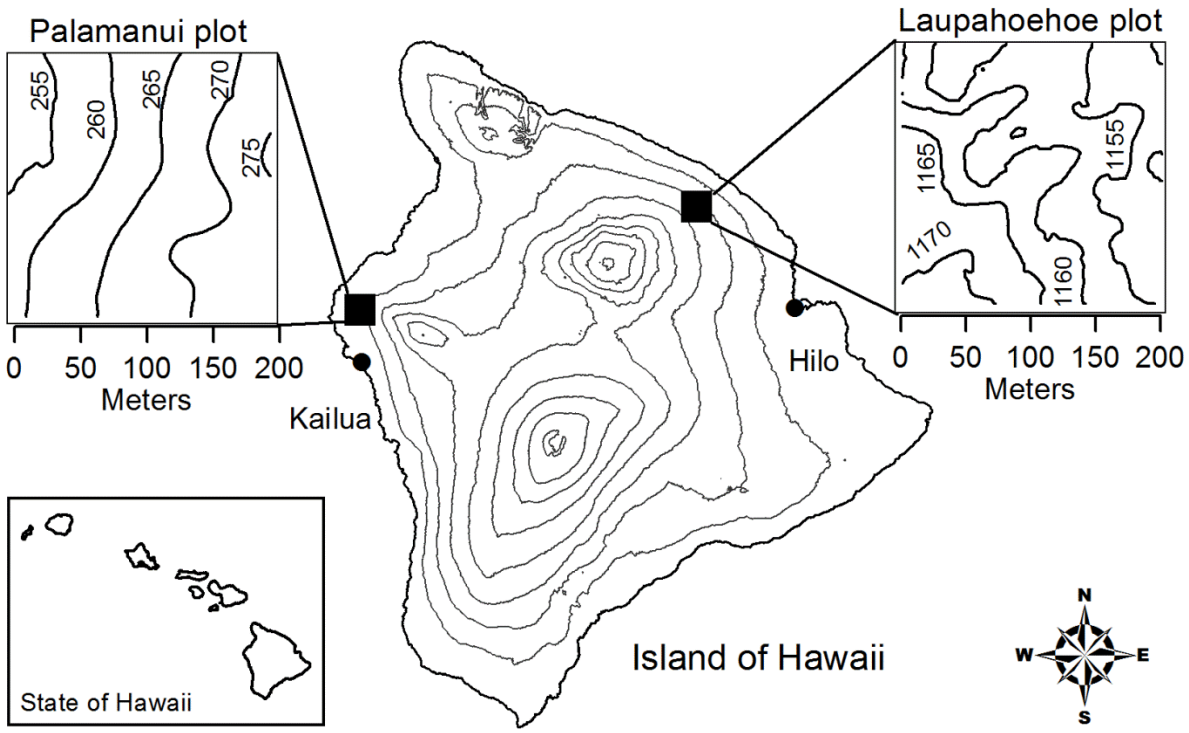
Palamanui plot
255
260
265
270
275
0 50 100 150 200
Meters
Laupahoehoe plot
1165
1155
1170
1160
0 50 100 150 200
Meters
Kailua
Hilo
Island of Hawaii
State of Hawaii
N
W
E
S

Figure 4.1

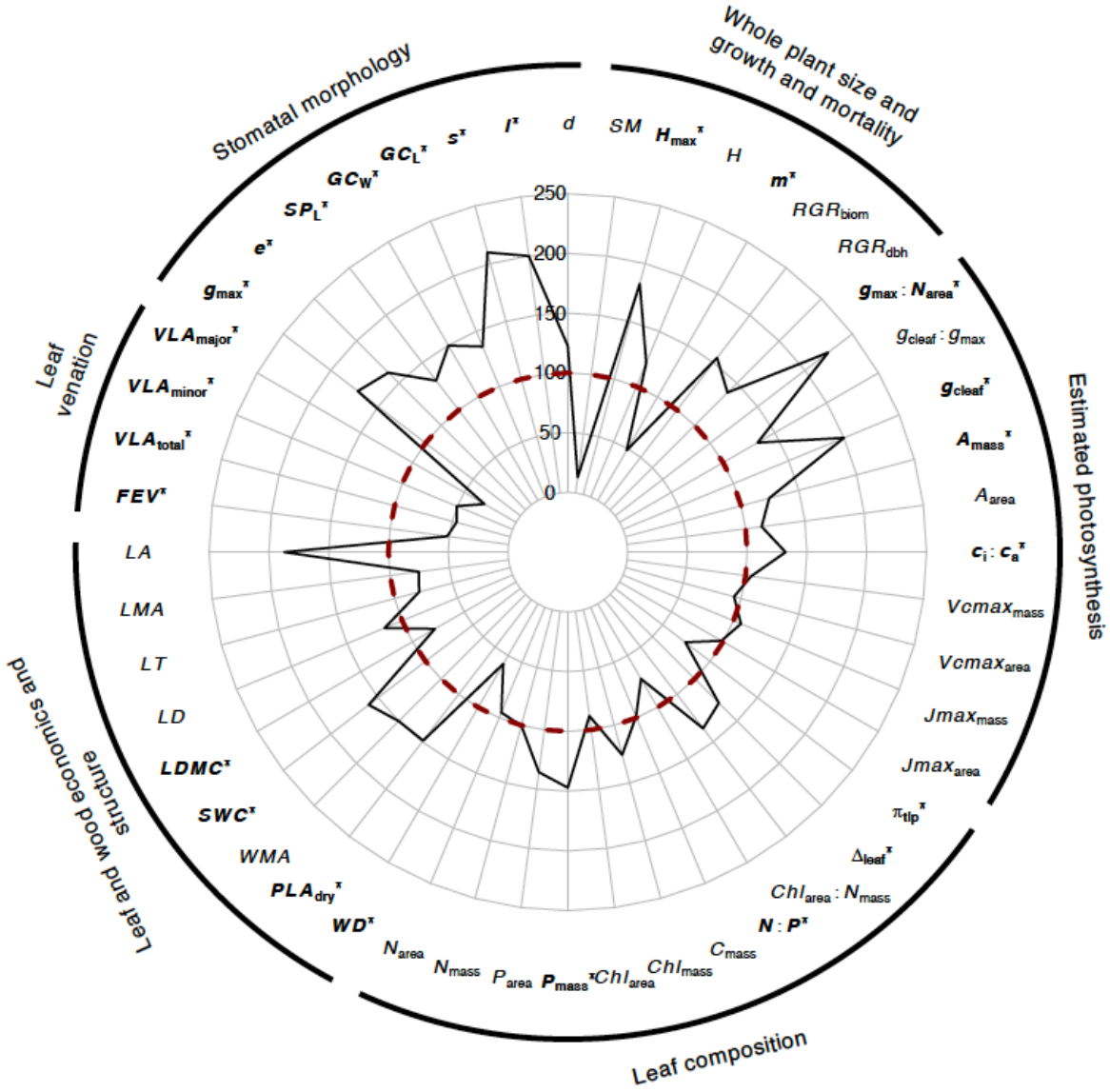
Stomatal morphology
Whole plant size and growth and mortality
Estimated photosynthesis
Leaf composition
Leaf and wood economics and structure
Leaf venation
250
200
150
100
50
0
l^{*}
d
SM
H_{max}^{*}
H
m^{*}
RGR_{biom}
RGR_{dbh}
$g_{max} : N_{area}^{*}$
$g_{cleaf} : g_{max}$
g_{cleaf}^{*}
A_{mass}^{*}
A_{area}
$c_i : c_a^{*}$
$Vcmax_{mass}$
$Vcmax_{area}$
$Jmax_{mass}$
$Jmax_{area}$
π_{tlp}^{*}
Δ_{leaf}^{*}
$Chl_{area} : N_{mass}$
$N : P^{*}$
C_{mass}
Chl_{mass}
Chl_{area}
P_{mass}^{*}
P_{area}
N_{mass}
N_{area}
WD^{*}
PLA_{dry}^{*}
WMA
SWC^{*}
$LDMC^{*}$
LD
LT
LMA
LA
FEV^{*}
VLA_{total}^{*}
VLA_{minor}^{*}
VLA_{major}^{*}
g_{max}^{*}
e^{*}
SP_L^{*}
GC_W^{*}
GC_L^{*}
s^{*}

Figure 4.2

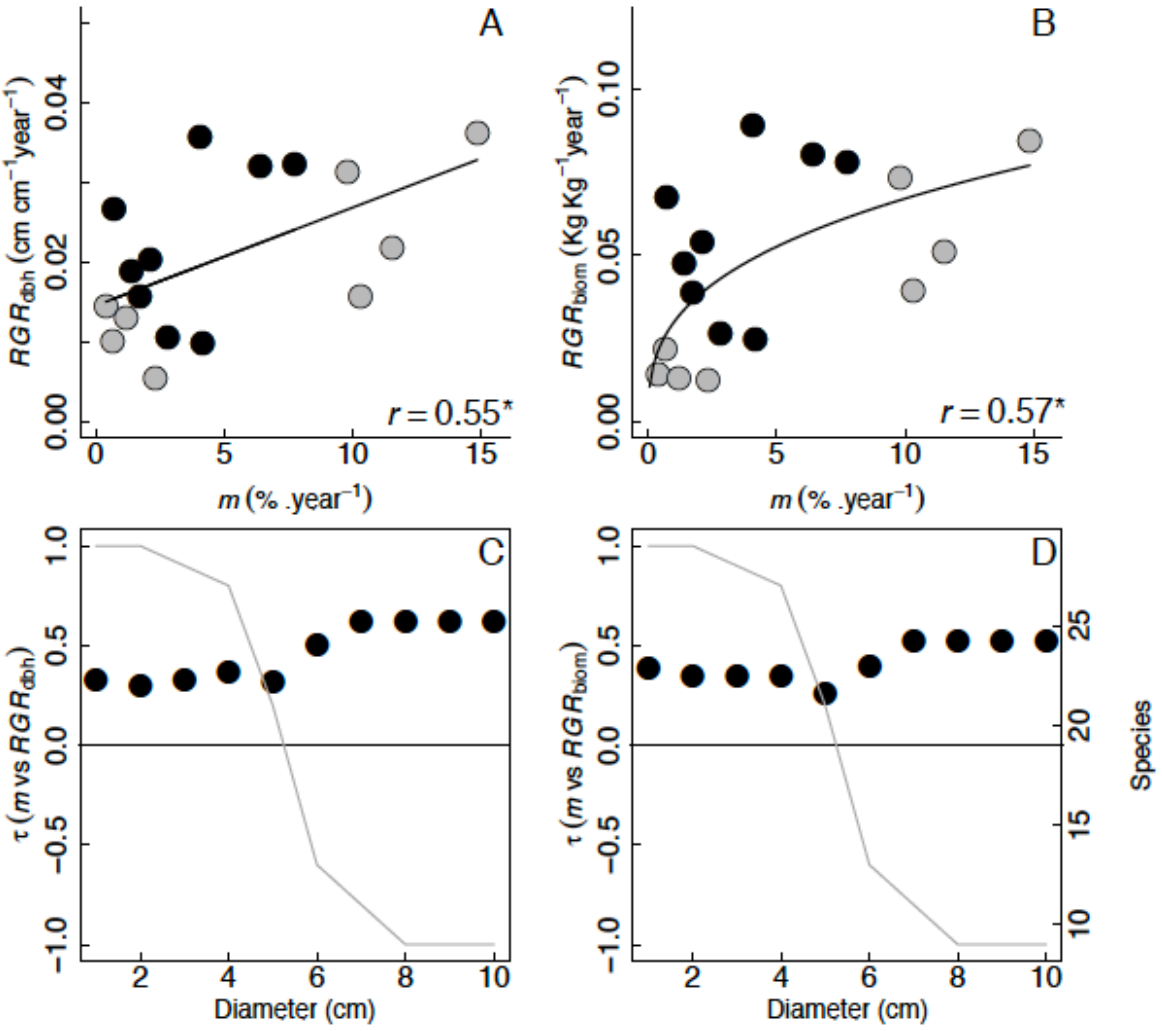
A
B
C
D
RGR_{dbh} (cm cm^{-1}year^{-1})
RGR_{biom} (Kg Kg^{-1}year^{-1})
$r = 0.55^{*}$
$r = 0.57^{*}$
m (% .year^{-1})
τ (m vs RGR_{dbh})
τ (m vs RGR_{biom})
Diameter (cm)
Species

Figure 4.3

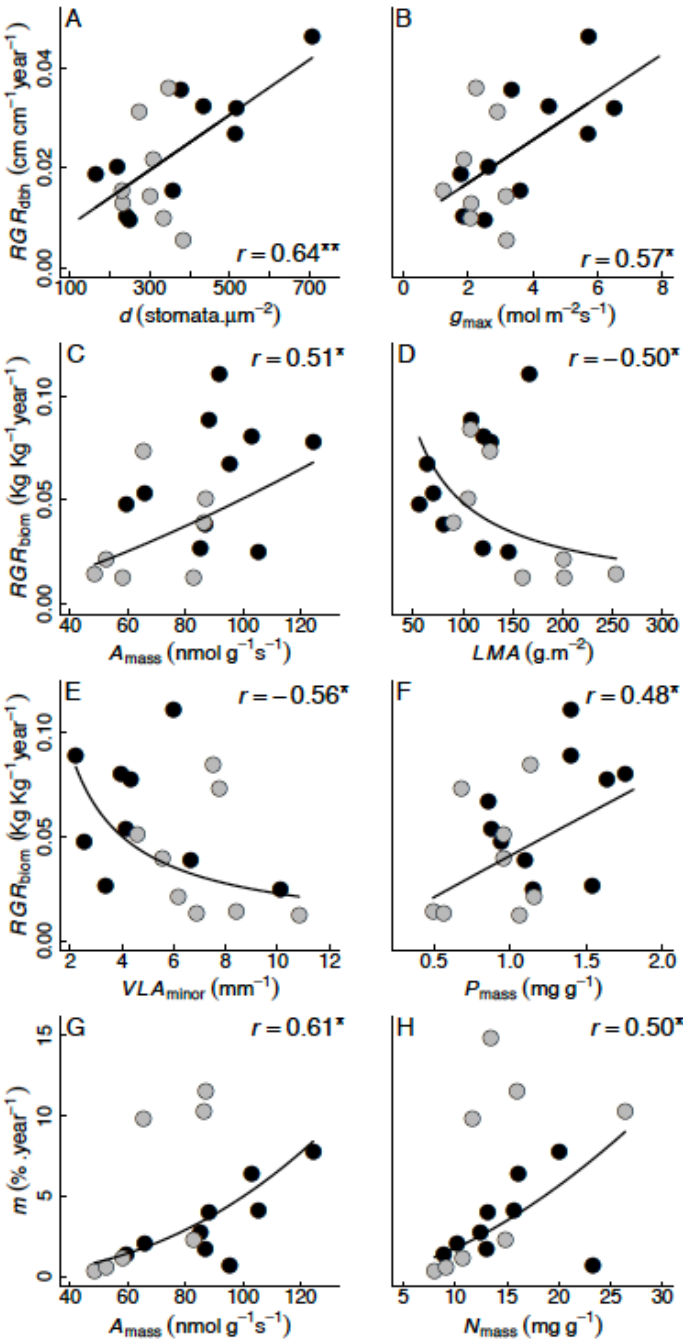
A
B
C
D
E
F
G
H
RGR_{dbh} (cm cm^{-1}year^{-1})
RGR_{biom} (kg Kg^{-1}year^{-1})
d (stomata.µm^{-2})
g_{max} (mol m^{-2}s^{-1})
A_{mass} (nmol g^{-1}s^{-1})
LMA (g.m^{-2})
VLA_{minor} (mm^{-1})
P_{mass} (mg g^{-1})
m (% .year^{-1})
N_{mass} (mg g^{-1})
$r = 0.64^{**}$
$r = 0.57^{*}$
$r = 0.51^{*}$
$r = -0.50^{*}$
$r = -0.56^{*}$
$r = 0.48^{*}$
$r = 0.61^{*}$
$r = 0.50^{*}$

Figure 4.4

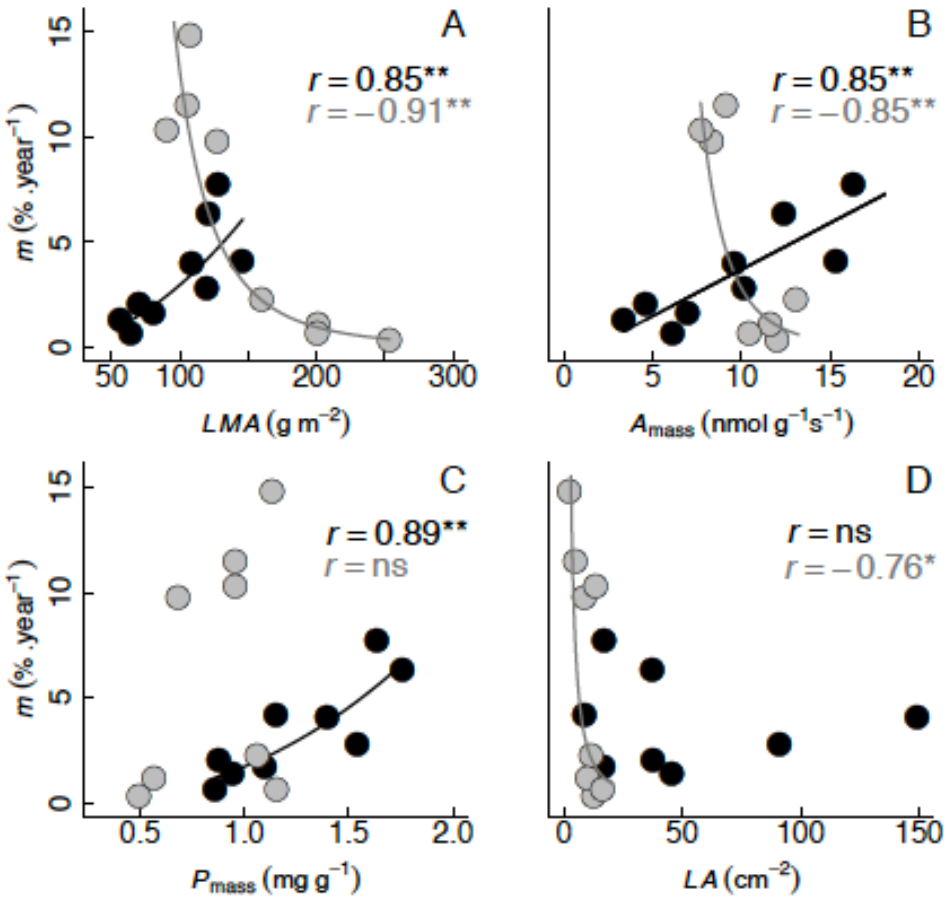
A
r = 0.85**
r = −0.91**
m (% .year⁻¹)
LMA (g m⁻²)
B
r = 0.85**
r = −0.85**
Amass (nmol g⁻¹s⁻¹)
C
r = 0.89**
r = ns
m (% .year⁻¹)
Pmass (mg g⁻¹)
D
r = ns
r = −0.76*
LA (cm⁻²)

Figure 4.5

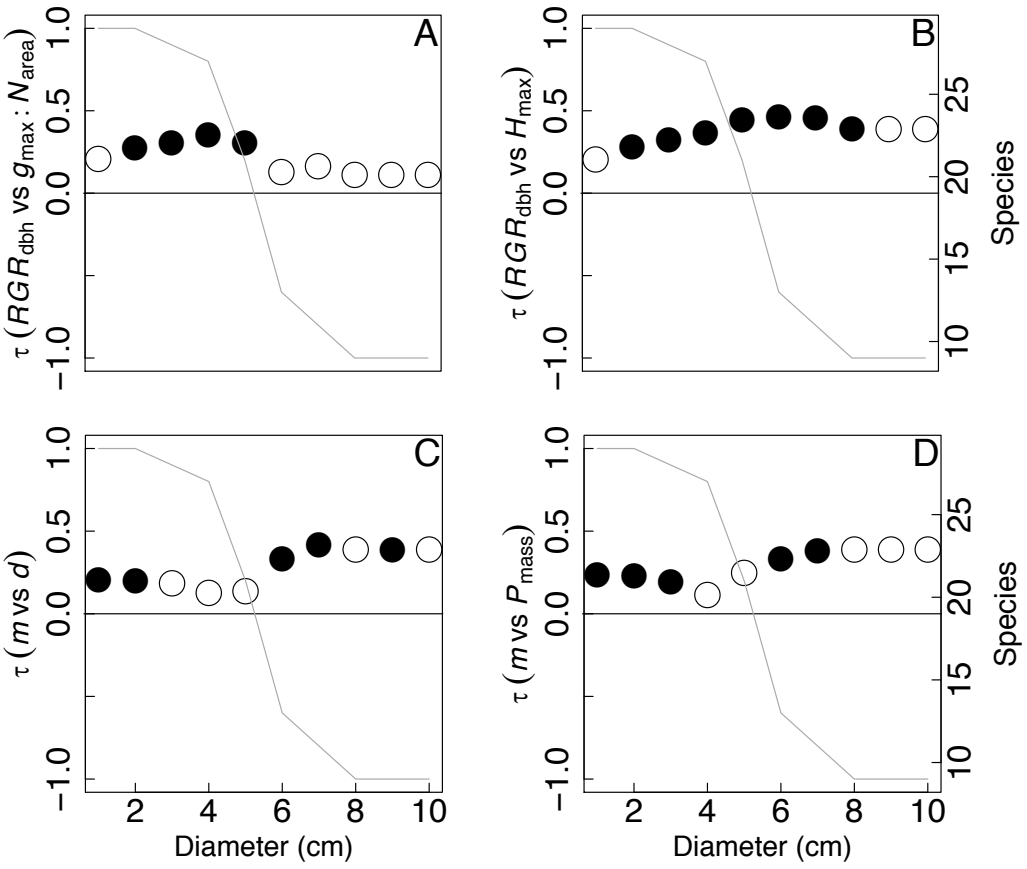
A
B
C
D
τ (RGR_dbh vs g_max : N_area)
τ (RGR_dbh vs H_max)
τ (m vs d)
τ (m vs P_mass)
1.0
0.5
0.0
−1.0
2
4
6
8
10
Diameter (cm)
25
20
15
10
Species

Figure 4.6

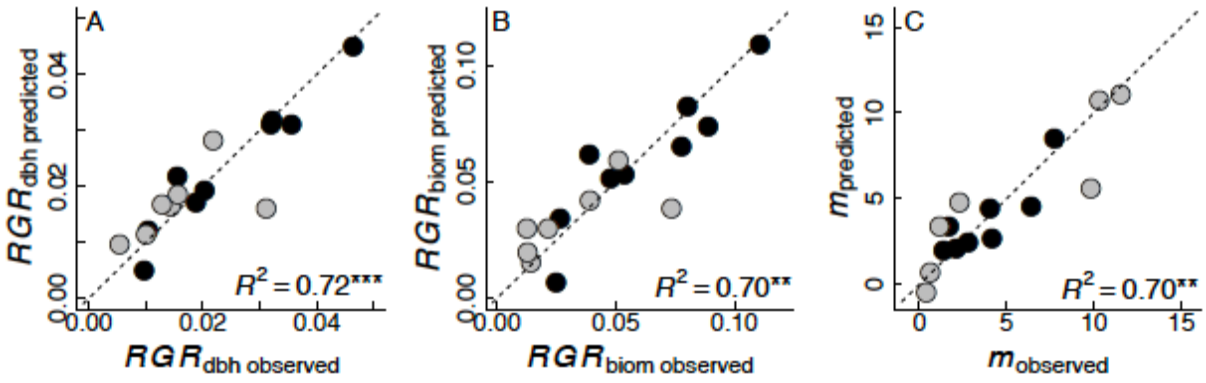
A
$RGR_{dbh\ predicted}$
$RGR_{dbh\ observed}$
$R^2 = 0.72^{***}$
B
$RGR_{biom\ predicted}$
$RGR_{biom\ observed}$
$R^2 = 0.70^{**}$
C
$m_{predicted}$
$m_{observed}$
$R^2 = 0.70^{**}$

Figure 4.7

Appendix 4.1. Supplementary methods

Study sites

The sites for the Hawaii forest dynamics plots were selected as ecologically relatively well preserved areas that are representative of a given forest type, with high native species cover, and a commitment by ownership to long-term conservation objectives. Notably, all forests in Hawai‘i are affected to some degree by altered trophic interactions due to invasion of non-native species or extinction of the native species, but this is not unique to Hawai‘i (Ziegler 2002; Harrison 2011; Ostertag *et al.* 2014).

Montane wet forest MWF. The 4-ha Laupāhoehoe FDP 19º55’ N, 155º17’ W is located on the northeast slope of Mauna Kea volcano within the Laupāhoehoe Natural Hawai‘i Area Reserve, Hawaii Division of Forestry and Wildlife, which makes up the wet forest unit of the Hawai‘i Experimental Tropical Forest HETF. The mean elevation of the plot is 1120 m.a.s.l. with slopes of 0–20%, and the overall direction of downslope is northwards towards the Pacific Ocean. The substrate within the plot is 4,000-14,000 years old (Vitousek & Farrington 1997). Interpolated mean annual precipitation, based on analysis of climate station data over 30 years, is 3440 mm with no distinct dry season and mean annual air temperature is 16ºC (Crews *et al.* 1995; Giambelluca *et al.* 2013). The forest consists of evergreen broad-leaved trees, and the 25–28 m canopy is dominated by *Metrosideros polymorpha* Myrtaceae and to a lesser extent, *Acacia koa* Fabaceae, with abundant tree ferns. Vegetation at the MWF is highly representative of this forest type in Hawai‘i (Ostertag *et al.* 2014).

Lowland dry forest LDF. The 4-ha Pālamanui FDP is a tropical dry forest, and an example of one of the world’s most endangered forest types. This FDP is located on a privately-owned tract of land on the northwest slope of Hualālai Volcano in the district of North Kona 240 m elevation, 19

º 44’ N, 155 º 59’ W. Geological substrate in the Pālamanui area consists of ‘a‘ālava with scattered pāhoehoe flows dating to 1,500–3,000 years old (Moore *et al.* 1987). Interpolated mean annual precipitation at the LDF site is 835 mm, with large within and between-year variability (Thaxton *et al.* 2010; Giambelluca *et al.* 2013). For the LDF, major rainfall events typically occur in the winter as low pressure storms ‘‘Kona lows’’ while summers tend to be dry and characterized by small convective storms. Mean daily air temperature is approximately 20ºC wrcc.dri.edu. Native vegetation consists of evergreen and deciduous broadleaved trees and shrubs that form an open-canopy forest that reaches heights of 7–8 m dominated by *Diospyros sandwicensis* Ebenaceae and *Psydrax odorata* Rubiaceae, with an understory of non-native shrubs and grasses (Ostertag *et al.* 2014).

Measurement of relative growth rates

A total of 21,805 individual trees of 29 species from both forest plots were measured for DBH in the first census, 2008, and the 18,745 of those trees that were alive were remeasured in the second census in 2013. The tree fern species (CIBCHA, CIBGLA, CIBMEN; Table 4.2), a monocot species (PLEHAW; Table 4.2), and two species that fulfilled the DBH requirement in only one of the two censuses (TREGRA and SIDFAL; Table 4.2) were included in trait analyses but not in growth and mortality analyses.

Stomatal and venation traits

We measured stomatal and vein traits on one leaf from each of three individuals per species. After rehydration, we fixed the leaves in FAA 48% ethanol: 10% formalin: 5% glacial acetic acid: 37%

water. From measured stomatal traits we calculated the maximum theoretical stomatal conductance g_{max}; (Franks & Farquhar 2007; Sack & Buckley 2016):

$$g_{\max} = \frac{bmds}{s^{0.5}}$$

In which b is a biophysical constant given as $b = \frac{D}{v}$, where D represents the diffusivity of CO_2 and water in air $m^2\ s^{-1}$ and v is the molar volume of air $m^3\ mol^{-1}$, so $b = 0.00126$; m is a morphological constant based on scaling factors representing the proportionality of stomatal dimensions $m = \frac{\pi c^2}{j^{0.5} 4hj + \pi}$, with c, h, and j treated as constants for the estimation of g_{max} c, h and $j = 0.5$; d is stomatal density, and s is stomatal size (Franks & Farquhar 2007; Franks *et al.* 2009; McElwain *et al.* 2016).

For the venation traits, FAA-fixed leaves were cleared in 5% sodium hydroxide followed by bleach, and then stained with safranin and fast green and scanned for major vein density (VLA_{major}). Minor and free ending vein densities (VLA_{minor} and FEV) were obtained from microscopy images of the top, middle and bottom of each leaf used for VLA_{major}. Detailed methods can be found in (Scoffoni *et al.* 2011).

Leaf and wood economics and structure and leaf composition

Leaf structure and composition traits were measured for three leaves per studied individual. Leaf saturated mass was measured using an analytical balance (0.01 mg; XS205; Mettler-Toledo, OH, USA) and leaf thickness LT using digital calipers (0.01 mm; Fowler, Chicago, IL, USA). The leaf area LA was measured using a flatbed scanner and analyzed using the software ImageJ (http://imagej.nih.gov/ij/). After scanning, leaves were placed in a drying oven at 70º for 72 h and their dry mass and area were measured again. From these measurements, we calculated the

percentage loss in area after dry PLA_{dry} as the percent decline in area from saturated to dry leaves,

$$PLA_{\text{dry}} = 100 - \left(\frac{Dry\ area}{Saturated\ area} \times 100\right)$$

(Witkowski & Lamont 1991; Ogburn & Edwards 2012; Pérez-Harguindeguy *et al.* 2013).

To determine concentration of leaf nitrogen, phosphorus and carbon per mass (N_{mass}, P_{mass} and C_{mass}), and carbon isotope ratio ($\delta^{13}C$); used to determine carbon isotope discrimination, leaves from three individuals per species were oven-dried at 70°C for 72 h, and whole leaf samples, excluding the petioles, were ground, weighed and analyzed using high temperature combustion in an elemental analyzer (Costech ECS 4010; Valencia, California, USA), with effluent passed into a continuous flow isotope ratio mass spectrometer (ThermoFinnigan Delta V Advantage with a Conflo III interface; ThermoFisher Scientific; Walthan, Massachusetts, USA; Fry *et al.* 1996; Pérez-Harguindeguy *et al.* 2013). For P_{mass}, samples were dry ashed, dissolved in HCl and analyzed using inductively-coupled plasma-optical emission spectrometry (Varian Vista MPX Instrument, Varian Inc., Palo Alto, California USA; Porder, Paytan & Vitousek 2004).

The chlorophyll concentration per area *Chl* was measured using a SPAD meter, which provides a correlate of total chlorophyll *a* + *b* concentration per area in SPAD units (Monje & Bugbee 1992; SPAD-502, Konica Minolta, Japan).

The carbon isotope discrimination (Δ_{leaf}; in parts per thousand, ‰) was calculated following Farquhar & Richards (1984) and using values of $\delta^{13}C$ air for the Island of Hawaii available from Allison, Francey & Krummel (2003) as:

$$\Delta_{\text{leaf}} = \frac{\delta^{13}C_{\text{air}} - \delta^{13}C_{\text{leaf}}}{1 + {\delta^{13}C_{\text{leaf}}}/{1000}}$$

The leaf ^{13}C isotope composition $\delta^{13}C_{leaf}$ used to calculate Δ_{leaf} was obtained from pulverized whole leaves for each study individual at the University of Hawaii at Hilo Analytical Laboratory facility, using an Isotope Ratio Mass Spectrometer Delta V IRMS, Thermo-Fisher, US.

Estimated photosynthesis traits

Using leaf N and P concentrations per mass and equations available from Domingues *et al.* (2010), we estimated maximum rate of carboxylation per area ($Vcmax_{area}$) and electron transport rate ($Jmax_{area}$) as:

$$log_{10}(Vcmax_{\text{area}}) = \min\{\alpha_N + \nu_N \times log_{10}(N_{\text{mass}});\ \alpha_P + \nu_P \times log_{10}(P_{\text{mass}})\}$$

and

$$log_{10}(Jmax_{\text{area}}) = \min\{\gamma_N + \varepsilon_N \times log_{10}(N_{\text{mass}});\ \gamma_P + \varepsilon_P \times log_{10}(P_{\text{mass}})\}$$

Where all coefficients are empirical constants: α_N = -1.16, ν_N = 0.70, α_P = -0.30, and ν_P = 0.85; γ_N = -1.22, ε_N = 0.92, γ_P = -0.11, ε_P = 0.66. The ratio between intercellular CO_2 concentration (c_i) and ambient CO_2 concentration (c_a) was estimated from $\delta^{13}C_{leaf}$ and Δ_{leaf} (Farquhar, O'Leary & Berry 1982; Franks *et al.* 2014) as:

$$c_i : c_a = \left[\frac{\Delta_{\text{leaf}} - a}{b - a}\right]$$

Where a is the carbon isotope fractionation due to diffusion of CO_2 in air (4.4‰), b is the fractionation associated with RuBP carboxylase taken as 30‰ and Δ_{leaf} is the carbon discrimination rate.

An estimate of leaf lifetime integrated CO_2 assimilation rate ($\bar{A}_{area}$) and stomatal conductance to CO_2 ($\bar{g}_{cleaf}$) were derived from $Vcmax_{mass}$, $Jmax_{mass}$ and isotope composition data using the Farquhar, von Caemmerer and Berry model with assumed constants (Franks, Drake & Beerling 2009). $\bar{A}_{mass}$ was calculated as:

$$\bar{A} = \min\{A_c, A_j\},$$

$$A_c = Vcmax_{\text{mass}} \left[\frac{\bar{c_i} - \Gamma^*}{\bar{c_i} + 622}\right] - R_d,$$

$$A_j = Jmax_{\text{mass}} \left[\frac{\bar{c_i} - \Gamma^*}{4\bar{c_i} + 296}\right] - R_d$$

where the CO_2 compensation point in the absence of mitochondrial respiration (Γ^*) was 37 μbar; and the mitochondrial respiration (R_d) was $0.01 * Vcmax_{\text{mass}}$. And $\bar{g}_{\text{cleaf}}$ was calculated as:

$$\bar{g}_{\text{cleaf}} = \frac{\bar{A}}{c_a - \bar{c_i}}, \text{and}$$

$$\bar{c_i} = c_a \left(\frac{\Delta_{\text{leaf}} - 4.4}{22.6}\right)$$

where c_a = 370 μmol mol^{-1}, is the atmospheric CO_2 mole fraction.

To convert $Vcmax_{\text{mass}}$, $Jmax_{\text{mass}}$, and $\bar{A}_{\text{mass}}$ to area-basis, we multiplied the traits values by *LMA*. We also calculated the ratio between $\bar{g}_{\text{cleaf}}$ and g_{max}, and the ratio between g_{max} and N_{area}.

Statistical analyses

We note that while we focus in this paper on frequentist statistical approaches as the most typically used in the field, we utilized a Bayesian approach to analyze the influence of tree size on trait-vital rate relationships, following (Iida *et al.* 2014), as this in our view is the most sophisticated existing analysis for testing that hypothesis. We estimated RGR_{dbh} and m at 1-cm intervals of DBH for each species.

Estimation of regression coefficients of relative growth rate in terms of diameter at breast height (RGR_{dbh}) using a hierarchical Bayesian approach

Following Iida *et* al. (2014), to estimate size-dependent RGR_{dbh} for each individual *i*th tree belonging to species *j* ($RGR\text{dbh}_{ij}$), we assumed that $RGR\text{dbh}_{ij}$ is a linear function of the natural logarithm of the initial diameter, $DBH1_{ij}$, with parameters for species *j* (α_{kj}; k=1, 2), that represent the sum of the community- and species-level parameters. We assumed that both parameters were normally distributed with mean μ_{kj} and precision $\gamma_{\kappa ij}$, $N(\mu_{kj}, \gamma_{\kappa ij})$. μ_{1j} and μ_{2j} are normally distributed with vague but proper priors with mean centered in 0 and variance of 10^4, $N(0,10^{-4})$. For the hyper-prior $\gamma_{\kappa ij}$, we assumed a Gamma distribution with both shape and scale parameters set as 10^{-2}, $G(10^{-2}, 10^{-2})$. The natural logarithm of the final stem diameter $DBH2_i$ was calculated as the sum of the natural logarithm of initial stem diameter $DBH1_i$ and the product of $RGR\text{dbh}_{ij}$ and the census interval of the *i*-th tree, Δt_i.

$$\ln(DBH2_i) = \ln(DBH1_i) + RGR\text{dbh}_{ij} \times \Delta t_i$$

$$RGR\text{dbh}_{ij} = \alpha_{1j} + \alpha_{2j} \times \ln(DBH1_i)$$

Posteriors were estimated via Markov Chain Monte Carlo implemented in JAGS Just Another Gibbs Sampler; (Plummer 2007) from R, using the package '*R2Jags*'. We ran the model for 90,000 iterations and 3 chains, with a thinning of 150, and burn-in of 30,000. All parameters converged in less than 20 lags before thinning. To test model fit, we plotted the observed species average RGR_{dbh} against the species average RGR_{dbh} predicted from the model and obtained an $R^2 = 0.96$.

Estimation of regression coefficients of mortality rate (m) using a hierarchical Bayesian approach

Following Iida *et* al. (2014), to estimate size-dependent *m* for each individual *i*th tree belonging to species *j* (m_{ij}), we first calculated the probability of survival of the *i*th individual tree (p_i) from observations of whether the tree survived the census period ($S_i = 1$) or not ($S_i = 0$). We assumed that S_i followed a Bernoulli distribution of the probability of survival (p_i). The p_i of the *i*th tree was calculated from the per capita annual mortality rate, m_{ij}, adjusted to the census interval (Δt_i). which was a function of the sum of species-specific parameters β_{kj} (k = 1, 2, 3). β_{1j} represented the initial mortality rate while parameters β_{2j} and β_{3j} represent the effect of *DBH*1 and ln(*DBH*1i) on m_{ij}. We assumed that all three parameters were normally distributed with mean μ_{kj} and precision $\gamma_{\kappa ij}$, $N(\mu_{kj}, \gamma_{\kappa ij})$. μ_{kj} had vague but proper priors with means centered in 0 and variance of 10^4, $N(0,10^{-4})$. For the hyper-prior distribution of $\gamma_{\kappa ij}$ we used a Gamma distribution with both shape and scale parameters set as 10^{-2}, $G(10^{-2}, 10^{-2})$.

$$S_i \sim Bernoulli(p_i)$$

$$p_i = \exp(-m_{ij} \times \Delta t_i)$$

$$\ln(m_{ij}) = \beta_{1j} + \beta_{2j} \times \ln(DBH1_i) + \beta_{3j} \times DBH1_i$$

We ran the model for 90,000 iterations and 3 chains, with a thinning of 150, and burn-in of 30,000, with a total of 120,000 iterations. All parameters converged in less than 20 lags before thinning. To test model fit, we plotted the observed species average *m* against the species average *m* predicted from the model and obtained an $R^2 = 0.97$.

Appendix 4.2. Supplementary results

Trait-trait coordination

The alternative measures of relative growth rates RGR_{dbh} and RGR_{biom} and mortality m were strongly intercorrelated (r ranged from 0.55 to 0.97; $P < 0.05$). Further, traits were highly inter-correlated within functional categories i.e., stomatal morphology traits, venation traits, leaf and wood economics and structure traits, and compositional traits when considering species from both forests together, and in the MWF and LDF separately. We focus here on analyses of trait correlations across both forests Table S4.5, with complete results for individual forests provided in Tables S4.5-S4.6.

Traits related to stomatal and epidermal pavement cell size SP_L, GC_L, GC_w, s, e were positively correlated (r = 0.64-0.97; $P < 0.05$). Stomatal size traits also had a positive relationship with i and g_{max} (r = 0.39-0.87; $P < 0.05$). The d was statistically independent of stomatal size traits, but negatively related to e (r = -0.54; $P < 0.01$) and positively with i and g_{max} (r = 0.66 and 0.74, respectively; $P < 0.001$).

Venation traits were all positively intercorrelated. VLA_{minor} was the main determinant of VLA_{total} (r = 0.99; $P < 0.001$), and strongly correlated with *FEV*s and VLA_{major} (r = 0.88 and 0.72, respectively; $P < 0.001$).

Leaf and wood economics spectrum and structure traits were intercorrelated. *LMA* was positively correlated with *LT* and *LD* (r = 0.34 and 0.64, respectively; $P < 0.05$). *LT* and *LD* were negatively correlated (r = -0.6; $P < 0.001$), and *WMA* was positively correlated with *LT* and negatively correlated with *LD* (r = 0.71 and -0.39, respectively; $P < 0.05$). *WD* and *LDMC* were positively correlated (r = 0.75; $P < 0.001$) and negatively correlated with *SWC*, *WMA*, *LA*, and

PLA_{dry} (r = -0.36 to -0.74; $P < 0.05$). *SWC*, *WMA*, *LA*, and PLA_{dry} were positively correlated (r = 0.37-0.72; $P < 0.05$).

Leaf compositional traits were also inter-correlated: *N* and *P* in area and mass basis were positively intercorrelated (r = 0.46-0.79; $P < 0.05$) and negatively correlated with Chl_{area}: N_{area} (r ranged from -0.4 to -0.94; $P < 0.05$). *N*:*P* was positively related to *N*, and negatively to *P* (r ranged from -0.58 to 0.38; $P < 0.05$). Additionally, P_{area} and P_{mass} were negatively correlated with C_{mass}, Chl_{area} and $|\pi_{tlp}|$ (r ranged from -0.34 to -0.52; $P < 0.05$). $|\pi_{tlp}|$ was positively correlated with C_{mass}, *N*:*P* and Chl_{area} (r ranged from 0.38 to 0.44; $P < 0.05$ and negatively with Δ_{leaf} r = -0.43; $P < 0.05$). These relationships led to positive correlations among estimated photosynthesis traits Table S4.5 as expected from their calculation, i.e., between $Jmax_{area}$ and $Vcmax_{area}$ (r = 0.99; $P < 0.001$) and $Jmax_{mass}$ and $Vcmax_{mass}$ (r = 0.95; $P < 0.001$). Estimated photosynthesis traits were positively intercorrelated (r ranging from 0.4 to 0.98; $P < 0.05$), except for the g_{max}:N_{area}, which was negatively correlated with all area-basis traits in the category (r ranging from -0.37 to -0.75; $P < 0.05$) and the c_i:c_a ratio, that was correlated only with $\overline{g}_{cleaf}$, $\overline{g}_{cleaf}$:g_{max} and g_{max}:N_{area} (r = 0.37 to 0.61; $P < 0.05$).

Mean height *H* had a positive relationship with H_{max} (r = 0.68; $P < 0.001$).

Across trait categories, we found a strong negative relationship between stomatal morphology traits and venation traits, especially between VLA_{minor} and *s* (r ranged from -0.4 to -0.66; $P < 0.05$). While most stomatal morphology traits were strongly correlated with vein traits, *d* was not. Vein traits also showed coordination with $|\pi_{tlp}|$ and *WD*, and Δ_{leaf}. Vein densities were positively correlated with $|\pi_{tlp}|$ and *WD* (r ranged from 0.39 to 0.71; $P < 0.05$), but negatively correlated with Δ_{leaf} (r ranged from -0.37 to -0.71; $P < 0.05$). Further, we found that $|\pi_{tlp}|$ and *WD* were negatively correlated with *LA* and PLA_{dry} (r ranged from -0.43 to -0.63; Table S4.5); $|\pi_{tlp}|$ was positively

correlated with *LMA* ($r = 0.46$, respectively; $P < 0.05$), while *WD* was positively correlated with C_{mass} ($r = 0.42$; $P < 0.05$) and negatively correlated with P_{area} and P_{mass} ($r = -0.6$, respectively; $P < 0.05$). Finally, $|\pi_{tlp}|$ and *WD* were negatively correlated with $\bar{A}_{mass}$, $\bar{g}_{cleaf}$ and c_i:c_a ratio (r ranged from -0.42 to -0.57; $P < 0.05$).

Appendix Table 4.1. Expectations for variation between forests in given traits, based on adaptive functions described in the previous literature on diverse species, given that the montane wet forest MWF has greater water and nutrient availability and lower light availability in the understorey than the LDF. "W" represents the expectation that, all else being equal, given the specific hypothesis, the wet forest would have a higher trait value than the dry forest on average, and "D" that the dry forest would have the higher trait value on average.

Trait	Expectation based on:	
	Water and nutrient availability higher in MWF than LDF	**Light availability higher in LDF**
Stomatal morphology		
d	W. More stomata per area enables greater CO_2 assimilation and promotes growth and competition (Hetherington & Woodward 2003) D. More stomata per area enables greater CO_2 assimilation in times when water is available and is selected when the period of available water is shorter (Maximov 1931; Grubb 1998; Scoffoni *et al.* 2011)	D. Shade tolerant species tend to have fewer stomata per area reflecting their lower limitation by CO_2 relative to irradiance (Givnish 1988)
i	W. Greater rates of stomatal development enable greater CO_2 assimilation and promotes growth and competition (Sack & Buckley 2016) D. Greater rates of stomatal development enable greater CO_2 assimilation in times when water is available and is selected when the period of available water is shorter (Maximov 1931; Grubb 1998; Scoffoni *et al*. 2011)	D. Shade tolerant species tend to have fewer stomata per epidermal cells reflecting their lower limitation by CO_2 relative to irradiance (Givnish 1988)
s	W. Larger guard cells and stomata result in larger pores, enabling greater CO_2 assimilation and promotes growth and competition (Hetherington & Woodward 2003). Smaller, denser stomatal guard cells and pores may increase the efficiency of CO_2 capture, and may enable more rapid stomatal responses to dehydration, protecting species facing drought (Franks & Farquhar 2007)	W. Shade tolerant species tend to have larger stomatal guard cells and pores, consistent with their lower densities and possibly reflecting less selection for rapid responses to dehydration (Givnish 1988)
GC_L	"	"
GC_W	"	"
SP_L	"	"

e	W. Epidermal pavement cell size typically scales with stomatal size (Beaulieu *et al.* 2008)	W. Epidermal pavement cell size typically scales with stomatal size (Beaulieu *et al.* 2008)
g_{max}	W. Higher g_{max} leads to higher potential CO_2 assimilation rate (Franks & Beerling 2009; Wang *et al.* 2015) D. Higher stomatal conductance enables greater CO_2 assimilation in times when water is available and is selected when the period of available water is shorter (Maximov 1931; Grubb 1998; Scoffoni *et al*. 2011)	D. Shade tolerant species tend to have lower stomatal conductance reflecting their lower limitation by CO_2 relative to irradiance (Givnish 1988)
Leaf venation		
VLA_{major}	W. Higher vein densities a would increase leaf hydraulic conductance and potentially photosynthetic rate and growth (Sack & Frole 2006; Brodribb, Feild & Jordan 2007; Sack & Scoffoni 2013; Iida *et al.* 2016; Scoffoni *et al*. 2016) D. Higher major vein densities will provide redundancy to protect from the detrimental effect of xylem embolism on leaf hydraulic function (Sack & Scoffoni 2013)	D. Shade tolerant species tend to have larger leaves, which tend to possess lower major vein densities (Sack *et al.* 2012)
VLA_{minor}	W. Higher vein densities a would increase leaf hydraulic conductance and potentially photosynthetic rate and growth (Sack & Frole 2006; Brodribb, Feild & Jordan 2007; Sack & Scoffoni 2013; Iida *et al.* 2016; Scoffoni *et al*. 2016) D. Higher minor vein densities enable greater stomatal conductance and CO_2 assimilation in times when water is available and is selected when the period of available water is shorter (Maximov 1931; Grubb 1998; Scoffoni *et al.* 2011)	D. Shade tolerant species tend to have lower minor vein densities, consistent with lower construction costs and their lower stomatal conductance reflecting their lower limitation by CO_2 relative to irradiance (Sack & Scoffoni 2013)
VLA_{total}	W. Higher vein densities a would increase leaf hydraulic conductance and potentially photosynthetic rate and growth (Sack & Frole 2006; Brodribb, Feild & Jordan 2007; Sack & Scoffoni 2013; Iida *et al.* 2016; Scoffoni *et al*. 2016) D. Higher major and minor vein densities and therefore total vein density enable greater leaf hydraulic safety and also stomatal conductance and CO_2 assimilation in times when water is available and is selected when the period of available water is shorter (Maximov 1931; Grubb 1998; Scoffoni *et al.* 2011)	D. Shade tolerant species tend to have lower vein densities, consistent with lower construction costs and their lower stomatal conductance reflecting their lower limitation by CO_2 relative to irradiance (Sack & Scoffoni 2013)
FEV	W. Higher free ending vein densities would increase leaf hydraulic conductance and potentially photosynthetic rate (Sack & Scoffoni 2013) D. Higher free ending vein densities enable greater stomatal conductance and CO_2 assimilation in times when water is available and is selected when the period of available water is shorter (Maximov 1931; Grubb 1998; Scoffoni *et al.* 2011)	D. Shade tolerant species may have lower free ending vein densities, associated with lower stomatal conductance reflecting their lower limitation by CO_2 relative to irradiance (Sack & Scoffoni 2013)
Leaf and wood economics and structure		

LA	W. Smaller leaves have higher major vein densities, which would provide greater leaf hydraulic safety, and have thinner boundaries enabling leaves to stay cool especially when transpirational cooling is not possible during drought (Sack *et al.* 2012; Wright *et al.* 2017)	W. Shade tolerant species tend to have larger leaves for greater efficiency in light capture relative to allocation to support (Niinemets 2001)
LMA	D. A lower *LMA* would be expected to promote more rapid relative growth rate, whereas a higher *LMA* would be associated with longer leaf lifetime and confer an advantage in stressful or low resource conditions (Evans 1973; Wright *et al.* 2004; Westoby & Wright 2006). High *LMA* leaves also may enable lower cuticular transpiration rates when stomata close due to lower surface area: volume and thicker cuticles, and may have higher elastic moduli which may enable greater water retention in leaves with lower wilting points (Niinemets 2001; Wright *et al.* 2004; Brodribb, Feild & Jordan 2007)	W. Shade-adapted evergreen species tend to have high LMA, associated with longer leaf lifespan and lower respiratory demand (Niinemets 2001; Lusk & Warton 2007; Poorter *et al.* 2009)
LT	D. Thinner leaves are associated with lower LMA and thus higher potential relative growth rate, and thicker leaves with higher LMA, longer leaf lifetimes and slower relative growth rates (Evans 1973; Niinemets 2001; Wright *et al.* 2004; Westoby & Wright 2006). Thicker leaves may also enable lower cuticular transpiration rates when stomata close due to lower surface area: volume and thicker cuticles, and may have higher elastic moduli which may enable greater water retention in leaves with lower wilting points (Niinemets 2001; Wright *et al.* 2004; Brodribb, Feild & Jordan 2007)	W. Shade-adapted evergreen species tend to have thicker leaves associated with higher LMA, longer leaf lifespan and lower respiratory demand (Niinemets 2001; Lusk & Warton 2007; Poorter *et al.* 2009)
LD	D. Less dense leaves are associated with lower LMA and thus higher potential relative growth rate, and denser leaves with higher LMA, longer leaf lifetimes and slower relative growth rates (Evans 1973; Niinemets 2001; Wright *et al.* 2004; Westoby & Wright 2006). Denser leaves may have higher elastic moduli which may enable greater water retention in leaves with lower wilting points (Niinemets 2001; Wright *et al.* 2004; Brodribb, Feild & Jordan 2007)	W. Shade-adapted evergreen species tend to have denser leaves associated with higher LMA, longer leaf lifespan and lower respiratory demand (Niinemets 2001; Lusk & Warton 2007; Poorter *et al.* 2009)
LDMC	D. Lower LDMC is related to lower LMA and thus higher potential relative growth rate, and higher LDMC leaves with higher LMA, longer leaf lifetimes and slower relative growth rates. Lower LDMC may also be linked with drought tolerance in certain ecosystems (Niinemets 2001; Diaz *et al.* 2016)	D. Lower LDMC is related to lower LMA, which may be linked with shade tolerance in evergreen forests see above (Niinemets 2001; Diaz *et al.* 2016)
SWC	W. Higher SWC is related to lower LMA and thus higher potential relative growth rate, and lower SWC leaves with higher LMA, longer leaf lifetimes and slower relative growth rates (Vendramini *et al.* 2002) D. High SWC may provide water storage to buffer low leaf water potentials during transpiration under soil and atmospheric drought, or to enable leaf survival after stomata close (Sack, Tyree & Holbrook 2005; Ogburn & Edwards 2012)	D. Lower SWC is related to higher LMA and longer leaf lifetimes, which would result in lower resource demand benefitting shade-tolerant evergreen species (Vendramini *et al.* 2002)
WMA	D. Lower WMA is related to lower LMA and thus higher potential relative growth rate, and higher SWC leaves with higher LMA, longer leaf lifetimes and slower relative growth rates (Vendramini *et al.* 2002). Conversely, high WMA may provide water storage to buffer low leaf water potentials during	D. Lower WMA is related to higher LMA and longer leaf lifetimes, which would result in lower resource demand benefitting shade-tolerant evergreen species (Vendramini *et al.* 2002)

	transpiration under soil and atmospheric drought, or to enable leaf survival after stomata close (Sack, Tyree & Holbrook 2005; Ogburn & Edwards 2012)	
PLA_{dry}	W. Leaves resistant to shrinkage may have higher elastic moduli, which may enable greater water retention in leaves with lower wilting points (Bartlett, Scoffoni & Sack 2012; Scoffoni *et al.* 2014)	NA
WD	D. A lower *WD*, being associated with higher hydraulic conductance and lower construction cost, would be expected to promote more rapid relative growth rate, whereas a higher *WD* would be associated with longer wood lifetimes and lower vulnerability to xylem embolism at the cost of potential relative growth rate (Hacke *et al.* 2001; Chave *et al.* 2009; Gleason *et al.* 2016).	W. A higher *WD* is associated with greater shade tolerance, potentially due to investment in longer wood lifetimes and thus reduction of resource demand (Givnish 1988)
Leaf composition		
N_{area}	W. Higher nutrient concentrations per leaf area or mass are linked with more rapid photosynthetic rates per leaf area or mass respectively (Wright *et al.* 2004) D. Higher nutrient concentrations enable greater CO_2 assimilation in times when water is available and is selected when the period of available water is shorter (Maximov 1931; Grubb 1998; Scoffoni *et al*. 2011)	D. Lower nutrient concentrations are associated with shade tolerance due to lower resource demand and lower limitation by CO_2 (Givnish 1988)
N_{mass}	"	"
P_{area}	"	"
P_{mass}	"	"
Chl_{area}	W. Higher *Chl* concentration per leaf area or mass may be linked with more rapid photosynthetic rates per leaf area or mass respectively (Chatuverdi, Raghubanshi & Singh 2011) D. Higher *Chl* concentrations may enable greater CO_2 assimilation in times when water is available and is selected when the period of available water is shorter (Maximov 1931; Grubb 1998; Scoffoni *et al*. 2011)	W. Higher *Chl* concentration per leaf area or mass may be linked with greater light harvesting potential, of benefit in the shade (Chatuverdi, Raghubanshi & Singh 2011)
Chl_{mass}	"	"
C_{mass}	W. Higher carbon concentration per mass is related to lower N and P concentrations per mass, which would be related to lower photosynthetic rates per leaf mass (Lambers & Poorter 2004)	W. Higher carbon concentration per mass is related to lower N and P concentrations per mass, which would be related to resource demand and assimilation rates as expected in shade adapted species (Elser *et al.* 2000; Lambers & Poorter 2004)
N:*P*	D. *N*:*P* is expected to be higher under conditions when P_{mass} is lower and growth is slower (Elser *et al.* 2000)	W. *N*:*P* is expected to be higher under conditions when P_{mass} is lower and growth is slower, as would be expected for shade-adapted species (Elser *et al.* 2000)

Chl_{area}:N_{area}	NA	W. Shade adapted species are expected to invest more strongly in light relative to carbon reactions, and thus to chlorophyll relative to Rubisco (Givnish 1988)
Δ_{leaf}	W. Higher stomatal conductance values integrated over leaf lifetimes would promote higher CO_2 assimilation rates and these would be associated with higher C isotope discrimination; drought tolerant species would have lower stomatal conductance over the leaf lifetime (Farquhar, Ehleringer & Hubick 1989; Donovan & Ehleringer 1994)	W. Higher stomatal conductance values integrated over leaf lifetimes would be associated with higher C isotope discrimination; shade tolerant species would have lower stomatal conductance over the leaf lifetime reflecting their lower CO_2 limitation (Farquhar, Ehleringer & Hubick 1989; Donovan & Ehleringer 1994)
$\lvert\pi_{tlp}\rvert$	D. Drought tolerant species should have lower wilting points i.e., higher $\lvert\pi_{tlp}\rvert$ to withstand lower soil water potentials (Bartlett, Scoffoni & Sack 2012)	NA
Estimated photosynthesis		
$Jmax_{area}$	W. Higher values for photosynthetic parameters would be associated with greater rates of CO_2 assimilation and growth (Farquhar, Ehleringer & Hubick 1989; Evans 2013) D. Higher values for photosynthetic parameters would be associated with greater rates of CO_2 assimilation and growth (Farquhar, Ehleringer & Hubick 1989; Evans 2013) in times when water is available and is selected when the period of available water is shorter (Maximov 1931; Grubb 1998; Scoffoni *et al.* 2011)	D. Higher values for photosynthetic parameters would be associated with greater rates of CO_2 assimilation and growth (Farquhar, Ehleringer & Hubick 1989; Evans 2013), and shade tolerant species would be expected to have lower growth associated with their lower resource demand
$Jmax_{mass}$	"	"
$Vcmax_{area}$	"	"
$Vcmax_{mass}$	"	"
c_i:c_a	W. Higher stomatal conductance values integrated over leaf lifetimes would be associated with higher c_i:c_a and should correspond to greater photosynthetic rates; drought tolerant species would have lower stomatal conductance over the leaf lifetime (Donovan & Ehleringer 1994; Wang *et al.* 2017).	D. Higher stomatal conductance values integrated over leaf lifetimes would be associated with higher c_i:c_a; shade tolerant species would have lower stomatal conductance over the leaf lifetime (Donovan & Ehleringer 1994)
$\bar{A}_{area}$	W. Higher photosynthetic rates should relate to greater productivity and competition, and drought tolerant species would have lower stomatal conductance and photosynthetic rates averaged over leaf lifetimes because of stomatal closure for water retention during dry periods (Franks & Beerling 2009)	D. Shade tolerant species would have lower stomatal conductance and photosynthetic rates averaged over leaf lifetimes because of stomatal closure for water retention during dry periods (Franks & Beerling 2009)
$\bar{A}_{mass}$	"	"
$\bar{g}_{cleaf}$	W. Higher stomatal conductance should enable greater photosynthetic rates and thereby greater productivity and competition (Franks & Beerling 2009)	"
$\bar{g}_{cleaf}$:g_{max}	W. Leaves operating at a greater proportion of their anatomical maximum stomatal conductance should enable greater photosynthetic rates and thereby greater productivity and competition (Franks & Beerling 2009)	NA

	D. Leaves operating at a greater proportion of their anatomical maximum stomatal conductance should enable greater photosynthetic rates in times when water is available and is selected when the period of available water is shorter (Maximov 1931; Grubb 1998; Scoffoni *et al.* 2011)	
g_{max}:N_{area}	W. Drought tolerant species should have lower stomatal conductance relative to photosynthetic rate and therefore relative to leaf nitrogen to enable higher water use efficiency (Wright, Reich & Westoby 2001)	NA
Whole plant size and growth		
RGR_{dbh},RGR_{biom}	W. Wetter forests have more resources and should support faster relative growth due to higher photosynthetic rates, while drought tolerant species have more conservative water use, so are not able to support fast growth due to low photosynthetic rates (Wright *et al.* 2004; Gibert *et al.* 2016)	D. Shade adapted species tend to grow slowly due to reduced competition and resource demand (Givnish 1988)
m	W. Wetter forests have more resources and should support faster relative growth due to higher photosynthetic rates, but species will be more sensitive to disturbances and when the conditions are not favorable, which may lead to higher *m* (Wright *et al.* 2010; McDowell *et al.* 2018) D. In dry forests species are grow under low water availability, which may lead to death due to xylem cavitation when droughts are more intense (McDowell *et al.* 2008, 2018).	W. Shading is expected to drive mortality in wet forests and has been associated with carbon starvation (Kobe & Coates 1997; Wright *et al.* 2010; McDowell *et al.* 2018)
H	W. Wetter forests have greater resources leading to preferential selection for mean and maximum height growth for increased competition, while in drier forests plants have lower allocation to mean and maximum height growth to maximize below ground allocation and minimize hydraulic pathlength susceptible to tension-driven embolism (Koch *et al*. 2004; King, Davies & Noor 2006)	NA
H_{max}	"	NA
SM	D. Species of more competitive ecosystems would have smaller seeds for greater dispersal potential (Gross 1984). Additionally, drought tolerant species would benefit from greater allocation to seed reserves to enable seedlings to establish rapidly when water is available (Khurana & Singh 2004)	W. Shade tolerant species would frequently benefit from greater allocation to seed reserves to enable establishment in low resource conditions (Gross 1984)

SUPPLEMENTARY MATERIALS

Supplementary data captions (see attached Excel Workbook)

Table S4.1. Range of species mean trait values in species from a Hawaiian Montane Wet Forest (MWF) and a Lowland Dry Forest (LDF), with mean and standard error (SE), and nested ANOVA results, where species were nested in forest types, and both were fixed as independent variables.

Table S4.2. *t*-test results table of analysis comparing the LDF and MWF.

Table S4.3. *F*-test results table of analysis comparing the variance in traits in the LDF and MWF.

Table S4.4. Correlation matrix with trait-trait correlation coefficients of the complete data-set (MWF + LDF species).

Table S4.5. Correlation matrix with trait-trait correlation coefficients of MWF species.

Table S4.6. Correlation matrix with trait-trait correlation coefficients of LDF species.

Table S4.7. Median values and 95% credible intervals of probability distribution of the posterior demographic parameters estimated using a hierarchical Bayesian approach for the complete data-set (MWF + LDF species).

Table S4.8. Correlations between traits hypothesized to be correlated with growth and mortality with P-values corrected using the Benjamini & Hochberg method (1950).

Table S4.9. Results from forward selection, backward elimination and stepwise regression procedures of variable selection for models to predict RGR_{dbh}, RGR_{biom} and m.

Supplementary figure captions

Figure S4.1. Relationships between growth rate in terms of above-ground biomass and A stomatal density and B maximum stomatal conductance. Black symbols, Montane Wet Forest MWF species; gray symbols, Lowland Dry Forest LDF. $RGR_{biom} = 3.02e^{-03} + 5.51e^{-05} * d$; $RGR_{biom} = 0.01 + 0.004 * g_{max}$. $*P < 0.05$, $**P < 0.01$, $***P < 0.001$.

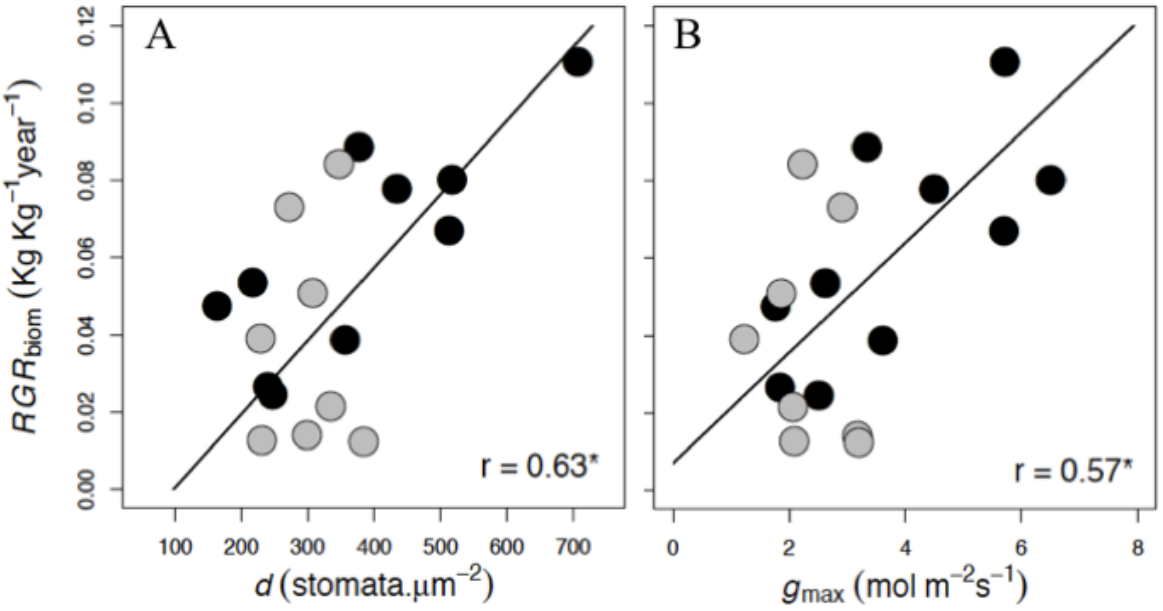
A
B
r = 0.63*
r = 0.57*
RGR_{biom} (Kg Kg^{-1}year^{-1})
0.00
0.02
0.04
0.06
0.08
0.10
0.12
100
200
300
400
500
600
700
d (stomata.µm^{-2})
0
2
4
6
8
g_{max} (mol m^{-2}s^{-1})

Figure S4.1

REFERENCES

Adler, P.B., Salguero-Gomez, R., Compagnoni, A., Hsu, J.S., Ray-Mukherjee, J., Mbeau-Ache, C., *et al.* (2014). Functional traits explain variation in plant life history strategies. *Proc Natl Acad Sci USA*, 111, 740–745.

Armbruster, W.S., Pélabon, C., Bolstad, G.H. & Hansen, T.F. (2014). Integrated phenotypes: understanding trait covariation in plants and animals. *Phil Trans R Soc B*, 369, 20130245.

Asefa, M., Cao, M., Zhang, G., Ci, X., Li, J. & Yang, J. (2017). Environmental filtering structures tree functional traits combination and lineages across space in tropical tree assemblages. *Sci Rep*, 7, 132.

Baltzer, J.L., Davies, S.J., Bunyavejchewin, S. & Noor, N.S.M. (2008). The role of desiccation tolerance in determining tree species distributions along the Malay–Thai Peninsula. *Funct Ecol*, 22, 221–231.

Bartlett, M.K., Klein, T., Jansen, S., Choat, B. & Sack, L. (2016). The correlations and sequence of plant stomatal, hydraulic, and wilting responses to drought. *Proc Natl Acad Sci USA*, 113, 13098–13103.

Bartlett, M.K., Scoffoni, C., Ardy, R., Zhang, Y., Sun, S., Cao, K., *et al.* (2012a). Rapid determination of comparative drought tolerance traits: using an osmometer to predict turgor loss point. *Methods Ecol Evol*, 3, 880–888.

Bartlett, M.K., Scoffoni, C. & Sack, L. (2012b). The determinants of leaf turgor loss point and prediction of drought tolerance of species and biomes: a global meta-analysis. *Ecol Lett*, 15, 393–405.

Beaulieu, J.M., Leitch, I.J., Patel, S., Pendharkar, A. & Knight, C.A. (2008). Genome size is a strong predictor of cell size and stomatal density in angiosperms. *New Phytol*, 179, 975–986.

Blackman, C.J., Brodribb, T.J. & Jordan, G.J. (2012). Leaf hydraulic vulnerability influences species' bioclimatic limits in a diverse group of woody angiosperms. *Oecologia*, 168, 1–10.

Brenes-Arguedas, T., Roddy, A.B., Kursar, T.A. & Tjoelker, M. (2013). Plant traits in relation to the performance and distribution of woody species in wet and dry tropical forest types in Panama. *Funct Ecol*.

Brodribb, T.J., Feild, T.S. & Jordan, G.J. (2007). Leaf maximum photosynthetic rate and venation are linked by hydraulics. *Plant Physiol*, 144, 1890–1898.

Brodribb, T.J., Feild, T.S. & Sack, L. (2010). Viewing leaf structure and evolution from a hydraulic perspective. *Functional Plant Biol*, 37, 488–498.

Brodribb, T.J., McAdam, S.A. & Carins Murphy, M.R. (2017). Xylem and stomata, coordinated through time and space: Functional linkages between xylem and stomata. *Plant Cell Environ*, 40, 872–880.

Chaturvedi, R.K., Raghubanshi, A.S. & Singh, J.S. (2011). Leaf attributes and tree growth in a tropical dry forest. *J Veg Sci*, 22, 917–931.

Chave, J., Andalo, C., Brown, S., Cairns, M.A., Chambers, J.Q., Eamus, D., *et al.* (2005). Tree allometry and improved estimation of carbon stocks and balance in tropical forests. *Oecologia*, 145, 87–99.

Chave, J., Coomes, D., Jansen, S., Lewis, S.L., Swenson, N.G. & Zanne, A.E. (2009). Towards a worldwide wood economics spectrum. *Ecol Lett*, 12, 351–366.

Chesson, P. (2000). Mechanisms of maintenance of species diversity. *Annu Rev Ecol Syst*, 31, 343–366.

Chevan, A. & Sutherland, M. (1991). Hierarchical partitioning. *Am Stat*, 45, 90–96.

Condit, R. (1998). Tropical Forest Census Plots.

Cornwell, W.K., Schwilk, D.W. & Ackerly, D.D. (2006). A trait-based test for habitat filtering: convex hull volume. *Ecology*, 87, 1465–1471.

Crews, T.E., Kitayama, K., Fownes, J.H., Riley, R.H., Herbert, D.A., Mueller-Dombois, D., *et al.* (1995). Changes in Soil Phosphorus Fractions and Ecosystem Dynamics across a LongChronosequence in Hawaii. *Ecology*.

Díaz, S., Kattge, J., Cornelissen, J.H.C., Wright, I.J., Lavorel, S., Dray, S., *et al.* (2016). The global spectrum of plant form and function. *Nature*, 529, 167–171.

Domingues, T.F., Meir, P., Feldpausch, T.R., Saiz, G., Veenendaal, E.M., Schrodt, F., *et al.* (2010). Co-limitation of photosynthetic capacity by nitrogen and phosphorus in West Africa woodlands. *Plant Cell Environ*.

Donovan, L.A. & Ehleringer, J.R. (1994). Carbon isotope discrimination, water-use efficiency, growth, and mortality in a natural shrub population. *Oecologia*, 100, 347–354.

Elser, J.J., Fagan, W.F., Denno, R.F., Dobberfuhl, D.R., Folarin, A., Huberty, A., *et al.* (2000). Nutritional constraints in terrestrial and freshwater foodwebs. *Nature*.

Evans, G.C. (1973). *The quantitative analysis of plant growth*. University of California Press, Berkeley and Los Angeles, California.

Evans, J.R. (2013). Improving photosynthesis. *Plant Physiol*, 162, 1780–1793.

Falcão, H.M., Medeiros, C.D., Silva, B.L.R., Sampaio, E.V.S.B., Almeida-Cortez, J.S. & Santos, M.G. (2015). Phenotypic plasticity and ecophysiological strategies in a tropical dry forest chronosequence: a study case with *Poincianella pyramidalis*. *For Ecol Manag*.

Farquhar, G., O'Leary, M. & Berry, J. (1982). On the relationship between carbon isotope discrimination and the intercellular carbon dioxide concentration in leaves. *Functional Plant Biol*, 9, 121.

Farquhar, G.D., Ehleringer, J.R. & Hubick, K.T. (1989). Carbon isotope discrimination and photosynthesis. *Annu Rev Plant Physiol Plant Mol Biol*, 40, 503–537.

Farquhar, G.D. & Richards, R.A. (1984). Isotopic composition of plant carbon correlates with water-use efficiency of Wheat genotypes. *Aust J Plant Physiol*, 11, 539–552.

Fine, P.V.A., Lohbeck, M., Lebrija-Trejos, E., Martínez-Ramos, M., Meave, J.A., Poorter, L., *et al.* (2015). Functional Trait Strategies of Trees in Dry and Wet Tropical Forests Are Similar but Differ in Their Consequences for Succession. *Plos One*.

Finegan, B., Peña-Claros, M., de Oliveira, A., Ascarrunz, N., Bret-Harte, M.S., Carreño-Rocabado, G., *et al.* (2015). Does functional trait diversity predict above-ground biomass and productivity of tropical forests? Testing three alternative hypotheses. *J Ecology*.

Fiske, I.J., Bruna, E.M. & Bolker, B.M. (2008). Effects of sample size on estimates of population growth rates calculated with matrix models. *PLoS ONE*, 3, e3080.

Fortini, L., Price, J., Jacobi, J., Vorsino, A., Burgett, J., Brinck, K., *et al.* (2013). *A Landscape-based assessment of climate change vulnerability for all native Hawaiian plant*. University of Hawaii Publisher, Hilo, HI.

Franks, P.J., Drake, P.L. & Beerling, D.J. (2009). Plasticity in maximum stomatal conductance constrained by negative correlation between stomatal size and density: an analysis using *Eucalyptus globulus*. *Plant Cell Environ*.

Franks, P.J. & Farquhar, G.D. (2007). The mechanical diversity of stomata and its significance in gas-exchange control. *Plant Physiol*, 143, 78–87.

Franks, P.J., Royer, D.L., Beerling, D.J., Van de Water, P.K., Cantrill, D.J., Barbour, M.M., *et al.* (2014). New constraints on atmospheric CO2concentration for the Phanerozoic. *Geophys Res Lett*.

Fry, B., Ganitt, R., Tholke, K., Neill, C., Michener, R.H., Mersch, F.J., *et al.* (1996). Cryoflow: Cryofocusing Nanomole Amounts of CO2, N2, and SO2 from an Elemental Analyzer for Stable Isotopic Analysis. *Rapid communications in mass spectrometry*.

Fyllas, N.M., Gloor, E., Mercado, L.M., Sitch, S., Quesada, C.A., Domingues, T.F., *et al.* (2014). Analysing Amazonian forest productivity using a new individual and trait-based model (TFS v.1). *Geosci Model Dev*, 7, 19.

Gaviria, J., Turner, B.L. & Engelbrecht, B.M.J. (2017). Drivers of tree species distribution across a tropical rainfall gradient. *Ecosphere*, 8, 16.

Giambelluca, T.W., Chen, Q., Frazier, A.G., Price, J.P., Chen, Y.-L., Chu, P.-S., *et al.* (2013). Online Rainfall Atlas of Hawai'i. *Bulletin of the American Meteorological Society*.

Gibert, A., Gray, E.F., Westoby, M., Wright, I.J., Falster, D.S. & Wilson, S. (2016). On the link between functional traits and growth rate: meta-analysis shows effects change with plant size, as predicted. *Journal of Ecology*.

Gil-Pelegrín, E., Saz, M.Á., Cuadrat, J.M., Peguero-Pina, J.J. & Sancho-Knapik, D. (2017). Oaks under Mediterranean-type Cclimates: functional response to summer aridity. In: *Oaks Physiological Ecology. Exploring the Functional Diversity of Genus Quercus L.*, Tree Physiology (eds. Gil-Pelegrín, E., Peguero-Pina, J.J. & Sancho-Knapik, D.). Springer International Publishing, Cham, pp. 137–193.

Givnish, T.J. (1987). Comparative studies of leaf form: assessing the relative roles of selective pressures and phylogenetic constraints. *New Phytol*, 106, 131–160.

Givnish, T.J., Pires, J.C., Graham, S.W., McPherson, M.A., Prince, L.M., Patterson, T.B., *et al.* (2005). Repeated evolution of net venation and fleshy fruits among monocots in shaded habitats confirms a priori predictions: evidence from an ndhF phylogeny. *Proc R Soc B*, 272, 1481–1490.

Gleason, S.M., Westoby, M., Jansen, S., Choat, B., Hacke, U.G., Pratt, R.B., *et al.* (2016). Weak tradeoff between xylem safety and xylem-specific hydraulic efficiency across the world's woody plant species. *New Phytol*, 209, 123–136.

Greenwood, S., Ruiz-Benito, P., Martínez-Vilalta, J., Lloret, F., Kitzberger, T., Allen, C.D., *et al.* (2017). Tree mortality across biomes is promoted by drought intensity, lower wood density and higher specific leaf area. *Ecol Lett*.

Grime, J.P. (2006). *Plant strategies, vegetation processes, and ecosystem properties*. 2nd edn. Chichester.

Gross, K.L. (1984). Effects of seed size and growth form on seedling establishment of six monocarpic perennial plants. *J Ecol*, 72, 369–387.

Grubb, P.J. (1998). A reassessment of the strategies of plants which cope with shortages of resources. *Perspect Plant Ecol Evol Syst*, 1, 3–31.

Hacke, U.G., Sperry, J.S., Pockman, W.T., Davis, S.D. & McCulloh, K.A. (2001). Trends in wood density and structure are linked to prevention of xylem implosion by negative pressure. *Oecologia*, 126, 457–461.

Harrison, R.D. (2011). Emptying the forest: hunting and the extirpation of wildlife from tropical nature reserves. *BioScience*.

Hastie, T. & Pregibon, D. (1992). Generalized linear models. In: *Statistical Models in S*. Wadsworth & Brooks/Cole, Pacific Grove, CA, pp. 195–246.

Hérault, B., Bachelot, B., Poorter, L., Rossi, V., Bongers, F., Chave, J., *et al.* (2011). Functional traits shape ontogenetic growth trajectories of rain forest tree species. *J Ecol*.

Hetherington, A.M. & Woodward, F.I. (2003). The role of stomata in sensing and driving environmental change. *Nature*.

Hurvich, C.M. & Tsai, C.-L. (1989). Regression and time series model selection in small samples. *Biometrika*, 76, 297–307.

Iida, Y., Poorter, L., Sterk, F., Kassim, A.R., Potts, M.D., kubo, T., *et al.* (2014). Linking size-dependent growth and mortality with architectural traits across 145 co-occurring tropical tree species. *Ecology*.

Iida, Y., Sun, I.F., Price, C.A., Chen, C.-T., Chen, Z.-S., Chiang, J.-M., *et al.* (2016). Linking leaf veins to growth and mortality rates: an example from a subtropical tree community. *Ecol Evol*.

Inman-Narahari, F., Ostertag, R., Asner, G.P., Cordell, S., Hubbell, S.P. & Sack, L. (2014). Trade-offs in seedling growth and survival within and across tropical forest microhabitats. *Ecology and Evolution*.

John, G.P., Scoffoni, C., Buckley, T.N., Villar, R., Poorter, H., Sack, L., *et al.* (2017). The anatomical and compositional basis of leaf mass per area. *Ecol Lett*, 20, 412–425.

Khurana, E. & Singh, J.S. (2004). Germination and seedling growth of five tree species from tropical dry forest in relation to water stress: impact of seed size. *J Trop Ecol*, 20, 385–396.

King, D.A., Davies, S.J. & Noor, N.S.Md. (2006). Growth and mortality are related to adult tree size in a Malaysian mixed dipterocarp forest. *For Ecol Manag*, 223, 152–158.

Kitajima, K. (1994). Relative Iimportance of photosynthetic traits and allocation patterns as correlates of seedling shade tolerance of 13 tropical trees. *Oecologia*, 98, 419–428.

Kobe, R.K. & Coates, K.D. (1997). Models of sapling mortality as a function of growth to characterize interspecific variation in shade tolerance of eight tree species of northwestern British Columbia. *Can J For Res*, 27, 10.

Koch, G.W., Sillett, S.C., Jennings, G.M. & Davis, S.D. (2004). The limits to tree height. *Nature*, 428, 851–854.

Kraft, N.J.B., Adler, P.B., Godoy, O., James, E.C., Fuller, S. & Levine, J.M. (2014). Community assembly, coexistence and the environmental filtering metaphor. *Funct Ecol*, 8.

Lambers, H. & Poorter, H. (2004). Inherent variation in growth rate between higher plants: a search for physiological causes and ecological consequences. In: *Advances in Ecological Research*. Elsevier, pp. 283–362.

Lavorel, S. & Garnier, E. (2002). Predicting changes in community composition and ecosystem functioning from plant traits: revisiting the Holy Grail. *Funct Ecol*, 16, 545–556.

Lebrija-Trejos, E., Meave, J.A., Poorter, L., Pérez-García, E.A. & Bongers, F. (2010). Pathways, mechanisms and predictability of vegetation change during tropical dry forest succession. *Perspectives in Plant Ecology, Evolution and Systematics*, 12, 267–275.

Levine, J.M., Bascompte, J., Adler, P.B. & Allesina, S. (2017). Beyond pairwise mechanisms of species coexistence in complex communities. *Nature*, 546, 9.

Li, L., McCormack, M.L., Ma, C., Kong, D., Zhang, Q., Chen, X., *et al.* (2015a). Leaf economics and hydraulic traits are decoupled in five species-rich tropical-subtropical forests. *Ecol Lett*.

Li, R., Zhu, S., Chen, H.Y.H., John, R., Zhou, G., Zhang, D., *et al.* (2015b). Are functional traits a good predictor of global change impacts on tree species abundance dynamics in a subtropical forest? *Ecol Lett*, 18, 1181–1189.

Liu, X., Swenson, N.G., Lin, D., Mi, X., Umana, M.N., Schmid, B., *et al.* (2016). Linking individual-level functional traits to tree growth in a subtropical forest. *Ecology*.

Lusk, C.H. & Warton, D.I. (2007). Global meta-analysis shows that relationships of leaf mass per area with species shade tolerance depend on leaf habit and ontogeny. *New Phytol*, 176, 764–774.

Markesteijn, L., Iraipi, J., Bongers, F. & Poorter, L. (2010). Seasonal variation in soil and plant water potentials in a Bolivian tropical moist and dry forest. *J Trop Ecol*, 26, 497–508.

Marks, C.O. & Lechowicz, M.J. (2006). Alternative designs and the evolution of functional diversity. *Am Nat*, 167, 55–66.

Maximov, N.A. (1931). The physiological significance of the xeromorphic structure of plants. *J Ecol*, 19, 273.

Mayfield, M.M., Boni, M.F. & Ackerly, D.D. (2009). Traits, Habitats, and Clades: Identifying Traits of Potential Importance to Environmental Filtering. *Am Nat*, 174, E1–E22.

McDowell, N., Allen, C.D., Anderson-Teixeira, K., Brando, P., Brienen, R., Chambers, J., *et al.* (2018). Drivers and mechanisms of tree mortality in moist tropical forests. *New Phytol*, 219, 851–869.

McDowell, N., Pockman, W.T., Allen, C.D., Breshears, D.D., Cobb, N., Kolb, T., *et al.* (2008). Mechanisms of plant survival and mortality during drought: why do some plants survive while others succumb to drought? *New Phytol*, 178, 719–739.

McElwain, J.C., Yiotis, C. & Lawson, T. (2016). Using modern plant trait relationships between observed and theoretical maximum stomatal conductance and vein density to examine patterns of plant macroevolution. *New Phytol*.

Messier, J., Lechowicz, M.J., McGill, B.J., Violle, C., Enquist, B.J. & Cornelissen, H. (2017). Interspecific integration of trait dimensions at local scales: the plant phenotype as an integrated network. *J Ecol*.

Monje, O.A. & Bugbee, B. (1992). Inherent Limitations of Nondestructive Chlorophyll Meters: A Comparison of Two Types of Meters. *HortScience*.

Moore, R.B., Clague, D.A., Rubin, M. & Bohrson, W.A. (1987). Hualalai-Volcano: a preliminary summary of geologic, petrologic, geophysical data. Volcanism in Hawaii.

Nathan, J., Osem, Y., Shachak, M. & Meron, E. (2016). Linking functional diversity to resource availability and disturbance: a mechanistic approach for water-limited plant communities. *J Ecol*, 104, 419–429.

Niinemets, Ü. (2001). Global-scale climatic controls of leaf dry mass per area, density, and thickness in trees and shrubs. *Ecol*, 82, 453–469.

Ogburn, R.M. & Edwards, E.J. (2012). Quantifying succulence: a rapid, physiologically meaningful metric of plant water storage. *Plant Cell Environ*.

Ogle, K. (2003). Implications of interveinal distance for quantum yield in C 4 grasses: a modeling and meta-analysis. *Oecologia*, 136, 532–542.

Osborne, C.P. & Sack, L. (2012). Evolution of C_4 plants: a new hypothesis for an interaction of CO_2 and water relations mediated by plant hydraulics. *Phil Trans R Soc B*, 367, 583–600.

Osone, Y., Ishida, A. & Tateno, M. (2008). Correlation between relative growth rate and specific leaf area requires associations of specific leaf area with nitrogen absorption rate of roots. *New Phytol*, 179, 417–427.

Ostertag, R., Inman-Narahari, F., Cordell, S., Giardina, C.P. & Sack, L. (2014). Forest structure in low-diversity tropical forests: a study of Hawaiian wet and dry forests. *PLoS ONE*.

Paine, C.E.T., Amissah, L., Auge, H., Baraloto, C., Baruffol, M., Bourland, N., *et al.* (2015). Globally, functional traits are weak predictors of juvenile tree growth, and we do not know why. *J Ecol*, 103, 978–989.

Pérez-Harguindeguy, N., Díaz, S., Garnier, E., Lavorel, S., Poorter, H., Jaureguiberry, P., *et al.* (2013). New handbook for standardised measurement of plant functional traits worldwide. *Aust J Bot*, 61.

Philipson, C.D., Dent, D.H., O'Brien, M.J., Chamagne, J., Dzulkifli, D., Nilus, R., *et al.* (2014). A trait-based trade-off between growth and mortality: evidence from 15 tropical tree species using size-specific relative growth rates. *Ecol Evol*.

Plummer, M. (2007). JAGS: A program for analysis of Bayesian graphical models using Gibbs sampling.

Poorter, H., Lambers, H. & Evans, J.R. (2014). Trait correlation networks: a whole-plant perspective on the recently criticized leaf economic spectrum. *New Phytologist*.

Poorter, L. (2009). Leaf traits show different relationships with shade tolerance in moist versus dry tropical forests. *New Phytologist*.

Poorter, L., Wright, S.J., Paz, H., Ackerly, D.D., Condit, R., Ibarra-Manríquez, G., *et al.* (2008). Are functional traits good predictors of demographic rates? Evidence from five neotropical forests. *Ecology*, 89, 1908–1920.

Prado-Junior, J.A., Schiavini, I., Vale, V.S., Raymundo, D., Lopes, S.F. & Poorter, L. (2016). Functional traits shape size-dependent growth and mortality rates of dry forest tree species. *J Plant Ecol*.

Price, J.P. & Clague, D.A. (2002). How old is the Hawaiian biota? Geology and phylogeny suggest recent divergence. *Proceedings of the Royal Society B: Biological Sciences*.

R Core Team. (2018). *R: a language and environment for statistical computing*. R Foundation for Statistical Computing.

Reich, P.B. (2014). The world-wide 'fast-slow' plant economics spectrum: a traits manifesto. *J Ecol*, 102, 275–301.

Russo, S.E., Jenkins, K.L., Wiser, S.K., Uriarte, M., Duncan, R.P. & Coomes, D.A. (2010). Interspecific relationships among growth, mortality and xylem traits of woody species from New Zealand: Tree growth, mortality and woody traits. *Functional Ecology*, 24, 253–262.

Sack, L. & Buckley, T.N. (2016). The developmental basis of stomatal density and flux. *Plant Physiol*.

Sack, L., Cowan, P.D., Jaikumar, N. & Holbrook, N.M. (2003a). The 'hydrology' of leaves: co-ordination of structure and function in temperate woody species. *Plant, Cell & Environment*.

Sack, L. & Frole, K. (2006). Leaf structural diversity is related to hydraulic capacity in tropical rain forest trees. *Ecology*, 87, 483–491.

Sack, L., Grubb, P.J. & Marañón, T. (2003b). The functional morphology of juvenile plants tolerant of strong summer drought in shaded forest understories in southern Spain. *Plant Ecology*.

Sack, L., Melcher, P.J., Liu, W.H., Middleton, E. & Pardee, T. (2006). How strong is intracanopy leaf plasticity in temperate deciduous trees? *J Bot*.

Sack, L. & Scoffoni, C. (2013). Leaf venation: structure, function, development, evolution, ecology and applications in the past, present and future. *New Phytol*.

Sack, L., Scoffoni, C., John, G.P., Poorter, H., Mason, C.M., Mendez-Alonzo, R., *et al.* (2013). How do leaf veins influence the worldwide leaf economic spectrum? Review and synthesis. *J Exp Bot*, 64, 4053–4080.

Sack, L., Scoffoni, C., McKown, A.D., Frole, K., Rawls, M., Havran, J.C., *et al.* (2012). Developmentally based scaling of leaf venation architecture explains global ecological patterns. *Nat Commun*, 3, 837.

Santiago, L.S., Kitajima, K., Wright, S.J. & Mulkey, S.S. (2004). Coordinated changes in photosynthesis, water relations and leaf nutritional traits of canopy trees along a precipitation gradient in lowland tropical forest. *Oecologia*, 139, 495–502.

Schimper, A.F.W. (1898). *Plant-geography upon a physiological basis*. Rev. and ed. Oxford: Clarendon Press.

Scoffoni, C., Chatelet, D.S., Pasquet-kok, J., Rawls, M., Donoghue, M.J., Edwards, E.J., *et al.* (2016). Hydraulic basis for the evolution of photosynthetic productivity. *Nat Plants*, 2, 16072.

Scoffoni, C., Rawls, M., McKown, A., Cochard, H. & Sack, L. (2011). Decline of leaf hydraulic conductance with dehydration: Relationship to leaf size and venation architecture. *Plant Physiol*.

Scoffoni, C., Vuong, C., Diep, S., Cochard, H. & Sack, L. (2014). Leaf Shrinkage with Dehydration: Coordination with Hydraulic Vulnerability and Drought Tolerance. *Plant Physiology*, 164, 1772–1788.

Seiwa, K. (2007). Trade-offs between seedling growth and survival in deciduous broadleaved trees in a temperate forest. *Ann Bot*, 99, 537–544.

Sheil, D., Burslem, D.F.R.P. & Alder, D. (1995). The Interpretation and Misinterpretation of Mortality Rate Measures. *J Ecol*, 83, 331.

Shipley, B., Belluau, M., Kühn, I., Soudzilovskaia, N.A., Bahn, M., Penuelas, J., *et al.* (2017). Predicting habitat affinities of plant species using commonly measured functional traits. *J Veg Sci*, 28, 1082–1095.

Sokal, R.R. & Rohlf, F.J. (2012). Biometry: the principles and practice of statistics in biological research.

Stahl, U., Reu, B. & Wirth, C. (2014). Predicting species' range limits from functional traits for the tree flora of North America. *Proc Natl Acad Sci USA*, 111, 13739–13744.

Sterck, F., Markesteijn, L., Schieving, F. & Poorter, L. (2011). Functional traits determine trade-offs and niches in a tropical forest community. *Proc Natl Acad Sci USA*, 108, 20627–20632.

Sterck, F.J., Van Gelder, H.A. & Poorter, L. (2006). Mechanical branch constraints contribute to life-history variation across tree species in a Bolivian forest. *J Ecology*, 94, 1192–1200.

Stratton, L., Goldstein, G. & Meinzer, F. (2000). Stem water storage capacity and efficiency of water transport: their functional significance in a Hawaiian dry forest. *Plant Cell Environ*, 23, 99–106.

Suarez, M.L. & Kitzberger, T. (2010). Differential effects of climate variability on forest dynamics along a precipitation gradient in northern Patagonia. *J Ecol*, 98, 1023–1034.

Thaxton, J.M., Cole, T.C., Cordell, S., Cabin, R.J., Sandquist, D.R. & Litton, C.M. (2010). Native Species Regeneration Following Ungulate Exclusion and Nonnative Grass Removal in a Remnant Hawaiian Dry Forest. *Pacific Science*.

Thomas, F.M. & Vesk, P.A. (2017). Are trait-growth models transferable? Predicting multi-species growth trajectories between ecosystems using plant functional traits. *PLOS ONE*, 12, e0176959.

Uriarte, M., Lasky, J.R., Boukili, V.K. & Chazdon, R.L. (2016). A trait-mediated, neighbourhood approach to quantify climate impacts on successional dynamics of tropical rainforests. *Funct Ecol*, 30, 157–167.

Venables, W. & Ripley, B. (2002). *Modern Applied Statistics with S*. 4th edn. Springer, New York, NY.

Vendramini, F., Díaz, S., Gurvich, D.E., Wilson, P.J., Thompson, K. & Hodgson, J.G. (2002). Leaf traits as indicators of resource-use strategy in floras with succulent species. *New Phytol*, 154, 147–157.

Violle, C., Navas, M.-L., Vile, D., Kazakou, E., Fortunel, C., Hummel, I., *et al.* (2007). Let the concept of trait be functional! *Oikos*, 116, 882–892.

Visser, M.D., Bruijning, M., Wright, S.J., Muller-Landau, H.C., Jongejans, E., Comita, L.S., *et al.* (2016). Functional traits as predictors of vital rates across the life cycle of tropical trees. *Funct Ecol*, 30, 168–180.

Vitousek, P.M. & Farrington, H. (1997). Nutrient limitation and soil development: Experimental test of a biogeochemical theory. *Biogeochemistry*.

Wagner, G.P. & Altenberg, L. (1996). Perspective: Complex Adaptations and the Evolution of Evolvability. *Evolution*, 50, 967.

Wagner, W.L., Herbst, D.R. & Sohmer, S. (1999). Manual of the flowering plants of Hawaii.

Walters, M.B. & Reich, P.B. (1999). Low-light carbon balance and shade tolerance in the seedlings of woody plants: do winter deciduous and broad-leaved evergreen species differ? *New Phytol*, 143, 143–154.

Wang, H., Prentice, I.C., Keenan, T.F., Davis, T.W., Wright, I.J., Cornwell, W.K., *et al.* (2017). Towards a universal model for carbon dioxide uptake by plants. *Nat Plants*.

Wang, R., Yu, G., He, N., Wang, Q., Zhao, N., Xu, Z., *et al.* (2015). Latitudinal variation of leaf stomatal traits from species to community level in forests: linkage with ecosystem productivity. *Sci Rep*.

Weiher, E. & Keddy, P.A. (1995). Assembly Rules, Null Models, and Trait Dispersion: New Questions from Old Patterns. *Oikos*, 74, 159.

Westoby, M., Falster, D.S., Moles, A.T., Vesk, P.A. & Wright, I.J. (2002). Plant ecological strategies: some leading dimensions of variation between species. *Annu Rev Ecol Syst*, 33, 125–159.

Westoby, M. & Wright, I.J. (2006). Land-plant ecology on the basis of functional traits. *Trends Ecol Evol*, 21, 261–268.

Witkowski, E.T.F. & Lamont, B.B. (1991). Leaf specific mass confounds leaf density and thickness. *Oecologia*.

Wright, I.J., Dong, N., Maire, V., Prentice, I.C., Westoby, M., Díaz, S., *et al.* (2017). Global climatic drivers of leaf size. *Science*, 357, 917–921.

Wright, I.J., Reich, P.B. & Westoby, M. (2001). Strategy shifts in leaf physiology, structure and nutrient content between species of high- and low-rainfall and high- and low-nutrient habitats. *Funct Ecol*, 15, 423–434.

Wright, I.J., Reich, P.B., Westoby, M., Ackerly, D.D., Baruch, Z., Bongers, F., *et al.* (2004). The worldwide leaf economics spectrum. *Nature*, 428, 821–827.

Wright, S.J., Kitajima, K., Kraft, N.J.B., Reich, P.B., Wright, I.J., Bunker, D.E., *et al.* (2010). Functional traits and the growth–mortality trade-off in tropical trees. *Ecology*.

Yang, J., Cao, M. & Swenson, N.G. (2018). Why functional traits do not predict tree demographic rates. *Trends Ecol Evol*, 33, 326–336.

Yang, Y., Morden, C.W., Sporck-Koehler, M.J., Sack, L. & Berry, P.E. (2016). *Repeated range expansion and niche shift in a volcanic hotspot archipelago: radiation of Hawaiian Euphorbia (Euphorbiaceae)* (preprint). Evolutionary Biology.

Zhu, S.-D., Song, J.-J., Li, R.-H. & Ye, Q. (2013). Plant hydraulics and photosynthesis of 34 woody species from different successional stages of subtropical forests. *Plant Cell Environ*, 36, 879–891.

Ziegler, A.C. (2002). Hawaiian natural history, ecology, and evolution.

CHAPTER 5

THE PREDICTION OF SPECIES AND ECOSYSTEM CLIMATE DISTRIBUTIONS ON THE BASIS OF MECHANISTIC FUNCTIONAL TRAITS

ABSTRACT

Anticipating shifts in the distributions of species and ecosystems under climate change depends on understanding species' preferred climate and their physiological vulnerability. Traits related to physiological tolerance have been widely used as a predictor of species preferred climate, however this assumption has remained controversial and largely untested. Here we show that mechanistic traits enable strong prediction of the mean warmest temperature, rainfall and aridity of the climatic range of diverse Californian plant species (n=107) and ecosystems (n= 6). The ability to predict climate from traits was stronger for species with narrow climate distributions, and was improved by sampling for traits closer to species' mean climates. Our analyses showed the importance of characterizing species' physiological vulnerabilities. We found species with less xeromorphic traits are projected to face greater climate aridification. The ability to predict a species' preferred climate from its traits has potential to improve global dynamic vegetation models to predict the impact of climate change and the design and prioritization of conservation efforts to protect the most vulnerable species.

INTRODUCTION

Functional traits have long held promise for predicting species' climatic niches (Soberón 2007; Laughlin *et al.* 2012; Peterson *et al.* 2012; Pollock *et al.* 2012; Shipley *et al.* 2017a; Vesk *et al.* 2020). Plant traits that influence growth, reproduction and survival (Lavorel & Garnier 2002; Violle *et al.* 2007; Poorter *et al.* 2008; Adler *et al.* 2014; Uriarte *et al.* 2016) are typically adapted or acclimated to environmental conditions (Albert *et al.* 2010a) and related to habitat type (Shipley *et al.* 2017b), geographic limits (Stahl *et al.* 2014) and abiotic and biotic conditions (Schimper 1898; Grubb 1998; Reich *et al.* 2003; Kattge *et al.* 2011; Drenovsky *et al.* 2012; Liu *et al.* 2021) (Appendix Table 5.1 and Fig. 5.1). Due to the rapid changes in climate, there is a growing need to characterize species' preferred habitats for conservation, and thus, increasing importance of measuring functional traits. Considering all living organisms, *y* vs. *x* plots of climate versus trait values are rare, with only a few examples, such as the prediction of species' native temperature distributions from body size ("Bergmann's Rule") across animal species, though this trend has been only sometimes supported (Geist 1986; Smith *et al.* 1995; Meiri & Dayan 2003). A greater potential would be expected for plants, as a rich literature describes how numerous phenotypic traits that influence growth, reproduction and survival (Lavorel & Garnier 2002; Violle *et al.* 2007; Poorter *et al.* 2008; Adler *et al.* 2014; Uriarte *et al.* 2016) are adapted or acclimated to environmental conditions (Albert *et al.* 2010a), and are linked to species' habitat type (Schimper 1898; Grubb 1998; Reich *et al.* 2003; Kattge *et al.* 2011; Drenovsky *et al.* 2012; Shipley *et al.* 2017a; Liu *et al.* 2021), and geographic limits (Stahl *et al.* 2014) (Appendix Table 5.1 and Fig. 5.1).

Yet, despite many enterprising paleoecological studies that have retrodicted *past* climates from fossil leaf traits, based on current trait-climate relationships (Wolfe 1978, 1995; Van Der

Burgh *et al.* 1993; McElwain & Chaloner 1995; Kürschner *et al.* 1996; Lockheart *et al.* 1997; McElwain 1998; Jacobs 1999; Royer 2001; Beerling & Royer 2002; Hatté & Schwartz 2003; Kowalski & Dilcher 2003; Greenwood 2007; Adams *et al.* 2008; Peppe *et al.* 2011, 2018; Yang *et al.* 2011, 2015a; Roth-Nebelsick *et al.* 2014; Steinthorsdottir *et al.* 2016; Eley & Hren 2018), only one pioneering study has tested the prediction of current climates, showing for trees of North America that climate distribution limits can be weakly predicted from easy to measure traits (Stahl *et al.* 2014), and no studies have directly tested the prediction of the mean of species' climatic distributions. The dearth of this approach may be due to many known factors that could in principle decouple climatic distributions from traits across species, including differences between fundamental and realized niches (Walter 1979; Brown 1984; Hanski *et al.* 1993; Wiens 2011; Lee-Yaw *et al.* 2016; Pérez-Ramos *et al.* 2019; Sheth *et al.* 2020), the indirect relationship between functional traits and fitness (Laughlin *et al.* 2020), intraspecific trait variation (Albert *et al.* 2010a, b; Violle *et al.* 2012; Siefert *et al.* 2015; Fyllas *et al.* 2020), trait multi-functionality (Sack & Buckley 2020), many-to-one mapping of traits to function (Alfaro *et al.* 2005; Marks & Lechowicz 2006) and nonequilibrium processes (Dobzhansky 1950; DeAngelis & Waterhouse 1987; Stevens 1989; Ohlemüller *et al.* 2008; Sheth *et al.* 2020) (Appendix Table 5.2).

Indeed, while strong adaptation of traits to climate has been reported for closely related species within lineages (Cochrane *et al.* 2016; Abdala-Roberts *et al.* 2018; Fletcher *et al.* 2018; Skelton *et al.* 2018; de la Riva *et al.* 2019; Ramírez-Valiente *et al.* 2020), and on average for communities across climatic gradients (Violle *et al.* 2007; Kichenin *et al.* 2013; Jager *et al.* 2015; Asner *et al.* 2017), relationships can be highly variable (Wright *et al.* 2005; Ordoñez *et al.* 2009; Moles *et al.* 2014; Costa-Saura *et al.* 2016). For example, across different species sets, the relationships of leaf nitrogen concentration with mean annual precipitation across species have

been reported as weakly positive (Mitchell *et al.* 2018), weakly negative (Santiago *et al.* 2004; Swenson & Weiser 2010) or not significant (Wright *et al.* 2005; Moles *et al.* 2014; Mitchell *et al.* 2018). However, the weakness of some reported trait-climate associations may have arisen at least in part from a range of methodological issues (Appendix Table 5.2).

Here, we provide a novel procedure to test whether traits can predict mean climate variables of diverse species and ecosystems (Appendix Table 5.1), across a strong precipitation gradient in California, a biodiversity hotspot (Appendix Table 5.3 and Fig. 5.2a). We sampled co-occurring species at few sites to reduce the effects of plasticity and ecotypic variation (Albert *et al.* 2010a, b; Violle *et al.* 2012; Siefert *et al.* 2015; Fyllas *et al.* 2020), used structural, hydraulic and economic traits (Appendix Table 5.1) that are putatively adapted to climatic aridity (Appendix Table 5.1; Table S5.1 and Fig. 5.1), and incorporated phylogenetic structure (Felsenstein 1985; Opedal *et al.* 2015).

We also clarified why species would deviate from the climate-trait relationship. We calculated species' trait-climate mismatch (Appendix Table 5.4) as their residuals from the all-species' trait vs. climate relationship, representing the degree that a species' traits do not conform to expectations based on its current climate distribution (Fig. 5.3a). We considered factors that might influence the trait-climate mismatch. Given the potential importance of plasticity and ecotypic sources of intraspecific variation, the trait-climate mismatch might be related to the difference in climate between the site at which species were sampled for trait measurements and the mean climate of its native range (Browne *et al.* 2019), the climate sampling bias (Appendix Table 5.4 and Fig. 5.3b). We also tested if the trait-climate mismatch values would be related to natural climatic distribution breadth, as species with broader climatic distributions would have greater likelihood of being sampled at a site further away in climate from the mean of their natural

distribution (Fig. 5.3c). Finally, we tested whether species with traits adapted to climatic aridity will be protected from future climate change, as would be expected if arid-adapted species are those occupying locations subject to stronger aridification. We thus tested potential associations of species' traits and trait-climate mismatch with projected reduction of current climate niche space.

METHODS

Study sites

We focused on six contrasting ecosystem types representing the range of biogeographic conditions in the California and Desert floristic provinces (CAFP, DFP; Appendix Table 5.3 and Fig. 5.2a). Together, the six sites contain vegetation of types that represent >247 km^2 of California, or 70% of its the terrestrial land area (Thorne *et al.* 2017). The sampling locations were distributed across a gradient of climatic aridity, including desert (Sweeney Granite Mountains Desert Research Center, part of the University of California Natural Reserve System, UCNRS), coastal sage scrub (located in the Centro de Investigación Científica y de Educación Superior de Ensenada and Cañon de Doña Petra, Baja California), chaparral (Stunt Ranch Santa Monica Mountains Reserve, UCNRS), montane wet forest (Yosemite Forest Dynamics Plot, part of the ForestGEO network (Anderson-Teixeira *et al.* 2015)), mixed riparian woodland (Onion Creek, near the Chickering American River Reserve, UCNRS) and mixed conifer-broadleaf forest (Angelo Coast Range Reserve, UCNRS).

To test predictions of climate-trait relationships for species and ecosystems, we sampled single representative ecosystems of widespread types. This approach is typical of ecophysiological studies comparing communities (Baltzer *et al.* 2008; Markesteijn *et al.* 2010; Zhu *et al.* 2013;

Blackman *et al.* 2014; Falcão *et al.* 2015; Medeiros *et al.* 2019), and enables rigorous tests of species' and ecosystem trait relationships to climate. However, we note that statistical differences between single specific ecosystems in trait means are not necessarily generalizable to the ecosystem type, but can represent hypotheses to be tested in future studies using replicate ecosystems of each type.

Sampling for leaf trait measurements

We sampled species among the most abundant at each site according to reserve managers and forest inventories. The species included in this study are taxonomically diverse, representing 31 plant families, and including many cases of closely related species that occur in contrasting environments (Fig. S5.1). Further, fifteen of the 107 species were selected in two ecosystems (and one species, *Eriogonum fasciculatum* in three ecosystems; Table S10). For 3-5 individuals of 14 to 26 species per site we collected a mature, sun-exposed and non-epicormic branch, with no signs of damage and herbivory using pole pruners or a slingshot. Branches were transported to the lab in dark plastic bags with moist paper and rehydrated overnight in a dark saturated atmosphere before harvesting current-year grown, fully expanded leaves for all subsequent analyses. For compound-leafed species, whole leaves were used.

Functional trait measurements

Maximum tree height (H_{max}) of all species was compiled from the Jepson Herbarium database (Jepson Flora Project 2021). When not available, the H_{max} was recorded as the maximum value reported on the Jepson eFlora website (https://ucjeps.berkeley.edu/eflora/). The remaining functional traits were measured for three sun leaves per individual. Leaf saturated mass was

measured using an analytical balance (0.01 mg; XS205; Mettler-Toledo, OH, USA). Leaf area (*LA*) was measured using a flatbed scanner and analyzed using the software (ImageJ; http://imagej.nih.gov/ij/). After scanning, leaves were oven-dried at 70º for 72 h before measurement of dry mass. Leaf mass per area (*LMA*) was calculated as lamina dry mass divided by *LA* (Pérez-Harguindeguy *et al.* 2013).

The concentrations of leaf nitrogen and carbon per mass (N_{mass} and C_{mass}) and the carbon isotope ratio ($\delta^{13}C$) were determined from oven-dried leaves by the by continuous flow dual isotope analysis (Center for Stable Isotope Biogeochemistry, University of California, Berkeley; CHNOS Elemental Analyzer interfaced to an IsoPrime100 mass spectrometer) (Kaklamanos *et al.* 2020). N_{mass} and C_{mass} were converted to a leaf area basis (N_{area} and C_{area}) by multiplying by *LMA*. The carbon isotope discrimination ($\Delta^{13}C$; in parts per thousand, ‰) was calculated following Farquhar and Richards(Farquhar & Richards 1984) as: $\Delta^{13}C = \frac{\delta^{13}C_{air} - \delta^{13}C_{leaf}}{1 + {\delta^{13}C_{leaf}}/{1000}}$, assuming $\delta^{13}C_{air}$ of -8 ‰ (NOAA Global Monitoring Laboratory 2018).

We measured the wood density (*WD*) from 5-cm branch segments after bark removal using the water displacement method (Pérez-Harguindeguy *et al.* 2013). Branch segments were immersed in water and the mass of the displaced water was recorded; branch segments were then oven-dried at 70º for 120 h and their dry mass was measured. *WD* was calculated as the segment dry mass divided by the mass of displaced water. Turgor loss point (π_{tlp}) was measured in two leaves from each of the 3-5 studied individuals. We used vapor-pressure osmometers (Vapro 5520 and 5600, Wescor, US) to obtain the osmotic concentration of the leaves and published calibration equations to estimate π_{tlp} (Bartlett *et al.* 2012a).

Environmental variables for species' native ranges

We obtained species occurrence data from the Global Biodiversity Information Facility (GBIF; references available in the Extended data) and we used R software (version 3.4.4 (R Core Team 2018)) to extract and calculate the mean, range and standard deviation of environmental variables of known occurrences across the range of distribution of each species. We focused on the relationships of traits with the mean climate of species distributions rather than the minimum or maximum values; assuming that gene flow occurs among populations of a given species across its native range, species' mean phenotypic trait values would be related to their mean climate (Sexton *et al.* 2009).

Occurrence records were downloaded using the '*rgbif*' package (Chamberlain *et al.* 2019) and filtered to keep herbarium records since 1950 and remove incomplete (latitude or longitude missing) and duplicated records, non-natural occurrences (e.g., records from botanical gardens or planted urban trees) (Riordan *et al.* 2015; Chamberlain *et al.* 2019). We calculated species climatic envelopes using species occurrence points and not maps of distribution ranges because we were interested in the relationship between species' traits and climate variables, whereas range maps are based on ecological niche models (Harrison 1997; Peterson 1999) (ENMs) that are partially calculated from environmental variables, and thus could potentially introduce circularity in our climate analyses (Šímová *et al.* 2018).

We extracted 30 environmental variables from open-access raster layers, relating to air temperature (WorldClim, CRU (Hijmans *et al.* 2005)), precipitation (WorldClim (Hijmans *et al.* 2005)), aridity (CGIAR-CSI, NCAR-UCAR (Zomer *et al.* 2008)) and soil characteristics (ISRIC Soilgrids (Hengl *et al.* 2017)) (see Table S5 for detailed description, download links and references for each variable). The raster layers with the same resolution were stacked using the *stack* function

from the '*raster'* package (Hijmans & van Etten 2012) and the environmental variables for each occurrence record were extracted using the *extract* function from the '*dismo'* package (Hijmans *et al.* 2011). Due to their coarse resolution, these environmental variables are effective in characterizing large scale patterns but do not reflect differences in microclimate, i.e., temperature, water and nutrient availability, irradiance and soil composition (Perez & Feeley 2020).

Species' vulnerability to climate change

We estimated the climate that would be experienced by each species according to future climate projections. The species-level projected future climate means were calculated as the average of four models that perform best in simulating both global and California climate (Lynn *et al.* 2015): the GFDL-CM3 (warm-dry; NOAA Geophysical Fluid Dynamics Laboratory, Princeton, N.J., USA), CNRM-CM5 (cool-wet; Centre National de Recherches Meteorologiques, Meteo-France, and Centre Europeen de Recherches et de Formation Avancee en Calcul Scientifique, Toulouse, France), CCSM4 (intermediate model; The National Science Foundation, The Department of Energy, and the National Center for Atmospheric Research, United States) and HadGEM2-CC (most distinct from the previous three; Met Office Hadley Centre, Fitzroy Road, Exeter, Devon, UK). From the open-access raster layers of the four models above (downloaded from the WorldClim website (Hijmans *et al.* 2005)), we extracted a total of 19 bioclimatic variables obtained for two climate change scenarios, the Representative Concentration Pathway (RCP) 4.5 and RCP 8.5 in 2070. The RCP 4.5 represents a moderate optimistic emission, whereas the RCP 8.5 represents a "high baseline" emission scenario (i.e., 90th percentile of a future without climate policy; a high emissions scenario would be the 95th percentile). We present analyses using the RCP 8.5 scenario in the main text and results from the RCP 4.5 in the supplemental files to emphasize

the potential consequences of increased emissions and expansion of coal use on species distributions, though this extreme scenario may be averted if policies aimed at reducing emissions continues to expand (van Vuuren *et al.* 2011; Ritchie & Dowlatabadi 2017).

After obtaining the current and projected future climate for the coordinates of all occurrences of each species, we calculated the percent of current occurrences that under projected future climates would shift to higher T_{max} and/or lower *MAP* by ≥ 2 standard deviations (SDs) of the current climate distribution (projected loss of climatically suitable habitats, *plch,* %; Table S5.13). Since in a normal distribution 95% of the data would be distributed 2SDs above or below the mean, occurrences outside this range were considered potential statistical outliers from typical species' climatic distribution. Thus, these occurrences were removed for the calculation of projected future species climatic distributions (Fig. S5.7). We used a 2 SD difference from the mean as a threshold because the typically recommended 3 SD threshold would include biologically unlikely values, such as negative *MAP* and T_{max} close to 50°C (Iglewicz & Hoaglin 1993).

Phylogenetic reconstruction

Sequences for all 107 species were automatically downloaded from GenBank and aligned with MAFFT (multiple alignment using fast Fourier transform; *Matrix Maker*; github.com/wf8/matrixmaker) (Freyman & Thornhill 2016). We focused on eight genes, ITS, matK, MatR, ndhF, rbcl, trnL-trnF, 18S, and atpB. Each species was represented with at least one up to seven gene accessions, with an average of 3.3 genes. The genes were then concatenated for each species, and a maximum likelihood analysis of the phylogenetic relationships was conducted using a General Time Reversible (GTR) model of substitution (*SeaView* version 4) (Gouy *et al.* 2010). To calibrate branch lengths, we used the *chronos* function in the R package '*ape*'(Paradis

& Schliep 2019). The species relationships recovered closely matched the Angiosperm Phylogeny Group consensus (Stevens 2019). The output of species branch lengths was utilized to incorporate species relatedness into downstream analyses.

Statistical analyses

All statistical analyses were performed and plots created using R software (versions 3.4.4 (R Core Team 2018) and 4.0.2 (R Core Team 2020)) and packages available from the CRAN platform. To test for differences among ecosystems in the mean climate their constituent species' distributions, we performed one-way ANOVAs with each environmental parameter as the dependent variable and ecosystem as the independent variable using the *aov* function from the '*stats'* package followed by a Tukey test at 5% probability when differences were detected using *TuckeyC* function from the package with the same name (Sokal & Rohlf 2012; R Core Team 2018). To test for differences in functional traits among ecosystems, we performed nested ANOVAs using the *aov* function, with functional traits coded as the dependent variable, ecosystem as the independent variable and species nested within ecosystems, followed by a Tukey test at 5% probability when differences were detected (Sokal & Rohlf 2012; R Core Team 2018). Trait and climate variables that did not fulfill the normality and homoscedasticity assumptions were $\log_{10}$-transformed prior to analyses. Variables that included both negative and positive numbers were incremented by a constant equal to the lowest species mean +1 before log-transformation, such that 1 was the lowest value for that variable (see Tables S5.2 and S5.6 for detailed description). Throughout the text, traits and climate variables were abbreviated in uppercase letters to differentiate them from the calculated indices of variation (Appendix Table 5.4), abbreviated in lowercase letters.

To summarize the variation in functional traits and the mean climate of the range of distribution of species, we performed principal component analyses (PCAs) on species means of eight nonredundant functional traits and climate variables using the *prcomp* function in the '*stats*' package (R Core Team 2018). All variables were log-scaled prior to analyses. We extracted the species scores (scaled to range from -1 to 1) of PC axes 1 and 2, and used them to summarize trait and climate main axes of variation in subsequent analyses.

To test species' trait-environment relationships while explicitly accounting for species relatedness, we performed phylogenetic generalized least-squares analyses (PGLS (Felsenstein 1985; Freckleton *et al.* 2002; Harmon 2019)) using the *pgls* function from the '*caper*' package (Orme *et al.* 2018) with lambda (λ) optimized using maximum likelihood. For cross-species analyses that required single values for given species, for the 15 species that were collected at more than one site, we calculated the mean trait values across the sites and assigned those species to the site most similar in aridity index (*AI*) to the mean for the range of distribution of that species. Analyses were performed for untransformed and log-transformed data, to test for either approximately linear or non-linear (i.e., approximate power-law) relationships respectively. To test trait-environment relationships across sites we calculated Pearson's correlations for untransformed and log-transformed data, and report the higher correlation value in the text (Table S5.4).

To test the prediction of climate from traits, we applied statistical regression methods (Stahl *et al.* 2014) after considering issues relating to causality. While in regressing or predicting a y-from an x-variable, in the purest sense, *y* should causally depend on *x*, and not vice versa. However, studies of traits and climate, causality might run either or both ways. Thus, a species' traits may depend on climate occupied during adaptation and acclimation, but the climate occupied by a

species would depend on its traits during processes such as immigration and community assembly. Notably, over very long scales of space and time (beyond those in this study), plant traits can influence climate (Boyce *et al.* 2009; Anderegg *et al.* 2019). To test the power of multiple traits to predict the mean environment of the distribution of each species within an evolutionary framework, we built multiple regression models using PGLS. We built models to predict maximum temperature of the warmest month (T_{max}), mean annual precipitation (*MAP*), aridity index (*AI*), soil pH ($Soil_{pH}$; high soil pH is associated with low concentration of exchangeable soil phosphate and iron (Tyler 1996)) and Climate-PC1 as dependent variables. We included eight of the 10 functional traits measured in this study as independent variables; to avoid strong collinearity, given that we included N_{mass}, we did not include N_{area} and $C{:}N$ in this analysis. To select the trait-based models that best predicted the target climate variables, we tested all possible predictor combinations and compared models using AICc (code available on C.M.'s GitHub). To determine the percentage contribution of each trait to the prediction of climate variables, we performed a hierarchical partitioning analysis using the '*hier.part'* package (Chevan & Sutherland 1991; Walsh & Mac Nally 2013).

To test the influence of intraspecific variation on functional traits, for the 15 species that were sampled at more than one site we calculated a between-site variation index (*bsv*; Appendix Table 5.4) values for trait and climate variables, $bsv_i = \frac{(max_i - min_i)}{max_i}$, where *i* represents the species and max_i and min_i are the maximum and minimum values of a trait or climate variable across sites (based on a commonly-used index, the phenotypic plasticity index (Valladares *et al.* 2000); Table S5.10). We analyzed the relationship across species among the trait and climate *bsv* indices using PGLS.

To test the ability to predict species' trait values from species' mean climate variables, we determined the relationships between the first axis of the Traits-PCA against that of the Climate-PCA using PGLS. For convenience of presentation, we re-scaled Climate-PC1 values (multiplied all scores by -1) such that the relationship between Traits-PC1 and Climate-PC1 was positive, and greater Climate-PC1 represented greater climatic aridity, as Traits-PC1 generally corresponded to traits adapted to aridity (see Results "*Trait variation in relation to climate across ecosystems*" and Table S5.5). The residuals from this model were considered as the "trait-climate mismatch" (*tcm*), i.e., an estimate of the amount of trait variation not explained by climate (Appendix Table 5.4). By this definition, species with higher *tcm* values had higher values overall for traits corresponding to adaptation to aridity than would be expected from the all-species trait-climate relationships. Given the definition of *tcm* as residuals from the trait-climate relationship, *tcm* was statistically independent of environmental variables and the Climate-PC1 (PGLS; Table S7). Thus, we avoided the circularity that would have arisen if we had defined *tcm* as the residuals of climate vs. traits, given our subsequent tests of the relationship of *tcm* with climate variables, that is, climate sampling bias (*csb*) and the breadth of species' climatic ranges. We calculated *csb* as the difference in a given climate variable between the sampling location and the mean of the range of distribution of a species (Browne *et al.* 2019) (e.g., $csb_{MAP} = MAP_{site} - MAP_{mean}$), by analogy to common garden studies that estimate "climate transfer distance" as the difference in a climate variable between the mean of the species' distribution and the location of the common garden. We defined the breadth of a species' climate niche as the 95th percentile – 5th percentile value. We tested whether across species, the *tcm* depended on the *csb* or the breadth of the climatic range using PGLS.

We tested the relationships of the projected loss of climatically suitable habitats (*plch,* %) with species' traits, current climatic distribution means and *tcm* using PGLS.

RESULTS

Trait variation in relation to climate

Species' differed strongly in the ten measured functional traits within and across the six California ecosystems (Table S5.2 and Fig. 5.2c-j). For individual traits, the ecosystem types explained 15-40% of variation, the species 42-79%, and 2-18% of variation was intraspecific (nested ANOVAs; Table S5.2). Species' traits varied with climatic aridity as hypothesized based on mechanistic theory (Appendix Table 5.1 and Fig. 5.1). Thus, species of more arid ecosystems had lower water potentials at wilting point (i.e., more negative π_{tlp}), higher leaf mass per area (*LMA*), nitrogen per leaf area (N_{area}), carbon-to-nitrogen ratio (*C*:*N*) and wood density (*WD*). By contrast, species of wetter ecosystems possessed traits associated with competitive resource use and photosynthetic productivity, including larger maximum height (H_{max}), carbon isotope discrimination ($\Delta^{13}C$), leaf area (*LA*) and nitrogen per leaf mass (N_{mass}), and with anti-herbivory defense, such as carbon per leaf mass (C_{mass}).

The strong covariation across California ecosystems (Baldwin 2014) in climate and in trait values was highlighted by principal component analyses (Climate-PCA and Traits-PCA). The first climate axis (Climate-PC1; Appendix Table 5.3and Fig. S5.2) encapsulated 79.1% of variation and corresponded to variables associated with climatic warmth and aridity across California, including higher mean annual temperature (*MAT*), maximum temperature of the warmest month (T_{max}), lower aridity index (*AI*), and annual precipitation (*MAP*), and more basic soil ($Soil_{pH}$). The second axis, Climate-PC2, explained 15.5% of variation and was related to the minimum

temperature of the coldest month (T_{min}). The Traits-PCA also showed a strong correspondence with adaptation to aridity. Traits-PC1 explained 37.2% of variation, with high values corresponding to trait xeromorphism, i.e., small *LA*, high *LMA*, high *WD*, low N_{mass} and π_{tlp}. Traits-PC2, which explained 23.8% of variation, was strongly related to H_{max} and C_{mass} (Table S5.5 and Fig. S5.2). Species' Traits-PC1 scores increased on average from wetter to drier ecosystems (one-way ANOVA; $p<0.01$; Table S5.6), and correlated with Climate-PC1 (phylogenetic generalized least squares, $r_{phy} = 0.59$; $p<0.001$; Table S5.7 and Fig. 5.3a), and species' Traits-PC2 scores were correlated with Climate-PC1 and 2 ($r_{phy} = 0.46$ and -0.40, respectively; $p<0.001$; Table S5.7).

Across the 107 species of six California ecosystems, individual species traits associated with adaptation to aridity were strongly associated with lower Climate-PC1 scores, and/or individual climate traits related to aridity (Table S5.7 and Figs. 5.2b, S5.1).

Trait-based climatic niche prediction

The strong relationships of species' traits with climate variables justified reversing the axes, to use species' traits to predict the mean climate of their native distributions. We found that traits considered individually and in combination had substantial predictive power for multiple climate variables. Species' Climate-PC1 scores were predicted by $|\pi_{tlp}|$ (Fig. 5.2b), *LMA,* N_{area}, *C*:*N*, *WD*, $\Delta^{13}C$, *LA,* N_{mass} and C_{mass} ($|r_{phy}|$= 0.22-0.63; $p < 0.05$; Table S5.7 and Fig. S5.5), and species' Climate-PC2 scores by Traits-PC2, $\Delta^{13}C$, *C*:*N*, H_{max}, N_{mass} and N_{area} ($|r_{phy}| = 0.22$-0.47; $p < 0.05$; Table S5.7). Across ecosystems, species' average values for Climate-PC1 was predicted by those for $|\pi_{tlp}|$ (Fig. 5.2b-inset), H_{max}, *WD* and C_{mass} ($|r_{site}| = 0.83$-0.94; $p < 0.05$; Table S5.4 and Fig S5.5-insets), though species' average Climate-PC2 were not predicted by average species trait values across ecosystems (Table S5.4). Individual traits also predicted individual mean climate variables

for species ranges, including *MAT*, T_{max}, T_{min}, *MAP*, P_{wet}, P_{dry}, *AI*, *GDD* and $Soil_{pH}$ ($|r_{phy}|$ ranged from 0.2 to 0.7; $p < 0.05$; Table S5.7).

We applied two multivariate approaches to further validate the trait-based prediction of the mean of species' climate distributions. First, we used phylogenetic regression models to predict Climate-PC1 based on eight traits selected for nonredundancy (Appendix Table 5.1), from which six traits were selected as best predictors of Climate-PC1, i.e., in order of importance, according to hierarchical partitioning analysis, $\Delta^{13}C$, *LMA*, $|\pi_{tlp}|$, C_{mass}, *WD* and N_{mass}; adjusted $R_{phy}^2 = 0.59$; $p < 0.001$; Table S5.8 and Fig. 5.4a). When averaging species' values for given ecosystems, the Climate-PC1 predicted by multivariate phylogenetic regression strongly predicted the average of observed Climate-PC1 scores ($R_{site}^2 = 0.87$; $p < 0.01$; Table S5.4 and Fig. 5.4a-inset). Multivariate phylogenetic regression models based on functional traits also predicted individual environmental variables, including T_{max}, *MAP*, *AI* and $Soil_{pH}$; the traits that were selected in the best-fit models for all four environmental variables and Climate-PC1 were $\Delta^{13}C$, *LMA* and C_{mass} (adjusted R_{phy}^2 ranged from 0.48 to 0.66; $p < 0.001$; Table S5.8 and Figs. 5.4a and S5.4). In a second approach, we used Traits-PC1 to predict Climate-PC1 across species ($R_{phy}^2 = 0.39$; $p<0.001$; Table S5.9 and Fig. 5.4b), and averaging scores for species, across ecosystems ($R_{site}^2 = 0.73$; $p < 0.05$; Table S5.4 and Fig. 5.4b-inset).

Species trait-climate mismatch

To test why species would deviate from the climate-trait relationship, we estimated species' trait-climate mismatch (*tcm*). We defined species' *tcm* as their residuals from the across-species relationship of Trait-PC1 to Climate-PC1; higher values correspond to traits that are more xeromorphic than expected based on the mean climate of their distribution (Fig. 5.3a). The species

with highest *tcm*, i.e., those for which climate was most weakly predicted from traits, included especially those with high *LMA* and low π_{tlp} , such as the conifers of the montane wet forest and mixed riparian woodland (*Abies concolor*, *A. magnifica, Calocedrus decurrens, Juniperus occidentalis*, *Pinus albicaulis*, *P. contorta*, *P. lambertiana*) and some of the most drought-tolerant species of each ecosystem (*Adenostoma fasciculatum*, *Arctostaphylos nevadensis*, *Quercus vacciniifolia*, *Arctostaphylos patula* and *Larrea tridentata*).

We tested whether *tcm* might arise due to plastic or ecotypic trait adjustment to climate, as this would may result in distance between species' trait values in the sampled ecosystem relative to the mean of their natural distribution. First, we confirmed the importance of intraspecific trait variation with respect to climate, focusing on the fifteen of the sampled species that occurred in two ecosystems. Across the 15 species, indices for the intraspecific variation in traits between sites ("between site variation indices", *bsv*, based on "plasticity index"(Valladares *et al.* 2000); Appendix Table 5.4) were correlated with indices for variation in climate between sites: *bsv* in $|\pi_{tlp}|$ was correlated with *bsv* in *AI*, *MAP* and P_{wet}; *bsv* in N_{mass} and *N*:*C* were correlated with *bsv* in *GDD* and/or T_{min}; and *bsv* in C_{mass} was correlated with *bsv* in with $Soil_{pH}$ ($|r_{phy}|$ = 0.59-0.62; $p <$ 0.05; Tables S5.10-S5.11 and Fig. S5.6).

Given the importance of plastic and/or ecotypic trait variation with climate, we tested its potential to explain species' *tcm*. Overall, species were sampled in locations representative of the mean of their natural climate distribution; the climate variables for the six ecosystems were correlated with the average of the mean climate variables of their component species' natural distributions (T_{max}, *MAP*, *AI*, $Soil_{pH}$ and Climate-PC1 scores; ordinary least squares regression, $|r|$ = 0.85-0.96; $p<0.05$; Table S8; Fig S3). However, the matching of climate between sampling location and natural distributions varied across species. Indeed, considering the two variables most

important for defining the aridity gradient, T_{max} and *MAP*, across species, *tcm* was related to the "climate sampling bias" (*csb*), i.e., the difference in climate between the species' sampling site and the mean climate of its native range (Fig. 5.3b) ($|r_{phy}|$ = 0.21-0.24; p<0.05; Table S5.7 and Fig. 5.5a-b). Thus, as expected based on plastic or ecotypic adjustment, species that were sampled at sites more arid than the mean of its range, had traits more xeromorphic than expected from the mean climate of its distribution (Figs. 5.3b and 5.5a-b). Additionally, species' absolute values for trait-climate mismatch (|*tcm*|) were related to their climatic breadths (95th percentile – 5th percentile; Appendix Table 5.4) in T_{max} (r_{phy} = 0.24; p<0.05; Table S5.7 and Fig. 5.5c), as expected given that more widely-distributed species would be on average adapted to climates more different from the mean of their natural distribution (Fig. 5.3c). For T_{max}, across species, *csb* and climatic breadth were statistically independent and each was associated independently with *tcm* (explaining 23% and 77% respectively of the overall relationship of *tcm* with *csb* and climatic breadth; (hierarchical partitioning; R_{phy}^2 = 0.16; p<0.001; Table S5.12). For *MAP*, species' *csb* and climatic breadth values were correlated (r_{phy} = 0.51; p<0.05; Table S5.7), and *csb* was sufficient to explain the relationship with *tcm* with no independent influence of climatic breadth (hierarchical partitioning; R_{phy}^2 = 0.06; p<0.05; Table S5.12).

Potential of traits to protect from climate-change related loss of climatically suitable habitats

We found that species with xeromorphic traits will not be protected from anticipated climate aridification. We estimated species' vulnerability to loss of climatically suitable habitats under future climate aridification (De Boeck *et al.* 2011; Duan *et al.* 2016; Hamerlynck *et al.* 2000) the percent of currently occupied locations that are projected for the year 2070 (Table S5.13) to increase in T_{max} or decrease in *MAP* by more than two standard deviations from the current mean,

the projected loss of climatically suitable habitats (*plch*, %; Appendix Table 5.4). Species' *plch* varied across species from 0 to 93%, with a median of 53% (Table S5.13); species with highest *plch* were *Ceanothus incanus, Ceanothus velutinus*, *Chamaebatia foliolosa* and *Corylus cornuta* (Fig. S5.3). On average, the *plch* was higher for species of wetter ecosystems (one-way ANOVA; $p < 0.001$; Table S5.6 and Fig. 5.6a), and those currently distributed with higher mean *MAP* and lower T_{max} (more negative Climate-PC1 scores; $r_{phy} = -0.50$; $p < 0.001$; Table S5.7 and Fig. 5.6b). Species with higher $\Delta^{13}C$, i.e., lower integrated water use efficiency, face greater *plch* ($r_{phy} = 0.20$; $p < 0.05$; Table S5.7 and Fig. 5.6c). Further, species with higher *tcm*, i.e., those more xeromorphic than expected for their climate, face higher *plch* ($r_{phy} = 0.23$; $p < 0.05$; Table S5.7 and Fig. 5.6d).

DISCUSSION

Our findings highlight the strong potential for traits to be used to estimate species' climate adaptation in the present and to anticipate their future vulnerability. Mechanistic functional traits have strong power for prediction of the climate of species' distributions and ecosystems. The striking correspondence of traits with climate variables would have arisen from millennia of evolution and community assembly matching plant physiology to climate (Mitchell *et al.* 2018), with a further reinforcement arising in cases when the ecosystems themselves influenced their local climate via the water cycle, soil accumulation and other processes (Bounoua *et al.* 2010; Crous 2019; Boyce & Lee 2010; Boyce *et al.* 2009; Wang *et al.* 2009). The generally poor explanatory power of many previous studies testing trait-climate relationships for diverse species at large geographical scales (Wright *et al.* 2001; Moles *et al.* 2014; Fyllas *et al.* 2020) may have arisen due to combining data for traits with less mechanistic significance, and from combining data across studies using varying methodology, and in addition to mismatch between species mean

climate and the local climate of their sampling location, especially when compiling large databases (Violle *et al.* 2007; Moles *et al.* 2014; Taugourdeau *et al.* 2014; Šímová *et al.* 2018; van der Plas *et al.* 2020; Vesk *et al.* 2020). Our approach depended on a novel procedure, including the measurement of multiple mechanistic traits for coexisting species using standardized protocols, and accounting for species' evolutionary histories. This approach resolved relationships despite many potential sources for mismatch of species' traits from their current climate distributions (Appendix Table 5.2). In particular, our quantification of *tcm* identified a strong influence of intra-specific variation due to species' plastic and ecotypic adjustments on species' deviation from the all-species climate versus trait relationship (Table S5.10), such that climate sampling bias and climatic range breadth influence *tcm* (Table S5.7).

Thus, the great potential for prediction of species' climate preferences from traits would be improved by sampling each species near to the center of its climate distributions. Further, we note that additional traits may significantly improve predictive power. Here, we focused on ten traits with theoretically-grounded support for a mechanistic importance, yet additional traits that contribute to vital rates and community assembly (Kraft *et al.* 2008, 2015; Poorter *et al.* 2008; Violle *et al.* 2011; Adler *et al.* 2014; Uriarte *et al.* 2016; Medeiros *et al.* 2019) include hydraulic vulnerability, stomatal and vein traits, photosynthetic responses and other nutrient concentrations, and in addition, life history traits such as seed size, especially if other life forms including non-woody species were considered. Furthermore, finer scale climate data, including microclimate based on topography and vegetation cover, and higher resolution of trait variation within and among populations of given species would likely increase prediction capacity.

The majority of the California species sampled are predicted to suffer larger loss of climatically suitable habitats under future climate warming (Table S5.13). Notably, this analysis

focused on mean projected climate variables is conservative as an estimate of niche loss, as it does not account for temperature and precipitation extremes, including multi-year droughts (Parsons *et al.* 2018; Germain & Lutz 2020). Species distributed in cool and wet climates or with a broader native range of precipitation face a greater risk of niche contraction under a shifting climate (Table S5.7 and Fig. 5.6a-b). This analysis emphasizes the urgency of quantifying species' climate vulnerability, as species with xeromorphic traits are not those facing the most extreme climate aridification.

This approach holds immense promise for key applications for management of native, endemic and rare species in many systems worldwide. First, trait-based estimation of species' current (and projected future) natural climatic ranges would enable existing and next generation dynamic global vegetation models (DGVMs) used to predict climate change impacts to improve the representation of range limits of species and plant functional types (Stahl *et al.* 2014; van Bodegom *et al.* 2014; Yang *et al.* 2015b, 2019). Second, the prioritization of species for conservation can ultimately be improved based on traits, i.e., focusing on those species most vulnerable (Foden *et al.* 2013; Loiseau *et al.* 2020). Third, the designation of habitats for the establishment of *ex-situ* conservation sites, can be informed by species' traits, especially for species reduced to relictual populations, extending previous approaches based on taxonomic and phylogenetic information (Brum *et al.* 2017) to prioritize physiological conservation efforts for the most vulnerable species.

ACKNOWLEDGMENTS

We acknowledge the indigenous peoples that stewarded the land and ecosystems studied in this project over millenia, including the Newe/ Kawaiisu/ Chemehuevi (Granites), Kizh/ Tongva/

Chumash/ Micqanaqa'n (Stunt Ranch and UCLA), Me-Wuk (Yosemite), Washoe/ Nisenan (Onion Creek) and Cahto (Angelo) peoples. We thank Alec Baird, Marvin Browne, Marissa Ochoa and Joseph Zailaa for discussion and for comments on early versions of the manuscript and the University of California Natural Reserve System (UCNRS) for maintaining the field sites and providing support for the field campaigns. We thank Jim Andre and Sarah Germain for assistance in the field. This work was funded by La Kretz Center Graduate Research Grants, UCNRS Stunt Ranch Reserve Research Grants, ESA Forrest Shreve Award, the National Science Foundation (Grants 1951244 and 2017949) and UCLA EEB Vavra Research Grants awarded to C.M. C.M. was supported by the Brazilian National Research Council (CNPq) through the Brazilian Science Without Borders Program (grant number: 202813/2014-2).

FIGURE CAPTIONS

Figure 5.1. The potential to predict plant climate distributions from mechanistic functional traits. Multiple traits are adapted and/or plastically adjusted to climatic aridity, from less xeromorphic in cool and wet climates to more xeromorphic in warm and dry climates (see Appendix Table 5.1 for expectations and rationales based on theory and previously published empirical work for each trait). Indeed, traits often adapt in suites due to co-optimization or trade-offs, conferring ensemble advantages in given environments. For example, "economics spectrum" traits tend to be correlated, such that rapidly-growing species of high resource environments have higher foliar nutrient concentrations and photosynthetic rates but shorter lived leaves than slow-growing species of lower-resource conditions (Wright *et al.* 2004; Reich 2014). Thus, xeromorphic species are expected to have smaller maximum heights (H_{max}), and to have leaves with lower turgor loss point (π_{tlp}; corresponding to more concentrated cell solutes as depicted) and lower carbon discrimination rate ($\Delta^{13}C$; corresponding to conservative stomatal opening as depicted), that are smaller in area (*LA*), higher in leaf mass per area (*LMA*; corresponding to denser or thicker leaves, as depicted), lower in leaf nitrogen per mass (N_{mass}) but higher in nitrogen per area (N_{area}; depicted with greenness), lower in leaf carbon per mass (C_{mass}; corresponding to greater herbivory, as depicted), and higher carbon to nitrogen ratio (*C*:*N;* reflecting greater investment in cell wall relative to chlorophyll as depicted) and higher wood density (*WD*, corresponding to more xylem cell wall tissue per area, as depicted). Created with BioRender.com.

Figure 5.2. Ecosystems distributed across an aridity gradient from Baja California (Mexico) to northern California (US), and aligned adaptive trait variation. (a) Photographs of the study ecosystems sampled in the peak of the Spring growing season, set in a map showing the rainfall

gradient. (b) Illustration of an across species climate-trait relationship: the first axis of a principal components analysis of species' climate variables (Climate-PC1) plotted against turgor loss point, π_{tlp} (main panel; phylogenetic generalized least squares; $\lambda = 0.83$; Table S5.7) and ecosystems (inset; ordinary least squares; Table S5.6); symbols as in Fig. 5.2a (**$p < 0.01$; ***$p < 0.001$). (c-j) Variation across ecosystems, from wettest to driest, in the eight mechanistic functional traits included in predictive models (Fig. 5.4), (c) maximum plant height (H_{max}; m), (d) leaf area (LA; cm^2), (e) carbon isotope discrimination ($\Delta^{13}C$; ‰), (f) carbon per mass (C_{mass}; $mg.g^{-1}$), (g) absolute turgor loss point (π_{tlp}; -MPa), (h) wood density (WD; $g.cm^{-3}$), (i) leaf mass per area, (LMA, $g.m^{-2}$) and (j) nitrogen per mass (N_{mass},; $mg.g^{-1}$). All eight traits were significantly different across ecosystems (Nested ANOVAs; Table S5.2; $p<0.001$).

Figure 5.3. The association of traits with climate across species and ecosystems, the derivation of trait-climate mismatch (*tcm*), and two potential influences arising from intra-specific trait variation. Symbols represent species of different ecosystems, with darker shades of blue representing greater water availability: mixed conifer-broadleaf forest (dark blue circles), mixed riparian woodland (triangles), montane wet forest (inverted triangles), chaparral (diamonds), coastal sage scrub (squares), desert (light blue circles). (a) A principal components analysis of species' climate variables and trait variables yielded first axes (Traits-PC1 and Climate-PC1, respectively) that represented climatic aridity and trait values associated with adaptation to aridity, and the two are strongly related across species (main plot; phylogenetic generalized least squares; $\lambda = 0.85$; Table S5.7) and ecosystems (inset; ordinary least squares; Table S5.6). Thus, the residuals from this relationship represent the trait-climate mismatch (*tcm*) where a species with higher values possesses traits more xeromorphic than expected from the all-species relationship.

(b) Given that species' traits may adjust plastically or genetically (ecotypically) in relation to climate, the *tcm* may depend on the "climate sampling bias" (*csb*), i.e., the difference between the climate of the species' sampling site (red or blue circle) and the mean climate of its native range (black star), where species sampled from a location more arid than the mean of its distribution would have a higher *csb* (red), and species sampled from a less arid location would have a lower *csb* (blue). (c) The magnitude of |*tcm*| may also depend on the breadth of species' climatic ranges, as species with wider climatic ranges (blue versus red) will have a larger likelihood of their traits being adjusted by adaptation and plasticity to sites further from their mean (black squares) (**$p < 0.01$; ***$p < 0.001$).

Figure 5.4. Prediction of species' native climate distribution means based on mechanistic functional traits for 107 species from six California ecosystems, demonstrated using two multivariate approaches. Symbols represent species of different ecosystems, with darker shades of blue representing greater water availability: mixed conifer-broadleaf forest (dark blue circles), mixed riparian woodland (triangles), montane wet forest (inverted triangles), chaparral (diamonds), coastal sage scrub (squares), desert (light blue circles). (a) Relationship of the first axis of a principal components analysis of species' climate variables (Climate-$PC1_{obs}$) to predicted values for Climate-PC1 based on functional traits using multiple regression: Climate-$PC1_{pred}$ = -3.31 – (0.14 × *LMA*) - (0.18 × *WD*) – (0.04 × N_{mass}) + (1.13 × C_{mass}) + (0.70 × $\Delta^{13}C$) – (0.17 × π_{tlp}); (phylogenetic generalized least squares, PGLS; $\lambda = 0.80$; Table S5.8). (b) Relationship between the Climate-$PC1_{obs}$ and predicted values for Climate-PC1 based on the first axis of a principal components analysis of species' traits, Traits-PC1 (Climate-$PC1_{pred\ Traits\text{-}PC1}$; Fig 5.3a; PGLS; $\lambda = 0.87$; Table S5.9). Main plots show relationships for species, and inset plots show the relationships

among ecosystem mean values, with the dashed lines representing the 1:1 relationship and dotted red lines the confidence intervals (*$p < 0.05$; **$p < 0.01$; ***$p < 0.001$).

Figure 5.5. Testing hypotheses for influences on trait-climate mismatch (*tcm*; the residuals from the all-species climate vs. traits relationship shown in Fig 5.3a) arising from intra-specific trait variation. Relationship between trait climate mismatch and species' climate sampling bias in terms of (a) maximum temperature of the warmest month, $csb_{T\max}$, and (b) mean annual precipitation, csb_{MAP} (PGLS; $\lambda = 0.86$ and 0.89, respectively; Table S5.7). (c) Relationship between the absolute trait-climate mismatch, $|tcm|$, and the range in maximum temperature of the warmest month, $T_{\max}$, of species climatic distributions (PGLS; $\lambda = 0.48$; Table S5.7). Symbols represent species of different ecosystems, with darker shades of blue representing greater water availability: mixed conifer-broadleaf forest (dark blue circles), mixed riparian woodland (triangles), montane wet forest (inverted triangles), chaparral (diamonds), coastal sage scrub (squares), desert (light blue circles) (*$p < 0.05$).

Figure 5.6. Species' vulnerability to future climate aridification. Projected loss of climatically suitable habitats, *plch*, is the species predicted climatic niche loss under a pessimistic ("business-as-usual") climate change scenario in 2070 (Representative Concentration Pathway, RCP 8.5; see Table S5.13 for results from a moderate emission scenario, RCP 4.5). Symbols represent species of different ecosystems, with darker shade of blue representing greater water availability: mixed conifer-broadleaf forest (dark blue circles), mixed riparian woodland (triangles), montane wet forest (inverted triangles), chaparral (diamonds), coastal sage scrub (squares), desert (light blue circles). (a) Variation across ecosystems in *plch*. Each point represents a species (analysis of

variance; Table S5.10; $p<0.001$). Relationships (phylogenetic generalized least squares; λ ranged from 0.46 to 0.59; Table S5.7) between (b) *plch* and the first axis of the climate PCA, Climate-PC1, (c) the log-transformed *plch* and log-transformed carbon isotope discrimination, $\Delta^{13}C$, and (d) *plch* and the trait-climate mismatch, *tcm*. $*p < 0.05$; $**p < 0.01$; $***p < 0.001$.

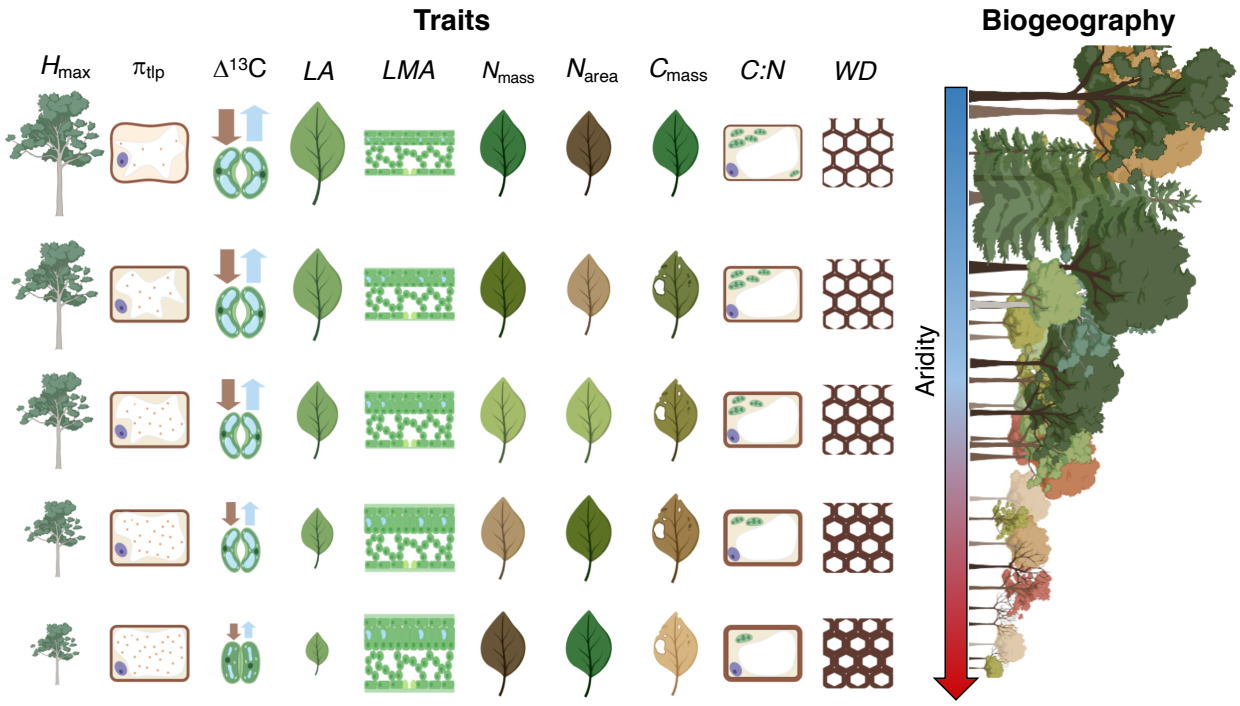
Traits
Biogeography
H_{max}
π_{tlp}
$\Delta^{13}C$
LA
LMA
N_{mass}
N_{area}
C_{mass}
C:N
WD
Aridity

Fig. 5.1

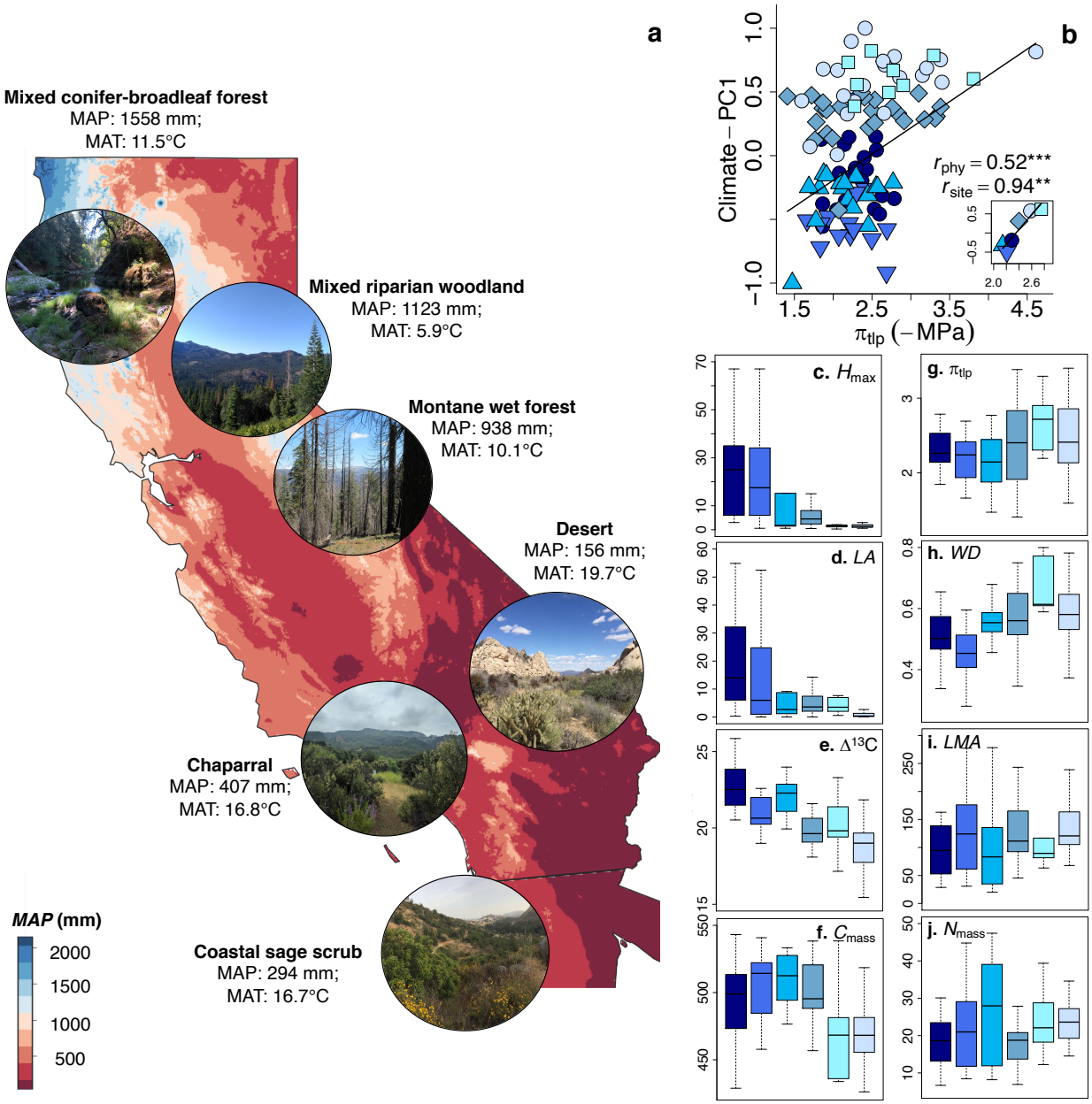
a
b
Mixed conifer-broadleaf forest
MAP: 1558 mm;
MAT: 11.5°C
Mixed riparian woodland
MAP: 1123 mm;
MAT: 5.9°C
Montane wet forest
MAP: 938 mm;
MAT: 10.1°C
Desert
MAP: 156 mm;
MAT: 19.7°C
Chaparral
MAP: 407 mm;
MAT: 16.8°C
Coastal sage scrub
MAP: 294 mm;
MAT: 16.7°C
MAP (mm)
2000
1500
1000
500
Climate – PC1
π_{tlp} (−MPa)
$r_{phy} = 0.52^{***}$
$r_{site} = 0.94^{**}$
c. H_{max}
d. LA
e. $\Delta^{13}C$
f. C_{mass}
g. π_{tlp}
h. WD
i. LMA
j. N_{mass}

Fig. 5.2

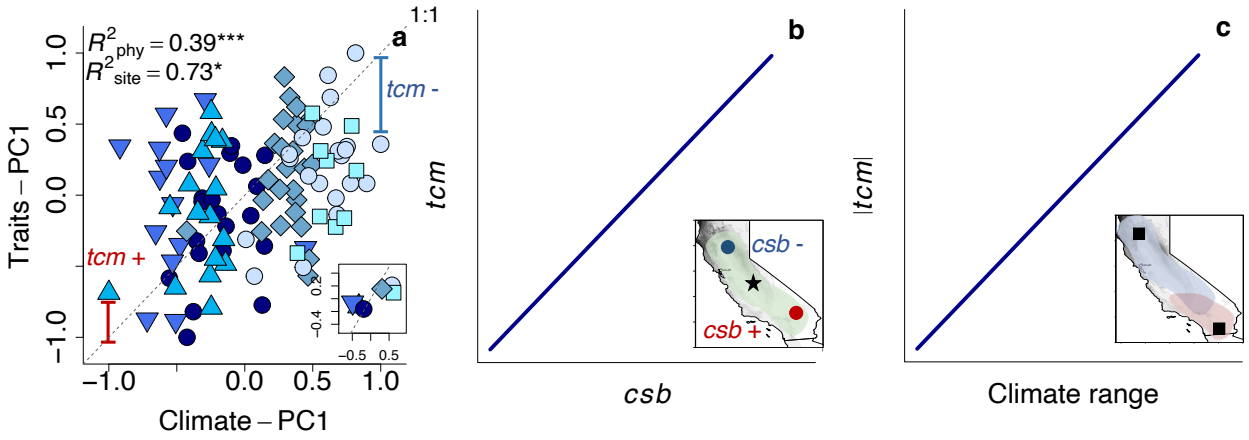
a
1:1
$R^2_{phy} = 0.39^{***}$
$R^2_{site} = 0.73^{*}$
tcm -
tcm +
Traits – PC1
Climate – PC1
tcm
b
csb -
csb +
csb
c
|tcm|
Climate range

Fig. 5.3

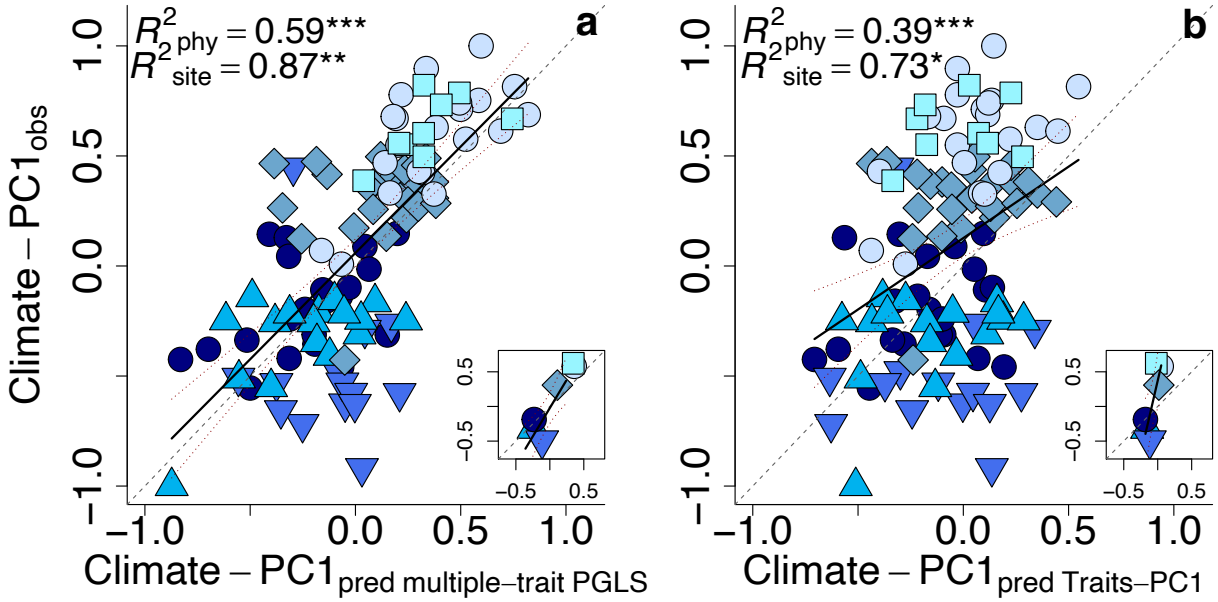
a
$R^2_{phy} = 0.59^{***}$
$R^2_{site} = 0.87^{**}$
Climate – PC1obs
Climate – PC1pred multiple–trait PGLS
b
$R^2_{phy} = 0.39^{***}$
$R^2_{site} = 0.73^{*}$
Climate – PC1pred Traits–PC1

Fig. 5.4

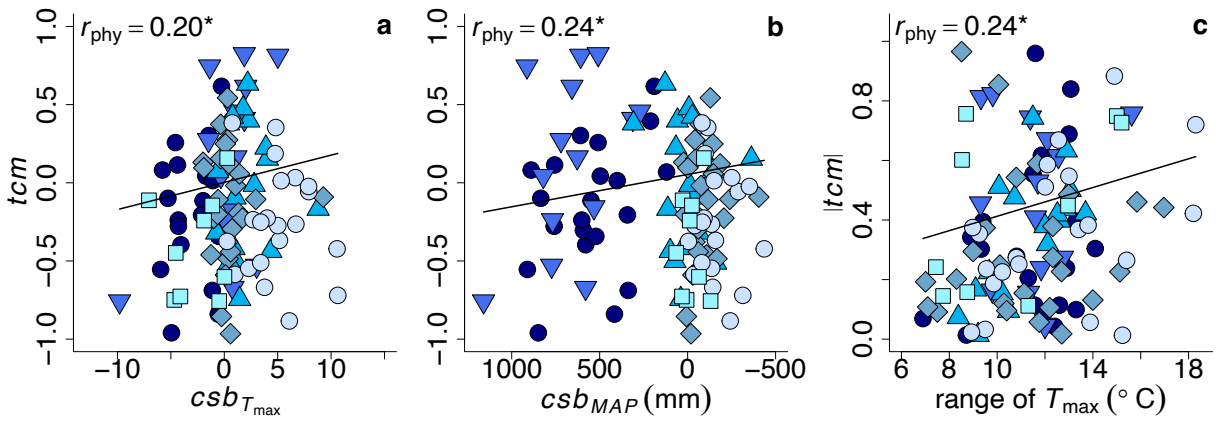
$r_{phy} = 0.20^*$
a
tcm
1.0
0.5
0.0
−0.5
−1.0
−10
0
5
10
$csb_{T_{max}}$
$r_{phy} = 0.24^*$
b
1000
500
0
−500
csb_{MAP} (mm)
$r_{phy} = 0.24^*$
c
|tcm|
0.8
0.4
0.0
6
8
10
14
18
range of T_{max} (° C)

Fig. 5.5

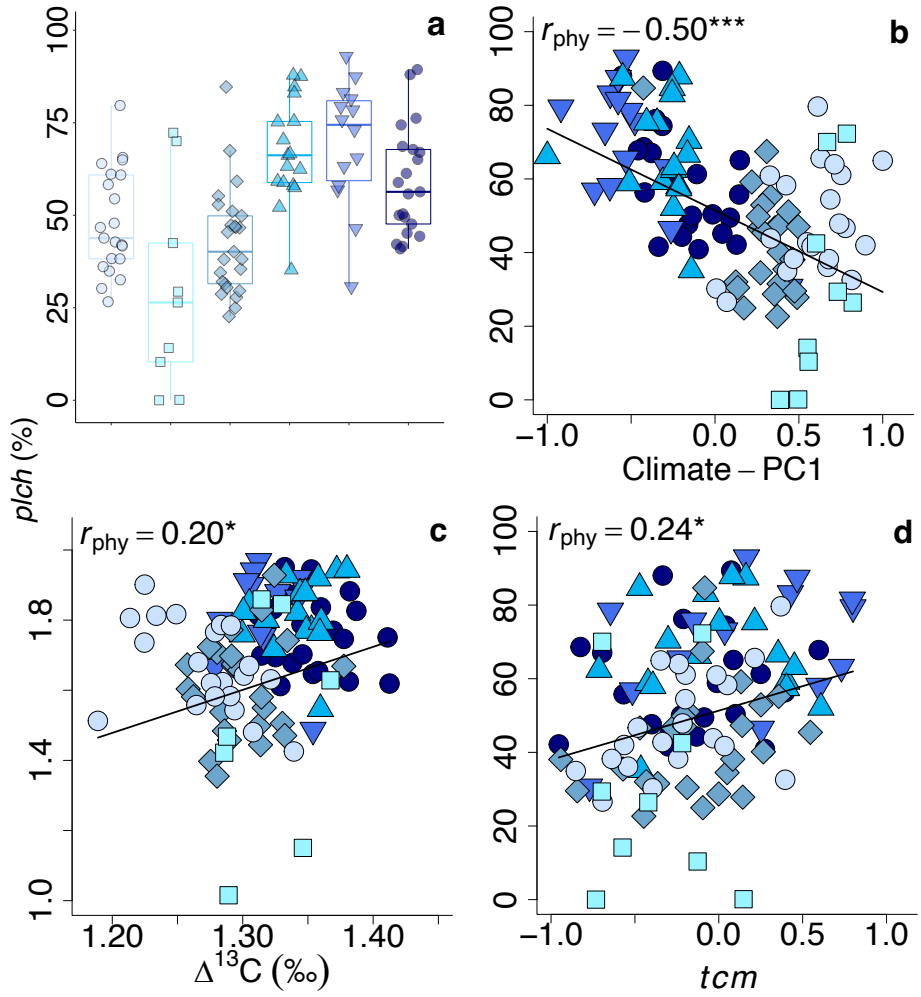
a
b
c
d
plch (%)
$r_{phy} = -0.50^{***}$
$r_{phy} = 0.20^{*}$
$r_{phy} = 0.24^{*}$
Climate – PC1
$\Delta^{13}C$ (‰)
tcm

Fig. 5.6

Appendix Table 5.1. Traits sampled for 107 California native woody species from six ecosystems distributed across a range of precipitation from Baja California (Mexico) to northern California (US), including symbols, units, and hypotheses for adaptation to climatic aridity (i.e., low precipitation, high temperature and high soil pH), based on previously published studies on a range of species, with references; a negative trend (indicated by "-") indicates the trait would decrease from the mixed conifer-broadleaf forest to the desert, and a positive trend (indicated by "+"), indicates the trait would increase (Fig 5.1).

Trait	Symbol	Units	Hypothesized relationship with climatic aridity	Reference for trends across species/ across ecosystems
Maximum plant height	H_{max}	m	-; when resources are abundant a greater height would enable stronger competition, and when resources are limited and temperatures high, lower stature would enable greater allocation below ground and reduced hydraulic pathlength susceptible to tension-driven embolism (Koch *et al.* 2004; King *et al.* 2006)	(Moles *et al.* 2009; Liu *et al.* 2019)
Osmotic potential at turgor loss (|absolute|)	$\|\pi_{tlp}\|$	MPa	+; higher $\|\pi_{tlp}\|$ (or wilting point) indicates greater capacity to maintain cell volume and turgor pressure, and to maintain open stomata during dehydration. It is strongly correlated with drought tolerance within and across species, i.e., more tolerant species tend to have larger $\|\pi_{tlp}\|$ and to withstand lower soil water potentials (Bartlett *et al.* 2012b)	(Fletcher *et al.* 2018; Griffin-Nolan *et al.* 2019)/ (Bartlett *et al.* 2012b)
Carbon isotope discrimination	$\Delta^{13}C$	‰	-; in C_3 photosynthetic species, higher $\Delta^{13}C$ values tend to correspond to high stomatal conductance integrated over leaf lifetimes, and may indicate higher CO_2 assimilation rates, whereas lower values tend to correspond to higher water use efficiency (i.e., assimilation relative to transpiratory water loss) integrated over the leaf lifetime (Farquhar *et al.* 1989)	(Hu *et al.* 2009)
Leaf area	*LA*	cm^2	-; smaller leaves have thinner boundaries enabling leaves to avoid dangerous overheating on hot days and chilling on cool nights, and potentially to achieve higher gas exchange rates when soil is moist and temperatures are moderate (Gibson 1998). Additionally, smaller leaves have smaller veins and xylem conduits, and higher major vein densities, which can provide greater hydraulic safety during dehydration (Sack *et al.* 2012; Wright *et al.* 2017)	(Wright *et al.* 2017)
Leaf mass per area	*LMA*	$g\ m^{-2}$	+; higher *LMA* tends to confer longer leaf lifetimes and thus a conservative resource allocation that is adaptive for leaves that persist through multiple droughts and for species on low fertility soils. A high *LMA* may also correspond to higher elastic moduli which may enable greater water retention in leaves with lower wilting points (Evans 1973; Wright *et al.* 2004; Westoby & Wright 2006; John *et al.* 2017) Additionally a high *LMA* may enable lower cuticular transpiration rates after stomata close due to lower surface area-to-volume ratio.	(Lamont *et al.* 2002; Wright *et al.* 2005; He *et al.* 2006; de la Riva *et al.* 2016)
Nitrogen per mass	N_{mass}	$mg\ g^{-1}$	-/+; higher N_{mass} tends to correspond to higher light-saturated photosynthetic rates per leaf mass, typical of species native to high resource availability(Wright *et al.* 2004). Higher N_{mass} can also provide drought adaptation by promoting both higher pulse-driven growth in periods of high water availability and a higher water use efficiency during moderate drought (Wright *et al.* 2001; Wright & Westoby 2002; Santiago *et al.* 2004)	(Field & Mooney 1986; Reich & Oleksyn 2004; Wright *et al.* 2005)
Nitrogen per area	N_{area}	$g\ m^{-2}$	+; higher N_{area} can also provide drought adaptation by promoting both higher pulse-driven growth in periods of high water availability and a higher water use efficiency during moderate drought (Cunningham *et al.* 1999; Wright *et al.* 2001)	(Wright *et al.* 2005; He *et al.* 2006)

Carbon per mass	C_{mass}	mg g^{-1}	-; higher C_{mass} is linked with higher lignin concentration, which may protect leaves against herbivory, thus a conservative resource allocation that is adaptive for leaves that persist through multiple droughts and for species on low fertility soils (Ma *et al.* 2018)	(Ma *et al.* 2018)
Carbon to nitrogen ratio	*C*:*N*	-	+; higher *C*:*N* ratio reflects investment in structural support relative to photosynthesis, resulting in thicker, sturdier, cell walls and thus a conservative resource allocation that is adaptive for leaves that persist through multiple droughts and for species on low fertility soils (Fang *et al.* 2019)	(Fang *et al.* 2019)
Wood density	*WD*	g cm^{-3}	+; higher *WD* is associated with longer wood lifetimes and with a conservative resource allocation strategy that is adaptive for species that persist through multiple droughts and for species on low fertility soils. In addition, higher *WD* can correspond to lower vulnerability to xylem embolism and survival during drought (Hacke *et al.* 2001; Chave *et al.* 2009; Gleason *et al.* 2016; Liang *et al.* 2021)	(Preston *et al.* 2006; Thomas *et al.* 2007)

Appendix Table 5.2. Many factors, not mutually exclusive, that would potentially impede trait-based prediction of the climate distribution of species and ecosystems by decoupling plant traits from the mean climate of their natural distributions, with supporting references.

Factor	Rationale
Fundamental vs. realized niches	A species' current distribution ("realized niche") may differ from that expected from its "fundamental niche", i.e., the set of abiotic environmental conditions in which species is able to live, as determined by its traits and physiological limits, due to dispersal limitation, disturbance and biotic interactions including competition (Brown 1984; Hanski *et al.* 1993; Wiens 2011; Peterson *et al.* 2012; Lee-Yaw *et al.* 2016), which can alter distributions in the field (Walter 1979; Pérez-Ramos *et al.* 2019; Sheth *et al.* 2020).
Traits and fitness are not directly related	Functional traits are frequently used as a metric for fitness, and assumed to influence success in a given environment, but this equivalence is not always straight forward, as functional traits are related to fitness through vital rates, and thus they might not predict fitness in many systems (Laughlin *et al.* 2020).
Trait plasticity and/or ecotypic differentiation	Trait plasticity, i.e., shift of phenotype in accordance with growing conditions, is essential for plant species survival in many environments (Valladares *et al.* 2000). Likewise, populations of given species may adapt to different conditions, leading to ecotypic variation. Both plasticity and ecotypic differentiation would result in intraspecific trait variation across environments. If species are collected at sites distant from the mean climate of their range, then plastic and ecotypic trait adjustment might weaken the association of measured traits with mean climate, as species' sampled trait values would reflect the sampled climate rather than the mean climate of the species' native range (Albert *et al.* 2010a, b; Violle *et al.* 2012; Siefert *et al.* 2015; Fyllas *et al.* 2020).
Trait multifunctionality	Given traits may be multifunctional and thus optimized in evolution and plasticity to multiple environmental factors (e.g., a trait may shift with herbivory, nutrient availability and aridity) and thus may be far from optimal for individual environmental factors, such as single climate variables (Sack & Buckley 2020).
Many-to-one mapping of traits to function	Adaptation to environmental conditions may be achieved through multiple alternative combinations of traits, such that individual traits would be weakly associated with environmental conditions (Alfaro *et al.* 2005; Marks & Lechowicz 2006).
Nonequilibrium processes	Species' distributions relate to dynamic processes including immigration, competition, evolution, and extinction under changing climates, and thus species' traits may not necessarily match their current distributions, and might better relate to their distribution under historical climates (Dobzhansky 1950; DeAngelis & Waterhouse 1987; Stevens 1989; Ohlemüller *et al.* 2008; Sheth *et al.* 2020).
Study methodology	*Traits with a limited direct mechanistic role* Since the publication of the leaf economics spectrum (Wright *et al.* 2004), ecologists have focused on the relationships of a core set of 5-8 traits and climate. However, these putative traits are not always mechanistically adaptive to given climate variables. For example, the leaf mass per area, *LMA*, has been frequently measured and framed as a drought tolerance trait. However, in many systems, *LMA* does not necessarily confer drought tolerance (e.g., in tropical rainforests, high *LMA* may be found in drought sensitive trees), though but in some species sets it is co-selected for with other traits, such as low turgor loss point (Buckley *et al.* 1980; Bartlett *et al.* 2012b). *Large variation in traits compiled from global databases* The frequent use of measurements compiled in databases from disparate locations, collected with different methods and with uncertainty in trait mean estimation contributes to weakness in the reported trait-climate associations (Moles *et al.* 2014; Violle *et al.* 2015; Šímová *et al.* 2018; van der Plas *et al.* 2020; Vesk *et al.* 2020). *Missing data in global databases* The relationship between given traits and climate variables might be weakened or missed due to many missing data points for species with restricted distributions and or/small populations, and for traits that are more measurement intensive (Taugourdeau *et al.* 2014). *Lack of phylogenetic structure* Since species have shared evolutionary histories, they cannot necessarily be considered independent data points. This nonindependence may violate one of the main assumptions of most statistical tests, so it is recommended that the phylogenetic structure is accounted for to fully resolve adaptive trait-trait and trait-

environment relationships across species. Phylogenetic approaches thus have potential to explain the large interspecific variation in many functional traits (Perez & Feeley 2020).

Microclimate

Species climatic ranges are typically calculated from large databases with coarse resolution (usually between 1 and 340 km^2). While these climatic ranges are effective in characterizing large scale patterns, the strength of trait-climate relationships could be improved if variation in microclimates, i.e., temperature, water and nutrient availability, irradiance and soil composition, were accounted for (Opedal *et al.* 2015).

Appendix Table 5.3. Ecosystems sampled across an aridity gradient in California, including site names, latitude and longitude of the site centroid, mean annual precipitation (*MAP*; mm), mean annual temperature (*MAT*; °C), mean elevation (m), and number of species sampled. Site climate was obtained from a 5-hectare circular area around each site's centroid.

Ecosystem	Site	Latitude	Longitude	*MAP* (mm)	*MAT* (ºC)	Elevation (m)	Number of species
Desert	Sweeney Granite Mountains Desert Center	34.7813355	-115.6559781	156	19.7	819	24
Coastal Sage Scrub	Centro de Investigación Científica y de Educación Superior de Ensenada and Cañon de Doña Petra	31.869475	-116.666892	294	16.7	342	14
Chaparral	Stunt Ranch Santa Monica Mountains Reserve	34.0955321	-118.66148	407	16.9	339	25
Montane Wet Forest	Yosemite National Park	37.8529772	-119.8312939	938	10.1	1629	20
Mixed Riparian Woodland	Onion Creek	39.274627	-120.3654455	1123	5.96	2060	19
Mixed conifer-broadleaf forest	Angelo Coast Range Reserve	39.7185431	-123.6550498	1558	11.6	526	21

Appendix Table 5.4. Indices of variation presented in the study, including abbreviations, definition, references and calculation.

Term	Abbreviation	Definition	Calculation
Trait-climate mismatch	*tcm*	The mismatch between the trait values measured for individuals occurring in the field and the trait values expected given the overall relationship of species' traits to their climatic distributions. The *tcm* represents the degree that a species' traits do not conform to expectations based on adaptation to its current climate distribution.	Calculated as the residuals from the all-species' trait *vs* climate relationship. In this study, species' scores in principal component axes of climate variables were used, and scaled such that higher *tcm* represents traits more putatively adapted to aridity than expected, i.e., "hyperxeromorphic". $tcm_i = obs\ Traits\ PC1_i - pred\ Traits\ PC1_i$, where *obs Traits PC1*$_i$ is the measured Traits-PC1 score and *pred Traits PC1*$_i$ is the Traits-PC1 score predicted from Climate-PC1 for each species *i*.
Climate sampling bias	*csb*	The difference between the climate of the site where a species' was sampled and the mean of its climatic distribution, calculated from current occurrences(Browne *et al.* 2019).	$csb_i = climate_{ij} - \overline{climate_i}$, where *climate*$_{ij}$ is the mean climate of the site *j* where species *i* was sampled from and *climate*$_i$ is the mean climate its distribution.
Climatic breath	-	The difference between the maximum and the minimum value of a climate variable for locations in which a given species occurs.	$breath_i = 95^{th}\ percentile_i - 5^{th}\ percentile_i$, where the *95*th *percentile*$_i$ represents the maximum and the *5*th *percentile*$_i$ represents the minimum values of a given climate variable for the range of distribution of each species *i*.
Between-site variation	*bsv*	An index of variation in values for trait and climate variables of a given species sampled from multiple sites, a measure of the intra-specific variation (see Table S2). While the *bsv* calculation is based on the plasticity index(Valladares *et al.* 2000), the *bsv* for traits does not quantify species' phenotypic plasticity, which can only be measured from controlled experiments, but rather a combination of genetic and plastic variation.	$bsv_i = \frac{(max_i - min_i)}{max_i}$, where *max*$_i$ is the maximum and *min*$_i$ is the minimum value of a given trait or climate variable for species *i*.
Projected loss of climatically suitable habitats	*plch*	The percent of occurrences of a given species that would be potentially outside of a given species' physiological limits under projected future climate change scenarios.	Calculated as the percent of current occurrences that under projected future climates would shift to higher T_{max} and/or lower *MAP* by ≥ 2 standard deviations of the current distributions of these climate variables.

SUPPLEMENTARY MATERIALS

Supplementary data captions (see attached Excel Workbook)

Table S5.1. (a) Environmental variables used to estimate climate for 107 species from six ecosystems across a climatic gradient in the California Floristic Province, including abbreviations, units, source database, metadata (raster layer title, timeframe of the dataset, the subset of the original dataset that was used to calculate species climate envelope, and the download date), and links to access datasets and references; (b) Future climate projection models, their sources, metadata (main characteristics, model developers, the subset of the original dataset that was used to calculate species climate envelope, download date), links to access datasets and references.

Table S5.2. Differences in functional traits among species and ecosystems, as indicated in nested analyses of variance, with species nested within ecosystems for 107 species from six ecosystems across a climatic gradient in the California Floristic Province. Traits deviating from assumptions of normality or homoscedasticity were log-transformed prior to the analysis (see legend below). Different letters indicate significant differences among groups (Tukey test). Blue highlighted cells indicate variables differing significantly different across sites ($p \leq 0.05$).

Table S5.3. Principal Components Analysis (PCA) axes scores, climate variable contribution, climate variable correlational values and importance of components that explain ~60% of the variation in the climate of species' native distribution for 107 species from six ecosystems across a climatic gradient in the California Floristic Province. Highlighted cells indicate strongest relationships (loadings > |0.6|).

Table S5.4. Associations of traits and environmental variables in a matrix presenting ahistorical correlation tests. In each cell, results are presented for Pearson tests on untransformed data and Pearson tests on log-transformed data. Blue highlighted cells indicate significant relationships for Pearson test on untransformed or log-transformed data (***$p \leq 0.001$; **$p \leq 0.01$; *$p \leq 0.05$).

Table S5.5. Principal Components Analysis (PCA) axes scores, trait contribution, trait correlational values and importance of components that explain ~60% of the variation in key functional traits of 107 species from six ecosystems across a climatic gradient in the California Floristic Province. Highlighted cells indicate strongest relationships (loadings > |0.6|).

Table S5.6. Differences in variables representing the climate of species' native distribution among ecosystems, as indicated in one-way analyses of variance for 107 species from six ecosystems across a climatic gradient in the California Floristic Province. Variables tested included modelled values for current and future conditions, climate sampling bias and projected niche loss. Variables deviating from assumptions of normality or homoscedasticity were log-transformed prior to the analysis (see legend below). Different letters indicate significant differences among groups (Tukey test). Blue highlighted cells indicate variables differing significantly different across sites ($p \leq 0.05$).

Table S5.7. Associations of traits and variables representing the climate of species' native distribution for 107 species from six ecosystems across a climatic gradient in the California Floristic Province using phylogenetic generalized least squares (PGLS) tests. Blue highlighted cells indicate significant relationships ($p \leq 0.05$).

Table S5.8. Multiple phylogenetic regression models predicting variables representing the climate of species' native distribution from mechanistic functional traits for 107 species from six ecosystems across a climatic gradient in the California Floristic Province; the full models and best-fit models built with log-transformed variables are shown. The best-fit models were chosen after AIC comparison of all possible models (ΔAICc < 2). Predictions were made of the first axis of a principal component analysis using 9 key climate and other environmental variables (Climate-PCA; Fig. 5.4a) and additionally, with a subset of six variables that have future estimates available from WorldClim (Fig. S5.6a). We use the Climate-PCA with 9 variables to summarize current climate and use the Climate-PCA with 6 variables when testing relationships with predicted future climate (2070). We also show models predicting individual environmental variables (Fig. S5.5). N=107 species.

Table S5.9. Phylogenetic regression models predicting the climate of species' native distribution from mechanistic functional traits for 107 species from six ecosystems across a climatic gradient in the California Floristic Province using scores from the first axis of the principal component axis of climate variables (Climate-PCA) as the dependent variable.

Table S5.10. Estimates of trait plasticity and environmental variation between sites for the fifteen species sampled in more than one ecosystem across a climatic gradient in the California Floristic Province. We present indices of between-site trait and climate variation [bsv_{trait} and bsv_{climate}; (MAX-MIN)/MAX; based on Valladares et al., 2000].

Table S5.11. Associations between trait plasticity and environmental variation between sites for the fifteen species sampled in more than one ecosystem across a climatic gradient in the California Floristic Province, assessed using phylogenetic generalized least squares (PGLS). Blue highlighted cells indicate trait relationships significant ($p \leq 0.05$).

Table S5.12. Multiple phylogenetic regression models to explain the trait-climate mismatch (*tcm*) from species' climate sampling bias (*csb*) and native ranges (95th - 5th percentile) of maximum temperature of the warmest month (T_{max}) and mean annual precipitation (*MAP*) for 107 species from six ecosystems across a climatic gradient in the California Floristic Province.

Table S5.13. Projected loss of climatically suitable habitats (*plch*) under future climatic aridification for 107 species from six ecosystems across a climatic gradient in the California Floristic Province, calculated as predicted percent reduction in number of occurrences given shifts of means of future climate scenarios (RCP 4.5 and 8.5 in 2070) 2 SDs above the maximum (for temperature variables, so warmer future) or below the minimum (for precipitation variables, so drier future) current climate means of the range of distribution of each species.

Supplementary figure captions

Figure S5.1. Phylogenetic tree showing evolutionary relationships among 107 species from six California ecosystems. Symbols represent species of different ecosystems, with darker shades of blue representing greater water availability: mixed conifer-broadleaf forest (dark blue circles), mixed riparian woodland (triangles), montane wet forest (inverted triangles), chaparral (diamonds), coastal sage scrub (squares), desert (light blue circles). Species were categorized according to the ecosystem they were sampled in (or, for species that occurred in multiple sites, that with climate closest to the mean aridity index, *AI*, of their climatic distribution).

Figure S5.2. Principal component analyses (PCA) of (a) mean climate variables for species' ranges of distribution (Table S5.3) and (b) a set of non-redundant species traits for 107 species from six California ecosystems (Table S5.5). The climate variables included were mean annual temperature, *MAT*, maximum temperature of the warmest month, T_{max}, minimum temperature of the coldest month, T_{min}, mean annual precipitation, *MAP*, precipitation of the wettest month, P_{wet}, precipitation of the dryest month, P_{dry}, aridity index, *AI*, growing degree-days, *GDD*, and soil pH, $Soil_{pH}$. For all tests of relationships with "Climate-PC1" we multiplied by "-1" so the relationship between Climate-PC1 and Traits-PC1 is positive, for clarity, as these reflected climatic aridity and adaptation to aridity respectively. The traits included were maximum adult height, H_{max}, turgor loss point, π_{tlp} (multiplied by "-1" prior to PCA), carbon isotope discrimination, $\Delta^{13}C$, leaf area, *LA*, leaf mass per area, *LMA*, foliar nitrogen and carbon concentrations, N_{mass} and C_{mass}, and wood density (*WD*). Symbols represent species of different ecosystems, with darker shades of blue representing greater water availability: mixed conifer-broadleaf forest (dark blue circles), mixed

riparian woodland (triangles), montane wet forest (inverted triangles), chaparral (diamonds), coastal sage scrub (squares), desert (light blue circles).

Figure S5.3. Relationships between the modelled climate of six California ecosystems and the average modelled climate of species' natural climatic distributions averaged for each ecosystem. (a) Maximum temperature of the warmest month, T_{max}, (b) mean annual precipitation, *MAP*, (c) aridity index, *AI*, and (d) soil pH, $Soil_{pH}$. Symbols represent species of different ecosystems, with darker shades of blue representing greater water availability: mixed conifer-broadleaf forest (dark blue circles), mixed riparian woodland (triangles), montane wet forest (inverted triangles), chaparral (diamonds), coastal sage scrub (squares), desert (light blue circles). The dashed gray lines represent the 1:1 relationship and the bars represent the standard errors of the *x*-axis means. $*p < 0.05$; $**p < 0.01$ (ordinary least squares; Table S5.4).

Figure S5.4. Prediction of the mean climate of species' distributions based on mechanistic functional traits for 107 species from six California ecosystems. Relationship between predicted and observed climate variables (phylogenetic generalized least squares; λ ranged from 0.70 to 0.76), (a) maximum temperature of the warmest month, T_{max}, (b) mean annual precipitation, *MAP*, (c) aridity index, *AI*, and (d) soil pH, $Soil_{pH}$. Refer to Table S5.8 for detailed model information. Inset plot shows the relationships for ecosystems based on averaging constituent species (ordinary least squares). Symbols represent species of different ecosystems, with darker shades of blue representing greater water availability: mixed conifer-broadleaf forest (dark blue circles), mixed riparian woodland (triangles), montane wet forest (inverted triangles), chaparral (diamonds), coastal sage scrub (squares), desert (light blue circles). The dashed lines represent the 1:1

relationship and dotted dark red lines represent the prediction intervals (*$p < 0.05$; **$p < 0.01$; ***$p < 0.001$).

Figure S5.5. Predicting the mean climate of species and ecosystems on the basis of mechanistic functional traits for 107 species from six California ecosystems. The first axis of the principal component analysis of climate variables (Climate-PC1; Fig S5.2) plotted against (a) log-transformed maximum plant height, H_{max}, (b) carbon isotope discrimination, $\Delta^{13}C$, (c) leaf area, *LA*, (d) leaf mass per area, *LMA*, (e) foliar nitrogen per mass, N_{mass}, (f) foliar nitrogen per area, N_{area}, (g) foliar carbon per mass, C_{mass}, (h) log-transformed carbon to nitrogen ratio, *C*:*N*, and (i) wood density, *WD*. Main plots show the relationships for species (phylogenetic generalized least squares; λ ranged from 0.64-0.84; Table S5.7), and inset plots for ecosystems (ordinary least squares; Table S5.6). Symbols represent species of different ecosystems, with darker shades of blue representing greater water availability: mixed conifer-broadleaf forest (dark blue circles), mixed riparian woodland (triangles), montane wet forest (inverted triangles), chaparral (diamonds), coastal sage scrub (squares), desert (light blue circles) (*$p < 0.05$; **$p < 0.01$; ***$p < 0.001$).

Figure S5.6. The influence of plasticity on functional traits for 15 species that were sampled from more than one California ecosystem (Table S5.10). For the 15 species, the relationship of the between-site variation in the osmotic potential at turgor loss, $bsv\pi_{tlp}$, with (a) the between-site variation in aridity, bsv_{AI}, and (b) the mean annual precipitation, bsv_{MAP} (phylogenetic generalized least squares; $\lambda = 0$; Table S5.11). Similar relationships were found for other traits and climate variables (Table S5.11). *$p < 0.05$.

Figure S5.7. Projected loss of climatically suitable habitats (*plch*) for four California native species under a pessimistic ("business-as-usual") climate change scenario (RCP 8.5; see Table S13 for RCP 4.5 results, which reflect a "moderate emissions" scenario) in terms of maximum temperature of the warmest month, $T_{max,}$ and mean annual precipitation, *MAP*. Maps show the current occurrences (all points) and the occurrences projected as >2SD higher in mean maximum temperature of the warmest month (T_{max}) and/or >2SD lower in mean annual precipitation (*MAP*) than current climate and would thus face extreme conditions if physiological adaption does not track changes in climate (red dots), to compare with occurrences that would be within the 2SD threshold (black dots). These four species were predicted to have the largest *plch* of the 107 species in this study: (a) *Ceanothus velutinus* of mixed riparian woodland, (b) *Ceanothus incanus* of mixed conifer-broadleaf forest, (c) *Corylus cornuta* of mixed conifer-broadleaf forest and (d) *Chamaebatia foliolosa* of montane wet forest.

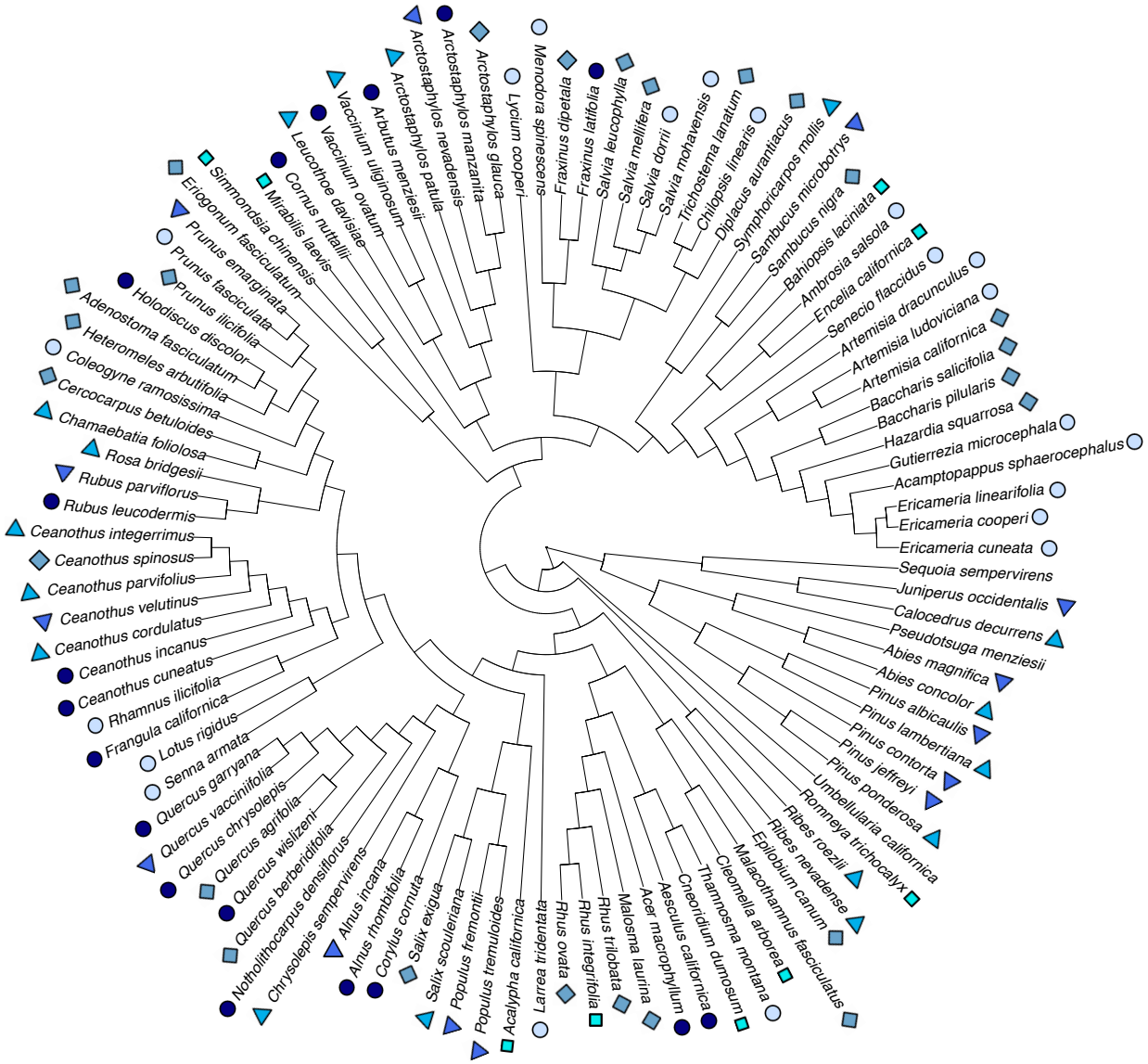
Arctostaphylos nevadensis
Arctostaphylos patula
Arctostaphylos manzanita
Arctostaphylos glauca
Arbutus menziesii
Vaccinium uliginosum
Vaccinium ovatum
Leucothoe davisiae
Cornus nuttallii
Mirabilis laevis
Simmondsia chinensis
Eriogonum fasciculatum
Prunus emarginata
Prunus fasciculata
Prunus ilicifolia
Holodiscus discolor
Adenostoma fasciculatum
Heteromeles arbutifolia
Coleogyne ramosissima
Cercocarpus betuloides
Chamaebatia foliolosa
Rosa bridgesii
Rubus parviflorus
Rubus leucodermis
Ceanothus integerrimus
Ceanothus spinosus
Ceanothus parvifolius
Ceanothus velutinus
Ceanothus cordulatus
Ceanothus incanus
Ceanothus cuneatus
Rhamnus ilicifolia
Frangula californica
Lotus rigidus
Senna armata
Quercus garryana
Quercus vacciniifolia
Quercus chrysolepis
Quercus agrifolia
Quercus wislizeni
Quercus berberidifolia
Notholithocarpus densiflorus
Chrysolepis sempervirens
Alnus incana
Alnus rhombifolia
Corylus cornuta
Salix exigua
Salix scouleriana
Populus fremontii
Populus tremuloides
Acalypha californica
Larrea tridentata
Rhus ovata
Rhus integrifolia
Rhus trilobata
Malosma laurina
Acer macrophyllum
Aesculus californica
Cneoridium dumosum
Thamnosma montana
Cleomella arborea
Malacothamnus fasciculatus
Epilobium canum
Ribes nevadense
Ribes roezlii
Romneya trichocalyx
Umbellularia californica
Pinus ponderosa
Pinus jeffreyi
Pinus contorta
Pinus lambertiana
Pinus albicaulis
Abies concolor
Abies magnifica
Pseudotsuga menziesii
Calocedrus decurrens
Juniperus occidentalis
Sequoia sempervirens
Ericameria cuneata
Ericameria cooperi
Ericameria linearifolia
Acamptopappus sphaerocephalus
Gutierrezia microcephala
Hazardia squarrosa
Baccharis pilularis
Baccharis salicifolia
Artemisia californica
Artemisia ludoviciana
Artemisia dracunculus
Senecio flaccidus
Encelia californica
Ambrosia salsola
Bahiopsis laciniata
Sambucus nigra
Sambucus microbotrys
Symphoricarpos mollis
Diplacus aurantiacus
Chilopsis linearis
Trichostema lanatum
Salvia mohavensis
Salvia dorrii
Salvia mellifera
Salvia leucophylla
Fraxinus latifolia
Fraxinus dipetala
Menodora spinescens
Lycium cooperi

Figure S5.1

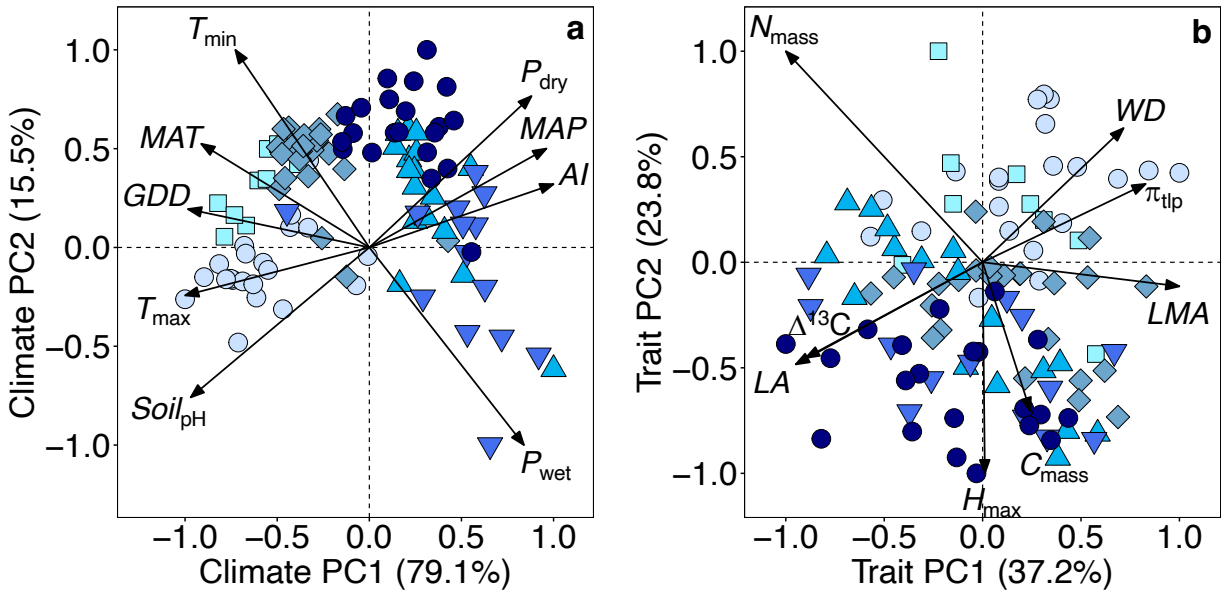
a
T_{min}
P_{dry}
MAT
MAP
AI
GDD
T_{max}
$Soil_{pH}$
P_{wet}
Climate PC2 (15.5%)
Climate PC1 (79.1%)
b
N_{mass}
WD
π_{tlp}
LMA
$\Delta^{13}C$
LA
C_{mass}
H_{max}
Trait PC2 (23.8%)
Trait PC1 (37.2%)

Figure S5.2

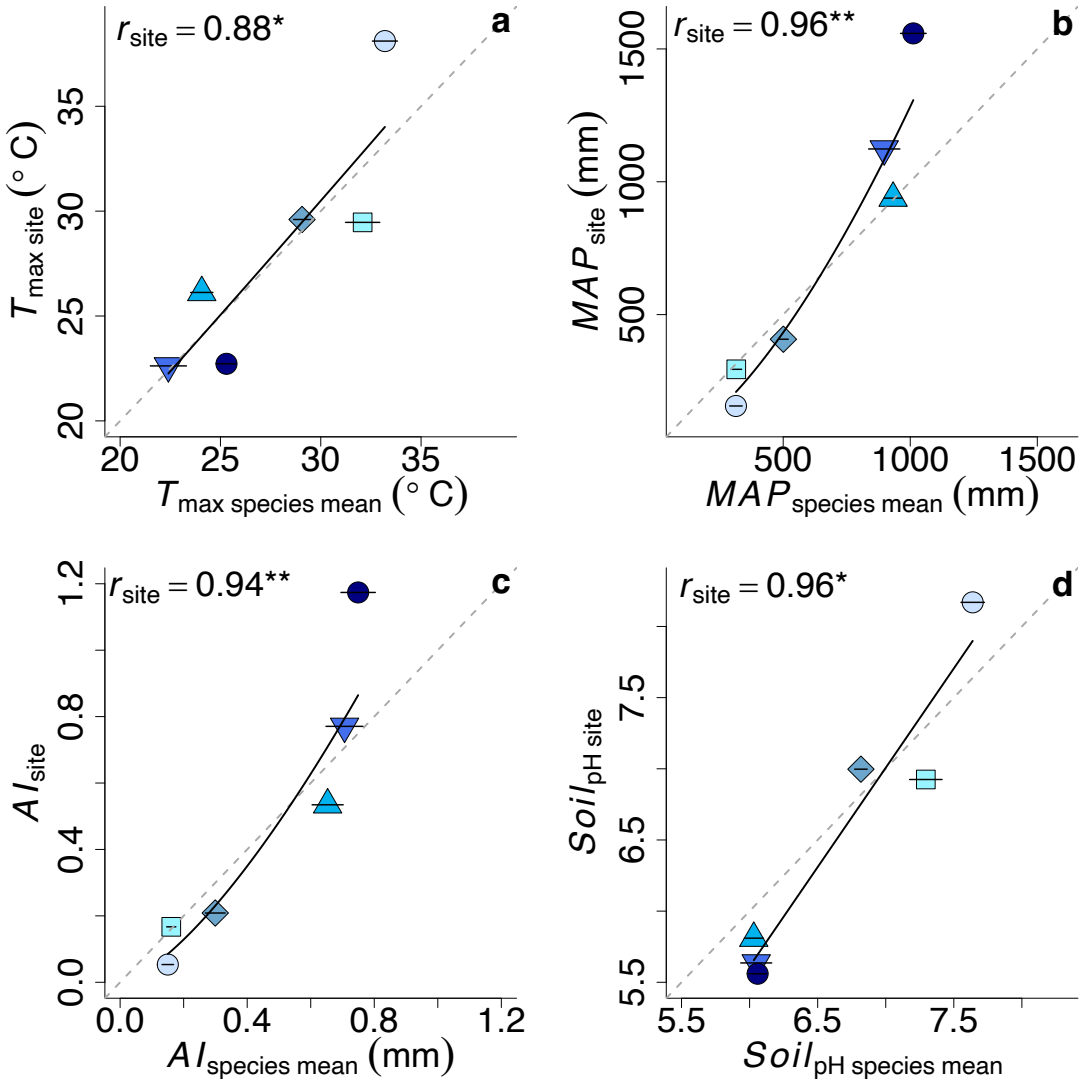
a
$r_{site} = 0.88^{*}$
$T_{max\ site}$ (° C)
$T_{max\ species\ mean}$ (° C)
20
25
30
35
b
$r_{site} = 0.96^{**}$
MAP_{site} (mm)
$MAP_{species\ mean}$ (mm)
500
1000
1500
c
$r_{site} = 0.94^{**}$
AI_{site}
$AI_{species\ mean}$ (mm)
0.0
0.4
0.8
1.2
d
$r_{site} = 0.96^{*}$
$Soil_{pH\ site}$
$Soil_{pH\ species\ mean}$
5.5
6.5
7.5

Figure S5.3

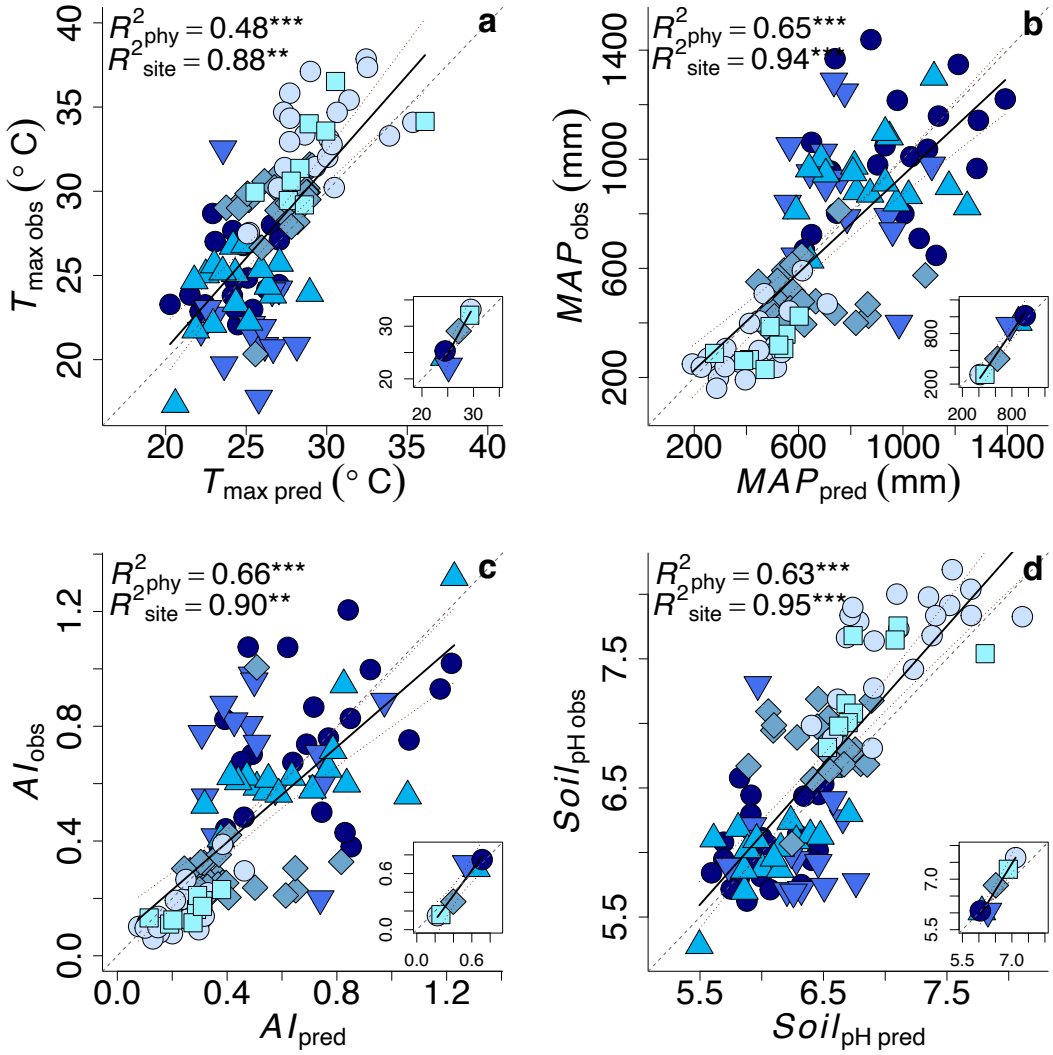
a
$R^2_{phy} = 0.48$***
$R^2_{site} = 0.88$**
$T_{max\ obs}$ (° C)
$T_{max\ pred}$ (° C)
b
$R^2_{phy} = 0.65$***
$R^2_{site} = 0.94$***
MAP_{obs} (mm)
MAP_{pred} (mm)
c
$R^2_{phy} = 0.66$***
$R^2_{site} = 0.90$**
AI_{obs}
AI_{pred}
d
$R^2_{phy} = 0.63$***
$R^2_{site} = 0.95$***
$Soil_{pH\ obs}$
$Soil_{pH\ pred}$

Figure S5.4

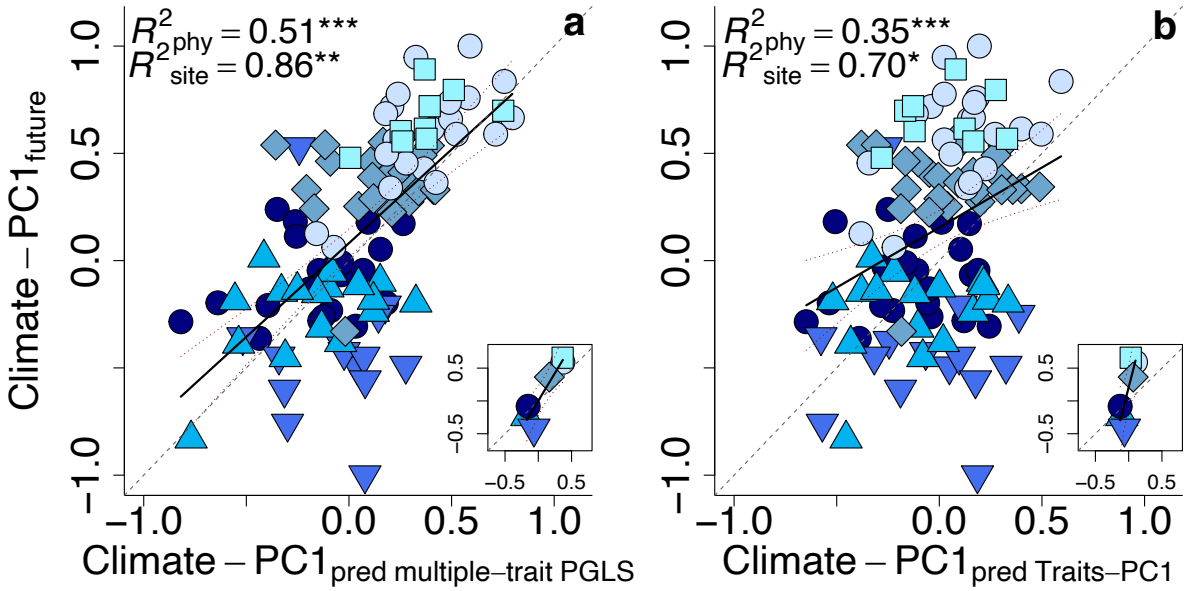
a
$R^2_{phy} = 0.51^{***}$
$R^2_{site} = 0.86^{**}$
Climate – PC1future
Climate – PC1pred multiple–trait PGLS
b
$R^2_{phy} = 0.35^{***}$
$R^2_{site} = 0.70^{*}$
Climate – PC1pred Traits–PC1

Figure S5.5

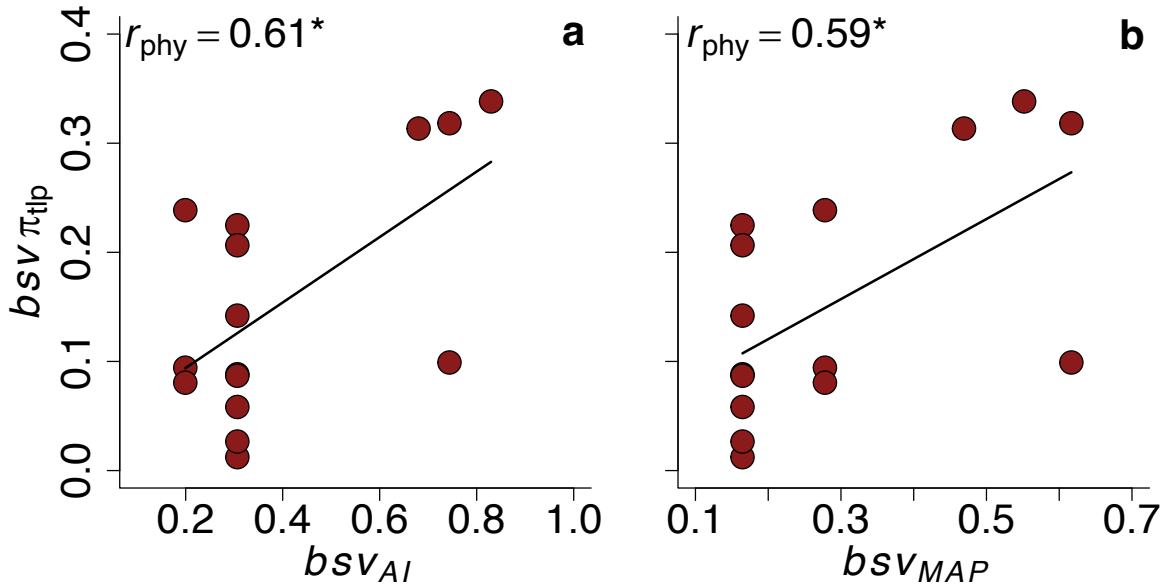
$r_{phy} = 0.61$*
a
$r_{phy} = 0.59$*
b
$bsv_{\pi tlp}$
0.0
0.1
0.2
0.3
0.4
0.2
0.4
0.6
0.8
1.0
bsv_{AI}
0.1
0.3
0.5
0.7
bsv_{MAP}

Figure S5.6

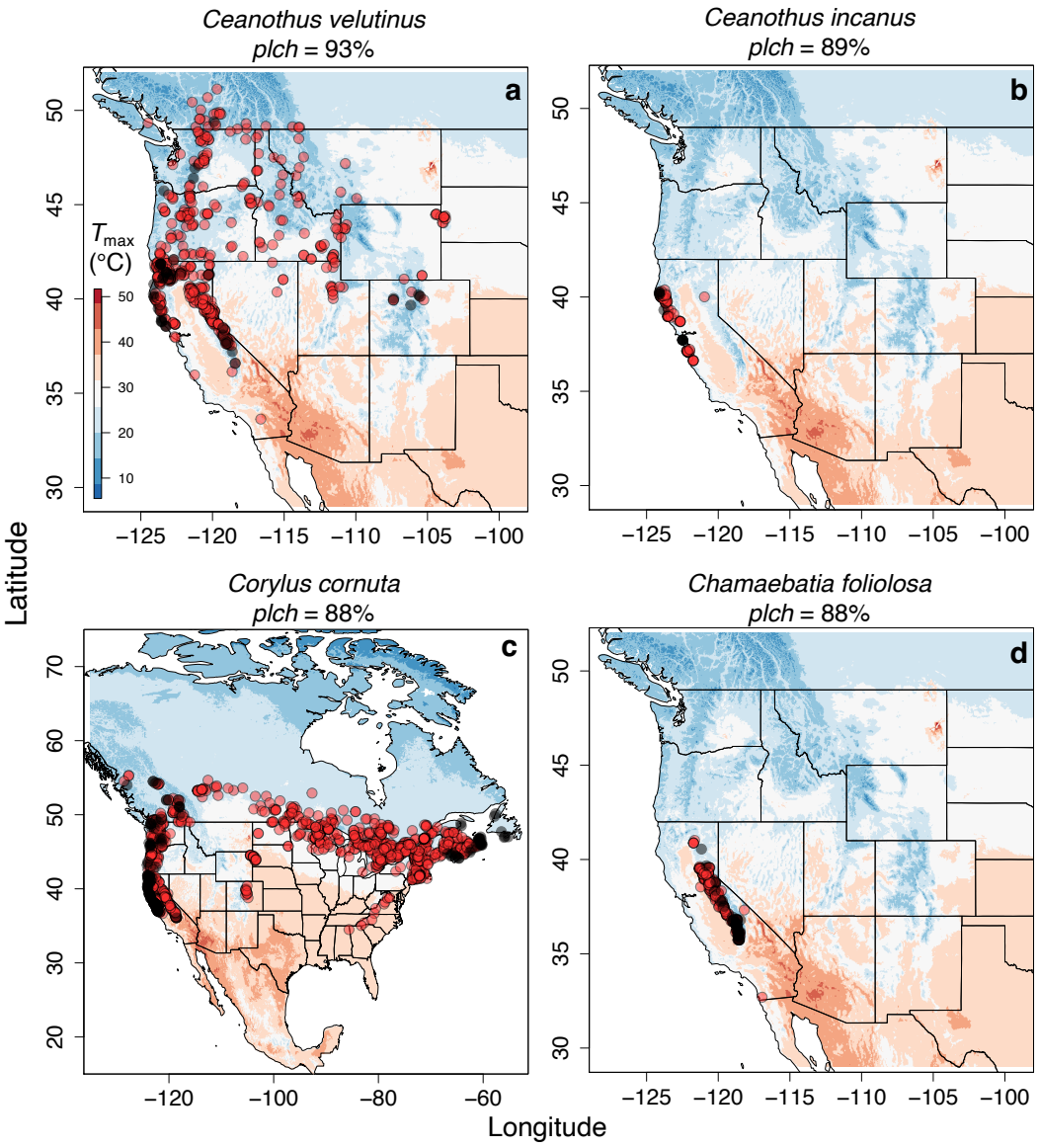
Ceanothus velutinus
plch = 93%
a
Ceanothus incanus
plch = 89%
b
Corylus cornuta
plch = 88%
c
Chamaebatia foliolosa
plch = 88%
d
Tmax (°C)
50
40
30
20
10
Latitude
Longitude

Figure S5.7

REFERENCES

Abdala-Roberts, L., Galmán, A., Petry, W.K., Covelo, F., de la Fuente, M., Glauser, G., *et al.* (2018). Interspecific variation in leaf functional and defensive traits in oak species and its underlying climatic drivers. *PLoS ONE*, 13, e0202548.

Adams, J.M., Green, W.A. & Zhang, Y. (2008). Leaf margins and temperature in the North American flora: Recalibrating the paleoclimatic thermometer. *Glob Planet Change*, 60, 523–534.

Adler, P.B., Salguero-Gomez, R., Compagnoni, A., Hsu, J.S., Ray-Mukherjee, J., Mbeau-Ache, C., *et al.* (2014). Functional traits explain variation in plant life history strategies. *Proc Natl Acad Sci USA*, 111, 740–745.

Albert, C.H., Thuiller, W., Yoccoz, N.G., Douzet, R., Aubert, S. & Lavorel, S. (2010a). A multi-trait approach reveals the structure and the relative importance of intra- vs. interspecific variability in plant traits. *Funct Ecol*, 24, 1192–1201.

Albert, C.H., Thuiller, W., Yoccoz, N.G., Soudant, A., Boucher, F., Saccone, P., *et al.* (2010b). Intraspecific functional variability: extent, structure and sources of variation. *J Ecol*, 98, 604–613.

Alfaro, M.E., Bolnick, D.I. & Wainwright, P.C. (2005). Evolutionary consequences of many-to-one mapping of jaw morphology to mechanics in labrid fishes. *Am Nat*, 165, E140–E154.

Anderegg, W.R.L., Trugman, A.T., Bowling, D.R., Salvucci, G. & Tuttle, S.E. (2019). Plant functional traits and climate influence drought intensification and land–atmosphere feedbacks. *Proc Natl Acad Sci USA*, 116, 14071–14076.

Anderson-Teixeira, K.J., Davies, S.J., Bennett, A.C., Gonzalez-Akre, E.B., Muller-Landau, H.C., Joseph Wright, S., *et al.* (2015). CTFS-ForestGEO: a worldwide network monitoring forests in an era of global change. *Glob Change Biol*, 21, 528–549.

Asner, G.P., Martin, R.E., Anderson, C.B., Kryston, K., Vaughn, N., Knapp, D.E., *et al.* (2017). Scale dependence of canopy trait distributions along a tropical forest elevation gradient. *New Phytol*, 214, 973–988.

Baldwin, B.G. (2014). Origins of plant diversity in the California Floristic Province. *Annu Rev Ecol Evol Syst*, 45, 347–369.

Baltzer, J.L., Davies, S.J., Bunyavejchewin, S. & Noor, N.S.M. (2008). The role of desiccation tolerance in determining tree species distributions along the Malay–Thai Peninsula. *Funct Ecol*, 22, 221–231.

Bartlett, M.K., Scoffoni, C., Ardy, R., Zhang, Y., Sun, S., Cao, K., *et al.* (2012a). Rapid determination of comparative drought tolerance traits: using an osmometer to predict turgor loss point. *Methods Ecol Evol*, 3, 880–888.

Bartlett, M.K., Scoffoni, C. & Sack, L. (2012b). The determinants of leaf turgor loss point and prediction of drought tolerance of species and biomes: a global meta-analysis. *Ecol Lett*, 15, 393–405.

Beerling, D.J. & Royer, D.L. (2002). Reading a CO2 signal from fossil stomata. *New Phytol*, 153, 387–397.

Blackman, C.J., Gleason, S.M., Chang, Y., Cook, A.M., Laws, C. & Westoby, M. (2014). Leaf hydraulic vulnerability to drought is linked to site water availability across a broad range of species and climates. *Ann Bot*, 114, 435–440.

van Bodegom, P.M., Douma, J.C. & Verheijen, L.M. (2014). A fully traits-based approach to modeling global vegetation distribution. *Proc Natl Acad Sci USA*, 111, 13733–13738.

Bounoua, L., Hall, F.G., Sellers, P.J., Kumar, A., Collatz, G.J., Tucker, C.J., *et al.* (2010). Quantifying the negative feedback of vegetation to greenhouse warming: a modeling approach. *Geophys Res Lett*, 37, L23701.

Boyce, C.K., Brodribb, T.J., Feild, T.S. & Zwieniecki, M.A. (2009). Angiosperm leaf vein evolution was physiologically and environmentally transformative. *Proc R Soc B*, 276, 1771–1776.

Boyce, C.K. & Lee, J.-E. (2010). An exceptional role for flowering plant physiology in the expansion of tropical rainforests and biodiversity. *Proc R Soc B*, 277, 3437–3443.

Brown, J.H. (1984). On the relationship between abundance and distribution of species. *Am Nat*, 124, 255–279.

Browne, L., Wright, J.W., Fitz-Gibbon, S., Gugger, P.F. & Sork, V.L. (2019). Adaptational lag to temperature in valley oak (*Quercus lobata*) can be mitigated by genome-informed assisted gene flow. *Proc Natl Acad Sci USA*, 116, 25179–25185.

Brum, F.T., Graham, C.H., Costa, G.C., Hedges, S.B., Penone, C., Radeloff, V.C., *et al.* (2017). Global priorities for conservation across multiple dimensions of mammalian diversity. *Proc Natl Acad Sci USA*, 114, 7641–7646.

Buckley, R.C., Corlett, R.T. & Grubb, P.J. (1980). Are the Xeromorphic Trees of Tropical Upper Montane Rain Forests Drought- Resistant? *Biotropica*, 12, 124–136.

Chamberlain, S., Ram, K., Mcglinn, D. & Barve, V. (2019). *rgbif: A programmatic interface to the Web Service methods provided by the Global Biodiversity Information Facility*.

Chave, J., Coomes, D., Jansen, S., Lewis, S.L., Swenson, N.G. & Zanne, A.E. (2009). Towards a worldwide wood economics spectrum. *Ecol Lett*, 12, 351–366.

Chevan, A. & Sutherland, M. (1991). Hierarchical partitioning. *Am Stat*, 45, 90–96.

Cochrane, A., Hoyle, G.L., Yates, C.J., Neeman, T. & Nicotra, A.B. (2016). Variation in plant functional traits across and within four species of Western Australian *Banksia* (Proteaceae) along a natural climate gradient: Variation in Plant Functional Traits. *Austral Ecology*, 41, 886–896.

Costa-Saura, J.M., Martínez-Vilalta, J., Trabucco, A., Spano, D. & Mereu, S. (2016). Specific leaf area and hydraulic traits explain niche segregation along an aridity gradient in Mediterranean woody species. *Perspect Plant Ecol Evol Syst*, 21, 23–30.

Crous, K.Y. (2019). Plant responses to climate warming: physiological adjustments and implications for plant functioning in a future, warmer world. *Am J Bot*, 106, 1049–1051.

Cunningham, S.A., Summerhayes, B. & Westoby, M. (1999). Evolutionary divergences in leaf structure and chemistry, comparing rainfall and soil nutrient gradients. *Ecol Monogr*, 69, 569–588.

De Boeck, H.J., Dreesen, F.E., Janssens, I.A. & Nijs, I. (2011). Whole-system responses of experimental plant communities to climate extremes imposed in different seasons. *New Phytol*, 189, 806–817.

DeAngelis, D.L. & Waterhouse, J.C. (1987). Equilibrium and nonequilibrium concepts in ecological models. *Ecol Monogr*, 57, 1–21.

Dobzhansky, T. (1950). Evolution in the tropics. *Am Sci*, 38, 208–221.

Drenovsky, R.E., Khasanova, A. & James, J.J. (2012). Trait convergence and plasticity among native and invasive species in resource-poor environments. *Am J Bot*, 99, 629–639.

Duan, H., Wu, J., Huang, G., Zhou, S., Liu, W., Liao, Y., *et al.* (2016). Individual and interactive effects of drought and heat on leaf physiology of seedlings in an economically important crop. *AoB PLANTS*, 9, plw090.

Eley, Y.L. & Hren, M.T. (2018). Reconstructing vapor pressure deficit from leaf wax lipid molecular distributions. *Sci Rep*, 8, 3967.

Evans, G.C. (1973). *The quantitative analysis of plant growth*. University of California Press, Berkeley and Los Angeles, California.

Falcão, H.M., Medeiros, C.D., Silva, B.L.R., Sampaio, E.V.S.B., Almeida-Cortez, J.S. & Santos, M.G. (2015). Phenotypic plasticity and ecophysiological strategies in a tropical dry forest chronosequence: a study case with *Poincianella pyramidalis*. *For Ecol Manag*.

Fang, Z., Li, D.-D., Jiao, F., Yao, J. & Du, H.-T. (2019). The Latitudinal Patterns of Leaf and Soil C:N:P Stoichiometry in the Loess Plateau of China. *Front Plant Sci*, 10, 85.

Farquhar, G.D., Ehleringer, J.R. & Hubick, K.T. (1989). Carbon isotope discrimination and photosynthesis. *Annu Rev Plant Physiol Plant Mol Biol*, 40, 503–537.

Farquhar, G.D. & Richards, R.A. (1984). Isotopic composition of plant carbon correlates with water-use efficiency of Wheat genotypes. *Aust J Plant Physiol*, 11, 539–552.

Felsenstein, J. (1985). Phylogenies and the comparative method. *Am Nat*, 125, 1–15.

Field, C. & Mooney, H.A. (1986). The photosynthesis-nitrogen relationships in wild plants. In: *On the economy of plant form and function*. Cambridge University Press, Cambridge, pp. 25–55.

Fletcher, L.R., Cui, H., Callahan, H., Scoffoni, C., John, G.P., Bartlett, M.K., *et al.* (2018). Evolution of leaf structure and drought tolerance in species of Californian *Ceanothus*. *Am J Bot*, 105, 1672–1687.

Foden, W.B., Butchart, S.H.M., Stuart, S.N., Vié, J.-C., Akçakaya, H.R., Angulo, A., *et al.* (2013). Identifying the world's most climate change vulnerable species: a systematic trait-based assessment of all birds, amphibians and corals. *PLoS ONE*, 8, e65427.

Freckleton, R.P., Harvey, P.H. & Pagel, M. (2002). Phylogenetic analysis and comparative data: a test and review of evidence. *Am Nat*, 160, 712–726.

Freyman, W.A. & Thornhill, A.H. (2016). *Matrix maker*.

Fyllas, N.M., Michelaki, C., Galanidis, A., Evangelou, E., Zaragoza-Castells, J., Dimitrakopoulos, P.G., *et al.* (2020). Functional trait variation among and within species and plant functional types in mountainous mediterranean forests. *Front Plant Sci*, 11, 212.

Geist, V. (1986). Bergmann's rule is invalid. *Can J Zool*, 65, 1035–1038.

Germain, S.J. & Lutz, J.A. (2020). Climate extremes may be more important than climate means when predicting species range shifts. *Clim Change*, 163, 579–598.

Gibson, A.C. (1998). Photosynthetic organs of desert plants. *BioScience*, 48, 911–920.

Gleason, S.M., Blackman, C.J., Chang, Y., Cook, A.M., Laws, C.A. & Westoby, M. (2016). Weak coordination among petiole, leaf, vein, and gas-exchange traits across Australian angiosperm species and its possible implications. *Ecol Evol*, 6, 267–278.

Gouy, M., Guindon, S. & Gascuel, O. (2010). SeaView version 4: a multiplatform graphical user interface for sequence alignment and phylogenetic tree building. *Mol Biol Evol*, 27, 221–224.

Greenwood, D.R. (2007). Fossil angiosperm leaves and climate: from Wolfe and Dilcher to Burnham and Wilf. *Cour Forsch-Inst Senckenberg*, 258, 95–108.

Griffin-Nolan, R.J., Ocheltree, T.W., Mueller, K.E., Blumenthal, D.M., Kray, J.A. & Knapp, A.K. (2019). Extending the osmometer method for assessing drought tolerance in herbaceous species. *Oecologia*, 189, 353–363.

Grubb, P.J. (1998). A reassessment of the strategies of plants which cope with shortages of resources. *Perspect Plant Ecol Evol Syst*, 1, 3–31.

Hacke, U.G., Sperry, J.S., Pockman, W.T., Davis, S.D. & McCulloh, K.A. (2001). Trends in wood density and structure are linked to prevention of xylem implosion by negative pressure. *Oecologia*, 126, 457–461.

Hamerlynck, E.P., Huxman, T.E., Loik, M.E. & Smith, S.D. (2000). Effects of extreme high temperature, drought and elevated CO2 on photosynthesis of the Mojave Desert evergreen shrub, *Larrea tridentata*. *Plant Ecol*, 148, 183–193.

Hanski, I., Kouki, J. & Halkka, A. (1993). Three explanations of the positive relationship between distribution and abundance of species. In: *Species diversity in ecological communities: historical and geographical perspectives*. The University of Chicago Press, Chicago, IL, USA, pp. 108–116.

Harmon, L.J. (2019). *Phylogenetic comparative methods*.

Harrison, S. (1997). How natural habitat patchiness affects the distribution of diversity in Californian serpentine chaparral. *Ecology*, 78, 1898–1906.

Hatté, C. & Schwartz, D. (2003). Reconstruction of paleoclimates by isotopic analysis: What can the fossil isotopic record tell us about the plant life of past environments? *Phytochem Rev*, 2, 163–177.

He, J.-S., Wang, Z., Wang, X., Schmid, B., Zuo, W., Zhou, M., *et al.* (2006). A test of the generality of leaf trait relationships on the Tibetan Plateau. *New Phytol*, 170, 835–848.

Hengl, T., Mendes de Jesus, J., Heuvelink, G.B.M., Ruiperez Gonzalez, M., Kilibarda, M., Blagotić, A., *et al.* (2017). SoilGrids250m: Global gridded soil information based on machine learning. *PLoS ONE*, 12, e0169748.

Hijmans, R.J., Cameron, S.E., Parra, J.L., Jones, P.G. & Jarvis, A. (2005). Very high resolution interpolated climate surfaces for global land areas. *Int J Climatol*, 25, 1965–1978.

Hijmans, R.J. & van Etten, J. (2012). *raster: Geographic analysis and modeling with raster data*. R. .

Hijmans, R.J., Phillips, S., Leathwick, J. & Elith, J. (2011). *Package 'dismo'*. R. .

Hu, J., Moore, D.J.P. & Monson, R.K. (2009). Weather and climate controls over the seasonal carbon isotope dynamics of sugars from subalpine forest trees. *Plant, Cell & Environment*.

Iglewicz, B. & Hoaglin, D.C. (1993). *How to detect and handle outliers*. ASQC basic references in quality control. ASQC Quality Press, Milwaukee, Wis.

Jacobs, B.F. (1999). Estimation of rainfall variables from leaf characters in tropical Africa. *Palaeogeogr Palaeoclimatol Palaeoecol*, 145, 231–250.

Jager, M.M., Richardson, S.J., Bellingham, P.J., Clearwater, M.J. & Laughlin, D.C. (2015). Soil fertility induces coordinated responses of multiple independent functional traits. *J Ecol*, 103, 374–385.

Jepson Flora Project. (2021). *Jepson eFlora*. *Jepson eFlora*. Available at: https://ucjeps.berkeley.edu/eflora/. Last accessed .

John, G.P., Scoffoni, C., Buckley, T.N., Villar, R., Poorter, H., Sack, L., *et al.* (2017). The anatomical and compositional basis of leaf mass per area. *Ecol Lett*, 20, 412–425.

Kaklamanos, G., Aprea, E. & Theodoridis, G. (2020). Mass spectrometry: principles and instrumentation. In: *Chemical Analysis of Food (Second Edition)* (ed. Pico, Y.). Academic Press, pp. 525–552.

Kattge, J., Díaz, S., Lavorel, S., Prentice, I.C., Leadley, P., Bönisch, G., *et al.* (2011). TRY - a global database of plant traits. *Glob Chang Biol*, 17, 2905–2935.

Kichenin, E., Wardle, D.A., Peltzer, D.A., Morse, C.W. & Freschet, G.T. (2013). Contrasting effects of plant inter- and intraspecific variation on community-level trait measures along an environmental gradient. *Funct Ecol*, 27, 1254–1261.

King, D.A., Davies, S.J. & Noor, N.S.Md. (2006). Growth and mortality are related to adult tree size in a Malaysian mixed dipterocarp forest. *For Ecol Manag*, 223, 152–158.

Koch, G.W., Sillett, S.C., Jennings, G.M. & Davis, S.D. (2004). The limits to tree height. *Nature*, 428, 851–854.

Kowalski, E.A. & Dilcher, D.L. (2003). Warmer paleotemperatures for terrestrial ecosystems. *Proc Natl Acad Sci USA*, 100, 167–170.

Kraft, N.J.B., Godoy, O. & Levine, J.M. (2015). Plant functional traits and the multidimensional nature of species coexistence. *Proc Natl Acad Sci USA*, 112, 797–802.

Kraft, N.J.B., Valencia, R. & Ackerly, D.D. (2008). Functional traits and niche-based tree community assembly in an Amazonian forest. *Science*, 322, 580–582.

Kürschner, W.M., van der Burgh, J., Visscher, H. & Dilcher, D.L. (1996). Oak leaves as biosensors of late Neogene and early Pleistocene paleoatmospheric CO2 concentrations. *Mar Micropaleontol*, 27, 299–312.

Lamont, B.B., Groom, P.K. & Cowling, R.M. (2002). High leaf mass per area of related species assemblages may reflect low rainfall and carbon isotope discrimination rather than low phosphorus and nitrogen concentrations. *Funct Ecol*, 16, 403–412.

Laughlin, D.C., Gremer, J.R., Adler, P.B., Mitchell, R.M. & Moore, M.M. (2020). The net effect of functional traits on fitness. *Trends Ecol Evol*, 35, 1037–1047.

Laughlin, D.C., Joshi, C., van Bodegom, P.M., Bastow, Z.A. & Fulé, P.Z. (2012). A predictive model of community assembly that incorporates intraspecific trait variation. *Ecol Lett*, 15, 1291–1299.

Lavorel, S. & Garnier, E. (2002). Predicting changes in community composition and ecosystem functioning from plant traits: revisiting the Holy Grail. *Funct Ecol*, 16, 545–556.

Lee-Yaw, J.A., Kharouba, H.M., Bontrager, M., Mahony, C., Csergő, A.M., Noreen, A.M.E., *et al.* (2016). A synthesis of transplant experiments and ecological niche models suggests that range limits are often niche limits. *Ecol Lett*, 19, 710–722.

Liang, X., Ye, Q., Liu, H. & Brodribb, T.J. (2021). Wood density predicts mortality threshold for diverse trees. *New Phytol*, 229, 3053–3057.

Liu, H., Gleason, S.M., Hao, G., Hua, L., He, P., Goldstein, G., *et al.* (2019). Hydraulic traits are coordinated with maximum plant height at the global scale. *Sci Adv*, 5, eaav1332.

Liu, H., Ye, Q., Gleason, S.M., He, P. & Yin, D. (2021). Weak tradeoff between xylem hydraulic efficiency and safety: climatic seasonality matters. *New Phytol*, 229, 1440–1452.

Lockheart, M.J., Van Bergen, P.F. & Evershed, R.P. (1997). Variations in the stable carbon isotope compositions of individual lipids from the leaves of modern angiosperms: implications for the study of higher land plant-derived sedimentary organic matter. *Org Geochem*, 26, 137–153.

Loiseau, N., Mouquet, N., Casajus, N., Grenié, M., Guéguen, M., Maitner, B., *et al.* (2020). Global distribution and conservation status of ecologically rare mammal and bird species. *Nat Commun*, 11, 5071.

Lynn, E., Chair, C., O'Daly, W., Keeley, F., Dsiwm, D., Woled, J., *et al.* (2015). *Perspectives and guidance for climate change*.

Ma, S., He, F., Tian, D., Zou, D., Yan, Z., Yang, Y., *et al.* (2018). Variations and determinants of carbon content in plants: a global synthesis. *Biogeosciences*, 15, 693–702.

Markesteijn, L., Iraipi, J., Bongers, F. & Poorter, L. (2010). Seasonal variation in soil and plant water potentials in a Bolivian tropical moist and dry forest. *J Trop Ecol*, 26, 497–508.

Marks, C.O. & Lechowicz, M.J. (2006). Alternative designs and the evolution of functional diversity. *Am Nat*, 167, 55–66.

McElwain, J.C. (1998). Do fossil plants signal palaeoatmospheric CO2 concentration in the geological past? *Phil Trans R Soc Lond B*, 353, 83–96.

McElwain, J.C. & Chaloner, W.G. (1995). Stomatal density and index of fossil plants track atmospheric carbon dioxide in the Paleozoic. *Ann Bot*, 76, 389–395.

Medeiros, C.D., Scoffoni, C., John, G.P., Bartlett, M.K., Inman-Narahari, F., Ostertag, R., *et al.* (2019). An extensive suite of functional traits distinguishes Hawaiian wet and dry forests and enables prediction of species vital rates. *Funct Ecol*, 33, 712–734.

Meiri, S. & Dayan, T. (2003). On the validity of Bergmann's rule: On the validity of Bergmann's rule. *Journal of Biogeography*, 30, 331–351.

Mitchell, N., Carlson, J.E. & Holsinger, K.E. (2018). Correlated evolution between climate and suites of traits along a fast-slow continuum in the radiation of *Protea*. *Ecol Evol*, 8, 1853–1866.

Moles, A.T., Perkins, S.E., Laffan, S.W., Flores-Moreno, H., Awasthy, M., Tindall, M.L., *et al.* (2014). Which is a better predictor of plant traits: temperature or precipitation? *J Veg Sci*, 25, 1167–1180.

Moles, A.T., Warton, D.I., Warman, L., Swenson, N.G., Laffan, S.W., Zanne, A.E., *et al.* (2009). Global patterns in plant height. *Journal of Ecology*, 97, 923–932.

NOAA Global Monitoring Laboratory. (2018). *NOAA Global Greenhouse Gas Reference Network*. *Earth System Research Laboratories*. Available at: https://www.esrl.noaa.gov/gmd/dv/data/. Last accessed .

Ohlemüller, R., Anderson, B.J., Araújo, M.B., Butchart, S.H.M., Kudrna, O., Ridgely, R.S., *et al.* (2008). The coincidence of climatic and species rarity: high risk to small-range species from climate change. *Biol Lett*, 4, 568–572.

Opedal, Ø.H., Armbruster, W.S. & Graae, B.J. (2015). Linking small-scale topography with microclimate, plant species diversity and intra-specific trait variation in an alpine landscape. *Plant Ecol Divers*, 8, 305–315.

Ordoñez, J.C., van Bodegom, P.M., Witte, J.-P.M., Wright, I.J., Reich, P.B. & Aerts, R. (2009). A global study of relationships between leaf traits, climate and soil measures of nutrient fertility. *Glob Ecol Biogeogr*, 18, 137–149.

Orme, D., Freckleton, R., Thomas, G., Petzoldt, T., Fritz, S., Isaac, N., *et al.* (2018). *caper: comparative analyses of phylogenetics and evolution in R*.

Paradis, E. & Schliep, K. (2019). ape 5.0: an environment for modern phylogenetics and evolutionary analyses in R. *Bioinformatics*, 35, 526–528.

Parsons, L.A., LeRoy, S., Overpeck, J.T., Bush, M., Cárdenes-Sandí, G.M. & Saleska, S. (2018). The threat of multi-year drought in Western Amazonia. *Water Resour Res*, 54, 5890–5904.

Peppe, D.J., Baumgartner, A., Flynn, A. & Blonder, B. (2018). Reconstructing Paleoclimate and Paleoecology Using Fossil Leaves. In: *Methods in Paleoecology* (eds. Croft, D.A., Su, D.F. & Simpson, S.W.). Springer International Publishing, Cham, pp. 289–317.

Peppe, D.J., Royer, D.L., Cariglino, B., Oliver, S.Y., Newman, S., Leight, E., *et al.* (2011). Sensitivity of leaf size and shape to climate: global patterns and paleoclimatic applications. *New Phytologist*, 190, 724–739.

Perez, T.M. & Feeley, K.J. (2020). Weak phylogenetic and climatic signals in plant heat tolerance. *J Biogeogr*, jbi.13984.

Pérez-Harguindeguy, N., Díaz, S., Garnier, E., Lavorel, S., Poorter, H., Jaureguiberry, P., *et al.* (2013). New handbook for standardised measurement of plant functional traits worldwide. *Aust J Bot*, 61.

Pérez-Ramos, I.M., Matías, L., Gómez-Aparicio, L. & Godoy, Ó. (2019). Functional traits and phenotypic plasticity modulate species coexistence across contrasting climatic conditions. *Nat Commun*, 10, 2555.

Peterson, A.T. (1999). Conservatism of ecological niches in evolutionary time. *Science*, 285, 1265–1267.

Peterson, A.T., Soberón, J., Pearson, R.G., Anderson, R.P., Martínez-Meyer, E., Nakamura, M., *et al.* (2012). *Ecological Niches and Geographic Distributions (MPB-49)*. Princeton University Press.

van der Plas, F., Schröder-Georgi, T., Weigelt, A., Barry, K., Meyer, S., Alzate, A., *et al.* (2020). Plant traits alone are poor predictors of ecosystem properties and long-term ecosystem functioning. *Nat Ecol Evol*, 4, 1602–1611.

Pollock, L.J., Morris, W.K. & Vesk, P.A. (2012). The role of functional traits in species distributions revealed through a hierarchical model. *Ecography*, 35, 716–725.

Poorter, L., Wright, S.J., Paz, H., Ackerly, D.D., Condit, R., Ibarra-Manríquez, G., *et al.* (2008). Are functional traits good predictors of demographic rates? Evidence from five neotropical forests. *Ecology*, 89, 1908–1920.

Preston, K.A., Cornwell, W.K. & DeNoyer, J.L. (2006). Wood density and vessel traits as distinct correlates of ecological strategy in 51 California coast range angiosperms. *New Phytol*, 170, 807–818.

R Core Team. (2018). *R: a language and environment for statistical computing*. R Foundation for Statistical Computing.

R Core Team. (2020). *R: a language and environment for statistical computing*. R Foundation for Statistical Computing.

Ramírez-Valiente, J.A., López, R., Hipp, A.L. & Aranda, I. (2020). Correlated evolution of morphology, gas exchange, growth rates and hydraulics as a response to precipitation and temperature regimes in oaks (*Quercus*). *New Phytol*, 227, 794–809.

Reich, P.B. (2014). The world-wide 'fast-slow' plant economics spectrum: a traits manifesto. *J Ecol*, 102, 275–301.

Reich, P.B. & Oleksyn, J. (2004). Global patterns of plant leaf N and P in relation to temperature and latitude. *Proc Natl Acad Sci USA*, 101, 11001–11006.

Reich, P.B., Wright, I.J., Cavender-Bares, J., Craine, J.M., Oleksyn, J., Westoby, M., *et al.* (2003). The evolution of plant functional variation: traits, spectra, and strategies. *Int J Plant Sci*, 164, S143–S164.

Riordan, E.C., Gillespie, T.W., Pitcher, L., Pincetl, S.S., Jenerette, G.D. & Pataki, D.E. (2015). Threats of future climate change and land use to vulnerable tree species native to Southern California. *Envir Conserv*, 42, 127–138.

Ritchie, J. & Dowlatabadi, H. (2017). Why do climate change scenarios return to coal? *Energy*, 140, 1276–1291.

de la Riva, E.G., Navarro, M.A., Montero, R.V., Oliva, F.G. & Oyama, K. (2019). The role of evapotranspiration on the foliar functional distribution of 28 *Quercus* species from Mexico and Spain. *Ecosistemas*, 28, 199–207.

de la Riva, E.G., Olmo, M., Poorter, H., Ubera, J.L. & Villar, R. (2016). Leaf Mass per Area (LMA) and Its Relationship with Leaf Structure and Anatomy in 34 Mediterranean Woody Species along a Water Availability Gradient. *PLoS ONE*, 11, e0148788.

Roth-Nebelsick, A., Oehm, C., Grein, M., Utescher, T., Kunzmann, L., Friedrich, J.-P., *et al.* (2014). Stomatal density and index data of *Platanus neptuni* leaf fossils and their evaluation as a CO2 proxy for the Oligocene. *Rev Palaeobot Palynol*, 206, 1–9.

Royer, D.L. (2001). Stomatal density and stomatal index as indicators of paleoatmospheric CO2 concentration. *Rev Palaeobot Palynol*, 114, 1–28.

Sack, L. & Buckley, T.N. (2020). Trait multi-functionality in plant stress response. *Integr Comp Biol*, 60, 98–112.

Sack, L., Scoffoni, C., McKown, A.D., Frole, K., Rawls, M., Havran, J.C., *et al.* (2012). Developmentally based scaling of leaf venation architecture explains global ecological patterns. *Nat Commun*, 3, 837.

Santiago, L.S., Kitajima, K., Wright, S.J. & Mulkey, S.S. (2004). Coordinated changes in photosynthesis, water relations and leaf nutritional traits of canopy trees along a precipitation gradient in lowland tropical forest. *Oecologia*, 139, 495–502.

Schimper, A.F.W. (1898). *Plant-geography upon a physiological basis*. Rev. and ed. Oxford: Clarendon Press.

Sexton, J.P., McIntyre, P.J., Angert, A.L. & Rice, K.J. (2009). Evolution and Ecology of Species Range Limits. *Annu. Rev. Ecol. Evol. Syst.*, 40, 415–436.

Sheth, S.N., Morueta-Holme, N. & Angert, A.L. (2020). Determinants of geographic range size in plants. *New Phytol*, 226, 650–665.

Shipley, B., Belluau, M., Kühn, I., Soudzilovskaia, N.A., Bahn, M., Penuelas, J., *et al.* (2017a). Predicting habitat affinities of plant species using commonly measured functional traits. *J Veg Sci*, 28, 1082–1095.

Shipley, B., Belluau, M., Kühn, I., Soudzilovskaia, N.A., Bahn, M., Penuelas, J., *et al.* (2017b). Predicting habitat affinities of plant species using commonly measured functional traits. *Journal of Vegetation Science*.

Siefert, A., Violle, C., Chalmandrier, L., Albert, C.H., Taudiere, A., Fajardo, A., *et al.* (2015). A global meta-analysis of the relative extent of intraspecific trait variation in plant communities. *Ecol Lett*, 18, 1406–1419.

Šímová, I., Violle, C., Svenning, J.-C., Kattge, J., Engemann, K., Sandel, B., *et al.* (2018). Spatial patterns and climate relationships of major plant traits in the New World differ between woody and herbaceous species. *J Biogeogr*, 45, 895–916.

Skelton, R.P., Dawson, T.E., Thompson, S.E., Shen, Y., Weitz, A.P. & Ackerly, D. (2018). Low vulnerability to xylem embolism in leaves and stems of north american oaks. *Plant Physiol*, 177, 1066–1077.

Smith, F.A., Betancourt, J.L. & Brown, J.H. (1995). Evolution of Body Size in the Woodrat over the Past 25,000 Years of Climate Change. *Science*, 270, 2012–2014.

Soberón, J. (2007). Grinnellian and Eltonian niches and geographic distributions of species. *Ecol Letters*, 10, 1115–1123.

Sokal, R.R. & Rohlf, F.J. (2012). Biometry: the principles and practice of statistics in biological research.

Stahl, U., Reu, B. & Wirth, C. (2014). Predicting species' range limits from functional traits for the tree flora of North America. *Proc Natl Acad Sci USA*, 111, 13739–13744.

Steinthorsdottir, M., Porter, A.S., Holohan, A., Kunzmann, L., Collinson, M. & McElwain, J.C. (2016). Fossil plant stomata indicate decreasing atmospheric CO2 prior to the Eocene–Oligocene boundary. *Clim Past*, 12, 439–454.

Stevens, G.C. (1989). The latitudinal gradient in geographical range: how so many species coexist in the tropics. *Am Nat*, 133, 240–256.

Stevens, P.F. (2019). *Angiosperm Phylogeny Website*. Available at: http://www.mobot.org/MOBOT/research/APweb/. Last accessed .

Swenson, N.G. & Weiser, M.D. (2010). Plant geography upon the basis of functional traits: an example from eastern North American trees. *Ecology*, 91, 2234–2241.

Taugourdeau, S., Villerd, J., Plantureux, S., Huguenin-Elie, O. & Amiaud, B. (2014). Filling the gap in functional trait databases: use of ecological hypotheses to replace missing data. *Ecol Evol*, 4, 944–958.

Thomas, D.S., Montagu, K.D. & Conroy, J.P. (2007). Temperature effects on wood anatomy, wood density, photosynthesis and biomass partitioning of Eucalyptus grandis seedlings. *Tree Physiol*, 27, 251–260.

Thorne, J.H., Choe, H., Boynton, R.M., Bjorkman, J., Albright, W., Nydick, K., *et al.* (2017). The impact of climate change uncertainty on California's vegetation and adaptation management. *Ecosphere*, 8, e02021.

Tyler, G. (1996). Soil chemical limitations to growth and development of Veronica officinalis L. and Carex pilulifera L. *Plant Soil*, 184, 281–289.

Uriarte, M., Lasky, J.R., Boukili, V.K., Chazdon, R.L. & Merow, C. (2016). A trait-mediated, neighbourhood approach to quantify climate impacts on successional dynamics of tropical rainforests. *Functional Ecology*.

Valladares, F., Wright, S.J., Lasso, E., Kitajima, K. & Pearcy, R.W. (2000). Plastic phenotypic response to light of 16 congeneric shrubs from a Panamanian rainforest. *Ecology*, 81, 1925–1936.

Van Der Burgh, J., Visscher, H., Dilcher, D.L. & Kurschner, W.M. (1993). Paleoatmospheric signatures in Neogene fossil leaves. *Science*, 260, 1788–1790.

Vesk, P.A., Morris, W.K., Neal, W.C., Mokany, K. & Pollock, L.J. (2020). Transferability of trait-based species distribution models. *Ecography*, 43, 1–14.

Violle, C., Bonis, A., Plantegenest, M., Cudennec, C., Damgaard, C., Marion, B., *et al.* (2011). Plant functional traits capture species richness variations along a flooding gradient. *Oikos*, 120, 389–398.

Violle, C., Borgy, B. & Choler, P. (2015). Trait databases: misuses and precautions. *J Veg Sci*, 26, 826–827.

Violle, C., Enquist, B.J., McGill, B.J., Jiang, L., Albert, C.H., Hulshof, C., *et al.* (2012). The return of the variance: intraspecific variability in community ecology. *Trends Ecol Evol*, 27, 244–252.

Violle, C., Navas, M.-L., Vile, D., Kazakou, E., Fortunel, C., Hummel, I., *et al.* (2007). Let the concept of trait be functional! *Oikos*, 116, 882–892.

van Vuuren, D.P., Edmonds, J., Kainuma, M., Riahi, K., Thomson, A., Hibbard, K., *et al.* (2011). The representative concentration pathways: an overview. *Climatic Change*, 109, 5–31.

Walsh, C. & Mac Nally, R. (2013). *hier.part: hierarchical partitioning*. R. .

Walter, H. (1979). *Vegetation of the Earth and Ecological Systems of the Geo-biosphere*. 2nd edn. Springer, New York.

Wang, H., Moore, M.J., Soltis, P.S., Bell, C.D., Brockington, S.F., Alexandre, R., *et al.* (2009). Rosid radiation and the rapid rise of angiosperm-dominated forests. *Proceedings of the National Academy of Sciences*, 106, 3853–3858.

Westoby, M. & Wright, I.J. (2006). Land-plant ecology on the basis of functional traits. *Trends Ecol Evol*, 21, 261–268.

Wiens, J.J. (2011). The niche, biogeography and species interactions. *Phil Trans R Soc B*, 366, 2336–2350.

Wolfe, J.A. (1978). A paleobotanical interpretation of tertiary climates in the Northern hemisphere: data from fossil plants make it possible to reconstruct tertiary climatic changes, which may be correlated with changes in the inclination of the earth's rotational axis. *Am Sci*, 66, 694–703.

Wolfe, J.A. (1995). Paleoclimatic estimates from tertiary leaf assemblages. *Annu Rev Earth Planet Sci*, 23, 119–142.

Wright, I.J., Dong, N., Maire, V., Prentice, I.C., Westoby, M., Díaz, S., *et al.* (2017). Global climatic drivers of leaf size. *Science*, 357, 917–921.

Wright, I.J., Reich, P.B., Cornelissen, J.H.C., Falster, D.S., Groom, P.K., Hikosaka, K., *et al.* (2005). Modulation of leaf economic traits and trait relationships by climate: Modulation of leaf traits by climate. *Glob Ecol Biogeogr*, 14, 411–421.

Wright, I.J., Reich, P.B. & Westoby, M. (2001). Strategy shifts in leaf physiology, structure and nutrient content between species of high- and low-rainfall and high- and low-nutrient habitats. *Funct Ecol*, 15, 423–434.

Wright, I.J., Reich, P.B., Westoby, M., Ackerly, D.D., Baruch, Z., Bongers, F., *et al.* (2004). The worldwide leaf economics spectrum. *Nature*, 428, 821–827.

Wright, I.J. & Westoby, M. (2002). Leaves at low versus high rainfall: coordination of structure, lifespan and physiology. *New Phytol*, 155, 403–416.

Yang, J., Spicer, R.A., Spicer, T.E.V., Arens, N.C., Jacques, F.M.B., Su, T., *et al.* (2015a). Leaf form-climate relationships on the global stage: an ensemble of characters: Global leaf form and climate relationships. *Glob Ecol Biogeogr*, 24, 1113–1125.

Yang, J., Spicer, R.A., Spicer, T.E.V. & Li, C.-S. (2011). 'CLAMP Online': a new web-based palaeoclimate tool and its application to the terrestrial Paleogene and Neogene of North America. *Palaeobio Palaeoenv*, 91, 163–183.

Yang, Y., Zhao, J., Zhao, P., Wang, H., Wang, B., Su, S., *et al.* (2019). Trait-Based Climate Change Predictions of Vegetation Sensitivity and Distribution in China. *Front Plant Sci*, 10, 908.

Yang, Y., Zhu, Q., Peng, C., Wang, H. & Chen, H. (2015b). From plant functional types to plant functional traits: a new paradigm in modelling global vegetation dynamics. *Prog Phys Geogr Earth Environ*, 39, 514–535.

Zhu, S.-D., Song, J.-J., Li, R.-H. & Ye, Q. (2013). Plant hydraulics and photosynthesis of 34 woody species from different successional stages of subtropical forests. *Plant Cell Environ*, 36, 879–891.

Zomer, R.J., Trabucco, A., Bossio, D.A. & Verchot, L.V. (2008). Climate change mitigation: A spatial analysis of global land suitability for clean development mechanism afforestation and reforestation. *Agric Ecosyst Environ*, 126, 67–80.

CHAPTER 6

VARIATION IN PLANT TRAIT NETWORKS ACROSS A GRADIENT OF ARIDITY IN CALIFORNIA

ABSTRACT

Plant ecological and physiological strategies are the result of multiple interactions among traits, and a deeper understanding of how traits involved in different axes of function are integrated can help us clarify how they contribute to species' ecological specializations, biogeographic distributions, and tolerance of climate change. We quantified an extensive set of 84 functional traits in 114 unique species sampled from six key ecosystems across a gradient of aridity in the California Floristic Province (CAFP), including desert, coastal sage scrub, chaparral, montane wet forest, mixed riparian woodland and mixed conifer-broad-leaf- forest sites. From trait measurements we built plant trait networks (PTNs) of each ecosystem and tested how their architecture (i.e., tightness and complexity) varied with climate. Functional traits and their pairwise relationships varied strongly across ecosystems. The PTNs became tighter (i.e., the traits that make up the network were more interconnected) and more complex (i.e., divided into more subcomponents or clusters) from high to low aridity environments, indicating that under more intense environmental pressure plant communities tend to become more functionally redundant. The use of PTNs enabled greater clarity and improved examination of the wider range of key plant traits.

INTRODUCTION

Functional traits are characteristics of an organism that influence their growth, reproduction and survival, and have long been used to predict species distributions, vital rates and responses to changing climates (Lavorel & Garnier 2002; Violle *et al.* 2007; Poorter *et al.* 2008; Adler *et al.* 2014; Stahl *et al.* 2014; Medeiros *et al.* 2019). Indeed, a great deal of research is focusing on how plant ecophysiological traits contribute to determining the composition of communities and range of climates in which species survive and compete (Engelbrecht et al., 2007). Yet, the power of these approaches has rarely been tested using large sets of physiological traits, or across California communities (Jacobsen et al., 2008; Sandel, Corbin & Krupa, 2011; Kraft et al., 2014). This is partially due to the difficulty of measuring more time-consuming physiological traits and the challenge of interpreting the complex inter-relationships within large sets of traits (Sack *et al.* 2013; Poorter *et al.* 2014; Messier *et al.* 2017; Belluau & Shipley 2018)

To deal with these issues, the field of functional ecology has dedicated much attention to the quest to find the "Holy Grail" traits, i.e., those that would efficiently summarize plant strategies alone or in combination with a few other traits, forming "axes" or "dimensions" of plant function (Grime 1979; Westoby 1998; Lavorel & Garnier 2002; Díaz *et al.* 2004, 2016; Wright *et al.* 2004; Funk *et al.* 2017). This approach is of practical use, providing approaches to estimate higher level processes, from species' tolerances to ecosystem function based on species' traits across a wide range of environments. Yet, that approach has been criticized as too reductionist, leading to low predictive value, and low resolution of true interactions among traits and important patterns of plant adaptation (He *et al.* 2020). Plant functional and ecological strategies are the result of multi-trait interactions, so shifts in a single trait could have cascading effects not only on traits that are directly related to it (and thus belonging to the same functional axis), but also traits that are

involved in mechanisms that are co-optimized with that target trait (He *et al.* 2020; Sack & Buckley 2020). Indeed, a deeper understanding of how traits involved in different axes of function (e.g., plant size, leaf and wood economics, photosynthesis, gas exchanges) are integrated can help us clarify how they contribute to species vital rates and tolerance to stresses across environments (Marks & Lechowicz 2006; Laughlin 2014; He *et al.* 2020).

One approach that has been used to integrate and help visualize the complexity of trait intercorrelations are the plant trait networks, henceforth PTNs (Messier *et al.* 2017; Flores-Moreno *et al.* 2019; Kleyer *et al.* 2019; He *et al.* 2020; Li *et al.* in review). Networks based on nodes and edges are based in graph theory and with applications in the fields of neuroscience, behavioral psychology and, more recently, elemental composition analyses (Salt *et al.* 2008; Markett *et al.* 2018; Tompson *et al.* 2018; Brooks *et al.* 2020; He *et al.* 2020). In these networks, traits are visualized as nodes and trait-trait relationships as connections of a network built from the statistical relationships between traits (Flores-Moreno *et al.* 2019; He *et al.* 2020). This approach also allows us to calculate parameters to describe the overall architecture of the network and the relative contribution of each trait to the overall topology (Flores-Moreno *et al.* 2019; He *et al.* 2020). Using these networks we can easily visualize traits that are involved in more than one function and can quantify how well connected a trait is relative to other traits in a network (Flores-Moreno *et al.* 2019; He *et al.* 2020). We are also able to identify functional clusters (or axes or dimensions) using a clustering algorithm, so in addition to clarifying the overall trait-trait coordination, we are able to identify the functional clusters that emerge from statistical relationships alone (Messier *et al.* 2017; Flores-Moreno *et al.* 2019; Kleyer *et al.* 2019; He *et al.* 2020).

This PTN approach thus has immense potential to resolve relationships among multiple traits; it allows not only the identification of trait clusters but also the relative importance of traits

within the network. We are also able to extract parameters that describe the overall architecture of the PTNs, which enables testing of relationships between entire PTNs and climate (Flores-Moreno *et al.* 2019; He *et al.* 2020). The key PTN parameters we are interested in are related to the tightness and complexity of the networks. The tightness describes how interdependent the traits are within the network; in tight PTNs the traits have a higher proportion of connections relative to all the possible connections. The complexity describes the overall functional structure of the network; networks with more clusters and clusters formed by less traits have a higher complexity. In other words, high complexity means lower functional redundancy (Flores-Moreno *et al.* 2019; He *et al.* 2020).

In this study, we quantified an extensive set of 84 functional traits in 114 unique species sampled from six key ecosystems across a gradient of aridity in the California Floristic Province (CAFP), including desert, coastal sage scrub, chaparral, montane wet forest, mixed riparian woodland and mixed conifer-broad-leaf- forest sites (Figs. 6.1 and 6.2a), representing around 70% of the land area of California (Thorne *et al.* 2017). From trait measurements we built PTNs of each ecosystem and tested how their architecture (i.e., tightness and complexity) varies with climate. Because these communities have highly contrasting characteristics, this approach will provide greater power for generalization, and the functional trait database will be of enormous value for researchers worldwide, particularly as data are currently lacking for the hydraulic behavior and vulnerability to drought for Californian species outside Chaparral systems (Jacobsen et al., 2008; Pivovaroff et al., 2016; Avila-Lovera, Zerpa & Santiago, 2017).

We expect that in the drier and/or hotter ecosystems, species will show constrained traits to improve water use efficiency and to tolerate water limitation, resulting in lower functional diversity and higher redundancy, and thus we hypothesized that PTNs will show lower

connectivity and modularity in high aridity environments. Conversely, we expect species from the wetter and/or cooler ecosystems to have a set of traits that would provide high photosynthetic and light capture efficiency to allow for fast growth, resulting in higher functional diversity. Thus, we hypothesize that PTNs will be more interconnected and complex in low aridity environments (Fig. 6.1).

METHODS

Study sites

We sampled branches from 683 trees from 114 unique species in six ecosystems representing the range of biogeographic conditions in the California and Desert floristic provinces (CAFP, DFP; Figs. 6.2a and S6.1). The species included in this study were taxonomically diverse, belonging to 37 botanical families, of which Asteraceae, Rosaceae, Rhamnaceae, Ericaceae and Pinaceae were the most representative. The CAFP is a plant-diverse and endemism rich biodiversity hotspot and has recently and currently experienced extreme drought with strong impacts on vegetation composition and diversity (Baldwin, 2014; McIntyre et al., 2015). The threats imposed by drought and fire lead to extreme urgency in understanding ecosystem function; according to Baldwin, 2014, the CAFP is the only North American province recognized by Conservation International as featuring amongst the 35 largest global biodiversity hotspots.

The six ecosystems included in this study were distributed across a gradient of climatic aridity, from dry to wet and warm to cool, and differed not only in their mean annual temperature and precipitation (*MAT* and *MAP*, respectively), but also their soil characteristics and plant community composition (Fig. S6.1). The desert site (Sweeney Granite Mountains Desert Research Center, part of the University of California Natural Reserve System, UCNRS) is characterized by

high *MAT* and low *MAP* concentrated in a few months a year. The soils are shallow, dry and basic. Most of the species are deciduous or semi-deciduous shrubs, such as *Ambrosia salsola*, *Ephedra californica* and *E. nevadensis*. The coastal sage scrub (located in the Centro de Investigación Científica y de Educación Superior de Ensenada and Cañon de Doña Petra, Baja California) is characterized by high *MAT* and low *MAP*. The soils are sandy, slightly acidic and very shallow. The landscape is dominated by sclerophyllous species, the majority being evergreen shrubs, such as *Adenostoma fasciculatum*, *Peritoma arborea* and *Simmondsia chinensis*. The chaparral site (Stunt Ranch Santa Monica Mountains Reserve, UCNRS) has a similar *MAT* to the coastal sage scrub coupled with higher *MAP* and deeper soils. The most common woody species are also evergreen shrubs, such as *Arctostaphylos glauca*, *Malosma laurina* and *Salvia leucophylla*. The montane wet forest (Yosemite Forest Dynamics Plot, part of the ForestGEO network (Anderson-Teixeira *et al.* 2015)) is characterized by a relatively high mean annual precipitation and mesic temperatures coupled with deep and acidic soils. The majority of the species are deciduous shrubs, such as *Rubus parviflorus* and *Vaccinium uliginosum*, but a significant proportion of the total biomass is accounted for by Gymnosperm species, such as *Abies concolor* and *Pinus lambertiana*. The mixed riparian woodland (Onion Creek, near the Chickering American River Reserve, UCNRS) is characterized by high *MAP* and low *MAT*. The soils are deep, acidic and have a high moisture content. The most common species were ecologically diverse; we sampled a similar number of evergreen shrubs, such as *Quercus vacciniifolia*, evergreen trees, such as *Pinus contorta*, deciduous shrubs, such as *Alnus incana*, and deciduous trees, such as *Populus tremuloides*. The sixth and last ecosystem is a mixed conifer-broadleaf forest (Angelo Coast Range Reserve, UCNRS), and is characterized by a combination of high *MAP*, *MAT*, deep, acidic and high moisture soils. The most abundant species were also very ecologically diverse; we sampled

evergreen shrubs, such as *Ceanothus incanus*, evergreen trees, such as *Umbellularia californica*, deciduous shrubs, such as *Cornus nuttalii*, and deciduous trees, such as *Quercus garryana*.

Sampling for leaf trait measurements

We sampled species among the most abundant at each site according to reserve managers and forest inventories. For 3-5 individuals of 19 to 28 species per site we collected a mature, sun-exposed and non-epicormic branch, with no signs of damage and herbivory using pole pruners or a slingshot. Branches were transported to the lab in dark plastic bags with moist paper and rehydrated overnight in a dark saturated atmosphere before harvesting current-year grown, fully expanded leaves for all subsequent analyses. For compound-leafed species, whole leaves were used.

Epidermal morphology

We measured epidermal traits on one leaf from each of three to five individuals per species. After rehydration, we fixed the leaves in FAA 48% ethanol: 10% formalin: 5% glacial acetic acid: 37% water. Epidermal measurements were obtained from microscopy images taken from nail varnish impressions of both leaf surfaces. From microscope images of the nail varnish peels we measured stomatal density (*d*), stomatal differentiation rate (or index; the number of stomata per numbers of stomata plus epidermal pavement cells, *i*), stomatal area (*s*), guard cell length and width (GC_l, GC_w), inner and outer stomatal pore length (SP_{il}, SP_{ol}), epidermal pavement cell area (*e*) and trichome density (*t*). We then calculated the maximum theoretical stomatal conductance g_{max} (Franks & Farquhar 2007; Sack & Buckley 2016) as: $g_{\max} = \frac{bmds}{s^{0.5}}$, in which *b* is a biophysical constant given as $b = \frac{D}{v}$, where *D* represents the diffusivity of CO_2 and water in air $m^2\ s^{-1}$ and *v* is

the molar volume of air m^3 mol^{-1}, so $b = 0.00126$; m is a morphological constant based on scaling factors representing the proportionality of stomatal dimensions $m = \frac{\pi c^2}{j^{0.5}4hj+\pi}$, with c, h, and j treated as constants for the estimation of g_{max} c, h and $j = 0.5$; d is stomatal density, and s is stomatal size (Franks & Farquhar 2007; Franks *et al.* 2009a; McElwain *et al.* 2016). To determine leaf-level epidermal trait values, for cell dimensions, we calculated an average value as the arithmetic mean of the abaxial and adaxial surfaces. For leaf-level cell densities and g_{max} we calculated a total trait value as the sum of abaxial and adaxial values. All images were analyzed and anatomical traits were measured using the software ImageJ (http://imagej.nih.gov/ij/).

Leaf economics and structure

Leaf saturated mass was measured using an analytical balance (0.01 mg; XS205; Mettler-Toledo, OH, USA) and leaf thickness (*LT*) using digital calipers (0.01 mm; Fowler, Chicago, IL, USA). The leaf area (*LA*) was measured using a flatbed scanner and analyzed using the software ImageJ (http://imagej.nih.gov/ij/). After scanning, leaves were oven-dried at 70º for 72 h and their dry mass and area were measured again. Leaf mass per area (*LMA*) was calculated as lamina dry mass divided by saturated area; leaf density (*LD*) as *LMA* divided by *LT*; saturated water content (*SWC*) as (saturated mass minus dry mass) divided by dry mass; saturated water mass per area (*SWMA*) as the (saturated mass minus dry mass) divided by saturated area; leaf dry matter content (*LDMC*) as dry mass divided by saturated mass; percentage loss in area after drying (PLA_{dry}) as the percent decline in area from saturated to dry leaves (Witkowski & Lamont 1991; Ogburn & Edwards 2012; Pérez-Harguindeguy *et al.* 2013). The petiole cross-sectional area (*PA*) was calculated as the area of an ellipse: $PA = \left[\pi \times \left(\frac{d_x}{2}\right)\right] \times \left[\pi \times \left(\frac{d_y}{2}\right)\right] \times l$, where d_x is the mean diameter at the x-axis of the petiole, d_y is the mean diameter at the y-axis of the petiole and l is the petiole length. The

petiole to leaf area ratio (*PA*:*LA*) was calculated as the petiole area divided by the leaf area and the petiole mass per area (*PMA*) was calculated as petiole dry mass divided by saturated area.

Wood economics and structure

We measured wood density (*WD*) from one 5 cm-branch segment of each of the studied individuals after bark removal by water-displacement (Pérez-Harguindeguy *et al.* 2013). Branch segments were immersed in water and the mass of the displaced water was recorded; branch segments were then oven-dried at 70º for 120 h and their dry mass was measured. *WD* was calculated as the segment dry mass divided by the mass of displaced water.

Leaf composition

The concentrations of four macronutrients (potassium, calcium, phosphorus and magnesium) and 12 micronutrients (iron, boron, manganese, sodium, zinc, copper, molybdenum, cobalt, aluminum, arsenic, cadmium, rubidium and strontium) were determined from ground oven-dried leaves using high throughput elemental profiling (ionomics; (Salt *et al.* 2008)) by the USDA-ARS/Danforth Center Ionomics facility at the Donald Danforth Plant Science Center. Elemental carbon and nitrogen concentrations and their isotope ratios ($\delta^{13}C$ and $\delta^{15}N$) were measured by the University of California, Berkeley, Center for Stable Isotope Biogeochemistry, by continuous flow dual isotope analysis using a CHNOS Elemental Analyzer interfaced to an IsoPrime100 mass spectrometer (Fry *et al.* 1996; Pérez-Harguindeguy *et al.* 2013). The concentrations of nutrients were converted from mass basis into area-basis by multiplying by *LMA*. The carbon isotope discrimination ($\Delta^{13}C$; in parts per thousand, ‰) was calculated following (Farquhar & Richards 1984). The chlorophyll concentration per area, Chl_{area}, was measured using a SPAD meter, which

provides a correlate of total chlorophyll *a* + *b* concentration per area in SPAD units ((Monje & Bugbee 1992); SPAD-502, Konica Minolta, Japan) and the chlorophyll concentration per mass was determined by dividing by *LMA* (Chl_{mass}). From nutrient measurements we calculated the ratio of carbon to nitrogen (*C*:*N*), nitrogen to carbon (*N*:*C*) and nitrogen to phosphorus (*N*:*P*).

We measured the turgor loss point (π_{tlp}) in two leaves per studied individual. We used a vapor-pressure osmometer (Vapro 5520, Wescor, US) to obtain the osmotic concentration of the leaves and used calibration equations to estimate π_{tlp} (Bartlett *et al.* 2012).

Estimated photosynthetic traits

We estimated maximum rate of carboxylation per mass ($Vc_{max\ mass}$) and electron transport rate ($J_{max\ mass}$) from leaf N and P concentrations per mass (Domingues *et al.* 2010; Medeiros *et al.* 2019; Maréchaux *et al.* 2020). The ratio between intercellular CO_2 concentration (c_i) and ambient CO_2 concentration (c_a) was estimated from $\Delta^{13}C$ (Farquhar *et al.* 1982; Franks *et al.* 2014). Estimates of leaf lifetime integrated CO_2 assimilation rate (A_{mass}) and stomatal conductance to CO_2 (g_{cleaf}) were derived from $Vc_{max\ mass}$, $J_{max\ mass}$ and isotope composition data using the Farquhar, von Caemmerer and Berry model (Franks *et al.* 2009a). To convert $Vc_{max\ mass}$, $J_{max\ mass}$, and A_{mass} to area-basis, we multiplied the trait values by *LMA*. We also calculated the ratio between g_{cleaf} and g_{max}, an index of the degree of stomatal opening relative to their anatomical maximum (McElwain *et al.* 2016), and the ratio between g_{max} and N_{area}, which is negatively related to water retention for a given investment in photosynthetic machinery (Wright *et al.* 2001).

Plant size and chromosome number

Species maximum height (H_{max}), seed dry mass values (SM) and the 2c number of chromosomes were compiled from the Ecological Flora of California database, part of the Jepson Flora Project (https://ucjeps.berkeley.edu/efc/). When not available, the H_{max} was recorded as the maximum value reported on the Jepson eFlora website (https://ucjeps.berkeley.edu/eflora/).

Climate of field sites

From open-access raster layers, we extracted a total of 30 environmental parameters relating to air temperature (WorldClim, CRU; (Hijmans *et al.* 2005)), precipitation (WorldClim; (Hijmans *et al.* 2005)), aridity (CGIAR-CSI, NCAR-UCAR; (Zomer *et al.* 2008)) and soil characteristics (ISRIC Soilgrids; (Hengl *et al.* 2017) from a 25-ha area around the centroid of each sampling location (see Table S1 for description, download links and references for each variable). Due to their coarse resolution, these environmental variables are effective in characterizing large scale patterns but do not reflect differences potential differences in microclimate within ecosystem, i.e., temperature, water and nutrient availability, irradiance and soil composition (Perez & Feeley 2020; Baird *et al.* 2021).

Plant trait networks

To build the plant trait networks (PTNs), functional traits were considered nodes and trait correlations were considered edges. We built trait-trait correlation matrices for each ecosystem from species mean values using ordinary least squares regression (OLS). The strength of the trait-trait relationships was described using correlation coefficients (r) and they were considered as edges if the $p < 0.05$. The matrices were then converted into adjacency matrices $A = [a_{i,j}]$, where

we assigned 1 to relationships that were above the significance threshold and 0 to those below the threshold ($a_{i,j} \in [0,1]$). These networks were visualized and all network parameters were calculated using functions available in the '*igraph'* package (version 1.2.6) in the R Software (R Core Team 2020).

We calculated five parameters to describe the overall topology of the PTNs, three that quantify the "tightness" of the PTN, the edge density (*ED*), the diameter (*D*) and the average path length (*AL*); and two parameters to quantify the "complexity" of the PTN, the average clustering coefficient (*AC*) and the modularity (*Q*) (He *et al.* 2020). The *ED* is the proportion of connections out of all possible connections, and thus, larger values of *ED* reflect a network that is more interconnected. *AL* is the network-averaged shortest distance between traits, and thus, high values reflect a high independence of traits. High values of *D*, which reflect high maximum shortest distances between traits in the network, also reflect a high independence of traits. *AC* is the network-averaged clustering coefficient of all traits, and thus, high values reflect a high division of the network into subcomponents. *Q* is the difference between the within-cluster connections and a null model where connections among traits are randomly distributed, and thus, high values reflect a tendency of the network to form clusters.

We also calculated parameters to describe the importance of traits within PTNs, two that quantify the "connectedness" of each trait, the degree (*K*) and closeness (*C*); and two that quantify the "centrality" of each trait, the betweenness (*B*), and the clustering coefficient (*CC*). For each trait, *K* is defined as the number of connections for a given trait, representing its centrality within the network. *C* represents the mean shortest path between a focal trait and all other traits in the network, so traits with high *C* values are traits closely connected to many other traits. *B* is a measure of the number of shortest paths going through a focal trait, and thus high values of *B*

reflect a trait that is a good mediator, intermediating other trait relationships. *CC* is the proportion of connections between a focal trait and its neighboring traits out of all possible connections, and thus traits with high *CC* are those at the center of different trait clusters. Traits with the highest *K* were considered "hub traits" and traits with highest *B* were considered "mediator traits".

Statistical analyses

All statistical analyses were performed and plots created using R software (version 4.0.2 (R Core Team 2020)) and packages available from the CRAN platform. We performed nested ANOVAs to test for differences in functional traits among ecosystems and species using the *aov* function, with functional traits coded as the dependent variable, ecosystem as the independent variable and species nested within ecosystem (Sokal & Rohlf 2012; R Core Team 2020).

To test the relationships between the PTN parameters (*ED*, *AL*, *D*, *AC* and *Q*) and climate of the six ecosystems, we performed ordinary least squares regression analyses (OLS) using the *lm* function from the '*stats'* package. We also tested the relationship between the number of species from each site used to build the PTNs and the network parameters. Analyses were performed in untransformed and log-transformed data, to test for either approximately linear or non-linear (i.e., approximate power-law) relationships, respectively.

RESULTS

Variation in traits across ecosystems

We found strong variation in functional traits across species and ecosystems. Of the 83 measured traits, 78 differed across species and 69 across ecosystems. Most of the variation in traits was explained by differences across species, 64%, with intraspecific and ecosystems explaining 18%

each (Table S2). Overall, in the more arid ecosystems (desert, coastal sage scrub and chaparral), species had smaller, denser and thicker leaves with higher trichome density, higher saturated water mass per area and smaller reduction in leaf area when dry, denser wood and more negative turgor loss points than species from the more mesic ecosystems (montane wet forest, mixed riparian woodland and mixed conifer-broadleaf forest) (Table S6.2). Species from more arid ecosystems also had higher leaf concentrations of area-based nutrients and lower concentrations of mass-based nutrients, such as carbon, nitrogen, potassium and phosphorus, high carbon to nitrogen ratio, high nitrogen isotope concentration and low carbon isotope discrimination rates. The photosynthetic traits followed the same pattern as the leaf nutrient concentrations; the area-based rates were higher in species sampled from the more arid ecosystems, but the mass-based rates were higher in species sampled from the less arid ecosystems (Table S6.2).

Variation in plant trait networks across ecosystems

The architecture and properties of the plant trait networks varied significantly across ecosystems. The PTNs of the drier sites were "looser" and less complex than the PTNs built from species sampled in the more mesic sites (Fig. 6.2b). The traits of the drier sites PTNs were overall less interconnected and were grouped into a smaller number of clusters. That is, these networks had lower values of *ED* and *AC* and higher values of *AL*, *D* and *Q* than the networks of the more mesic sites (Table 6.1).

From the PTNs we were also able to identify traits that are central to the functioning of the networks, such as traits with high connectivity, *K* (hub traits), and traits with high betweenness, *B* (mediator traits). Across the PTNs from the six ecosystems, C_{area}, *LMA*, $Vc_{\text{max area}}$, Chl_{mass} and *N*:*C* can be considered hub traits, with an average of 39.667, 39.333, 35.167, 32.333 and 30.667

connections each. The traits with highest values of *B* were the K_{mass}, C_{area}, *LMA*, *LD* and *LDMC* with average *B* of 113.752, 106.956, 100.024, 99.255 and 98.208 respectively (Fig. 6.3).

Relationship between PTN architecture and climate

The tightness and complexity of the PTNs varied with climate. The *ED* decreased with the mean annual temperature, *MAT* (r = -0.83; p<0.05; Table S6.5 and Fig. 6.4a) and increased with the $soil_{depth}$ (r = 0.84; p<0.05; Table S6.5 and Fig. 6.4d). The *AL* decreased with $soil_{depth}$ (r = -0.84; p<0.05; Table S6.5 and Fig. 6.4h) while *AC* decreased with *MAT* (r = -0.87; p<0.05; Table S6.5 and Fig. 6.4i). The *Q* was the network parameter most strongly correlated with climate; *Q* increased with *MAT* (r = 0.90; p<0.05; Table S6.5 and Fig. 6.4m) and decreased with increasing mean annual precipitation, *MAP*, aridity index, *AI*, and $soil_{depth}$ (r ranging from -0.90 to -0.81; p<0.05; Table S6.5 and Figs. 6.4n-p). Four of the five PTN parameters were independent of the number of species included in the correlative matrix; *AC*, however, decreased with the number of species (r = -0.82; p<0.05; Table S6.5 and Fig. S6.3)

DISCUSSION

Functional traits and their correlative relationships varied strongly across ecosystems (Tables S6.2-S6.3). In this study, we found that both the number and the direction of trait-trait relationships shifted across ecosystems in response to the climatic aridity, and that mean annual temperature and the soil depth were strongly associated with these shifts in trait intercorrelations (Lusk & Warton 2007; Medeiros *et al.* 2019). These results also indicate that different combinations of traits are selected for in different environments. For example, high photosynthetic rate is an advantageous trait for plants growing in resource-rich environments, since it allows them to grow

taller faster and thus outcompete co-occurring plants (Farquhar *et al.* 1989; Franks *et al.* 2009b). However, under water and nutrient limitation, the maintenance of fast photosynthetic rates could increase the risk of embolism and lead to hydraulic failure (Wong *et al.* 1979; Bartlett *et al.* 2016; Martin-StPaul *et al.* 2017; Henry *et al.* 2019).

This environmental "context-dependence" of the network of trait-trait relationships is likely a co-product of the multifunctionality of traits (Medeiros *et al.* 2019; Sack & Buckley 2020). Since each trait may be involved in multiple functions and/or the function of a given trait may be influenced indirectly by traits to which they are not mechanistically related, across environments different conformations of the trait-trait connections might be more advantageous and thus selected for (Sack & Buckley 2020). In this study, the PTNs became tighter (i.e., the traits that make up the network were more interconnected) and more complex (i.e., divided into more subcomponents or clusters) from high to low aridity environments. This pattern indicates that under more intense environmental pressure the plant communities tend to become more functionally redundant, likely because a smaller number of alternative trait combinations would be advantageous for survival and competition under the more restrictive growing conditions (He *et al.* 2020; Li *et al.* in review). Functional redundancy is associated with higher stability, given that it may help maintain ecosystem processes in the face of disturbances, such as extreme climatic events (Cowling *et al.* 1994; Pillar *et al.* 2013; Biggs *et al.* 2020). The less arid and more resource-rich ecosystems are able to support a higher number of organisms, due to the larger amount of water and soil nutrients (Harrison *et al.* 2020). In these environments, plant species that become abundant tend to be highly specialized to use specific resources, thus in these sites we find PTN that reflect higher functional diversity (Spasojevic *et al.* 2014; Harrison *et al.* 2020). This PTN findings translated well into the species' phenological strategies; in the more arid ecosystems we found dominance of one or two

functional types, while in the less arid ecosystems more combinations were abundant, without a clear dominating strategy (Spasojevic *et al.* 2014).

Our results of the analyses of the relationships between PTNs and the climate of the sampling location further corroborate our interpretation of the network-level architecture parameters above (Table 6.1). The topology of the PTNs shifted with the climate of sampling locations (Flores-Moreno *et al.* 2019; He *et al.* 2020; Li *et al.* in review). *MAT* and $soil_{depth}$ were the climate variables more strongly correlated with the topology of PTNs. In the sampling locations with shallower soils and warmer temperatures the PTNs were looser, with lower edge density and clustering coefficient and higher modularity (Fig. 6.4). The water availability (through *MAP* and *AI*) did not significantly influence the tightness of PTNs, but were negatively related to the modularity. The absence of a relationship between PTN tightness and water availability might be a result of the optimization of drought adaptation in species native across CAFP (Bohnert *et al.* 1995; Harrison *et al.* 2020). The $soil_{depth}$ was the second environmental variable most correlated with PTN topology; possibly due to deeper soils being older and richer in nutrients, organic matter and water (Abd-Elmabod *et al.* 2017; Rajakaruna & Boyd 2019). Combined, *MAT*, *MAP* and $soil_{depth}$ were strong climatic drivers of PTN topology.

The PTNs allowed us to identify the traits with larger connectiveness, *K*, and betweenness, *B*, in each of the six ecosystems. These traits are of special importance for the functional stability of the ecosystem due to the dependence of other trait on these traits (Fig. 6.3) (Flores-Moreno *et al.* 2019; He *et al.* 2020; Li *et al.* in review). The traits that emerged as hub and mediator traits were traits typically associated with leaf structural support, photosynthesis and fluxes, so their relative importance within the network was not surprising. Although these traits are important hubs they might also be connected to more traits for different reasons. For example, *LMA*, the second

most connected traits across all six ecosystems, is mechanistically involved in many aspects of physiology, such as photosynthesis and tolerance to drought (Pérez-Harguindeguy *et al.* 2013; Sack *et al.* 2013; de la Riva *et al.* 2016; John *et al.* 2017; Sack & Buckley 2020). It is also a component of many other traits since it mediates the conversion of trait values from mass to area-based (Wright *et al.* 2004). It is also noteworthy that since traits are grouped according to their statistical relationships, traits that belong to functional modules with more traits will likely have more hub or mediator traits, but those are highly coordinated and at times functionally redundant (Li *et al.* in review).

The use of PTNs enabled greater clarity and improved examination of the wider range of key plant traits. Our results reinforce the idea that traits have limited meaning when alone. Using a wide range of traits provides insight into the modular nature of trait function and overall physiological and ecological strategies of different plant species and ecosystems. Ultimately, PTNs provide a promising avenue to explore the adaptive strategies of plants and help with the identification of important candidate traits to include in models of future species distributions and ecosystem resilience in response to changes in climate.

ACKNOWLEDGEMENTS

We acknowledge the indigenous peoples that stewarded the land and ecosystems studied in this project over millenia, including the Newe/ Kawaiisu/ Chemehuevi (Granites), Kizh/ Tongva/ Chumash/ Micqanaqa'n (Stunt Ranch and UCLA), Me-Wuk (Yosemite), Washoe/ Nisenan (Onion Creek) and Cahto (Angelo) peoples. We thank the University of California Natural Reserve System (UCNRS), Yosemite Field Station and ForestGEO for maintaining the field sites and providing support for the field campaigns. We thank Jim Andre and Sarah Germain for assistance

in the field and Jessica Smith, Star Kent, Saba Ebrahimi, Hana Lee, Anasik Yadegarian, Aimee Varnado, Erin Solis, Kevin Zhang, Jonnby Laguardia, Glen Grewal, Manan Mehta, Evanie Huang, Leane Nasrallah, Joshua Kim, Sarah Kady, Linh Ngau, Amika Verma, Brayden Leyva, Adam Perez, Rachel Min, Vionna Liu, Avshalom Berrol, Michael Yu, Charanpreet Rai and Etham Lam for assistance in the lab. This work was funded by La Kretz Center Graduate Research Grants, UCNRS Stunt Ranch Reserve Research Grants, ESA Forrest Shreve Award, the National Science Foundation (Grants 1951244 and 2017949) and UCLA EEB Vavra Research Grants awarded to C.M. C.M. was supported by the Brazilian National Research Council (CNPq) through the Brazilian Science Without Borders Program (grant number: 202813/2014-2).

Table 6.1. Network-level parameters that quantify the tightness (edge density, *ED*, diameter, *D*, and average path length, *AL*) and complexity (average clustering coefficient, *AC*, and the modularity, *Q*) of plant trait networks built from species sampled in sites across a climatic gradient in the California Floristic Province. Higher values of *ED* reflect more interdependence of traits within the network, higher *D* and *AL* reflect more independence of traits within the network; higher values of *AC* reflect a network that is divided into more subcomponents; higher values of *Q* reflect higher clustering of traits.

Network	**Tightness**			**Complexity**	
	ED	*AL*	*D*	*AC*	*Q*
Desert	0.162	2.173	5	0.460	0.299
Coastal sage scrub	0.132	2.528	6	0.516	0.408
Chaparral	0.200	2.097	5	0.552	0.234
Montane wet forest	0.269	2.003	5	0.684	0.072
Mixed riparian woodland	0.258	2.002	5	0.648	0.061
Mixed conifer-broadleaf forest	0.210	2.034	4	0.556	0.107
Combined species	*0.361*	*1.691*	*4*	*0.581*	*0.043*

FIGURE CAPTIONS

Figure 6.1. Variation in climate and hypothesized ecological characteristics across the sites representative of the six ecosystems included in this study. The climatic aridity (i.e., high temperatures, low precipitation and low aridity index) increased from the mixed conifer-broadleaf forest site to the desert site. We hypothesized the environmental pressure (i.e., stress) would increase with climatic aridity, due to the constraints imposed by the combination of low water availability and warm temperatures that results in a high vapor pressure deficit, resulting in higher risk of embolism and hydraulic failure. Conversely, we hypothesized the competitive pressure to increase from the desert to the mixed conifer-broadleaf forest site. In resource rich environments (i.e., high nutrient and water availability) more species are able to germinate, but due to high density of individuals, the competitive pressure would be higher (for light, for example), so slow growing species would be less competitive. The combination of low environmental and high competitive pressures would theoretically result in high functional diversity. Thus, we expect the functional diversity to increase from high to low climatic aridity, since to survive under high environmental pressure species would need highly specialized strategies to survive the lack of resources and under high competitive pressure, species would need to grow fast and have more potential niches to fill. These hypotheses would be reflected in the architecture of plant trait networks (PTNs) as looser and less modular networks in high aridity environments and more interconnected and complex networks in resource rich environments.

Figure 6.2. Plant trait networks built from species sampled in six different ecosystems across the California Floristic province. (a) Map showing the centroid of the sampling location of each of the six ecosystems in a landscape of aridity. Symbols represent different ecosystems, with darker

shades of blue representing greater water availability: mixed conifer-broadleaf forest (dark blue circles), mixed riparian woodland (triangles), montane wet forest (inverted triangles), chaparral (diamonds), coastal sage scrub (squares), desert (light blue circles). (b) Plant trait networks (PTNs) built from species sampled in each of the six ecosystems. All networks were built from a matrix of trait-trait correlations, which were considered significant when $p < 0.05$. Nodes with the same colors were grouped into the same modules by the clustering algorithm (Table S3).

Figure 6.3. Variation in trait-level parameters of the networks build from traits measured on species from six ecosystem types across the California Floristic Province. Each boxplot shows the median, interquartile range, and minimum maximum values of parameters describing trait connectivity and centrality (a) degree of connectedness, *K*, and (b) betweeness, *B,* across networks. Traits with high values of *K* were considered "hub traits" and traits with high values of *B* were considered "mediator traits" (Table S4).

Figure 6.4. Relationships between network parameters and the climate of the sampling location of six ecosystem types across the California Floristic Province. Relationships between the mean annual temperature (*MAT*), mean annual precipitation, (*MAP*), aridity index (*AI*) and soil depth ($soil_{\text{depth}}$) with the edge density, *ED* (a-d), average path length, *AL* (e-h), average clustering coefficient, *AC* (i-l), and modularity, *Q* (m-p). Symbols represent different ecosystems, with darker shades of blue representing greater water availability: mixed conifer-broadleaf forest (dark blue circles), mixed riparian woodland (triangles), montane wet forest (inverted triangles), chaparral (diamonds), coastal sage scrub (squares), desert (light blue circles). Solid lines describe the fit of ordinary least squares regression analyses (OLS; Table S5). $*p < 0.05$.

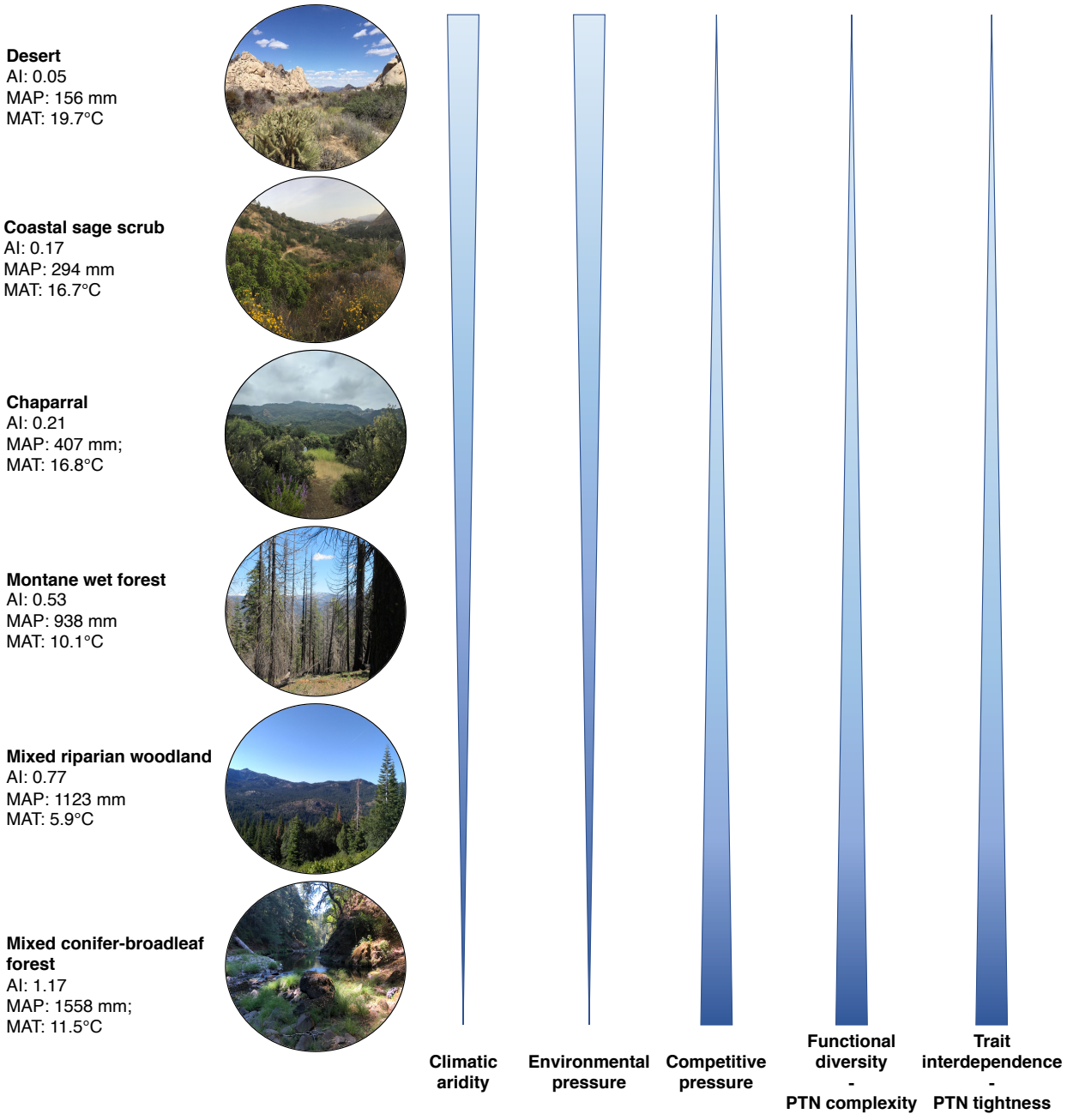
Desert
AI: 0.05
MAP: 156 mm
MAT: 19.7°C
Coastal sage scrub
AI: 0.17
MAP: 294 mm
MAT: 16.7°C
Chaparral
AI: 0.21
MAP: 407 mm;
MAT: 16.8°C
Montane wet forest
AI: 0.53
MAP: 938 mm
MAT: 10.1°C
Mixed riparian woodland
AI: 0.77
MAP: 1123 mm
MAT: 5.9°C
Mixed conifer-broadleaf forest
AI: 1.17
MAP: 1558 mm;
MAT: 11.5°C
Climatic aridity
Environmental pressure
Competitive pressure
Functional diversity - PTN complexity
Trait interdependence - PTN tightness

Figure 6.1

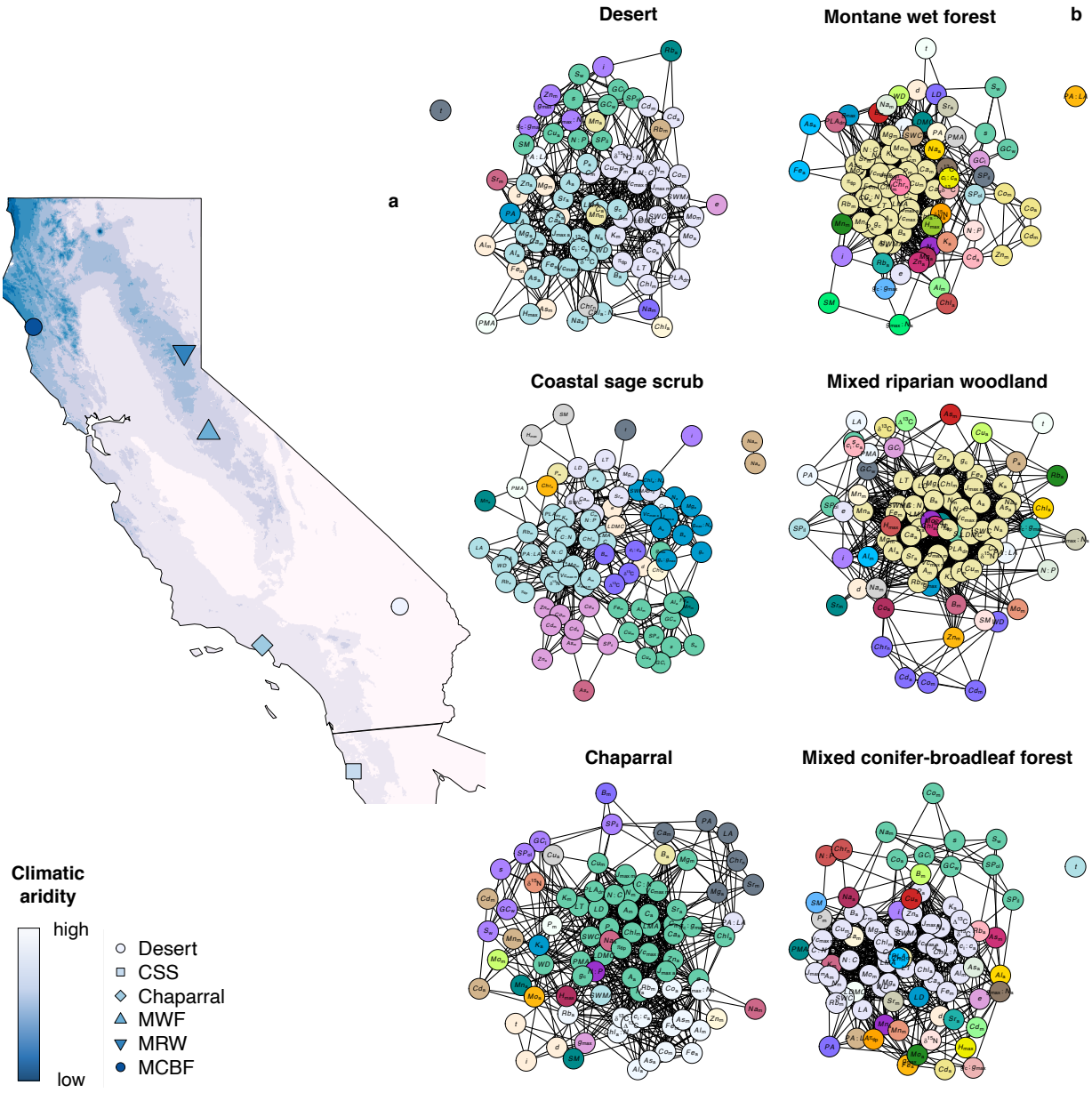
a
b
Desert
Montane wet forest
Coastal sage scrub
Mixed riparian woodland
Chaparral
Mixed conifer-broadleaf forest
Climatic aridity
high
low
Desert
CSS
Chaparral
MWF
MRW
MCBF

Figure 6.2

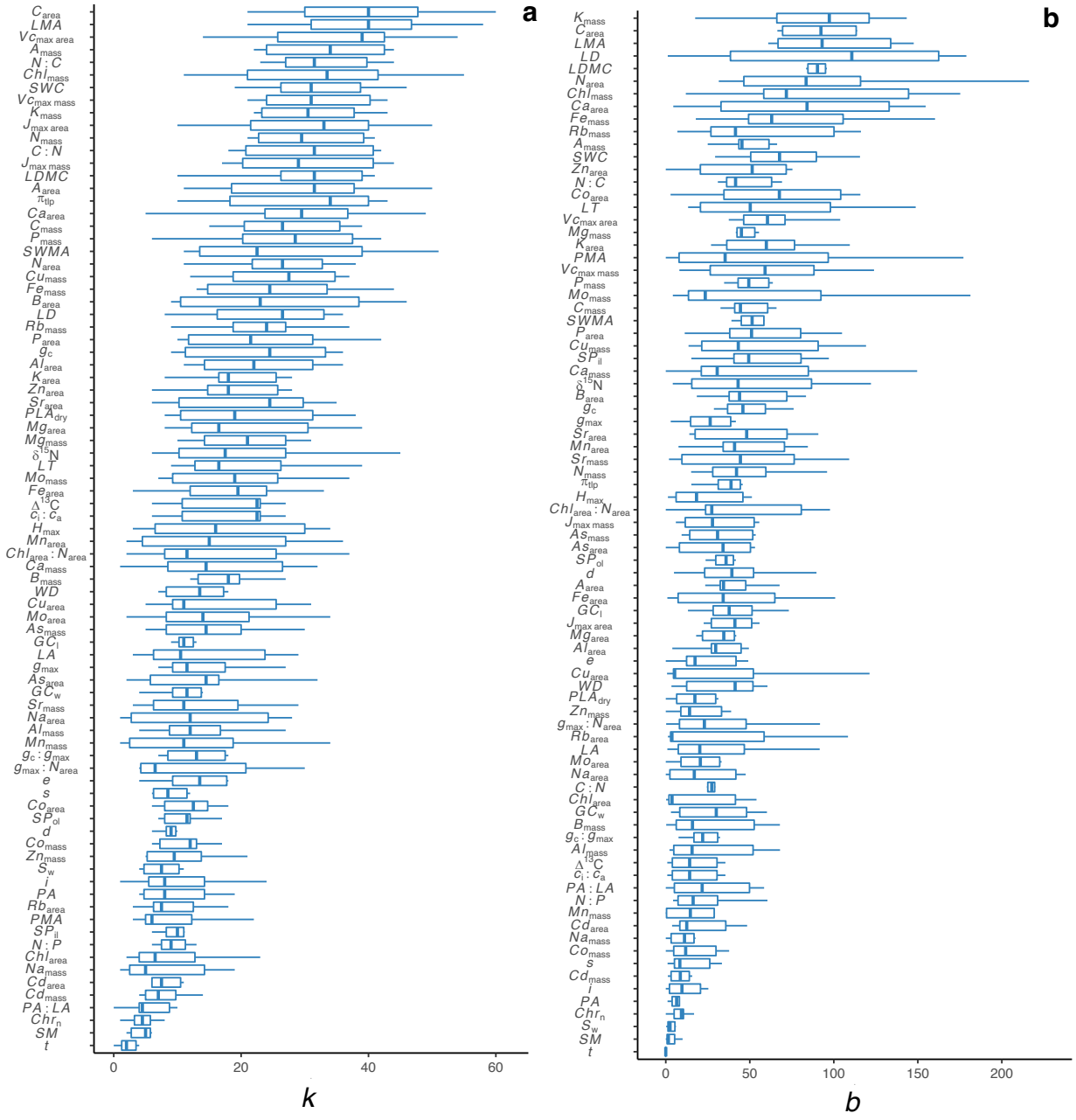

Figure 6.3

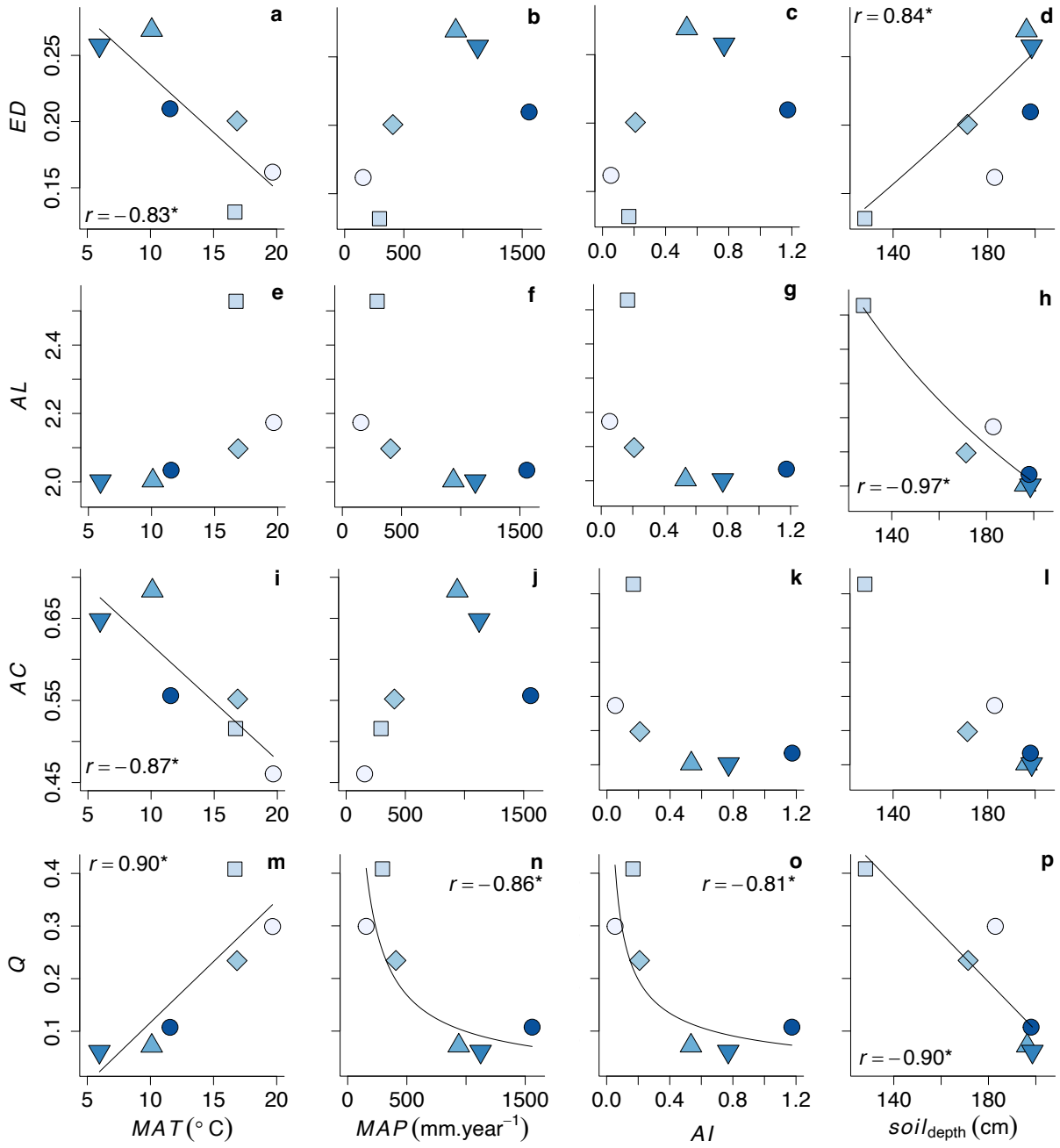
a
b
c
d
e
f
g
h
i
j
k
l
m
n
o
p
ED
AL
AC
Q
r = −0.83*
r = 0.84*
r = −0.97*
r = −0.87*
r = 0.90*
r = −0.86*
r = −0.81*
r = −0.90*
MAT (° C)
MAP (mm.year−1)
AI
soildepth (cm)

Figure 6.4

SUPPLEMENTARY MATERIALS

Supplementary data captions (see attached Excel Workbook)

Table S6.1. Environmental variables obtained for the six sites sampled across a climatic gradient in the California Floristic Province, including abbreviations, units, source database, metadata (raster layer title, timeframe of the dataset, the subset of the original dataset that was used to calculate species climate envelope, and the download date), and links to access datasets and references.

Table S6.2. Differences in functional traits among species and ecosystems, as indicated in nested analyses of variance, with species nested within ecosystems for 136 unique species from six ecosystems across a climatic gradient in the California Floristic Province. Traits deviating from assumptions of normality or homoscedasticity were log-transformed prior to the analysis (see legend below). Different letters indicate significant differences among groups (Tukey test). Highlighted cells indicate variables differing significantly different across sites ($p \leq 0.05$).

Table S6.3. Associations of traits in a matrix presenting results of ahistorical correlation tests on log-transformed data for the complete set of 136 species. Highlighted cells indicate significant relationships (***$p \leq 0.001$; **$p \leq 0.01$; *$p \leq 0.05$).

Table S6.4. Trait-level ahistorical plant network parameters for each of the six sites (built from the complete dataset with 136 species).

Table S6.5. Associations of plant trait network parameters from the PTN built from six ecosystems across the California Floristic Province and environmental variables of the sampling location. Matrix presents results of Pearson correlation tests on raw and log-transformed data. Highlighted cells indicate significant relationships (***$p \leq 0.001$; **$p \leq 0.01$; *$p \leq 0.05$).

Supplementary figure captions

Figure S6.1. Diversity in growth and leaf habit, leaf morphology, maximum height, H_{max}, seed mass, *SM*, leaf area, *LA*, stomatal density, *d*, stomatal size, *s*, and trichome density, *t*, across all 136 species sampled from six ecosystem types across California. All pictures belong to CD Medeiros personal database, with the exception of the pictures of *Mirabilis laevis* and seeds of *Vaccinium uliginosum* and *Aesculus californica,* modified from Calscape.com (by Steven M. Norris) and WikiCommons.

Figure S6.2. Plant trait network built from all 114 species sampled in six different ecosystems across the California Floristic province. Nodes with the same colors were grouped into the same clusters by the clustering algorithm (Table S6.3).

Figure S6.3. Relationships between network parameters and the number of species included in the PTN of the six ecosystem types across the California Floristic Province. Relationships between the number of species with the tightness parameters (a) edge density, *ED*, (b) average path length, *AL*, (c) network diameter, *D*; and complexity parameters, (d) average clustering coefficient, *AC*, and (e) modularity, *Q*. Symbols represent different ecosystems, with darker shades of blue representing greater water availability: mixed conifer-broadleaf forest (dark blue circles), mixed riparian woodland (triangles), montane wet forest (inverted triangles), chaparral (diamonds), coastal sage scrub (squares), desert (light blue circles). Solid lines describe the fit of ordinary least squares regression analyses (OLS; Table S6.5). $*p < 0.05$.

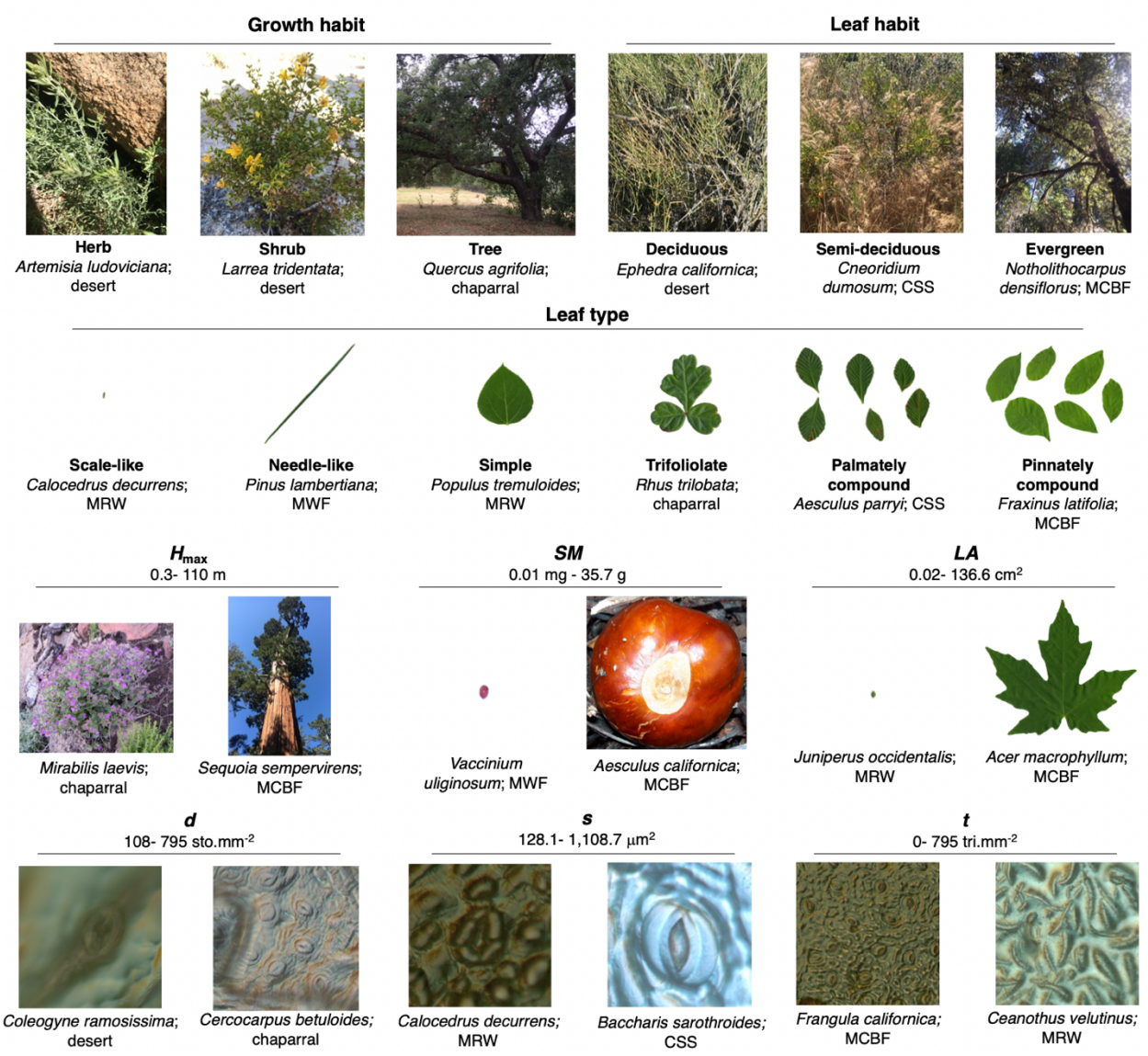
Growth habit
Leaf habit
Herb
Artemisia ludoviciana; desert
Shrub
Larrea tridentata; desert
Tree
Quercus agrifolia; chaparral
Deciduous
Ephedra californica; desert
Semi-deciduous
Cneoridium dumosum; CSS
Evergreen
Notholithocarpus densiflorus; MCBF
Leaf type
Scale-like
Calocedrus decurrens; MRW
Needle-like
Pinus lambertiana; MWF
Simple
Populus tremuloides; MRW
Trifoliolate
Rhus trilobata; chaparral
Palmately compound
Aesculus parryi; CSS
Pinnately compound
Fraxinus latifolia; MCBF
H_{max}
0.3- 110 m
SM
0.01 mg - 35.7 g
LA
0.02- 136.6 cm^2
Mirabilis laevis; chaparral
Sequoia sempervirens; MCBF
Vaccinium uliginosum; MWF
Aesculus californica; MCBF
Juniperus occidentalis; MRW
Acer macrophyllum; MCBF
d
108- 795 sto.mm^{-2}
s
128.1- 1,108.7 μm^2
t
0- 795 tri.mm^{-2}
Coleogyne ramosissima; desert
Cercocarpus betuloides; chaparral
Calocedrus decurrens; MRW
Baccharis sarothroides; CSS
Frangula californica; MCBF
Ceanothus velutinus; MRW

Figure S6.1

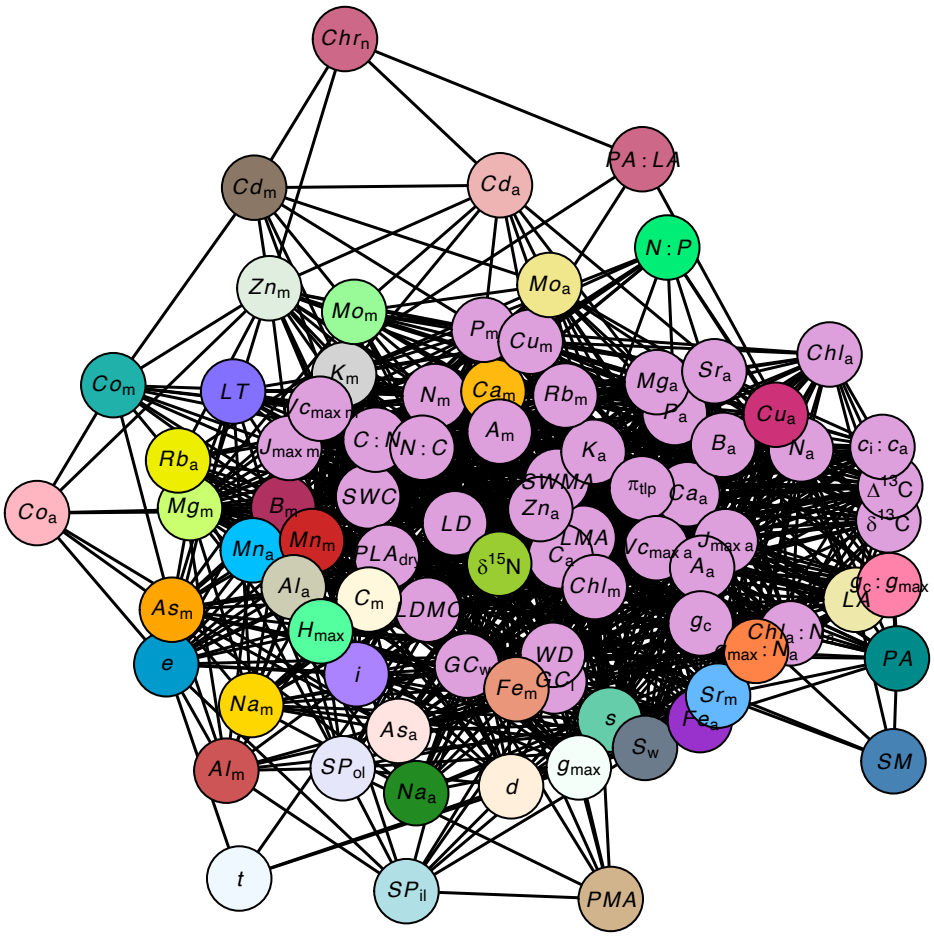
Chr_n
PA : LA
Cd_m
Cd_a
N : P
Zn_m
Mo_a
Mo_m
P_m
Cu_m
Chl_a
Co_m
LT
K_m
Sr_a
Mg_a
N_m
Ca_m
Rb_m
P_a
Cu_a
Vcmax m
A_m
B_a
N_a
c_i : c_a
Rb_a
Jmax m
C : N
N : C
K_a
SWMA
π_tlp
Ca_a
Δ13C
Co_a
Mg_m
B_m
SWC
Zn_a
δ13C
LD
LMA
Mn_a
Mn_m
PLA_dry
δ15N
C_a
Vcmax a
Jmax a
A_a
Al_a
C_m
Chl_m
g_c : g_max
LA
As_m
LDMC
g_c
H_max
Chl_a : N_a
PA
e
i
GC_w
WD
Fe_m
GC_l
Sr_m
Na_m
s
Fe_a
As_a
S_w
SM
Al_m
SP_ol
g_max
Na_a
d
t
SP_il
PMA

Figure S6.2

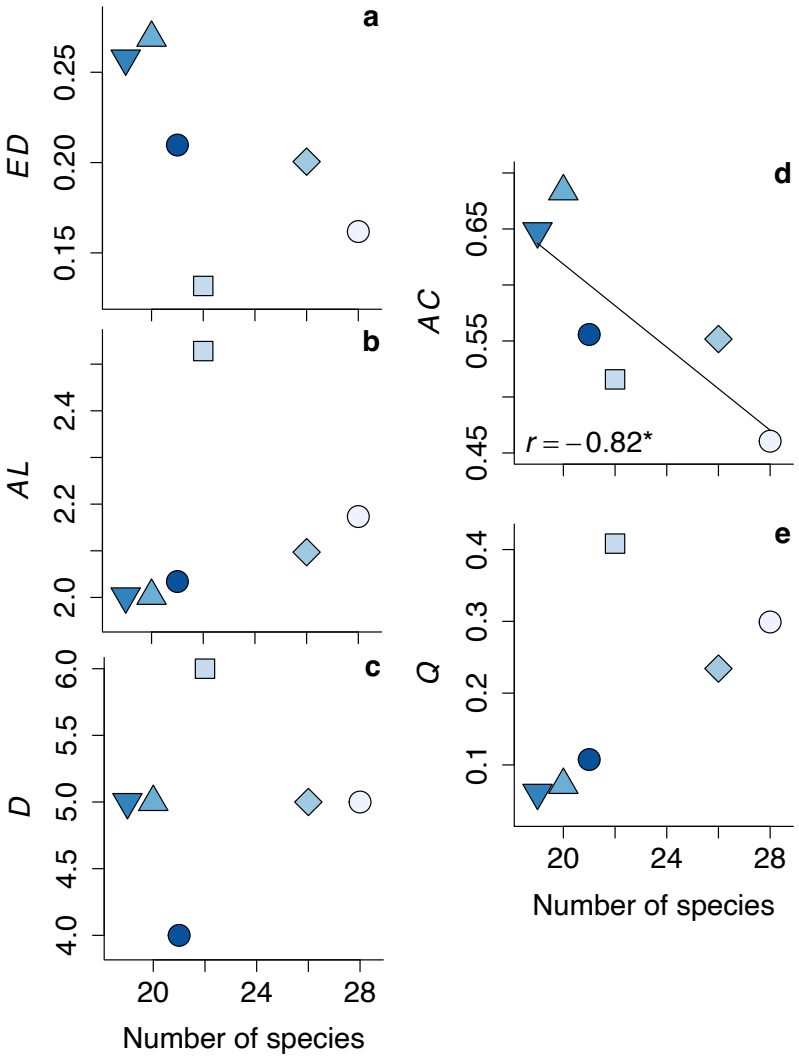
a
ED
0.15
0.20
0.25
b
AL
2.0
2.2
2.4
c
D
4.0
4.5
5.0
5.5
6.0
20
24
28
Number of species
d
AC
0.45
0.55
0.65
r = −0.82*
e
Q
0.1
0.2
0.3
0.4
20
24
28
Number of species

Figure S6.3

REFERENCES

Abd-Elmabod, S.K., Jordán, A., Fleskens, L., Phillips, J.D., Muñoz-Rojas, M., van der Ploeg, M., *et al.* (2017). Modeling Agricultural Suitability Along Soil Transects Under Current Conditions and Improved Scenario of Soil Factors. In: *Soil Mapping and Process Modeling for Sustainable Land Use Management*. Elsevier, pp. 193–219.

Adler, P.B., Salguero-Gomez, R., Compagnoni, A., Hsu, J.S., Ray-Mukherjee, J., Mbeau-Ache, C., *et al.* (2014). Functional traits explain variation in plant life history strategies. *Proc Natl Acad Sci USA*, 111, 740–745.

Anderson-Teixeira, K.J., Davies, S.J., Bennett, A.C., Gonzalez-Akre, E.B., Muller-Landau, H.C., Joseph Wright, S., *et al.* (2015). CTFS-ForestGEO: a worldwide network monitoring forests in an era of global change. *Glob Change Biol*, 21, 528–549.

Baird, A.S., Taylor, S.H., Pasquet-Kok, J., Vuong, C., Zhang, Y., Watcharamongkol, T., *et al.* (2021). Developmental and biophysical determinants of grass leaf size worldwide. *Nature*, 592, 242–247.

Bartlett, M.K., Klein, T., Jansen, S., Choat, B. & Sack, L. (2016). The correlations and sequence of plant stomatal, hydraulic, and wilting responses to drought. *Proc Natl Acad Sci USA*, 113, 13098–13103.

Bartlett, M.K., Scoffoni, C., Ardy, R., Zhang, Y., Sun, S., Cao, K., *et al.* (2012). Rapid determination of comparative drought tolerance traits: using an osmometer to predict turgor loss point. *Methods Ecol Evol*, 3, 880–888.

Belluau, M. & Shipley, B. (2018). Linking hard and soft traits: Physiology, morphology and anatomy interact to determine habitat affinities to soil water availability in herbaceous dicots. *PLoS ONE*, 13, e0193130.

Biggs, C.R., Yeager, L.A., Bolser, D.G., Bonsell, C., Dichiera, A.M., Hou, Z., *et al.* (2020). Does functional redundancy affect ecological stability and resilience? A review and meta-analysis. *Ecosphere*, 11.

Bohnert, H.J., Nelson, D.E. & Jensen, R.G. (1995). Adaptations to Environmental Stresses. *Plant Cell*, 7, 1099–1111.

Brooks, D., Hulst, H.E., de Bruin, L., Glas, G., Geurts, J.J.G. & Douw, L. (2020). The Multilayer Network Approach in the Study of Personality Neuroscience. *Brain Sciences*, 10, 915.

Cowling, R.M., Esler, K.J., Midgley, G.F. & Honig, M.A. (1994). Plant functional diversity, species diversity and climate in arid and semi-arid southern Africa. *Journal of Arid Environments*, 27, 141–158.

Díaz, S., Hodgson, J.G., Thompson, K., Cabido, M., Cornelissen, J.H.C., Jalili, A., *et al.* (2004). The plant traits that drive ecosystems: Evidence from three continents. *Journal of Vegetation Science*.

Díaz, S., Kattge, J., Cornelissen, J.H.C., Wright, I.J., Lavorel, S., Dray, S., *et al.* (2016). The global spectrum of plant form and function. *Nature*, 529, 167–171.

Domingues, T.F., Meir, P., Feldpausch, T.R., Saiz, G., Veenendaal, E.M., Schrodt, F., *et al.* (2010). Co-limitation of photosynthetic capacity by nitrogen and phosphorus in West Africa woodlands. *Plant Cell Environ*.

Farquhar, G., O'Leary, M. & Berry, J. (1982). On the relationship between carbon isotope discrimination and the intercellular carbon dioxide concentration in leaves. *Functional Plant Biol*, 9, 121.

Farquhar, G.D., Ehleringer, J.R. & Hubick, K.T. (1989). Carbon isotope discrimination and photosynthesis. *Annu Rev Plant Physiol Plant Mol Biol*, 40, 503–537.

Farquhar, G.D. & Richards, R.A. (1984). Isotopic composition of plant carbon correlates with water-use efficiency of Wheat genotypes. *Aust J Plant Physiol*, 11, 539–552.

Flores-Moreno, H., Fazayeli, F., Banerjee, A., Datta, A., Kattge, J., Butler, E.E., *et al.* (2019). Robustness of trait connections across environmental gradients and growth forms. *Global Ecol Biogeogr*, 28, 1806–1826.

Franks, P.J., Drake, P.L. & Beerling, D.J. (2009a). Plasticity in maximum stomatal conductance constrained by negative correlation between stomatal size and density: an analysis using *Eucalyptus globulus*. *Plant Cell Environ*.

Franks, P.J., Drake, P.L. & Beerling, D.J. (2009b). Plasticity in maximum stomatal conductance constrained by negative correlation between stomatal size and density: an analysis using *Eucalyptus globulus*. *Plant Cell Environ*.

Franks, P.J. & Farquhar, G.D. (2007). The mechanical diversity of stomata and its significance in gas-exchange control. *Plant Physiol*, 143, 78–87.

Franks, P.J., Royer, D.L., Beerling, D.J., Van de Water, P.K., Cantrill, D.J., Barbour, M.M., *et al.* (2014). New constraints on atmospheric CO2concentration for the Phanerozoic. *Geophys Res Lett*.

Fry, B., Ganitt, R., Tholke, K., Neill, C., Michener, R.H., Mersch, F.J., *et al.* (1996). Cryoflow: Cryofocusing Nanomole Amounts of CO2, N2, and SO2 from an Elemental Analyzer for Stable Isotopic Analysis. *Rapid communications in mass spectrometry*.

Funk, J.L., Larson, J.E., Ames, G.M., Butterfield, B.J., Cavender-Bares, J., Firn, J., *et al.* (2017). Revisiting the H oly G rail: using plant functional traits to understand ecological processes. *Biol Rev*, 92, 1156–1173.

Grime, J.P. (1979). *Plant strategies and vegetation processes*. 1st edn. Wiley, Chichester.

Harrison, S., Spasojevic, M.J. & Li, D. (2020). Climate and plant community diversity in space and time. *Proc Natl Acad Sci USA*, 117, 4464–4470.

He, N., Li, Y., Liu, C., Xu, L., Li, M., Zhang, J., *et al.* (2020). Plant Trait Networks: Improved Resolution of the Dimensionality of Adaptation. *Trends Ecol Evol*, 35, 908–918.

Hengl, T., Mendes de Jesus, J., Heuvelink, G.B.M., Ruiperez Gonzalez, M., Kilibarda, M., Blagotić, A., *et al.* (2017). SoilGrids250m: Global gridded soil information based on machine learning. *PLoS ONE*, 12, e0169748.

Henry, C., John, G.P., Pan, R., Bartlett, M.K., Fletcher, L.R., Scoffoni, C., *et al.* (2019). A stomatal safety-efficiency trade-off constrains responses to leaf dehydration. *Nat Commun*, 10, 3398.

Hijmans, R.J., Cameron, S.E., Parra, J.L., Jones, P.G. & Jarvis, A. (2005). Very high resolution interpolated climate surfaces for global land areas. *Int J Climatol*, 25, 1965–1978.

John, G.P., Scoffoni, C., Buckley, T.N., Villar, R., Poorter, H., Sack, L., *et al.* (2017). The anatomical and compositional basis of leaf mass per area. *Ecol Lett*, 20, 412–425.

Kleyer, M., Trinogga, J., Cebrián-Piqueras, M.A., Trenkamp, A., Fløjgaard, C., Ejrnaes, R., *et al.* (2019). Trait correlation network analysis identifies biomass allocation traits and stem specific length as hub traits in herbaceous perennial plants. *J Ecol*, 107, 829–842.

Laughlin, D.C. (2014). The intrinsic dimensionality of plant traits and its relevance to community assembly. *J Ecol*, 102, 186–193.

Lavorel, S. & Garnier, E. (2002). Predicting changes in community composition and ecosystem functioning from plant traits: revisiting the Holy Grail. *Funct Ecol*, 16, 545–556.

Li, Y., He, N., Liu, C., Zhang, J., Xu, L., Hou, J., *et al.* (in review). Climate shapes leaf trait networks across forests at continental scale.

Lusk, C.H. & Warton, D.I. (2007). Global meta-analysis shows that relationships of leaf mass per area with species shade tolerance depend on leaf habit and ontogeny. *New Phytol*, 176, 764–774.

Maréchaux, I., Saint-André, L., Bartlett, M.K., Sack, L. & Chave, J. (2020). Leaf drought tolerance cannot be inferred from classic leaf traits in a tropical rainforest. *J Ecol*, 108, 1030–1045.

Markett, S., Montag, C. & Reuter, M. (2018). Network Neuroscience and Personality. *Personality Neuroscience*, 1, e14.

Marks, C.O. & Lechowicz, M.J. (2006). Alternative designs and the evolution of functional diversity. *Am Nat*, 167, 55–66.

Martin-StPaul, N., Delzon, S. & Cochard, H. (2017). Plant resistance to drought depends on timely stomatal closure. *Ecol Lett*, 20, 1437–1447.

McElwain, J.C., Yiotis, C. & Lawson, T. (2016). Using modern plant trait relationships between observed and theoretical maximum stomatal conductance and vein density to examine patterns of plant macroevolution. *New Phytol*.

Medeiros, C.D., Scoffoni, C., John, G.P., Bartlett, M.K., Inman-Narahari, F., Ostertag, R., *et al.* (2019). An extensive suite of functional traits distinguishes Hawaiian wet and dry forests and enables prediction of species vital rates. *Funct Ecol*, 33, 712–734.

Messier, J., Lechowicz, M.J., McGill, B.J., Violle, C., Enquist, B.J. & Cornelissen, H. (2017). Interspecific integration of trait dimensions at local scales: the plant phenotype as an integrated network. *J Ecol*.

Monje, O.A. & Bugbee, B. (1992). Inherent Limitations of Nondestructive Chlorophyll Meters: A Comparison of Two Types of Meters. *HortScience*.

Ogburn, R.M. & Edwards, E.J. (2012). Quantifying succulence: a rapid, physiologically meaningful metric of plant water storage. *Plant Cell Environ*.

Perez, T.M. & Feeley, K.J. (2020). Weak phylogenetic and climatic signals in plant heat tolerance. *J Biogeogr*, jbi.13984.

Pérez-Harguindeguy, N., Díaz, S., Garnier, E., Lavorel, S., Poorter, H., Jaureguiberry, P., *et al.* (2013). New handbook for standardised measurement of plant functional traits worldwide. *Aust J Bot*, 61.

Pillar, V.D., Blanco, C.C., Müller, S.C., Sosinski, E.E., Joner, F. & Duarte, L.D.S. (2013). Functional redundancy and stability in plant communities. *J Veg Sci*, 24, 963–974.

Poorter, H., Lambers, H. & Evans, J.R. (2014). Trait correlation networks: a whole-plant perspective on the recently criticized leaf economic spectrum. *New Phytologist*.

Poorter, L., Wright, S.J., Paz, H., Ackerly, D.D., Condit, R., Ibarra-Manríquez, G., *et al.* (2008). Are functional traits good predictors of demographic rates? Evidence from five neotropical forests. *Ecology*, 89, 1908–1920.

R Core Team. (2020). *R: a language and environment for statistical computing*. R Foundation for Statistical Computing.

Rajakaruna, N. & Boyd, R.S. (2019). Edaphic Factor. In: *Encyclopedia of Ecology*. Elsevier, pp. 361–367.

de la Riva, E.G., Olmo, M., Poorter, H., Ubera, J.L. & Villar, R. (2016). Leaf Mass per Area (LMA) and Its Relationship with Leaf Structure and Anatomy in 34 Mediterranean Woody Species along a Water Availability Gradient. *PLoS ONE*, 11, e0148788.

Sack, L. & Buckley, T.N. (2016). The developmental basis of stomatal density and flux. *Plant Physiol*.

Sack, L. & Buckley, T.N. (2020). Trait multi-functionality in plant stress response. *Integr Comp Biol*, 60, 98–112.

Sack, L., Scoffoni, C., John, G.P., Poorter, H., Mason, C.M., Mendez-Alonzo, R., *et al.* (2013). How do leaf veins influence the worldwide leaf economic spectrum? Review and synthesis. *J Exp Bot*, 64, 4053–4080.

Salt, D.E., Baxter, I. & Lahner, B. (2008). Ionomics and the study of the plant ionome. *Annu Rev Plant Biol*, 59, 709–733.

Sokal, R.R. & Rohlf, F.J. (2012). Biometry: the principles and practice of statistics in biological research.

Spasojevic, M.J., Grace, J.B., Harrison, S. & Damschen, E.I. (2014). Functional diversity supports the physiological tolerance hypothesis for plant species richness along climatic gradients. *J Ecol*, 102, 447–455.

Stahl, U., Reu, B. & Wirth, C. (2014). Predicting species' range limits from functional traits for the tree flora of North America. *Proc Natl Acad Sci USA*, 111, 13739–13744.

Thorne, J.H., Choe, H., Boynton, R.M., Bjorkman, J., Albright, W., Nydick, K., *et al.* (2017). The impact of climate change uncertainty on California's vegetation and adaptation management. *Ecosphere*, 8, e02021.

Tompson, S.H., Falk, E.B., Vettel, J.M. & Bassett, D.S. (2018). Network Approaches to Understand Individual Differences in Brain Connectivity: Opportunities for Personality Neuroscience. *Personality Neuroscience*, 1, e5.

Violle, C., Navas, M.-L., Vile, D., Kazakou, E., Fortunel, C., Hummel, I., *et al.* (2007). Let the concept of trait be functional! *Oikos*, 116, 882–892.

Westoby, M. (1998). A leaf-height-seed (LHS) plant ecology strategy scheme. *Plant Soil*, 199, 213–227.

Witkowski, E.T.F. & Lamont, B.B. (1991). Leaf specific mass confounds leaf density and thickness. *Oecologia*.

Wong, S.C., Cowan, I.R. & Farquhar, G.D. (1979). Stomatal conductance correlates with photosynthetic capacity. *Nature*, 282, 424–426.

Wright, I.J., Reich, P.B. & Westoby, M. (2001). Strategy shifts in leaf physiology, structure and nutrient content between species of high- and low-rainfall and high- and low-nutrient habitats. *Funct Ecol*, 15, 423–434.

Wright, I.J., Reich, P.B., Westoby, M., Ackerly, D.D., Baruch, Z., Bongers, F., *et al.* (2004). The worldwide leaf economics spectrum. *Nature*, 428, 821–827.

Zomer, R.J., Trabucco, A., Bossio, D.A. & Verchot, L.V. (2008). Climate change mitigation: A spatial analysis of global land suitability for clean development mechanism afforestation and reforestation. *Agric Ecosyst Environ*, 126, 67–80.

CHAPTER 7

CONCLUSIONS AND FUTURE DIRECTIONS

My PhD focused on an increasingly critical topic in ecology and evolution—the integration of leaf and whole-plant traits to explaining and predicting plant vital rates and vegetation distributions with respect to climate. During my PhD, I have quantified a comprehensive set of leaf, stem and whole-plant traits and their relationships with vital rates and climate for study systems across scales, from ecotypes of model species *Arabidopsis thaliana* (Chapter 2), to species of the oak genus (Chapter 3), species of Hawaiian wet versus dry forest (Chapter 4), and species and ecosystems across California (Chapters 5 and 6). Beyond providing new synthesis of the variation of trait-climate relationships across scales, this work has led to specific discoveries, including the developmental basis of *Arabidopsis* stomatal adaptation to climate (Chapter 2), the evolution of California native oak species traits in modules (Chapter 3), the variation in traits and their influence on vital rates across species native to contrasting forests of Hawai‘i (Chapter 4), the statistical predictability of species' climate distributions across California (Chapter 5) and the variation in the intercorrelated networks of traits across a gradient of aridity in California (Chapter 6).

More specifically, In Chapter 2, I found that across natural *Arabidopsis* ecotypes, the maximum stomatal conductance, g_{max}, was determined mainly by the epidermal cell size and the stomatal initiation rate, with a much smaller effect of the stomatal size. The anatomical determination of stomatal density and g_{max} by the epidermal cell size and the stomatal initiation rate suggests that these traits would be loci for selection, and potential targets for improved crops. By contrast, stomatal size was not a key driver of stomatal density or g_{max}, indicating that theory that g_{max} is strongly influenced by stomatal packing and the stomatal size vs. density trade-off—

which was weak in this study—would not apply across *Arabidopsis* ecotypes (Franks & Farquhar 2007; Ohsumi *et al.* 2007; Franks *et al.* 2009; Camargo & Marenco 2011; Wang *et al.* 2015; Dittberner *et al.* 2018; Kardiman & Ræbild 2018; Yin *et al.* 2020). To our knowledge, this is the first study to show quantitatively that the maximum anatomical stomatal conductance and its relationship with climate is developmentally determined by the area of epidermal pavement cells and the stomatal initiation rate and not the stomatal size (Sack & Buckley 2016).

In Chapter 3, in California oaks, I tested hypotheses for trait co-evolution within and across structure-function modules, defined based on ecophysiological theory (plant size, leaf size, flux-related, economics, ecological stoichiometry and drought response modules). I also tested the contribution of shared evolutionary history to the formation of trait modules within plant trait networks (PTNs) and identified the key traits within the PTNs. I found that traits varied strongly among and within California oak species, with significantly more correlations within than among theoretically expected structure-function modules and strong influence of shared evolutionary histories. The central, "indicator traits" of the leaf size, ecological stoichiometry and drought-tolerance modules were positively correlated with climatic aridity of species' native distributions. Photosynthetic traits and the leaf turgor loss point were disproportionately important to the topology of the PTNs. Ultimately, the evolution of traits within modules highlights the complexity of the integrated phenotypes (He *et al.* 2020; Sack & Buckley 2020).

In Chapter 4, I used functional traits to test hypotheses for Hawaiian wet montane and lowland dry forests (MWF and LDF respectively). I found that The MWF species' traits were associated with adaptation to high soil moisture and nutrient supply, and greater shade tolerance, whereas the LDF species' traits were associated with drought tolerance. On average, MWF species achieved greater maximum heights than LDF species and had leaves with larger

epidermal cells, higher maximum stomatal conductance and CO_2 assimilation rate, lower vein lengths per area, higher saturated water content and greater shrinkage when dry, lower dry matter content, higher phosphorus concentration, lower nitrogen to phosphorus ratio, high chlorophyll to nitrogen ratio, high carbon isotope discrimination, high stomatal conductance to nitrogen ratio, less negative turgor loss point, and lower *WD*. Functional traits were more variable in the MWF than LDF. Across both forests, functional traits were correlated within modules, and predicted species' *RGR* and *m* across forests, with stronger relationships when stratifying by tree size (Iida *et al.* 2014; Prado-Junior *et al.* 2016). Models based on multiple traits predicted vital rates across forests (R^2 = 0.70-0.72; $p < 0.01$). Given the power to predict vital rates, this work can enable scaling up from the traits of component species to ecosystem and eventually global vegetation processes.

In Chapter 5, I showed that species differed strongly in their functional traits within and across the six California ecosystems, with traits varying with climatic aridity as hypothesized based on mechanistic theory (Evans 1973; Farquhar *et al.* 1989; Cunningham *et al.* 1999; Hacke *et al.* 2001; Wright *et al.* 2001, 2004; Wright & Westoby 2002; Koch *et al.* 2004; Santiago *et al.* 2004; King *et al.* 2006; Poorter *et al.* 2009; Bartlett *et al.* 2012; Sack *et al.* 2012; Gleason *et al.* 2016; John *et al.* 2017; Ma *et al.* 2018; Fang *et al.* 2019; Liang *et al.* 2021). I showed that traits considered individually and in combination had substantial power to predict the mean values for climate variables representing the range of species and ecosystems, despite the strong influence of many factors, such as intra-specific variation due to species' plastic and ecotypic adjustments, that could in principle decouple climatic distributions from traits across species (Dobzhansky 1950; Walter 1979; Brown 1984; DeAngelis & Waterhouse 1987; Stevens 1989; Hanski *et al.* 1993; Ohlemüller *et al.* 2008; Albert *et al.* 2010a, b; Wiens 2011; Violle *et al.* 2012; Siefert *et al.*

2015; Lee-Yaw *et al.* 2016; Pérez-Ramos *et al.* 2019; Fyllas *et al.* 2020; Laughlin *et al.* 2020; Sheth *et al.* 2020). I also showed that the potential for prediction of species' climate preferences from traits was improved using my approach of including traits with mechanistic significance, and measured with consistent methodology and would be further increased by sampling each species near to the center of its climate distributions (Violle *et al.* 2007; Moles *et al.* 2014; Taugourdeau *et al.* 2014; Šímová *et al.* 2018; van der Plas *et al.* 2020; Vesk *et al.* 2020).

In Chapter 6, I found strong variation in functional traits across California species of six ecosystems, with 78 of the 83 measured traits differing across species and 69 differing across the ecosystems. In the more arid ecosystems, species had smaller, denser and thicker leaves with higher trichome density, higher saturated water mass per area and smaller reduction in leaf area when dry, denser wood and more negative turgor loss points than species from the more mesic ecosystems. The topology of the PTNs shifted with the climate of sampling locations (Flores-Moreno *et al.* 2019; He *et al.* 2020; Li *et al.* in review). In the sampling locations with shallower soils and warmer temperatures the PTNs were looser, with lower edge density and clustering coefficient and higher modularity (Fig. 4). The water availability did not significantly influence the tightness of PTNs, but was negatively related to the modularity. The traits that emerged as hub and mediator traits in the PTNs were traits typically associated with leaf structural support, photosynthesis and fluxes. These results reinforce the idea that traits have limited meaning when considered alone. Using a wide range of traits provides insight into the modular nature of trait function and overall physiological and ecological strategies of different plant species and ecosystems. Ultimately, PTNs provide a promising avenue to explore the adaptive strategies of plants and help with the identification of important candidate traits to include in models of future species distributions and ecosystem resilience in response to changes in climate.

My PhD work opens new possibilities for using mechanistically informative traits to parameterize process-based models to test the ability to predict growth and mortality rates from trait networks, spatial neighborhoods, local topography, and climate across forests worldwide. These models will be critical tools for predicting the trajectory of future climate change, and for identifying the species and ecosystems that require the most urgent management.

REFERENCES

Albert, C.H., Thuiller, W., Yoccoz, N.G., Douzet, R., Aubert, S. & Lavorel, S. (2010a). A multi-trait approach reveals the structure and the relative importance of intra- vs. interspecific variability in plant traits. *Funct Ecol*, 24, 1192–1201.

Albert, C.H., Thuiller, W., Yoccoz, N.G., Soudant, A., Boucher, F., Saccone, P., *et al.* (2010b). Intraspecific functional variability: extent, structure and sources of variation. *J Ecol*, 98, 604–613.

Bartlett, M.K., Scoffoni, C. & Sack, L. (2012). The determinants of leaf turgor loss point and prediction of drought tolerance of species and biomes: a global meta-analysis. *Ecol Lett*, 15, 393–405.

Brown, J.H. (1984). On the relationship between abundance and distribution of species. *Am Nat*, 124, 255–279.

Camargo, M.A.B. & Marenco, R.A. (2011). Density, size and distribution of stomata in 35 rainforest tree species in Central Amazonia. *Acta Amaz.*, 41, 205–212.

Cunningham, S.A., Summerhayes, B. & Westoby, M. (1999). Evolutionary divergences in leaf structure and chemistry, comparing rainfall and soil nutrient gradients. *Ecol Monogr*, 69, 569–588.

DeAngelis, D.L. & Waterhouse, J.C. (1987). Equilibrium and nonequilibrium concepts in ecological models. *Ecol Monogr*, 57, 1–21.

Dittberner, H., Korte, A., Mettler-Altmann, T., Weber, A.P.M., Monroe, G. & de Meaux, J. (2018). Natural variation in stomata size contributes to the local adaptation of water-use efficiency in *Arabidopsis thaliana*. *Mol Ecol*, 27, 4052–4065.

Dobzhansky, T. (1950). Evolution in the tropics. *Am Sci*, 38, 208–221.

Evans, G.C. (1973). *The quantitative analysis of plant growth*. University of California Press, Berkeley and Los Angeles, California.

Fang, Z., Li, D.-D., Jiao, F., Yao, J. & Du, H.-T. (2019). The Latitudinal Patterns of Leaf and Soil C:N:P Stoichiometry in the Loess Plateau of China. *Front Plant Sci*, 10, 85.

Farquhar, G.D., Ehleringer, J.R. & Hubick, K.T. (1989). Carbon isotope discrimination and photosynthesis. *Annu Rev Plant Physiol Plant Mol Biol*, 40, 503–537.

Flores-Moreno, H., Fazayeli, F., Banerjee, A., Datta, A., Kattge, J., Butler, E.E., *et al.* (2019). Robustness of trait connections across environmental gradients and growth forms. *Global Ecol Biogeogr*, 28, 1806–1826.

Franks, P.J., Drake, P.L. & Beerling, D.J. (2009). Plasticity in maximum stomatal conductance constrained by negative correlation between stomatal size and density: an analysis using *Eucalyptus globulus*. *Plant Cell Environ*.

Franks, P.J. & Farquhar, G.D. (2007). The mechanical diversity of stomata and its significance in gas-exchange control. *Plant Physiol*, 143, 78–87.

Fyllas, N.M., Michelaki, C., Galanidis, A., Evangelou, E., Zaragoza-Castells, J., Dimitrakopoulos, P.G., *et al.* (2020). Functional trait variation among and within species and plant functional types in mountainous mediterranean forests. *Front Plant Sci*, 11, 212.

Gleason, S.M., Westoby, M., Jansen, S., Choat, B., Hacke, U.G., Pratt, R.B., *et al.* (2016). Weak tradeoff between xylem safety and xylem-specific hydraulic efficiency across the world's woody plant species. *New Phytol*, 209, 123–136.

Hacke, U.G., Sperry, J.S., Pockman, W.T., Davis, S.D. & McCulloh, K.A. (2001). Trends in wood density and structure are linked to prevention of xylem implosion by negative pressure. *Oecologia*, 126, 457–461.

Hanski, I., Kouki, J. & Halkka, A. (1993). Three explanations of the positive relationship between distribution and abundance of species. In: *Species diversity in ecological communities: historical and geographical perspectives*. The University of Chicago Press, Chicago, IL, USA, pp. 108–116.

He, N., Li, Y., Liu, C., Xu, L., Li, M., Zhang, J., *et al.* (2020). Plant Trait Networks: Improved Resolution of the Dimensionality of Adaptation. *Trends Ecol Evol*, 35, 908–918.

Iida, Y., Poorter, L., Sterk, F., Kassim, A.R., Potts, M.D., kubo, T., *et al.* (2014). Linking size-dependent growth and mortality with architectural traits across 145 co-occurring tropical tree species. *Ecology*.

John, G.P., Scoffoni, C., Buckley, T.N., Villar, R., Poorter, H., Sack, L., *et al.* (2017). The anatomical and compositional basis of leaf mass per area. *Ecol Lett*, 20, 412–425.

Kardiman, R. & Ræbild, A. (2018). Relationship between stomatal density, size and speed of opening in Sumatran rainforest species. *Tree Physiol*, 38, 696–705.

King, D.A., Davies, S.J. & Noor, N.S.Md. (2006). Growth and mortality are related to adult tree size in a Malaysian mixed dipterocarp forest. *For Ecol Manag*, 223, 152–158.

Koch, G.W., Sillett, S.C., Jennings, G.M. & Davis, S.D. (2004). The limits to tree height. *Nature*, 428, 851–854.

Laughlin, D.C., Gremer, J.R., Adler, P.B., Mitchell, R.M. & Moore, M.M. (2020). The net effect of functional traits on fitness. *Trends Ecol Evol*, 35, 1037–1047.

Lee-Yaw, J.A., Kharouba, H.M., Bontrager, M., Mahony, C., Csergő, A.M., Noreen, A.M.E., *et al.* (2016). A synthesis of transplant experiments and ecological niche models suggests that range limits are often niche limits. *Ecol Lett*, 19, 710–722.

Li, Y., He, N., Liu, C., Zhang, J., Xu, L., Hou, J., *et al.* (in review). Climate shapes leaf trait networks across forests at continental scale.

Liang, X., Ye, Q., Liu, H. & Brodribb, T.J. (2021). Wood density predicts mortality threshold for diverse trees. *New Phytol*, 229, 3053–3057.

Ma, S., He, F., Tian, D., Zou, D., Yan, Z., Yang, Y., *et al.* (2018). Variations and determinants of carbon content in plants: a global synthesis. *Biogeosciences*, 15, 693–702.

Moles, A.T., Perkins, S.E., Laffan, S.W., Flores-Moreno, H., Awasthy, M., Tindall, M.L., *et al.* (2014). Which is a better predictor of plant traits: temperature or precipitation? *J Veg Sci*, 25, 1167–1180.

Ohlemüller, R., Anderson, B.J., Araújo, M.B., Butchart, S.H.M., Kudrna, O., Ridgely, R.S., *et al.* (2008). The coincidence of climatic and species rarity: high risk to small-range species from climate change. *Biol Lett*, 4, 568–572.

Ohsumi, A., Kanemura, T., Homma, K., Horie, T. & Shiraiwa, T. (2007). Genotypic variation of stomatal conductance in relation to stomatal density and length in rice (*Oryza sativa* L.). *Plant Prod Sci*, 10, 322–328.

Pérez-Ramos, I.M., Matías, L., Gómez-Aparicio, L. & Godoy, Ó. (2019). Functional traits and phenotypic plasticity modulate species coexistence across contrasting climatic conditions. *Nat Commun*, 10, 2555.

van der Plas, F., Schröder-Georgi, T., Weigelt, A., Barry, K., Meyer, S., Alzate, A., *et al.* (2020). Plant traits alone are poor predictors of ecosystem properties and long-term ecosystem functioning. *Nat Ecol Evol*, 4, 1602–1611.

Poorter, H., Niinemets, Ü., Poorter, L., Wright, I.J. & Villar, R. (2009). Causes and consequences of variation in leaf mass per area (LMA): a meta-analysis. *New Phytol*, 182, 565–588.

Prado-Junior, J.A., Schiavini, I., Vale, V.S., Raymundo, D., Lopes, S.F. & Poorter, L. (2016). Functional traits shape size-dependent growth and mortality rates of dry forest tree species. *J Plant Ecol*.

Sack, L. & Buckley, T.N. (2016). The developmental basis of stomatal density and flux. *Plant Physiol*.

Sack, L. & Buckley, T.N. (2020). Trait multi-functionality in plant stress response. *Integr Comp Biol*, 60, 98–112.

Sack, L., Scoffoni, C., McKown, A.D., Frole, K., Rawls, M., Havran, J.C., *et al.* (2012). Developmentally based scaling of leaf venation architecture explains global ecological patterns. *Nat Commun*, 3, 837.

Santiago, L.S., Kitajima, K., Wright, S.J. & Mulkey, S.S. (2004). Coordinated changes in photosynthesis, water relations and leaf nutritional traits of canopy trees along a precipitation gradient in lowland tropical forest. *Oecologia*, 139, 495–502.

Sheth, S.N., Morueta-Holme, N. & Angert, A.L. (2020). Determinants of geographic range size in plants. *New Phytol*, 226, 650–665.

Siefert, A., Violle, C., Chalmandrier, L., Albert, C.H., Taudiere, A., Fajardo, A., *et al.* (2015). A global meta-analysis of the relative extent of intraspecific trait variation in plant communities. *Ecol Lett*, 18, 1406–1419.

Šímová, I., Violle, C., Svenning, J.-C., Kattge, J., Engemann, K., Sandel, B., *et al.* (2018). Spatial patterns and climate relationships of major plant traits in the New World differ between woody and herbaceous species. *J Biogeogr*, 45, 895–916.

Stevens, G.C. (1989). The latitudinal gradient in geographical range: how so many species coexist in the tropics. *Am Nat*, 133, 240–256.

Taugourdeau, S., Villerd, J., Plantureux, S., Huguenin-Elie, O. & Amiaud, B. (2014). Filling the gap in functional trait databases: use of ecological hypotheses to replace missing data. *Ecol Evol*, 4, 944–958.

Vesk, P.A., Morris, W.K., Neal, W.C., Mokany, K. & Pollock, L.J. (2020). Transferability of trait-based species distribution models. *Ecography*, 43, 1–14.

Violle, C., Enquist, B.J., McGill, B.J., Jiang, L., Albert, C.H., Hulshof, C., *et al.* (2012). The return of the variance: intraspecific variability in community ecology. *Trends Ecol Evol*, 27, 244–252.

Violle, C., Navas, M.-L., Vile, D., Kazakou, E., Fortunel, C., Hummel, I., *et al.* (2007). Let the concept of trait be functional! *Oikos*, 116, 882–892.

Walter, H. (1979). *Vegetation of the Earth and Ecological Systems of the Geo-biosphere*. 2nd edn. Springer, New York.

Wang, R., Yu, G., He, N., Wang, Q., Zhao, N., Xu, Z., *et al.* (2015). Latitudinal variation of leaf stomatal traits from species to community level in forests: linkage with ecosystem productivity. *Sci Rep*.

Wiens, J.J. (2011). The niche, biogeography and species interactions. *Phil Trans R Soc B*, 366, 2336–2350.

Wright, I.J., Reich, P.B. & Westoby, M. (2001). Strategy shifts in leaf physiology, structure and nutrient content between species of high- and low-rainfall and high- and low-nutrient habitats. *Funct Ecol*, 15, 423–434.

Wright, I.J., Reich, P.B., Westoby, M., Ackerly, D.D., Baruch, Z., Bongers, F., *et al.* (2004). The worldwide leaf economics spectrum. *Nature*, 428, 821–827.

Wright, I.J. & Westoby, M. (2002). Leaves at low versus high rainfall: coordination of structure, lifespan and physiology. *New Phytol*, 155, 403–416.

Yin, Q., Tian, T., Kou, M., Liu, P., Wang, L., Hao, Z., *et al.* (2020). The relationships between photosynthesis and stomatal traits on the Loess Plateau. *Glob Ecol Conserv*, 23, e01146.